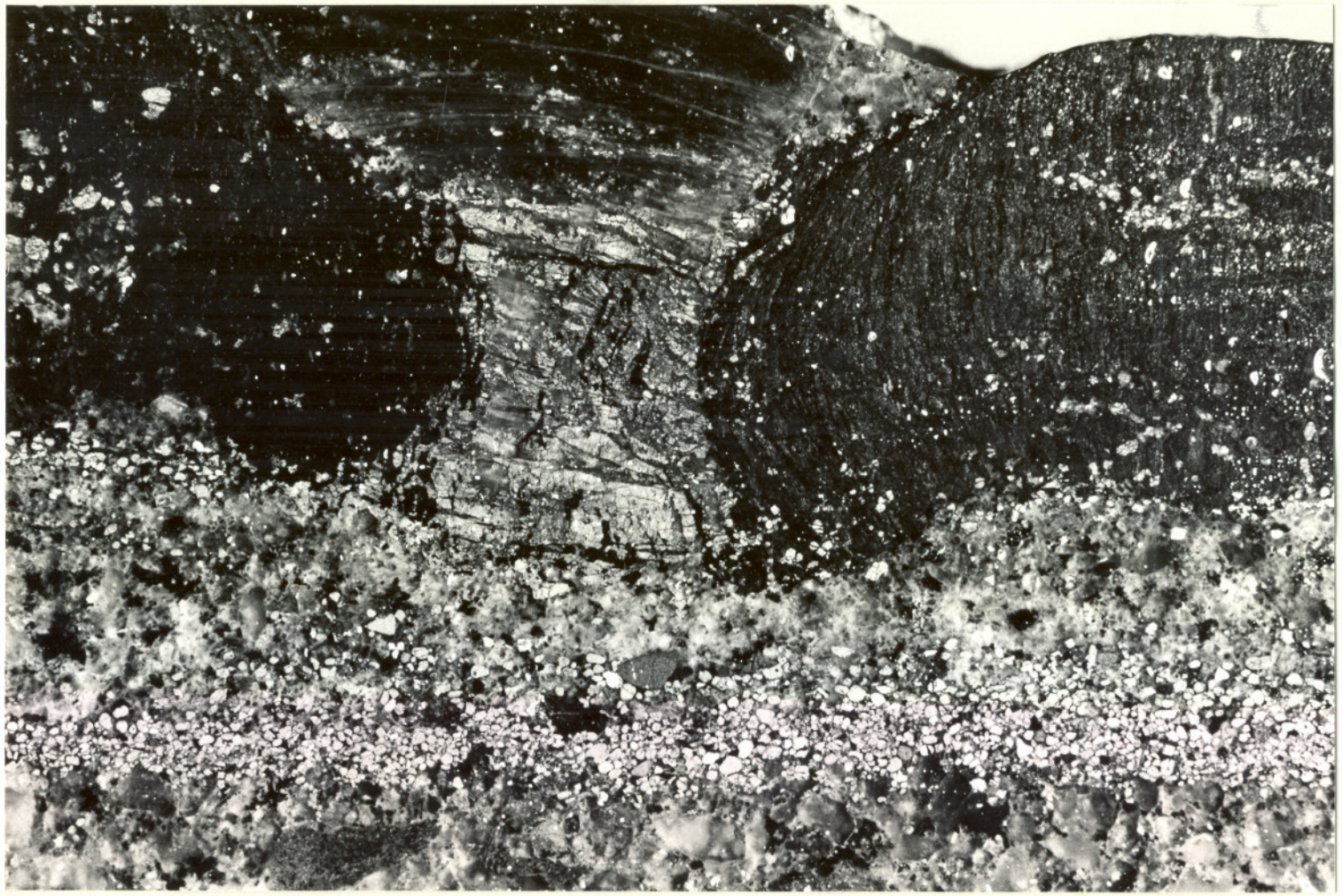
# THE GEOCHEMICAL HISTORY OF THE SEDIMENTARY ROCKS OF THE WITWATERSRAND AS REFLECTED IN THE MINERALOGY OF THE HEAVY-MINERAL ASSEMBLAGE OF THE URANIUM-BEARING REEFS OF THE CENTRAL RAND GROUP

**Georgette SMITS, BSc., Hons., MSc**

Thesis accepted in the Faculty of Science of the Potchefstroom University for Christian Higher Education in fulfilment of the requirements for the degree of Doctor of Science

| | |
|---|---|
| Supervisors | : Prof. S.A. de Waal |
| | : Prof. J. Markgraaff |
| External Co-supervisor | : Prof. J.N.Beukes |



A kerogen seam at the base of the Basal Reef on President Brand G.M.

# SYNOPSIS

The well-known Archaean gold deposit on the Witwatersrand is the world's principal source of this precious metal. A tectonically active hinterland comprising Archaean granite-greenstone terrane and pre-Witwatersrand sediments provided the detritus which was deposited at major points of fluvial influx along the northern and western periphery of the Witwatersrand Basin during the sedimentation of the Central Rand Group.

The geochemical characteristics of the environment which prevailed at the earth's surface at the time of sedimentation can be reconstructed from the response of the detrital constituents to the changes in surficial conditions during the different stages of the exogenic cycle and after burial at the final site of deposition. The information is provided by the following groups of minerals:

(1) those that must have been common in the source rocks but are absent in the reefs,
(2) constituents that were preserved during the exogenic cycle, including those altered before denudation of the provenance area, and
(3) altered or neoformed products of post-burial origin.

The absence of carbonates, sulphides other than pyrite, sulphates, apatite, iron oxides, and primary silicates suggest that the surface conditions during denudation in the provenance area and *en route* to the depositional environment must have been acid. The silicates that survived the pre-depositional processes or formed soon after deposition were subjected to diagenesis and metamorphism. The metamorphic silicate assemblage:

chloritoid-pyrophyllite-chlorite II*b*-muscovite $2M_1$,

indicates that the sedimentary rocks attained the lower stage of low-grade metamorphism at a temperature below 400°C and a pressure of about 3 kbar.

The thorough elimination of iron oxides and the alteration of ilmenite to leucoxene pseudomorphs by the removal of iron at, or close to the earth's surface was a common process during the Archaean. The dissolution of iron requires neutral to acid conditions, and the required level of acidity increases with an increase in oxidation potential.

Detrital uraninite, pyrite, chlorite, and biotite, which react readily under modern (oxidizing) surface conditions, were preserved during the exogenic cycle. Low surface temperatures and rapid erosion and accumulation of large supplies of debris could have delayed the reaction of these oxygen-consuming minerals during denudation, erosion, and transportation. When the detritus arrived at the plane of final deposition, part of the unoxidized uraninite was encapsulated by microbiota, which prevented its reaction, while the remaining portion of uraninite became a constituent of the heavy-mineral assemblage. The common presence of relict uraninite in the matrix of the conglomerates indicates that uranium was dissolved from uraninite which was not shielded by organic matter. The shape

of these partly or entirely leached grains was preserved by cutans which precipitated during the removal of uranium. The dissolved uranium was recaptured by dissolved titanium, and the two phases reprecipitated as the uranous titanate species, viz brannerite and uraniferous leucoxene of variable composition.

In the Dominion Reef, at the base of the sedimentary succession that filled the basin, and in some of the reefs near the top of the supergroup, part of the uraninite was transformed *in situ* to coffinite through the addition of silica, a process which requires an alkaline-reducing environment. Such conditions were found, for example, in stagnant pools on the depositional plane onto which a braided channel pattern developed.

Owing to the addition of titania and silica, the neoformed uranous titanates and coffinite occupied much more space than the original uraninite, hence, the alteration of uraninite and, likewise, the formation of cutans took place at a time that the porosity of the sediment made provision for expansion and for the free circulation of pore solutions, i.e. shortly after burial.

The missing minerals and the behaviour of ilmenite and the iron oxides indicate that the conditions at the Archaean earth's surface was distinctly acid. It is generally assumed that the partial pressure of carbon dioxide in the primitive atmosphere was much higher than it is at present, a condition which must have increased the acidity of the rain water, groundwater and surface waters.

Of the oxygen-consuming minerals, only uraninite was oxidized, which implies that the uranium oxide was the most efficient sink for oxygen. The oxidation of uraninite after deposition at the palaeosurface without that of the detrital minerals pyrite, chlorite, and biotite, indicates that only limited amounts of oxygen must have been available at the time of sedimentation.

# SAMEVATTING

Die welbekende goudafsetting van Argeïese ouderdom wat aan die Witwatersrand voorkom is die wêreld se vernaamste bron van goud. 'n Tektonies aktiewe brongebied bestaande uit 'n Argeïese graniet-groensteenterrein en voor-Witwatersrandse sedimente het die detritus verskaf. Hierdie detritus is afgesit by belangrike rivierinvloeipunte langs die noordelike en westelike buiterand van die Witwatersrandkom tydens die sedimentasie van die Groep Sentraal-Rand.

Die geochemiese kenmerke van die omgewing wat ten tye van die sedimentasie aan die oppervlak van die aarde geheers het, kan gerekonstrueer word op grond van die reaksie wat die detritale mineraalbestanddele ondergaan het weens veranderinge in die oppervlaktoestande tydens die verskillende stadiums van die eksogene siklus en na begrawing op die finale afsettingsterrein. Inligting in die verband word deur die volgende mineraalgroepe verskaf:

(1) dié wat algemeen in die brongesteentes voorgekom het, maar afwesig is in die riwwe,
(2) bestanddele wat behoue gebly het tydens die eksogene siklus, insluitende dié wat voor denudasie van die herkomsgebied verander het, en
(3) veranderde of nuutgevormde produkte wat na die begrawing ontstaan het.

Die afwesigheid van karbonate, sulfiede behalwe piriet, sulfate, apatiet, ysteroksiede, en primêre silikate, dui daarop dat die oppervlaktoestande tydens denudasie in die herkomsgebied en onderweg na die afsetomgewing suur moes gewees het. Die silikate wat die voorafsettingsprosesse oorleef het, of kort na die afsetting gevorm het, het diagenese en metamorfose ondergaan. Die metamorfiese silikaatgroep

chloritoied-pirofilliet-chloriet II*b*-muskoviet $2M_1$

dui daarop dat die sedimentêre gesteentes die onderste stadium van laegraadse metamorfose bereik het, naamlik by 'n temperatuur onder 400°C en 'n druk van ongeveer 3 kbar.

Die deeglike uitskakeling van ysteroksiedes en die verandering van ilmeniet in leukokseenpseudomorfe deur die verwydering van yster dui daarop dat die loging van yster, op of naby die aardoppervlak, 'n algemeen proses was tydens die Argeïese tyd. Die oplossing van yster vereis neutrale tot suur toestande en die vereiste suurgehalte neem toe met 'n toename in die oksidasie-potensiaal.

Detritale uraniniet, piriet, chloriet en biotiet wat onder moderne (oksiderende) oppervlaktoestande maklik reageer, is tydens die eksogene siklus bewaar. Lae oppervlak temperature en vinnige erosie en die akkumulasie van groot hoeveelhede puin kan die reaksie van hierdie suurstofverbruikende minerale tydens denudasie, erosie en vervoer vertraag het. Toe die detritus op die finale afsettingsvlak aangekom het, is 'n gedeelte van die ongeoksideerde uraniniet deur mikrobiota gekapsuleer wat voorkom het dat dit reageer terwyl die oorblywende gedeelte van die uraniniet 'n bestanddeel van die

swaarmineraalgroep geword het. Die algemene teenwoordigheid van uraninietoorblyfsels in die matriks van die konglomerate toon aan dat die uraan opgelos is uit uraniniet wat nie deur organiese materiaal afgeskerm was nie. Die vorm van hierdie gedeeltelik of heeltemaal geloogde korrels is bewaar deur kutane wat tydens die verwydering van uraan neergeslaan het. Die opgeloste uraan is weer deur opgeloste titaan vasgevang en die twee fases het weer neergeslaan as uraantitanaatspecies, naamlik branneriet en uraanhoudende leukokseen met 'n veranderlike samestelling.

In die Dominion-rif, aan die voet van die opeenvolging van sedimente wat die kom gevul het, en in sommige van die riwwe nader aan die bokant van die supergroup, is deel van die uraniniet ter plaatse in coffiniet verander deur die byvoeging van silika, 'n proses wat 'n alkaliese reduserende omgewing vereis. Sulke toestande is byvoorbeeld gevind in die staande poele op die afsettingsvlak waarop 'n gevlegde kanaalpatroon ontwikkel het.

As gevolg van die byvoeging van titaanoksied en silika het die nuutgevormde uraantitanate en coffiniet meer ruimte as die oorspronklike uraniniet in beslag geneem. Die verandering van die uraniniet asook die vorming van kutane het dus plaasgevind op 'n tydstip toe die poreusheid van die sediment, uitsetting en die vrye sirkulasie van porieoplossings toegelaat het - d.w.s. kort na die begrawing.

Die ontbrekende minerale en die gedrag van ilmeniet en die ysteroksiede toon dat die toestande op die Argeïese aardoppervlak duidelyk suur was. Daar word algemeen aanvaar dat die deeldruk van koolstofdioksied in die primitiewe atmosfeer baie hoër was as wat dit tans is - 'n toestand wat die suurheid van reënwater, grondwater en die oppervlakwater moes verhoog het.

Van die suurstofverbruikende minerale is net uraniniet geoksideer wat daarop dui dat die uraanoksied die doeltreffendste opvanger vir suurstof was. Die oksidasie van uraniniet na afsetting op die paleo-oppervlak, sonder dat die detritale minerale piriet, chloriet en biotiet geoksideer het, toon aan dat daar ten tye van die sedimentasie slegs beperkte hoeveelhede suurstof beskikbaar moet gewees het.

CONTENTS


1. INTRODUCTION 1

1.1. Intent of Study 1
1.2. Method of Study and Mode of Presentation 5
1.3. Previous Work 8

2. GENERAL REVIEW OF THE WITWATERSRAND SUPERGROUP 11

2.1. Tectonic and Sedimentological Framework of the Witwatersrand Deposits 111
2.2. Lithological Characteristics of the Reefs of the Central Rand Group 112

2.2.1. Conglomeratic Units 13
2.2.2. Unconformities 13
2.2.3. Concentratioan of Heavy Minerals 15
2.2.4. Mechanical Abrasion of Detritus 16

2.3. Mineralization of the Reefs 16
2.4. Post-depositional Processes 17
2.5. Age Limits of the Witwatersrand Supergroup 17

3. DESCRIPTION OF HEAVY MINERALS IN THE CENTRAL RAND GROUP 21

3.1. Phyllosilicates and Chloritoid 26

3.1.1. Chlorite 26
3.1.2. Muscovite and Sericite 30
3.1.3. Pyrophyllite and Chloritoid 41

3.2. Sulphides and Sulpharsenides 49

3.2.1. Pyrite 49
3.2.2. Pyrrhotite 51
3.2.3. Other Sulphides 51
3.2.4. Sulpharsenides and -antimonides 53

3.3. Accessory Minerals 56

3.3.1. Titanium-bearing Minerals 57
3.3.2. Chromite 61
3.3.3. Zircon 66
3.3.4. Tourmaline 66
3.3.5. Graphite 66

3.4. Polymineralic Spheroids 66
3.5 Gold 69
3.6. Platinum Group Minerals 72
3.7 Uranium-bearing Minerals 75
3.7.1. Uraninite 76
3.7.2. Uraninite-bearing Kerogen 81
3.7.3. Uranous Titanates 86
3.7.4. (U,Th)-silicates 91
3.7.5. Pitchblende and Secondary Coffinite 109
3.7.6. Thorian Zircon 109

4. INTERPRETATION AND DISCUSSION OF MINERALOGICAL OBSERVATIONS IN THE REEFS OF THE CENTRAL RAND GROUP 111

4.1. Minerals that are Absent 111
4.1.1. Ilmenite, Magnetite, Hematite, and Ferrihydrite 114
4.1.2. Carbonates, Sulphates, and Silicates 118
4.1.3. Apatite 120
4.1.4. Framboidal Pyrite 121
4.1.5. Sphalerite, Galena, Chalcopyrite, Pyrrhotite, and Pentlandite 121

4.2. Minerals that were Preserved 122
4.2. 1. Uraninite 122
4.2. 2. Gold 124
4.2. 3. Platinum Group Minerals 129
4.2. 4. Pyrite 131
4.2. 5. Chloritized iron-bearing Minerals and Chlorite Pseudomorphs 131
4.2..6. Rutile-leucoxene Pseudomorphs 132
4.2. 7. Sericite, Muscovite, and Pseudomorphs after Biotite 134
4.2. 8. Zircon, thorian Zircon, and Tourmaline 134
4.2. 9. Chromite 134
4.2.10. Sulpharsenides 135
4.2.11. Polymineralic Spheroids 135
4.2.12. Rare accessory Minerals 136

4.3. Altered and Neoformed Minerals 137
4.3.1. Kerogen 137
4.3.1.1. Kerogen-Uraninite Association 141
4.3.1.2. Kerogen-Gold Association 144
4.3.1.3. Kerogen-Gersdorffite Association 145

4.3.2. Authigenic Uranium-bearing Minerals and Cutans 146
4.3.2.1. Relict Uraninite and Cutans 141
4.3.2.2. Uranous Titanates 150
4.3.2.3. (U,Th)-silicates 155
4.3.2.4. Pitchblende and Secondary coffinite 161
4.3.3. Rutile and Leucoxene of authigenic Origin 161
4.3.4. The Metamorphic Assemblage 162
4.3.4.1. Chlorite 169
4.3.4.2. Muscovite-Sericite 171
4.3.4.3. Pyrophyllite 171
4.3.4.4. Chloritoid 173
4.3.4.5. Authigenic Sulphides and Gersdorffite and Recrystallization of Gold 174
4.3.4.6. Tourmaline overgrowth 175
4.3.4.7. Other metamorphic Parameters in the Witwatersrand 175
5. THE PALAEOENVIRONMENT OF THE EARTH'S SURFACE DURING WITWATERSRAND TIMES 177
5.1. Geologic Setting 177
5.2. The primitive Atmosphere and Biosphere 179
5.2.1. Influence of Climate 182
5.3. Geochemical Aspects 183
5.3.1. Pre-depositional Mineral Modifications 185
5.3.2. Weathering Profiles 186
5.3.2.1. Palaesols in the Central Rand Group 186
5.3.2.2. Palaeosols in the Archaean Granite Basement 187
5.3.3. Geochemical Indicators in the Reefs of the Central Rand Group 188
6. CONCLUSIONS
ACKNOWLEDGEMENTS
REFERENCES

## APPENDICES

A. PHOTOMICROGRAPHS OF MINERALOGICAL FEATURES OF INTEREST IN THE WITWATERSRAND REEFS
B. LIST OF ABBREVIATIONS

## LIST OF TABLES

1. Stratigraphic column for the Witwatersrand Supergroup in the. Central Rand and Dominion Group 3
2. Reefs from which samples were investigated 4
3. Age determinations of rocks and minerals associated with sedimentary rocks of the Witwatersrand Supergroup 18
4. Ideal compositions and average electron-microprobe compositions of silicates in the CRG 27
5. Range of trace element contents of CRG silicates determined on the electron microprobe 27
6. Textural varieties of chlorite in the CRG reefs 31
7. Minerals associated with chlorite in the CRG reefs 32
8. Optical varieties of chlorite in the CRG reefs 32
9. Quantitative electron-microprobe analyses of the Witwatersrand chlorite 33-37
10. Average chlorite formulae for individual gold mines 38
11. Textural varieties of muscovite in the CRG reefs 42
12. Quantitative electron-microprobe analyses of Witwatersrand sericite 43,44
13. Textural varieties of pyrophyllite in the CRG reefs 45
14. Quantitative electron-microprobe analyses of the Witwatersrand pyrophyllite 46,47
15. Quantitative electron-microprobe analyses of the Witwatersrand chloritoid 48
16. Textural varieties of pyrite in the CRG reefs 50
17. Textural varieties of pyrrhotite in the CRG reefs 52
18. Textural varieites of galena in the CRG reefs and Dominion Reef 52
19. Textural data of sulpharsenides in the CRG reefs 55
20. Textural varieties of authigenic rutile in the CRG reefs 58
21. Textural varieties of anatase in the CRG reefs 58
22. Detailed information on rutile-leucoxene pseudomorphs in the CRG reefs 59
23. Electron-microprobe analyses of titanium oxides in the CRG reefs 60
24. Variation in oxide composition of chromite in the Vaal Reef 62
25. Types of alterations of chromite in the CRG reefs 64
26. Electron-microprobe analyses of zinc-bearing chromites 65
27. Mineralogical data of zircon in the CRG reefs 67
28. Textural varieties of graphite in the CRG reefs 68

29. Mode of occurrence of gold in the CRG reefs 70
30. Chemical composition of gold particles in the CRG reefs 73
31. Fineness of gold from placers and hydrothermal veins 73
32. Data on platinum group minerals in the CRG reefs 74
33. Compositional range of PGE from the Main, Bird, Kimberley, Elsburg, VCR, and Black Reefs 75
34. Mineralogical data of uraninite in the CRG reefs and the Dominion Reef 77
35. Electron-microprobe analyses of uraninite in the CRG reefs 78
36. Compositional data on uraninite in sediments of Early Proterozoic age 79
37. $UO_2$, $UO_3$, and PbO contents of uraninite concentrates of the Dominion, Main, Vaal, and Carbon Reef Leader Reefs 80
38. Mineralogical information of uraninite-bearing kerogen in the CRG reefs 83
39. Chemical analyses of uraninite-bearing kerogen in CRG reefs 85
40. Chemical analyses of kerogen in the CRG reefs 85
41. Textural data on brannerite in the CRG reefs 87
42. Textural data of uraniferous leucoxene in the CRG reefs 87
43. Properties of brannerite of occurrences elsewhere in the world 89
44. X-ray diffraction data for several brannerites 90
45. Electron-microprobe analyses of brannerite in the CRG reefs 92
46. Compositions of brannerite and uraniferous leucoxene from various localities in the world 93
47. Optical and physical properties of thorium-bearing silicates 95
48. Compositions of thorium silicates from the Witwatersrand and elsewhere 95
49. Average electron-microprobe analyses of radioactive minerals in the Dominion Reef 96
50. Comparison of analytical data of uranothorite 94
51. Textural varieties of thorian coffinite in the CRG reefs and the Dominion Reef 98
52. Optical and physical properties of coffinite 99
53. X-ray diffraction data for thorium and uranium silicates 100
54. Electron-microprobe analyses of coffinite from the Witwatersrand 101
55. Composition of coffinites occurring in other deposits in the world 102
56. Electron-microprobe analyses of Y-phosphates 103
57. Diffraction data of coffinite patterns of mushy anatase in the Witwatersrand 103
58. Electron-microprobe analyses of coffinite associated with mushy anatase 108
59. Electron-microprobe analyses of uraninite and coffinite of primary and secondary origin in the Monarch Reef, West Rand Goldfield 108
60. Compositions of minerals of the thorite-zircon group 110
61. Genetic classification of heavy minerals in the CRG reefs and the Dominion Reef 112
62. Isotopic composition of kerogen, sulphides, and sulphates 117

63. Geochemical response of gold in different natural environments 127
64. Some properties of platinum group elements 130
65. Modes of precipitation of uranous titanates 153
66. Possible precursor minerals of present metamorphic phyllosilicate assemblage 163
67. Indicator minerals for the type of source rocks of the CRG reefs and the Dominion Reef 173
68. Range and average of total rock analyses of reefs on the OFS, Klerksdorp, West Wits Line, and West Rand G.F. 184

## LIST OF FIGURES

1. Location of Witwatersrand Basin 2
2. Location of gold mines from which rock samples were studied 7
3. Schematic illustration of depositional planes at major points of fluvial influx 12
4. Schematic diagram of the seven goldfields along the periphery of the Witwatersrand Basin 12
5. a. Pebble-supported conglomerate underlain by fine-grained quartzite 14
b. Kerogen seam overlying quartzite which encloses foresets of kerogen 14
6. Photomicrographs of phyllosilicates 22
7. Photomicrographs of green and purple chlorite 24
8. Photomicrographs of phyllosilicates 28
9. Graphic representation of average compositions of chlorite in the reefs of the CRG 39
10. Classification of chlorites in the CRG reefs according to relation between octahedral $Fe^{2+}$:$R^{2+}$ and tetrhedral Si:Al 39
11. Diagram showing relation between Al(IV) and Al(VI) contents of chlorites of the CRG reefs compared with those classified by Foster (1962) 40
12. Diagram showing relation between $K^+$ and $Al^{3+}$(VI)-$Al^{3+}$(IV) for sericite from the Witwatersrand (this study) and muscovite and illite from other locations 40
13. Possible precipitation paths for pyrite 54
14. Ternary diagram of compositions of detrital and authigenic sulpharsenides in the CRG reefs 54
15. Compositional field of Witwatersrand chromites 63
16. Composition of (U,Th)-silicates in (U+Th)-Si-$H_2O$ system in mass per cent 104
17. Composition of (U,Th)-silicates in the U-Th-Si system in mass per cent 105
18. Backscattered electron and X-ray distribution images for uranium, titanium, and silicon 107
19. Stability fields for ilmenite, magnetite + rutile, and hematite + rutile in natural waters 113
20. Eh-pH diagram of iron oxides and sulphides in water at 25°C and 1 atm 119

21. a. Eh-pH diagram for Au-Cl-S-$H_2O$ at 25°C, 1 atm
b. Eh-pH diagram for Au-CN-$H_2O$ system at 25°C, 1 atm
c. Solubility curves for three thio-gold commplexes 127
22. Solubility of components released during weathering in relatioan to pH 138
23. Van Krevelen diagram illustrating the diagenetic pathways for different types of organic matter 138
24. Eh-pH diagram in the U-$O_2$-$CO_2$-$H_2O$ system at 25°C and a typical groundwater $CO_2$ pressure of $10^{-2}$ atm 148
25. Parageneses of very-low and low metamorphic grades illustrated in an AMF projection plane 163
26. Graphic representation in an AFM projection plane of parageneses and the compositional ranges of chloritoid ;and chlorites found in the uranium-bearing CRG reefs 164
27. Petrogenetic grid of metamorphic reactions relevant to the Witwatersrand rocks 166
28. Correlation between the thermal indicators for coal, hydrocarbon, and minerals 167
29. Eh-pH diagram at 25°C and 1 atm on which surface conditions are indicated that prevailed at the earth's surface during the Witwatersrand sedimentation 192

## LIST OF FIGURES IN APPENDIX A

A. 1. Photomicrographs of phyllosilicates
A. 2. Photomicrographs of chlorite
A. 3. Photomicrographs of phyllosilicates
A. 4. Photomicrographs of phyllosilicates
A. 5. Photomicrographs of chloritoid and pyrite
A. 6. Photomicrographs of pyrite
A. 7. Photomicrographs of pyrite
A. 8. Photomicrographs of sulphides, chromite, tantalaeschynite, and gar net
A. 9. Photomicrographs of gersdorffite
A.10. Photomicrographs of cheralite, titania, and chromite
A.11. Photomicrographs of titania
A.12. Photomicrographs of chromite
A.13. Photomicrographs of chromite, zircon, and gold
A.14. Photomicrographs of graphite intergrown with chlorite
A.15. Photomicrographs of graphite inclusions in quartz
A.16. Photomicrographs of polymineralic spheroids
A.17. Photomicrographs of gold
A.18. Photomicrographs of gold
A.19. Photomicrographs of uraninite

A.20. Photomicrographs of altered uraninite and seam of kerogen
A.21. Photomicrographs of uraninite-bearing kerogen
A.22. Photomicrographs of kerogen
A.23. Photomicrographs of uranous titanates
A.24. Photomicrographs of kerogen
A.25. Photomicrographs of boudinage in kerogen and of uranous titanates
A.26. Photomicrographs of uranous titanates
A.27. Photomicrographs of uraniferous leucoxene and coffinite
A.28. Photomicrographs of coffinite, pitchblende, and secondary coffinite
A.29. Photomicrographs of brannerite
A.30. Photomicrographs of thorite and mushy anatase

# 1. INTRODUCTION

Quartz-pebble conglomerate ore deposits of Archaean and Early Proterozoic age represent the earliest known sedimentary concentrations of gold and uranium. Of these deposits, only the Witwatersrand in South Africa and those in the Elliot Lake-Blind River region in Canada are of economic importance. This type of sedimentary deposits exhibits similar mineral assemblages as well as genetic and geochemical characteristics. They formed at a critical point in the evolution of the atmosphere, referred to as the oxyatmoversion (Mossman & Harron, 1983).

Two essential factors influenced their formation, i.e. a specific tectonic regime in the provenance and depositional area (Pretorius, 1976) and the absence of vegetation (Cloud, 1976), which promoted uninhibited disintegration and denudation of the rocks. The disappearance of the quartz-pebble conglomerate type of uranium deposits from the geological record and the simultaneous appearance of red-bed sediments (Cloud, 1976) about 2,0 Ga ago, denote a global control of the geochemical conditions in which the composition of the atmosphere and the evolution of the biosphere played an important role.

The Witwatersrand Basin and the Dominion Reef and Evander subsidiary depositories, respectively west of the Klerksdorp Goldfield (G.F.) and at the northeastern tip of the basin, are located on the Kaapvaal Craton (Fig. 1), an Archaean crustal fragment made up of granites and gneisses which encloses remnants of infolded supracrustal rocks of the greenstone belt.

Gold and uranium mineralization of economic importance is found in some of the conglomerates (referred to as reefs when mineralized) present in the Central Rand Group (CRG), the upper portion of the sediments (Table 1) that filled the Witwatersrand Basin.

## 1.1. Intent of Study

Over the period 1981 to 1984, a mineralogical investigation was carried out for metallurgical purposes at the Council for Mineral Technology (Mintek), Randburg. From this study, it became evident that the heavy-mineral assemblages of the sedimentary rocks of the Witwatersrand are a valuable source of

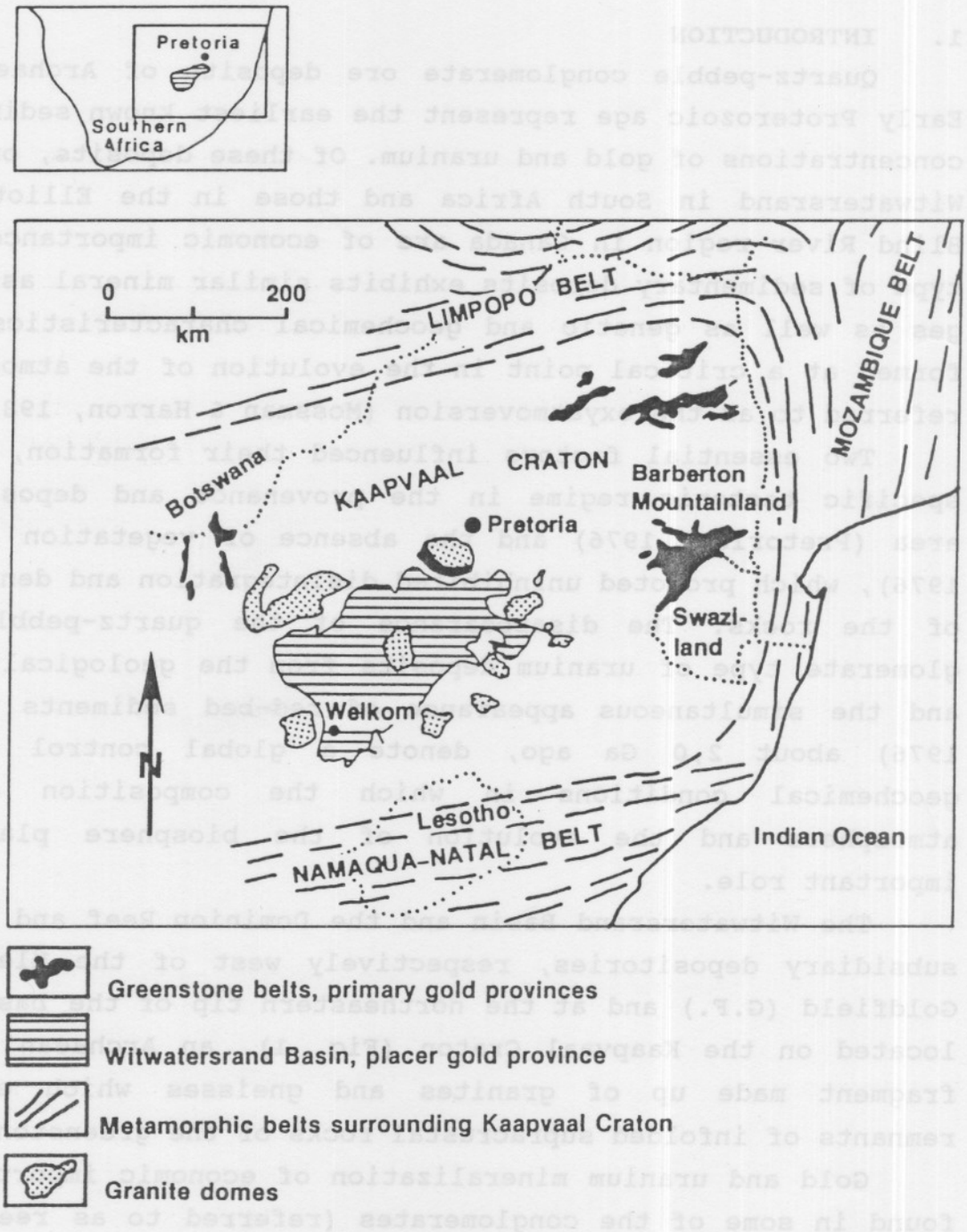



Fig. 1 Location of Witwatersrand Basin (after Thiel *et al.*, 1979)

Table 1 Stratigraphic column for the Witwatersrand Supergroup in The Central Rand and Dominion Group (S.A.C.S., 1980)

| Supergroup | Group | Subgroup | Formation |
|---|---|---|---|
| Witwatersrand 11000 m | Central Rand | Turffontein 1700 m* | Mondeor Conglomerate<br>Elsburg Quartzite<br>Kimberley Conglomerate |
| | | | Booysens Shale |
| | | Johannesburg 1400 m | Krugersdorp<br>Bird Conglomerate<br>Luipaardsvlei Quartzite<br>Livingstone Conglomerate<br>Randfontein Quartzite<br>Johnston Conglomerate<br>Langlaagte Quartzite |
| | West Rand | Jeppestown 1400 m | Roodepoort<br>Crown<br>Florida Quartzite |
| | | Government 2000 m | Witpoortjie<br>Coronation Shale<br>Promise Quartzite |
| | | Hospital Hill 1700 m | Brixton<br>Parktown Shale<br>Orange Grove Quartzite |
| | Dominion | Syferfontein 2100 m | Syferfontein Porphyry |
| | | Rhenosterhoek 600 m | Rhenosterhoek Andesite<br>Rhenosterspruit Quartzite |

*) Thicknesses compiled from type areas (Tankard et al., 1982)

information with regard to the geochemical conditions they were subjected to before or after they became exposed to the atmosphere.

Although the mineralogy of the reefs in the Witwatersrand has been studied by many (Section 1.3), none of the investigators used the information provided by the heavy-mineral assemblages to the full extent. When one critically analyzes the geological record preserved in today's mineral constituents of the reefs of the CRG, it is possible to make inferences with respect to the type of processes which operated before, during, and after the various stages of the exogenic cycle. In other words, the cause of change is deduced from the effect it had on the minerals. Understanding of the geochemical processes also contributes to that of the primitive atmosphere and its evolution in the course of geologic time.

Certain minerals have been altered or entirely eliminated before arrival at the final site of deposition, while others were transformed, replaced, or precipitated after burial on the depositional plane. The present mineral assemblage offers clues on factors, which controlled the behaviour of the minerals at the time that the Witwatersrand Basin was created and filled with clastic material. They are:

(1) the conditions which controlled processes that took place in the source rocks before denudation (Robb & Meyer, 1985; Grandstaff *et al.*, 1986),
(2) the geochemical environment at the earth's surface in the provenance and the final site of deposition,
(3) the possible influence of the climate, temperature, and the composition of the primitive atmosphere,
(4) the role of the microorganisms which grew in stagnant pools on unconformities in the depositional environment,
(5) the effects of weathering and diagenesis after final deposition, and
(6) the metamorphic grade and peak temperature which was attained after burial (Phillips, 1987).

Except for the first and last, the above-mentioned topics have not been dealt with in the literature, or only touched upon.

In this study, an attempt is made to reconstruct, with the aid of certain scientific principles, the geochemical path followed by the heavy minerals as manifested in today's mineral constituents of the reefs of the CRG. In addition an extensive

database of the chemical and textural properties of the heavy minerals which may be observed in the conglomerates from the Central Rand Group is provided. Some previously proposed concepts have been included or extended on, in the analysis and the interpretation of the behaviour of the minerals, but several new ideas are advanced.

The decoding of the physicochemical conditions, which prevailed at the earth's surface during the time that the Witwatersrand Basin was filled, from the information retained by the heavy-mineral constituents appeared to be an extremely stimulating and rewarding exercise.

### 1.2. Method of Study and Mode of Presentation

The mineralogical information was gathered from the following:

(1) the microscopic study of 933 polished sections and 552 thin sections of rock samples of the reefs of the CRG summarized in Table 2 (Fig. 2),
(2) identification by X-ray diffraction (XRD),
(3) qualitative analysis on the scanning electron microscope (SEM),
(4) quantitative analysis of silicates, uranium-bearing minerals and other heavy minerals on the electron microprobe (EMP),
(5) concentrates of uraninite from Blyvooruitzicht Gold Mine (G.M.), West Wits Line G.F., and Vogelstruisbult G.M., East Rand G.F.,
(6) a handspecimen of brannerite of hydrothermal origin, and
(7) polished and thin sections of gold-bearing metagreywackes of Sheba gold mine and schists of Consort gold mine in the Barberton Mountain Land.

For comparative purposes, microscopic findings of the Dominion Reef were, where applicable, included in the interpretation of the mineralogical observations. Polished and thin sections from the Sheba and Consort gold mines were also studied, because the provenance of the Witwatersrand deposit was supposedly made up of similar rocks (Viljoen *et al.*, 1970). The properties of brannerite of hydrothermal origin were compared with those of the 'brannerite'-type minerals in the Witwatersrand, which are beyond doubt of post-depositional origin.

Table 2 Reefs from which samples were investigated

| Goldfield and gold mine | Name of the reef |
|---|---|
| EVANDER | |
| Leslie<br>Kinross<br>Winkelhaak<br>Bracken | Kimberley Reef |
| EAST RAND | |
| Grootvlei<br>Marievale | Main and Kimberley Reefs,<br>Booysens Shale |
| CENTRAL RAND | |
| Durban Roodepoort Deep<br>South Roodepoort | Main Reef |
| WEST RAND | |
| West Rand Consolidated | Upper Monarch Reefs;<br>Zone 2 Reef<br>Zone 4 Reef<br>Monarch Reef<br>White Reef |
| Randfontein Estates<br>Cooke Section | Monarch Reef, UE1a and E9Gd,<br>or Composite Reef |
| Western Areas | UE1a and E9Ec Reefs |
| Luipaardsvlei* | Monarch Reef |
| East Champ d'Or* | Monarch Reef |
| WEST WITS LINE | |
| Blyvooruitzicht | Carbon Leader |
| West Driefontein | Ventersdorp Contact Reef (VCR) |
| Western Deep Levels | Black Bar and Green Bar |
| Kloof | Libanon Shale |
| KLERKSDORP | |
| Hartebeestfontein<br>Buffelsfontein<br>Western Reefs<br>Vaal Reefs East<br>Vaal Reefs South | Vaal Reef for all; Elsburg no. 5<br>and VCR for Western Reefs |
| Rietkuil<br>Bramley | Dominon Reef |
| ORANGE FREE STATE | |
| President Brand | Basal Reef |
| President Steyn | Steyn Reef, locally underlain by<br>Lower Reef |
| Harmony Complex | Basal Reef, Leader Reef, or<br>Composite Reef |
| Beisa | Beisa Reef |
| Oryx | Kalkoenkrans Reef |

*) including polished sections of Liebenberg (1955)

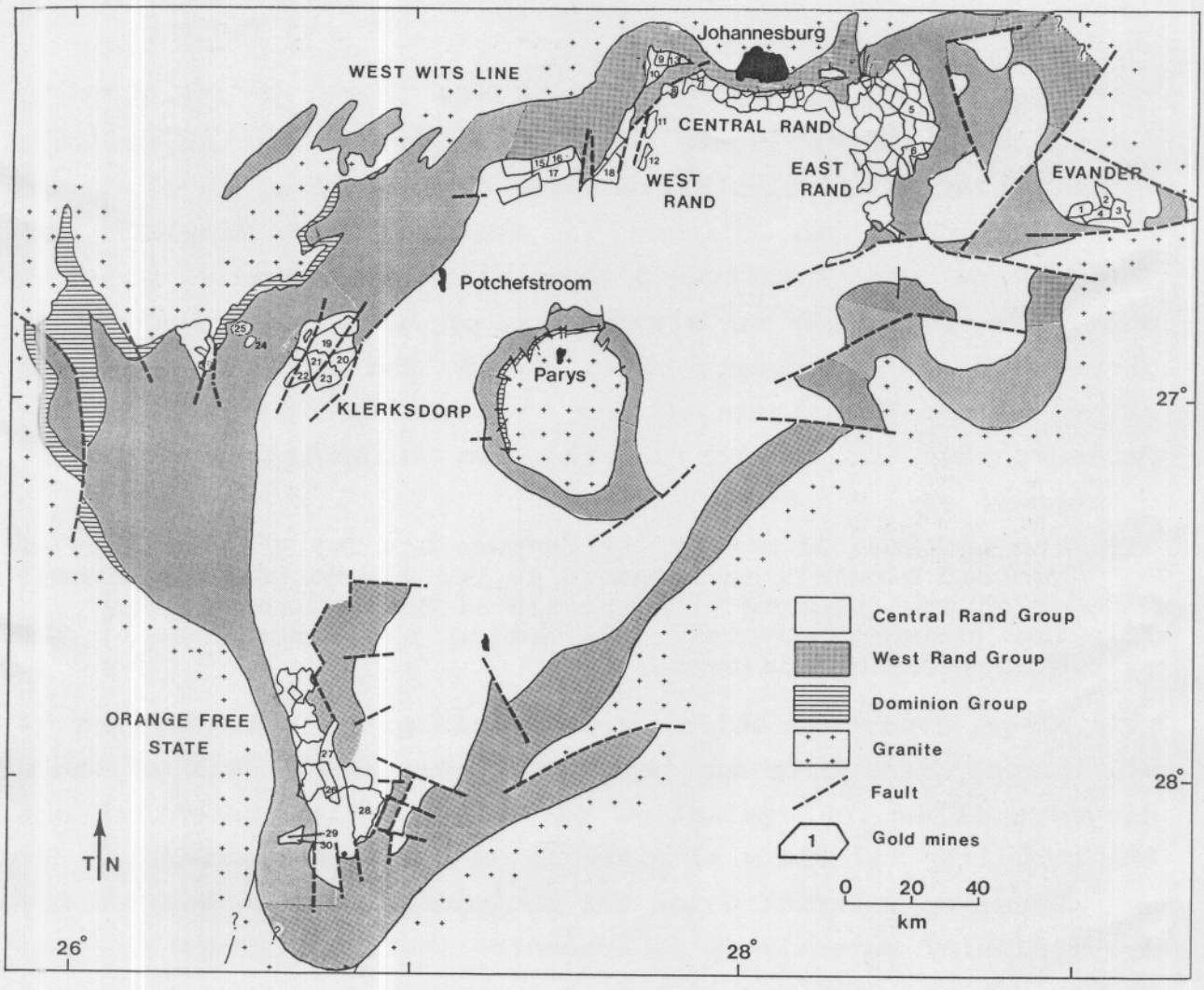



Fig. 2 Location of gold mines from which rock samples were studied. Map of suboutcrops of Dominion, West Rand and Central Rand Groups (after Borchers, 1964)

1. Leslie
2. Kinross
3. Winkelhaak
4. Bracken
5. Grootvlei
6. Marievale
7. Durban Roodepoort Deep
8. South Roodepoort
9. West Rand Consolidated
10. Randfontein Estates
11. Cooke Section
12. Western Areas
13. Luipaardsvlei
14. East Champ d'Or
15. Blyvooruitzicht
16. West Driefontein
17. Western Deep Levels
18. Kloof
19. Hartebeestfontein
20. Buffelsfontein
21. Western Reefs
22. Vaal Reefs East
23. Vaal Reefs South
24. Rietkuil
25. Bramley
26. President Brand
27. President Steyn
28. Harmony Complex
29. Beisa
30. Oryx

The heavy minerals present in the reefs of the CRG are described in Chapter 3 and their behaviour during the exogenic cycle, chiefly based on microscopic observations, is discussed and interpreted in Chapter 4. Textural and mineralogical features of the constituents were used to determine at which stage the formation or elimination of certain minerals took place, i.e. in the source rocks, during the exogenic cycle, or after final deposition during weathering, diagenesis, or metamorphism. In Chapter 5, the two following aspects are discussed:

(1) the geochemical conditions responsible for the reaction of certain minerals in response to the change in environment, which are inferred with the aid of Eh-pH diagrams, and
(2) the atmospheric conditions during the deposition of the Witwatersrand sediments.

Eh-pH diagrams, which were introduced by Baas Becking *et al.* (1960) have been an important tool in the study. These diagrams allow the evaluation of the oxidation potential and the stability relations of minerals and aqueous species.

Detailed information on the individual constituents of the heavy-mineral assemblages is presented in tables. The abbreviations that are used are listed in Appenix B on a page which can be unfolded. The description of colours is based on the Rock-Color Chart of the Geological Society of America (1963).

## 1.3. Previous Work

Numerous papers and theses have been written covering various geological topics of specific areas in the seven goldfields which have been developed since the discovery of gold in 1886 by Harrison (Pretorius, 1986). Several of these essays deal with the sedimentological aspects of the reefs of the CRG. From this information, Pretorius (1976) reconstructed the tectonic setting and depositional environment of the Witwatersrand Basin.

The most important contributions on the mineralogy of the sedimentary rocks came from: Liebenberg (1955), Ramdohr (1955, 1957, 1958a and b, 1961), Schidlowski (1966a to e, 1967, 1968), Hallbauer (1975, 1981, 1983), Feather (1976), and Smits (1984a and b, 1985 a to d, 1986, 1987). Feather and Koen (1975) reviewed the mineralogy of the Witwatersrand deposit in detail.

Because of its relationships with both detrital and authigenic components, a controversy on the genesis of gold existed for many years. 'Hydrothermalists', mainly represented by Graton (1930) and Davidson and Bowie (1951), opposed 'placerists', a group to which Young (1917), Ramdohr (1955), Liebenberg (1955), and Schidlowski (1968) belonged.

Liebenberg (1955) concluded from his study that gold and uraninite were of detrital origin, but that both had been subjected to post-depositional modifications. He endorsed the 'modified placer' theory, proposed in 1916 by Mellor, who assumed that gold and uraninite were reconstituted after burial.

Several investigators (Hallbauer, 1975; Pretorius, 1976; Reimer, 1984; Mossman & Dexter-Deyer, 1985) believe that gold arrived at the fan in the colloidal state, organically bound, or in the form of complex ions. However, the variation in the concentrations of silver and mercury even at very short distance between gold particles in the same hand-specimen rules out that it was transported in solution and precipitated after deposition (Von Gehlen, 1983). In view of its fine-grained nature, Nami (1982) believes that the gold has been transported in suspension.

The presence of radioactive matter was first mentioned by Rogers in 1915 (Whiteside, 1970), and in 1920 again by Pirow. Cooper (1923) reported that the radioactivity was caused by several types of uraninite. In 1955 Liebenberg and Ramdohr (English translation 1958) published their work on the mineralogy of the Witwatersrand. In addition to uraninite, they reported the occurrence of two unknown uranium-bearing minerals, which Schidlowski (1966a) identified on the EMP as (U,Ti)-bearing minerals.

Schidlowski also published papers on uraninite (1966b) and thucholite (1966c and e), a term introduced by Ellsworth (1928) for radioactive hydrocarbon found in pegmatites in Canada. Because the thucholite is insoluble in organic solvents, it should be referred to as kerogen. In this treatise, the term *uraninite-bearing kerogen* will therefore be used instead of thucholite.

Simpson and Bowles (1977) concluded from their study on the EMP that uranium oxide of post-depositional origin is also present in the reefs as very fine-grained material of low thorium content. It is associated with clay minerals and occurs in the matrix or is enclosed by kerogen. The authors postulate that it precipitated from uranyl, $UO_2^{2+}$, which formed after deposition on the fan and, after burial, was reduced to pitchblende. On the other hand, Thiel *et al.* (1979) believe that the authigenic uranium oxide represents uranium which was redistributed during metamorphism.

Because at today's surface conditions, uraninite and pyrite readily react with ground- and surface waters, their occurrence in conglomerates of Archaean and Early Proterozoic led many investigators to conclude that the primitive atmosphere was deficient in oxygen, or even anoxic (Cloud, 1976). Kimberley and Dimroth (1976), Dimroth (1979), and Clemmey (1981) expressed reservations concerning the use of uraninite and pyrite as indicators for an anoxic atmosphere. These objections are based on two modern examples in which uraninite and pyrite are preserved during transportation, i.e. in British Columbia, Canada (Steacy, 1953), and in the Indus River in Kashmir (Zeschke, 1960). In both instances, the debris originates from regions of extreme cold with little or no vegetation cover present, so that chemical breakdown is sluggish, and rock weathering is dominated by mechanical disintegration. Note that permafrost conditions would inhibit stripping of regolith or pre-existing sediments, unless seasonal fluvial activity would generate erosion and transportation of sediments under these conditions (Sutherland, 1985).

# 2. GENERAL REVIEW OF THE WITWATERSRAND SUPERGROUP

## 2.1. Tectonic and Sedimentological Framework of the Witwatersrand Deposits

The composite thickness of the strata in the Witwatersrand Supergroup has been estimated at 11 000 m, but the complete succession has nowhere been encountered (Pretorius, 1981). The predominantly argillaceous sediments of the West Rand Group (WRG), which were deposited in a tide-dominated basin (Watchorn, 1980), show an increase in grain size in an upward stratigraphic direction and a general trend towards the development of conglomerates, which first appear in the Government and Jeppestown Subgroups.

Recurrent tectonic instability in the provenance along the western and northern periphery of the depository during Central Rand times gave rise to the development of 'alluvial fans' Pretorius (1976) at sites of major fluvial influx (Fig. 3) and to cyclic sedimentation, first noticed by Sharpe (1949). In contrast with the sediments of the WRG, which have been deposited in an open basin (Tankard *et al.*, 1982), the sediments of the CRG suggest that sedimentation took mainly place in a closed basin (Pretorius, 1976). Recently, it was found that certain sediments indicate periods of marine activity (Bailey, *et al.*, 1989). In the present thesis, it is assumed that the depositional sites are alluvial planes.

The seven goldfields, i.e. Orange Free State (OFS), Klerksdorp, West Wits Line, West Rand, Central Rand, East Rand, and Evander are located on the six known 'alluvial fans' (Fig. 4), which occupy areas between 100 and 400 $km^2$. Each cycle starts with a conglomeratic unit, which is overlain by quartzites in which the grain size gradually decreases upwards (Pretorius, 1976). In addition to the detritus supplied by the provenance, the proximal facies of the sediments of the WRG (which extended beyond the area occupied by the CRG rocks) must have been a major source of debris for the CRG sediments (Vos, 1975), in which gold and uraninite had already been preconcentrated.

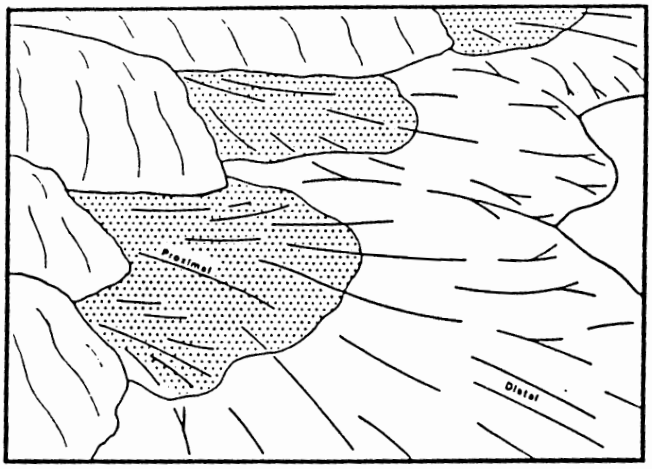



Fig. 3 Schematic illustration of depositional planes at major points of fluvial influx (after Reading, 1979)

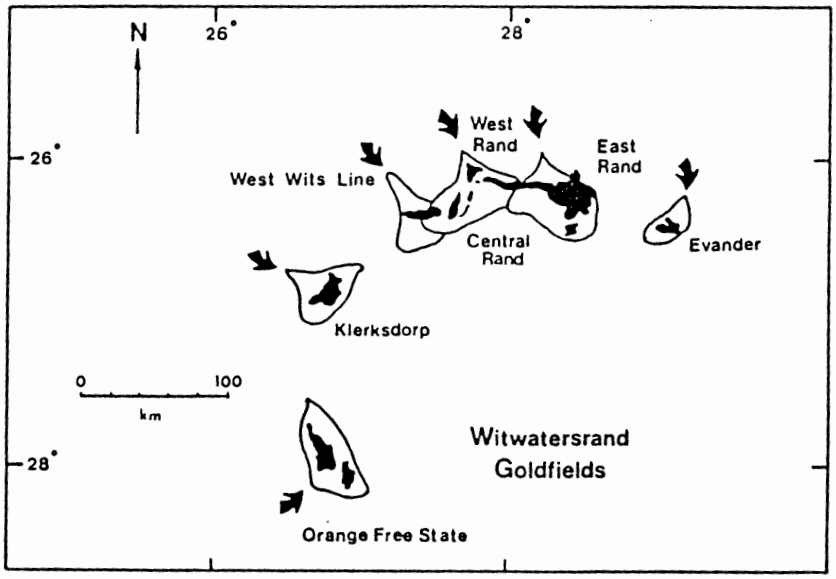



Fig. 4 Schematic diagram of the seven goldfields along the periphery of the Witwatersrand Basin (after Pretorius, 1976)

Information obtained from boreholes indicate that the southeastern margin of the basin was passive and that little sediment was derived from the southeast (Pretorius, 1976).

## 2.2. Lithological Characteristics of the Reefs of the Central Rand Group

The CRG comprises conglomerates, grits, quartz or lithic arenites, quartz wackes, argillaceous rocks and, in the northeastern part of the basin, the Bird Amygdaloid.

### *2.2.1. Conglomeratic Units*

The palaeoplacers, which form the main host rock for the gold-uranium mineralization, constitute approximately 8% of the total thickness of the sedimentary sequence of the Witwatersrand Supergroup. About 2,5% of the total thickness of rudites is mined (Pretorius, 1976). The productive reefs are generally less than 50 cm wide (ibid.).

The *banket*-type, pebble-supported reefs (Fig. 5a) were deposited closer to the apex of the aluvial plane than the uranium-bearing conglomerates, known as the *carbon seam*-type reefs which are a distal facies in relatively flat parts of the palaeosurfaces. The latter small-pebble conglomerates owe their name to the presence of discontinuous patches of uraninite-bearing kerogen at their base (Fig. 5b), which represent microbial communities that grew in shallow, waterlogged depressions (Hallbauer, 1975). For this type of reef, Nami (1982) distinguishes between a *channel* facies of stream deposits in which conglomerate and quartzite alternate, and an *interchannel* facies of conglomerate sheets, which represents debris-flow deposits. The carbon seam-type of reef is restricted to certain reefs in the Johannesburg Subgroup in the western half of the basin.

The pebble framework of the conglomerates acted as a mechanical trap for the sand-size fraction in which the pebbles were set and in which phyllosilicates filled the interstices between quartz and heavy minerals (pretorius, 1976).

### *2.2.2. Unconformities*

Angular unconformities, which truncate the underlying sediments (on average 250 m thick), separate the major sedimentation cycles of the CRG (Pretorius, 1976). They mark

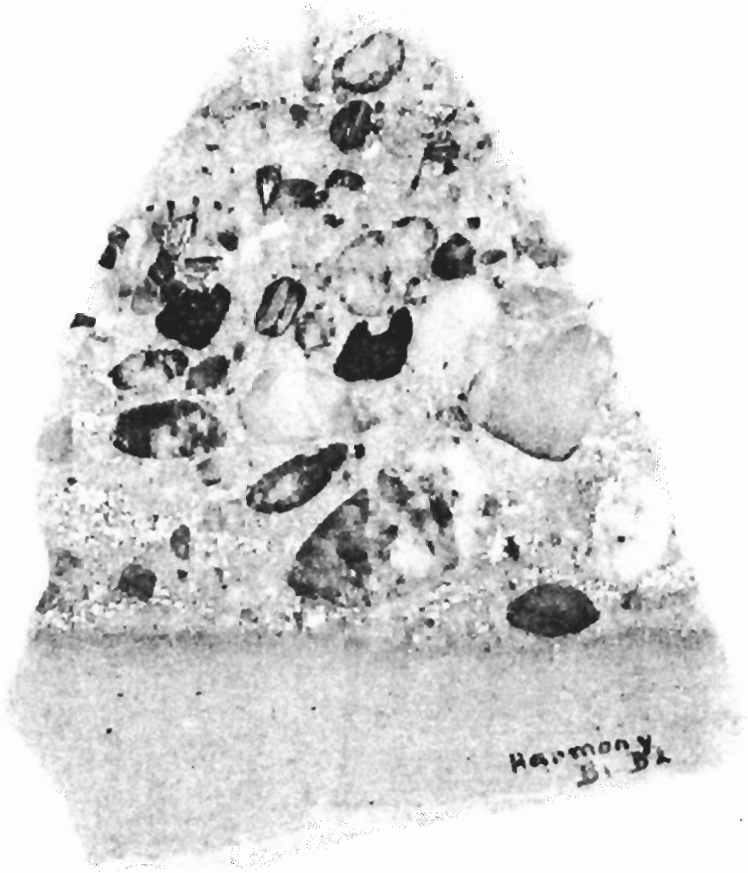



Fig. 5a Pebble-supported conglomerate underlain by fine-grained quartzite (Harmony G.M.; largest pebble 40 mm)

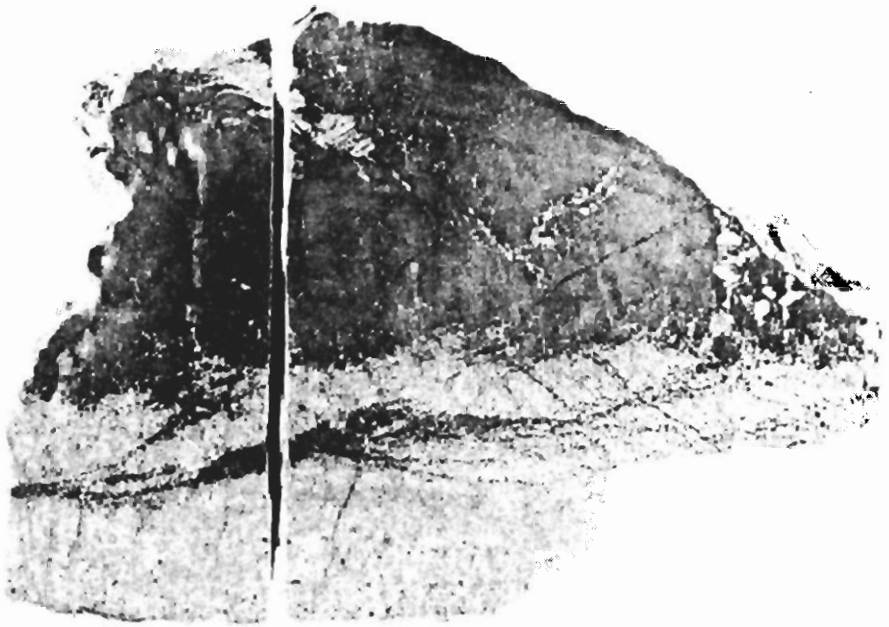


Fig. 5b Kerogen seam (black) overlying quartzite which encloses foresets of kerogen (Beisa Reef; height of rock specimen 12 cm)

lengthy breaks in sedimentation and are palaeosurfaces which, if not permanently or periodically covered by water, were exposed to surficial conditions. In the distal areas, the topographic relief of the unconformities is in the order of 0,5 m (Minter, 1972) but, near the fanhead, incisions made by rivers may reach depths up to 6,0 m (Tankard *et al.*, 1982).

The fabric of the conglomerates indicates that the concentration of heavy minerals mainly took place prior to the deposition of the pebble fraction of the conglomeratic units or of the individual pulses within such a unit (Pretorius, 1976). The major uranium-bearing reefs of the carbon-seam type, viz Basal Reef, Vaal Reef, and Carbon Leader, likewise rest on this type of unconformities (ibid. 1976). It follows that the unconformities have played a predominant role in the concentration of heavy minerals and the contemporaneous growth of microbiota.

### *2.2.3. Concentration of Heavy Minerals*

The selective concentration of minerals is characterized by the removal of the less dense minerals. Because greater energy is required to dislodge the denser particles (Reid & Frostick, 1985), the process enhances the accumulation of heavy minerals. Preconcentration of debris also takes place in temporary depository sites (Meade, 1982) *en route* from the source rocks to the point of final deposition. Such 'stopovers' serve as source points for further concentration of heavy minerals.

Koen (1961), Coetzee (1965), and Hiemstra (1968) established that the pyrite, zircon, chromite, and uraninite particles were in approximate hydraulic equilibrium with each other, but that the accompanying gold particles were smaller than the calculated size for their hydraulic equilibrium in relation to the other heavy minerals. From large-scale flume experiments, Nami (1982) concluded that the theoretical concept of the mobility of minerals according to their hydraulic equilibrium cannot be applied when different flow velocities, depths of water, and other sedimentological parameters exist side by side. The settling equivalence of clasts of different

densities is then superseded by entrainment equivalence (Reid & Frostick, 1985), and flow separation (Best & Brayshaw, 1985). Separation of grains takes place at abrupt changes in the streambed geometry, where shearflow develops. At such sites, heavy minerals are entrained, and will be deposited if a sudden drop in velocity occurs. These processes must have influenced the segregation and concentration of certain heavy minerals in the reefs of the CRG.

*2.2.4. Mechanical Abrasion of Detritus*

The pebbles and most of the heavy minerals, in particular pyrite, chromite and uraninite, show a high degree of roundness, which is indicative of their detrital origin. Small particles transported by surface waters tend to be less round than large ones. Below a certain threshold value which varies, among other factors, with the density of the grain relative to that of the transport medium, the particles will not be rounded (Utter, 1980). For quartz, this value is 0,1 mm in water (Pettijohn, 1957). Utter (1980) used this value to calculate the threshold sizes of the mentioned heavy minerals found in the reefs. He concluded that the roundness of the detrital grains in the Witwatersrand, including that of uraninite (for which the threshold value is 44 μm), can be attributed to normal mechanical abrasion during transport.

## 2.3. Mineralization of the Reefs

Gold, uraninite, and other heavy minerals are confined to conglomerates, pyritic foresets and laminations within quartzites, and less commonly, to thin layers of extreme mineralization which overlie some of the conglomerates. Examples of the last-named horizons are the U-seam on top of the UE1a Reef in Cooke Section (Tucker, 1980), and the 2,5 cm thick layer overlying the Upper Reef of the Dominion Reef (Hiemstra, 1968).

The midfan sector of the 'aluvial fans' formed the optimum site for the deposition of gold and uraninite (Pretorius, 1976). High gold values are found in the proximal zone of this sector, where it is associated with buckshot pyrite and leucoxene pseudomorphs. In the distal portion, uraninite is more abundant than gold, which here is finer-grained. The two ore minerals are often enclosed in kerogen seams. The

concentration of gold and uraninite prior to the deposition of the pebble fraction may be as much as a thousand times higher (Table A.31) than the amount of gold dispersed throughout the reef.

## 2.4. Post-depositional Processes

After deposition, the sediments were subjected to further weathering, diagenesis, and regional burial metamorphism. Despite their age, they only show low-grade metamorphism.

The northern margin of the basin was subjected to thrust faulting (McCarthy *et al.*, 1982; Roering, 1984, 1986), and post-depositional faulting strongly partitioned the sedimentary succession (McKinney *et al*, 1964; Wilson *et al.*, 1964). Dykes and sills of the Ventersdorp age and younger, which intruded the Witwatersrand strata along existing fault planes, occupy 5 to 10% of the space in the pile of sedimentary rocks (Pretorius, 1976). Their thermal influence on the adjacent rocks is limited to a narrow strip at the contact.

Quartz veins, ranging in length from a few, to tens of metres and rarely wider than two metres traverse the rocks (Burger *et al.*, 1962). These veins, which often entered along the same fault planes as the dykes, are essentially barren. Quartz, which filled dilational fractures that formed during compaction, may carry small amounts of sphalerite, galena, pyrrhotite, and chalcopyrite.

## 2.5. Age Limits of the Witwatersrand Supergroup

The geochronological data available for the granite floor, the detrital uraninite grains, and the lavas of the Dominion Group and the Ventersdorp Supergroup are listed in Table 3.

Direct dating of the Witwatersrand sedimentary rocks appears to be difficult. Minimum and maximum ages of the overlying rocks of the Ventersdorp Supergroup and underlying granite-greenstone rocks bracket the period of the Witwatersrand sedimentation. The Makwassie porphyry in Klerksdorp yielded a U-Pb age of 2699 Ma (Armstrong *et al.*, 1986). The younger age of 2300 Ma determined for the Ventersdorp lavas (Van Niekerk & Burger, 1964) is the same as that, which has recently (Allsopp *et al.*, 1986) been established for the major resetting age of uraninite enclosed by kerogen. Allsopp *et al.*

Table 3 Age determinations of rocks and minerals associated with sedimentary rocks of the Witwatersrand Supergroup

| Rock sequence or mineral | Age, Ma* | Method | Reference |
|---|---|---|---|
| Ventersdorp Supergroup | 2300 (100) | U-Pb | Van Niekerk and Burger, 1964 |
| | 2643 ( 80) | U-Pb | Van Niekerk and Burger, 1978 |
| | 2350 (160)** | Pb-Pb | Armstrong et al., 1986 |
| | 2370 ( 70)** | Pb-Pb | |
| | 2699 ( 16) | U-Pb | |
| Uraninite in CRG reefs | 2040 ( 60) | U-Pb | Louw, 1954 |
| | | U-Pb | Wetherill, 1956 |
| | | U-Pb | Burger et al., 1962 |
| | | U-Pb | Köppel and Saager, 1974 |
| | | U-Pb | Rundle and Snelling, 1977 |
| Uraninite in kerogen | 2320 ( 50) | U-Pb | Allsop et al., 1986 |
| Uraninite in Dominion Reef | 3080 (100) | U-Pb | Nicolaysen et al., 1962 |
| Uraninite | 3050 ( 50) | U-Pb | Rundle and Snelling, 1977 |
| Dominion Group | 2820 ( 55) | Rb-Sr | Allsopp, 1964 |
| | 2800 ( 60) | U-Pb | Van Niekerk and Burger, 1969b |
| | 3060 | U-Pb | Armstrong, 1987 |
| Archaean Granite | 2900 (150) | U-Pb | Nicolaysen et al., 1962 |
| | 3260 (100) | Rb-Sr | Allsopp, 1964 |
| | 3360 (100) | U-Pb | Van Niekerk and Burger, 1969a |
| | 2800 | Pb-Pb | Barton et al., 1986 |
| | 3050 | Pb-Pb | |

*) 2300 (100) means 2300 ± 100
**) Regarded to represent a resetting event (Armstrong et al., 1986)

(1986) consider this date to represent a metamorphic overprint on all rocks, i.e. granites, lavas and sediments, which has reset the rubidium-strontium isotope system.

New ages were also obtained for the Archaean granites underlying the Witwatersrand sedimentary rocks (Barton *et al.*, 1986). The oldest granite is dated at 3050 Ma, whereas the youngest was emplaced 2800 Ma ago. However, the most recent dating of zircons from rhyolites in the Dominion Group revealed an age of 3060 Ma (Armstrong, personal communication, 1987). This age is close to the age of the zircons from a rhyolite of the Pongola Supergroup (Hegner *et al.*, 1984). What is more, the mineral assemblage of the uranium-bearing conglomerate in the Mozaan Group of this Supergroup is very similar to that of the Dominion Reef (Smits, 1978).

Internationally the boundary between Archaean and Early Proterozoic is taken at 2500 Ma (James, 1978). According to the latest geochronological information, deposition of the Witwatersrand sediments started midway in the Archaean, in contrast to the quartz-pebble conglomerate, deposits in the Elliot Lake, Canada and Jacobina, Brazil, which are of Early Proterozoic age. The newly determined age of the Dominion Reef also implies that stabilization of the granite-greenstone craton in South Africa was achieved well ahead of that on other continents.

In conclusion it can be said that, although the sedimentological character of the Witwatersrand deposit is of typical Proterozoic character, it is of Archaean age.

## 3. DESCRIPTION OF HEAVY MINERALS IN THE CENTRAL RAND GROUP

Mineralogical observations of the heavy minerals in the reefs of the CRG and of certain minerals of the Dominion Reef (Table 6), which provide information on their geochemical and sedimentological history, will be summarized under the following headings:

phyllosilicates and chloritoid,
sulphides and sulpharsenides,
accessory minerals,
polymineralic spheroids,
gold,
platinum group minerals (PGM), and
uranium-bearing minerals.

In the absence of feldspar in the sediments of the CRG, all constituents, except quartz, fall under the category of heavy minerals of relative densities above about 2,8. Detailed information on texture, morphology, other properties, and composition of the heavy minerals is summarized and pictured in tables and diagrams. Photomicrographs of mineralogical features of specific interest are compiled in Appendix A. Their numbers are preceded by A.

### 3.1. Phyllosilicates and Chloritoid

The major phyllosilicates found in the sediments of the CRG are *chlorite*, *muscovite*, *sericite*, and *pyrophyllite* which, like *chloritoid*, are of post-burial origin. *Kaolinite* and *illite* are extremely rare. Small amounts of both minerals have been recorded by X-ray diffractograms. They were also observed in thin sections of the Vaal Reef from the Vaal Reefs South and Western Reefs G.M. Some kaolinite was also found in the E9Ec Reef in the Western Areas G.M.

The phyllosilicates occur in two modes, viz (1) fine-grained interstitial fillings (Fig. 6a and A.1e) and (2) coarse particles of obvious detrital origin. The second category comprises:

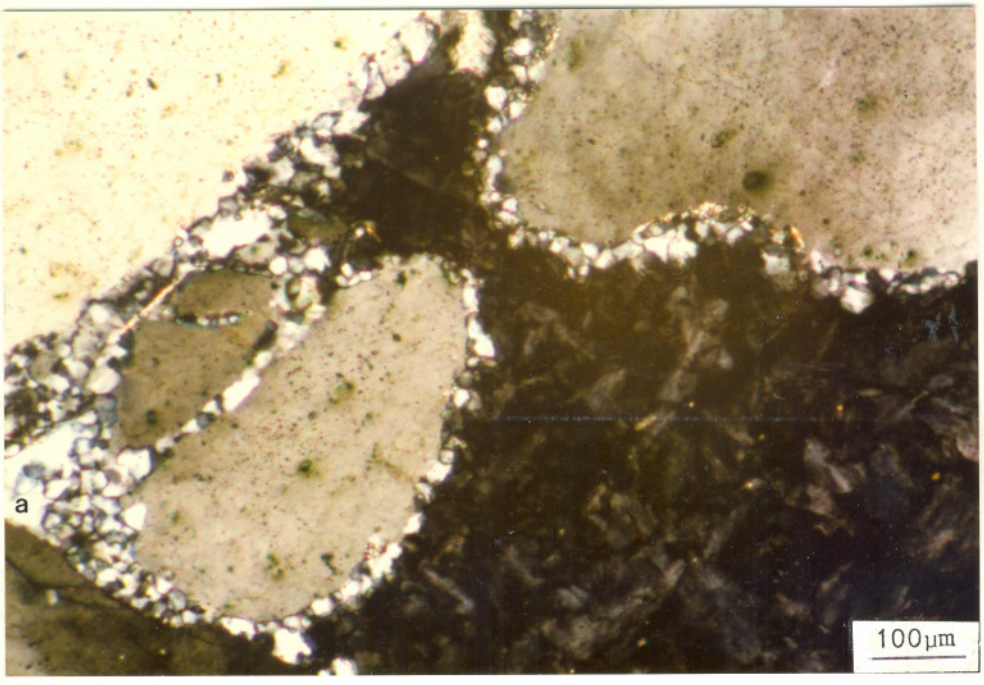
(1) well-rounded detrital chlorite of dimensions equivalent to pyrite (Figs. 7b and A.5g), or three to four times larger (Fig. 6b),

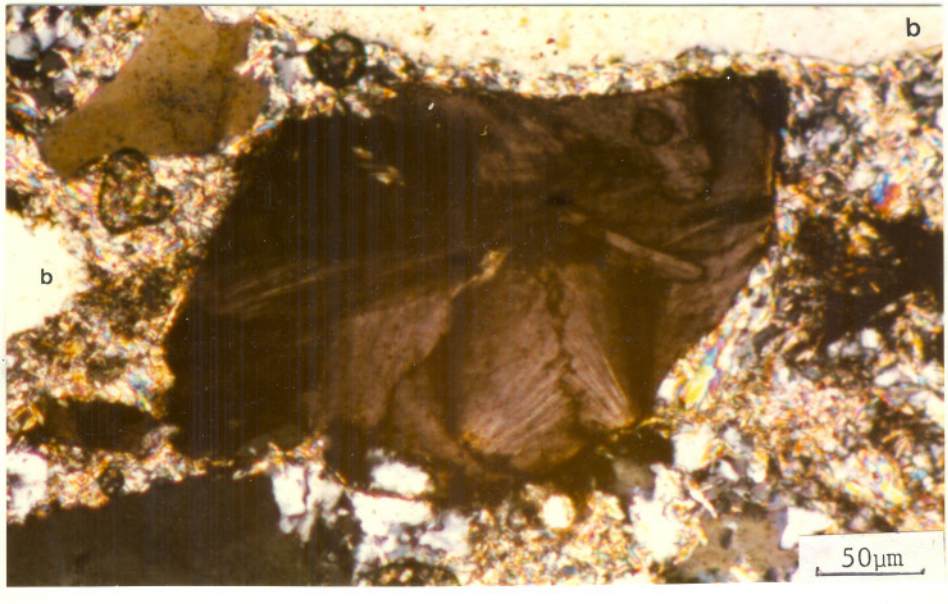
Figure 6 Photomicrographs of phyllosilicates
Transmitted light

a. Fine-grained, tufted 'purple' chlorite defined by a layer of authigenic quartz. Basal Reef, Harmony G.M.

b. Detrital particle of coarse 'purple' chlorite flakes, possibly pseudomorphous after amphibole or pyroxene. Vaal Reef, Vaal Reefs East G.M.

c. Incoherent intergrowth of 'green' chlorite and muscovite winding along strongly embayed quartz grains of the matrix, bordered by fine-grained intergrowth of sericite/pyrophyllite. Carbon Leader, Western Deep Levels G.M.


a
100µm


b
b
50µm

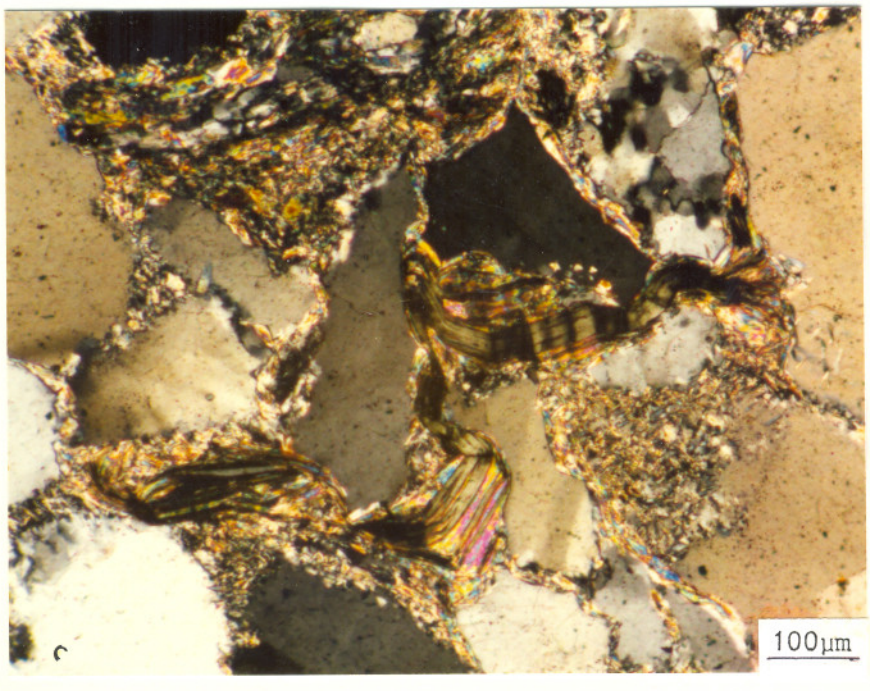
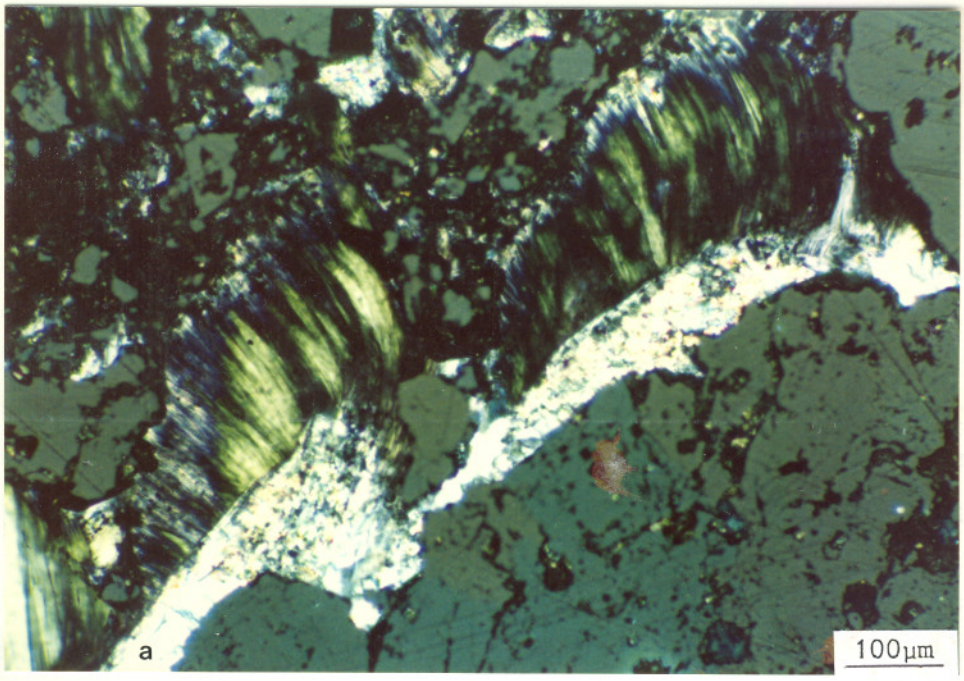

c
100µm

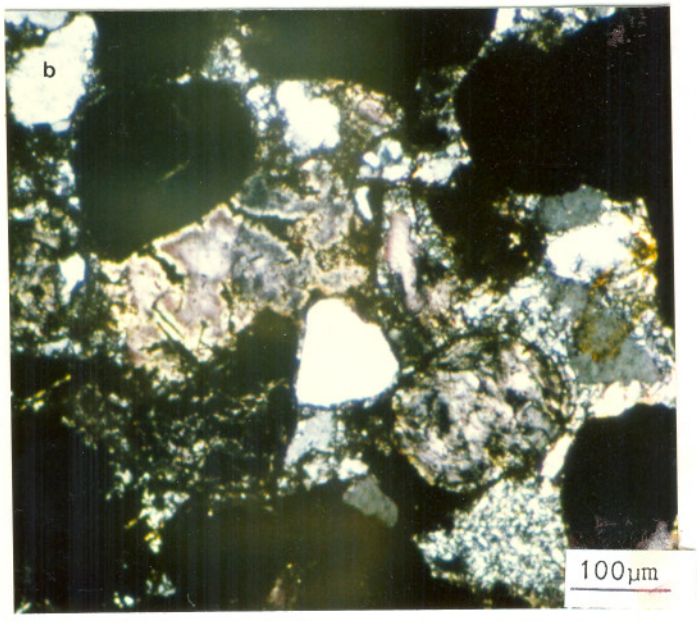
Figure 7 Photomicrographs of green and purple chlorite
Transmitted light

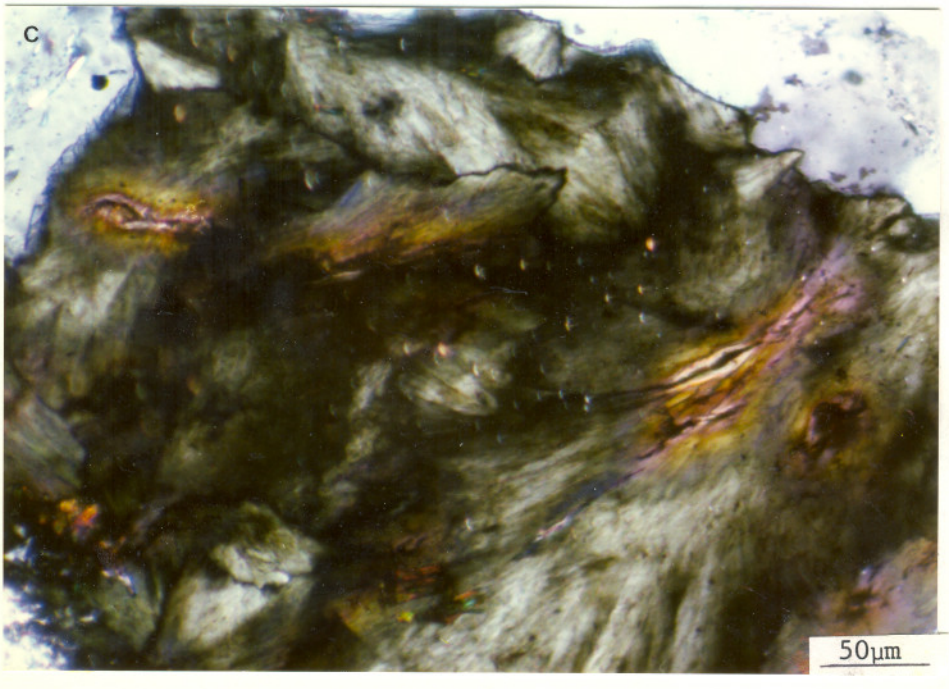
a. Pressure fringes on pyrite (greenish grey) filled with curved, columnar 'green' chlorite. The tip of the chlorite is incipiently altered to the purple variety, followed by little quartz (white). Between pyrite and chlorite, pyrophyllite or muscovite precipitated parallel to the surface of the pyrite. Its kinked texture indicates that it was subjected to stress after its formation. UE1a Reef, Cooke Section.

b. 'Purple' chlorite at left is marginally discoloured (pale brown) by a uraniferous leucoxene coating (black). In right bottom corner, a rounded detrital chlorite particle (purple). Quartz grain in the centre (white). Vaal Reef, Buffelsfontein G.M.

c. Particle composed of coarse flakes of 'green' chlorite with small inclusions of uraniferous leucoxene. Alpha radiation discoloured the surrounding chlorite (brown to pale brown). At top left a small area of 'purple' chlorite is present. Vaal Reef, Buffelsfontein G.M.


a
100μm


b
100μm


c
50μm

(2) flakes reminiscent of biotite composed of one or more of the phyllosilicates, which flex along the quartz grains of the matrix (Fig. 6c), and
(3) uncommon, undeformed muscovite flakes (Fig. 8d).

Many of the phyllosilicates have been silicified to a lesser or greater extent. The silicification process is particularly advanced in the Vaal Reef where ghost patterns of small prisms of rutile (Figs. A.1a and b) or strips of chlorite (Fig. A.1c) indicate the earlier presence of biotite. However, authigenic overgrowth of quartz on the sand- to silt-sized quartz grains in the matrix is rare (Fig. A.4h).

In Table 4, the average composition of these minerals is compared with the ideal one, and Table 5 lists the range of concentrations of trace elements present in the silicates.

All phyllosilicates and the chloritoid are of metamorphic origin. Chlorite and muscovite occur in the final stable polytype, respectively IIb and $2M_1$, which is reached during metamorphism. Two mineral assemblages are recognized in the sediments:

chloritoid-pyrophyllite-muscovite/sericite-quartz (Fig. 8c), and

chloritoid-chlorite-muscovite/sericite-quartz (Fig. 8d).

The two parageneses may occur at short distances of one another, indicating that the precipitation of chloritoid was controlled by the amount of pyrophyllite and chlorite locally available. The first paragenesis is found in the Green Bar, the second in the Black Bar, which occur in the sediments overlying the Carbon Leader in the West Wits Line G.F. The two argillaceous rocks are different facies from the same sediment. The green and black colours are imparted respectively by sericite and chlorite.

*Metamorphic fabrics* have only rarely been noticed in the sediments. Slip-shearing and schistosity occur in the very thin muddrapes which locally close off a sedimentary cycle. The Black Bar in the West Wits Line G.F. shows a phyllitic fabric and at the contact with the underlying quartzite, microfolds may occur.

*3.1.1. Chlorite*

In contrast with the quartzites, where sericite is the major phyllosilicate, chlorite is common in the conglomerates,

Table 4 Ideal compositions and average electron-microprobe compositions of silicates

| Mineral | $K_2O + Na_2O$ | MgO | FeO | $Al_2O_3$ | $SiO_2$ | $H_2O$ |
|---|---|---|---|---|---|---|
| *Ideal composition* | | | | | | |
| Sericite | 11,8 | – | – | 38,4 | 45,3 | 4,5 |
| Pyrophyllite | – | – | – | 28,3 | 66,7 | 5,0 |
| Iron chlorite | – | – | 50,3 | 14,3 | 25,3 | 10,1 |
| Magnesium chlorite | – | 36,3 | – | 18,3 | 32,4 | 13,0 |
| Chloritoid | – | – | 28,5 | 40,5 | 23,9 | 7,1 |
| *Actual average composition* | | | | | | |
| Sericite | 9,3 | – | – | 39,3 | 46,9 | 4,5 |
| Pyrophyllite | – | – | – | 28,3 | 66,7 | 5,0 |
| Iron chlorite | – | 6,9 | 32,4 | 26,1 | 23,3 | 11,3 |
| Magnesium chlorite | – | 22,4 | 14,5 | 24,9 | 26,2 | 12,0 |
| Chloritoid | – | 2,4 | 24,7 | 41,3 | 24,3 | 7,3 |

Table 5 Range of trace element contents of CRG silicates determined on the electron microprobe

| | chlorite | sericite | pyrophyllite | chloritoid |
|---|---|---|---|---|
| $Na_2O$ | 0 - 0,6 | 0,2 - 1,6 | 0 - 0,6 | 0 - 0,1 |
| $K_2O$ | 0 - 0,1 | m.e. | 0 - 0,9 | 0 - 0,2 |
| FeO | m.e. | 0 - 0,7 | 0 - 0,9 | m.e. |
| MgO | m.e. | 0,1 - 0,6 | 0 - 0,4 | m.e. |
| CaO | 0 - 0,07 | 0 - 0,02 | 0,04 - 0,14 | 0 - 0,01 |
| $TiO_2$ | 0 - 0,2 | 0 - 0,1 | 0 - 0,1 | 0 - 0,02 |
| MnO | 0 - 0,7 | 0 - 0,04 | 0 - 0,04 | 0,1 - 1,1 |
| ZnO | 0 - 0,2 | 0 - 0,6 | 0 - 0,1 | 0 - 0,1 |
| $UO_2$ | 0 - 0,05 | 0 - 0,05 | tr | 0 - 0,02 |
| $Cr_2O_3$ | 0 - 1,3 | 0 - 0,9* | 0 - 0,2 | 0 - 0,1 |

m.e. major element in the silicate tr trace

*) Cr only present in fuchsitic sericite

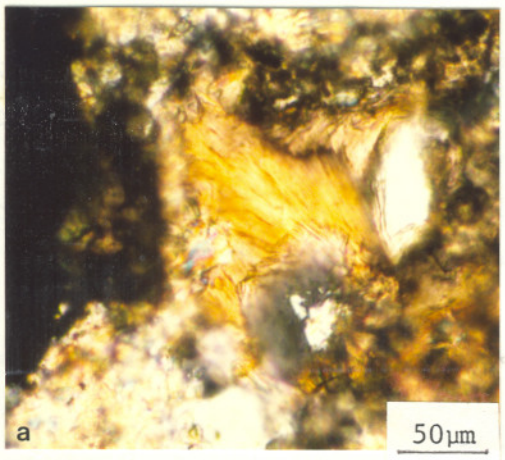
Figure 8 Photomicrographs of phyllosilicates
Transmitted light

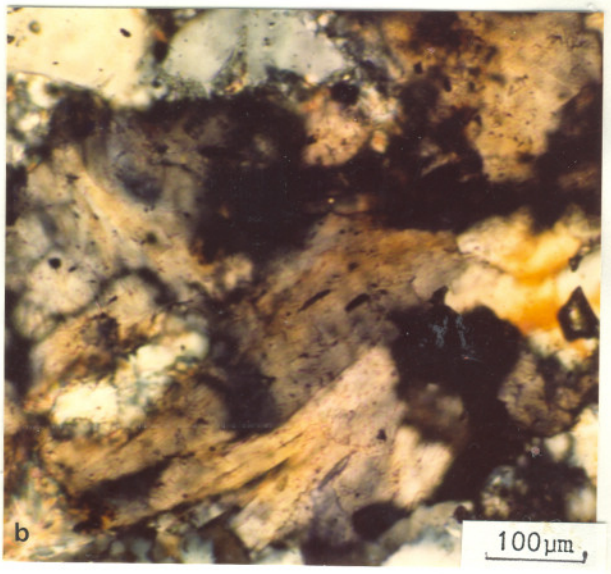
a. 'Orange' chlorite flake. Vaal Reef, Western Reefs G.M.

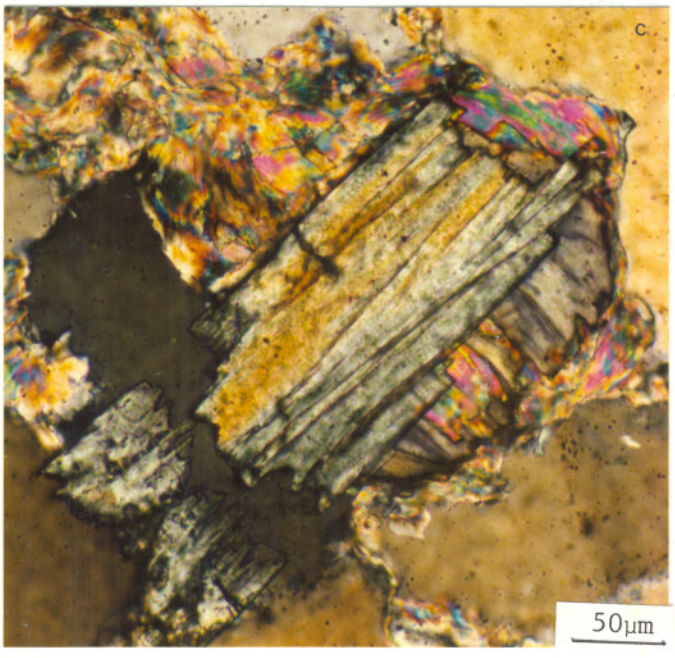
b. Pale 'purple' chlorite blended with the orange variety. Vaal Reef, Hartebeestfontein G.M.

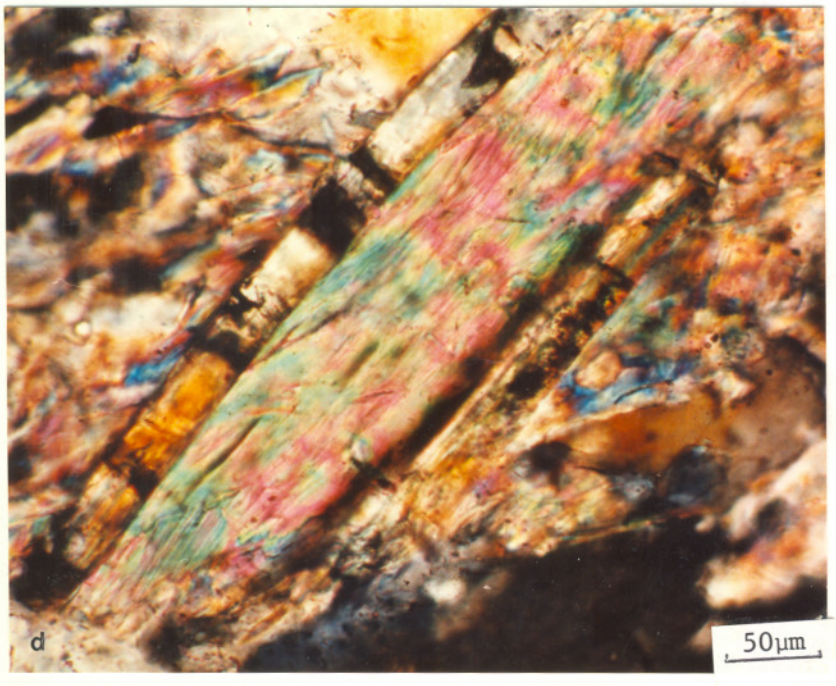
c. Chloritoid (grey and brown) blade, diagonally across the micrograph, is surrounded by whorly sericite (mixed bright colours). Curved purple chlorite occurs on the lower side of the blade at right angles to it. Carbon Leader, Western Deep Levels G.M.

d. Muscovite (pink and brilliant green), flanked by chloritoid (white, light brown, and black), and surrounded by a fine-grained mixture of sericite and pyrophyllite. E9Gd, Cooke Section.


a
50µm


b
100µm


c
50µm


d
50µm

particularly in the Dominion Reef, Ventersdorp Contact Reef (VCR) and Black Reef, where it imparts a black colour to the rock. The association of chlorite with pyrite concentrations is conspicuous. In the sediments of the West Rand and West Wits Line G.F., the chlorite has been replaced by chloritoid (Fig. A.1d).

The chlorite displays variation in texture (Table 6) and frequently encloses (Table 7) sulphides (Figs. A.3d and e), gold, rutile, and (U,Ti)-bearing minerals (Fig. A.3f). Three types of chlorite can be distinguished by their anomalous interference colours, which are here accordingly referred to as the 'green', 'purple', and 'orange' variety (Figs. 7 and 8a and b; Table 8). EMP analyses (Table 9) indicate that the 'green' chlorite contains more magnesium than iron, the 'orange' type more iron than magnesium, and that the 'purple' variety takes an intermediate position. Table 10 summarizes the average chlorite formulae for individual gold mines.

The composition of the chlorites is pictured in several types of diagrams (Figs. 9 to 11). The aluminium content of the chlorites in the CRG ranges from 25 to 29% and is higher than that of the analyses published by Deer *et al.* (1962) and Foster (1962; Fig. 11) in which the concentration is less than 24%.

According to the classification scheme proposed by Bayliss (1975) and accepted by the AIPEA Nomenclature Committee (Bailey, 1980), the chlorite species fall in the series between the Mg-end member clinochlore and the Fe-end member chamosite.

*3.1.2. Muscovite and Sericite*

Muscovite is a constituent of the pseudomorphs after biotite (Fig. 6c and A.2b), and only rarely occurs as undeformed detrital grains. Sericite fills the open space between the quartz grains (Fig. A.1e) in the matrix of the conglomerates and quartzites.

The sedimentary cycles of the CRG are locally terminated by a 1 to 2 cm-thick argillaceous layer, particularly enriched in sericite, usually mixed with pyrophyllite (Fig. 6c). Fuchsitic sericite of characteristic pale green colour, imparted by the presence of trace amounts of chromium, is a fairly common constituent of the sediments on the West Rand and

Table 6 Textural varieties of chlorite in the CRG reefs

| Morphology | Size, mm | Distribution | Probable precursor |
|---|---|---|---|
| (1) Aggregates of flakes arranged in tufts; matted texture (Fig. 6a) | 0,02 to 0,04 | Interstitial filling in groundmass of conglomerates | Clay minerals |
| (2) Randomly orientated aggregates of coarse flakes (Figs. 6b and 7c) | 0,10 to 0,20 | Heavy-mineral constituent | Large grains: detrital amphibole or pyroxene<br>Small grains: pseudomorphs after detrital py (Fig. A.2f), asp (Fig. A.2g), chr (Fig.A.2h), and garnet. Usually grains are coated by film of non-oriented br crystals |
| (3) Coarse flakes (Fig. A.3b) of coherently or incoherently intergrown (White et al., 1985) chl-musph. Boudinaged (Figs. A.2a and 6c) and kinked (Figs. A.2b and c) grains common. Ghost textures of silicified flakes can be recognized by rutile prisms (Fig. A.1a) or by preserved chl lamellae (Fig. A.1c) | <1,00 | Flexed between q grains in matrix | Detrital biotite |
| (4) Whorls (Fig. A.2d) | <0,07 | Associated with microstylolites | Authigenic origin |
| (5) Vermicular stacks of basal sections in curved aggregates (Fig. A.2e), referred to as 'helminth' (Troger, 1967) | 0,07 | Enclosed by q at shear planes | Authigenic origin |
| (6) Columnar, curved chl (Fig. 7a) at right angles to the surface of py grains. Sometimes in 2 or 3 consecutive layers pointing to interrupted periods of stress. Curved habit results from rotation during shearing (Spry, 1969) | <0,20 | Filling pressure fringes on opposite ends of detrital py | Neoformed product |

Table 7 Minerals associated with chlorite in the CRG reefs

| Mineral | Size, mm | Description |
|---|---|---|
| (1) Titania | 0,05 to 0,15 | An, lc, or prisms of rut are dispersed throughout chl (Fig. A.3a) or occur along cleavage in bio pseudomorphs |
| (2) Gold | 0,05 | Equant, irregular-shaped inclusions (Fig. A.3c) |
| (3) Sulphides | <0,20 | Irregular-shaped inclusions of cp, gn (Fig. A.3d), sl (Fig. A.3e), po, py, or ur. tit. (Fig. A.3f) |
| (4) Brannerite and uraniferous leucoxene | <0,05 | Ur. tit. discoloured adjacent chl (Figs. 7b and c). Common phenonon in Vaal Reef. Small chl haloes (0,05 mm) remained unchanged when surrounding ph.sil. was altered to ph or ser (Figs. A.3g and h) or chlort (Figs.A.3d and e). Common feature in Carbon Leader |

Table 8 Optical varieties of chlorite in CRG reefs

| Anomalous interference colours | Fe/Fe+Mg | Occurrence |
|---|---|---|
| Green chlorite* greyish green (Figs. 7a and c) | 0,26 to 0,38 | Elsburg Reefs. West Rand G.F., and Kalkoenkrans Reef, OFS G.F. |
| Purple chlorite* greyish purple to very dusky purple (Figs. 6a, b and 7b). The colour becomes paler, the higher the iron content (Fig. 8b) | 0,45 to 0,70 | Basal Reef, OFS G.F. and Vaal Reef, Klerksdorp G.F.. Replaces green variety |
| Orange chlorite greyish orange to dark yellow orange Fig. 8a) | ~ 0,70 | Seldom as separate flakes in Basal and Vaal Reefs. Blended with purple variety (Fig. 8b) in same reefs. Chl discoloured by U-bearing titania (Figs. 7b and c) acquired similar colour and composition |

*) Iron-bearing detrital minerals such as, py, chr, asp, and gar are replaced by green and purple varieties

Table 9

Quantitative electron-microprobe analyses of Witwatersrand chlorite

| | West Rand G.F. | | Carletonville G.F. | | | | | | | | | | | | | | |
|---|---|---|---|---|---|---|---|---|---|---|---|---|---|---|---|---|---|
| Chlorite | WA 1216/2A-1 | WA 1216/2A2 | WDL 828/1A-1 | WDL 828/3-1 | WDL 828/3-3 | WDL 828/2-2 | WDL 828/2-3 | WDL 653/1-1 | WDL 653/1-2 | WDL 653/1-3 | WDL 653/2-1 | WDL 653/2-3 | BV 670/1-1 | BV 670/1-2 | BV 670/4-2-1 | BV 670/3-1 | BV 670/3-4 | BV 670/2-2 |
| $SiO_2$ | 25,190 | 24,978 | 23,362 | 22,355 | 22,388 | 21,653 | 22,271 | 25,149 | 24,977 | 24,477 | 24,789 | 24,972 | 22,317 | 32,257 | 30,202 | 23,910 | 23,839 | 23,661 |
| $Al_2O_3$ | 27,530 | 27,317 | 25,650 | 25,858 | 26,650 | 27,390 | 27,071 | 22,938 | 23,726 | 23,844 | 22,877 | 24,217 | 27,326 | 24,986 | 28,59 | 25,414 | 26,129 | 26,429 |
| $K_2O$ | 0,003 | 0,001 | 0,005 | 0,003 | 0,003 | 0,016 | 0,016 | 0,002 | 0,003 | 0,002 | 0,004 | - | 0,014 | 0,551 | 1,946 | 0,021 | 0,149 | - |
| $Na_2O$ | 0,030 | - | - | 0,017 | 0,033 | - | - | - | - | 0,016 | - | - | - | 0,058 | 0,305 | 0,024 | - | - |
| MgO | 17,563 | 18,340 | 12,609 | 12,233 | 12,502 | 10,281 | 12,445 | 18,545 | 18,836 | 17,74 | 15,376 | 18,961 | 12,642 | 10,938 | 9,699 | 10,282 | 10,463 | 12,065 |
| FeO | 17,174 | 16,878 | 24,353 | 23,046 | 24,124 | 27,692 | 24,869 | 20,407 | 19,792 | 20,879 | 20,714 | 18,857 | 24,199 | 20,051 | 17,715 | 28,233 | 26,998 | 24,775 |
| ZnO | 0,061 | 0,025 | 0,017 | - | 0,043 | - | - | 0,059 | 0,099 | 0,013 | 0,060 | 0,078 | 0,038 | 0,053 | 0,037 | 0,072 | 0,044 | 0,033 |
| MnO | 0,324 | 0,294 | 0,083 | 0,142 | 0,064 | 0,019 | 0,011 | 0,580 | 0,622 | 0,627 | 0,765 | 0,579 | 0,003 | 0,053 | 0,014 | 0,032 | 0,052 | 0,012 |
| $Cr_2O_3$ | 0,779 | 0,747 | 0,973 | 0,801 | 1,078 | 0,722 | 0,733 | 0,153 | 0,120 | 0,150 | 0,132 | 0,176 | 0,590 | 0,659 | 0,537 | 0,269 | 0,297 | 0,282 |
| $TiO_2$ | 0,037 | 0,031 | 0,106 | 0,128 | 0,065 | 0,029 | 0,040 | 0,046 | 0,030 | 0,036 | 0,483 | 0,043 | 0,028 | 0,184 | 0,052 | 0,061 | 0,080 | 0,044 |
| CaO | 0,024 | - | - | 0,023 | 0,002 | - | - | - | 0,005 | - | 0,002 | - | - | 0,005 | 0,006 | - | - | 0,002 |
| $UO_2$ | - | - | 0,017 | 0,048 | 0,045 | 0,008 | - | 0,009 | 0,041 | 0,012 | - | - | 0,003 | - | - | 0,015 | 0,009 | - |
| Total | 88,715 | 88,611 | 87,175 | 84,654 | 86,997 | 87,81 | 87,456 | 87,888 | 88,251 | 87,796 | 85,202 | 87,883 | 87,16 | 89,795 | 89,103 | 88,333 | 88,06 | 87,303 |
| | | | Number of ions (based on 14 oxygens) | | | | | | | | | | | | | | | |
| Si | 2,5 | 2,5 | 2,5 | 2,4 | 2,4 | 2,3 | 2,3 | 2,6 | 2,5 | 2,5 | 2,6 | 2,5 | 2,3 | 3,1 | - | 2,5 | 2,5 | 2,5 |
| $Al^{iv}$ | 1,5 | 1,5 | 1,5 | 1,6 | 1,6 | 1,7 | 1,7 | 1,4 | 1,5 | 1,5 | 1,4 | 1,5 | 1,7 | 0,9 | - | 1,5 | 1,5 | 1,5 |
| $Al^{vi}$ | 1,7 | 1,7 | 1,7 | 1,7 | 1,7 | 1,8 | 1,7 | 1,4 | 1,4 | 1,4 | 1,5 | 1,4 | 1,7 | 2,0 | - | 1,7 | 1,8 | 1,8 |
| K | tr | tr | tr | tr | tr | tr | tr | tr | tr | tr | tr | - | tr | 0,07 | - | tr | 0,02 | - |
| Na | tr | - | - | tr | tr | - | - | - | - | tr | - | - | - | 0,01 | - | tr | - | - |
| Mg | 2,6 | 2,7 | 2,0 | 2,0 | 2,0 | 1,6 | 2,0 | 2,8 | 2,9 | 2,7 | 2,4 | 2,9 | 2,0 | 1,6 | - | 1,6 | 1,6 | 1,9 |
| Fe | 1,4 | 1,4 | 2,1 | 2,1 | 2,1 | 2,5 | 2,2 | 1,7 | 1,7 | 1,8 | 1,8 | 1,6 | 2,1 | 1,6 | - | 2,5 | 2,4 | 2,1 |
| Zn | tr | tr | tr | - | tr | - | - | tr | tr | tr | tr | tr | tr | tr | - | tr | tr | tr |
| Mn | 0,03 | 0,02 | tr | 0,01 | tr | tr | tr | 0,05 | 0,05 | 0,05 | 0,07 | 0,05 | tr | tr | - | tr | tr | tr |
| Cr | 0,06 | 0,06 | 0,08 | 0,07 | 0,09 | 0,06 | 0,06 | 0,01 | tr | 0,01 | 0,01 | 0,01 | 0,05 | 0,05 | - | 0,02 | 0,02 | 0,02 |
| Ti | tr | tr | tr | tr | tr | tr | tr | tr | tr | tr | 0,04 | tr | tr | 0,01 | - | tr | tr | tr |
| Ca | tr | - | - | tr | tr | - | - | - | tr | - | tr | - | - | tr | - | - | - | tr |
| U | - | - | tr | tr | tr | tr | - | tr | tr | tr | - | - | tr | - | - | tr | tr | - |

WA = Western Areas

WDL = Western Deep Levels

BV = Blyvooruitzicht

Computer programme for the calculation of the formulae was written by Dr. M. Southwood, Mineralogy Division, Mintek (1983)

Table 9 cont.

| Chlorite | Klerksdorp G.F. | | | | | | | | | | | | | | | | | |
|---|---|---|---|---|---|---|---|---|---|---|---|---|---|---|---|---|---|---|
| | WR 818/1-3 | WR 791/1-1 | WR 791/1-2 | WR 791/1-3 | WR 791/1-4 | WR 791/1-6 | WR 826/1-1 | WR 826/1-2 | BF 797/1-2 | BF 797/1-3-1 | BF 797/1-3-2 | BF 797/1-4-1 | BF 797/1-1A | BF 797/1-1B | BF 797/1-1C | BF 616/1-1-1 | BF 616/1-1-2 | BF 616/1-1-3 |
| $SiO_2$ | 22,815 | 24,627 | 27,567 | 22,864 | 20,879 | 23,010 | 24,622 | 24,420 | 21,500 | 27,027 | 26,789 | 25,751 | 25,356 | 25,518 | 24,894 | 20,519 | 23,824 | 21,589 |
| $Al_2O_3$ | 23,846 | 25,499 | 28,009 | 25,775 | 28,078 | 25,998 | 22,178 | 22,517 | 29,172 | 26,932 | 27,455 | 22,570 | 23,353 | 23,478 | 24,250 | 29,091 | 27,932 | 27,642 |
| $K_2O$ | 0,012 | 0,109 | 0,670 | 0,002 | - | 0,013 | 0,002 | 0,010 | 0,060 | 0,791 | 0,646 | 0,004 | 0,006 | 0,005 | - | 0,040 | 0,696 | 0,006 |
| $Na_2O$ | 10,622 | 0,090 | 0,028 | 0,059 | 0,146 | - | - | - | 0,569 | 1,372 | 1,031 | - | - | 0,097 | 0,017 | - | 0,099 | - |
| MgO | 12,741 | 11,741 | 10,635 | 9,095 | 9,775 | 8,728 | 13,213 | 12,309 | 6,041 | 7,769 | 8,188 | 20,163 | 22,069 | 21,890 | 21,849 | 7,588 | 7,284 | 8,563 |
| FeO | 14,854 | 26,708 | 24,144 | 31,515 | 28,641 | 32,013 | 25,783 | 27,243 | 28,650 | 25,290 | 25,299 | 16,915 | 13,785 | 13,940 | 14,057 | 30,080 | 26,085 | 29,312 |
| ZnO | - | 0,066 | 0,023 | 0,153 | 0,049 | 0,068 | 0,047 | 0,061 | 0,046 | 0,031 | 0,089 | 0,073 | 0,010 | 0,067 | 0,034 | 0,114 | 0,087 | 0,115 |
| MnO | 0,698 | 0,185 | 0,151 | 0,262 | 0,166 | 0,291 | 0,251 | 0,407 | 0,272 | 0,240 | 0,188 | 0,087 | 0,004 | 0,020 | 0,035 | 0,239 | 0,197 | 0,234 |
| $Cr_2O_3$ | 0,613 | 0,319 | 0,311 | 0,258 | 0,484 | - | 0,042 | 0,062 | 0,384 | 0,073 | 0,041 | 0,931 | 0,824 | 0,850 | 0,992 | 0,203 | 0,147 | 0,181 |
| $TiO_2$ | 7,162 | 0,012 | 0,015 | 0,025 | 0,015 | 0,057 | 0,043 | 0,030 | 0,030 | 0,042 | 0,041 | 0,125 | 0,076 | 0,072 | 0,074 | 0,049 | 0,072 | 0,047 |
| CaO | 0,177 | 0,011 | - | - | - | 0,006 | - | - | - | 0,008 | 0,006 | - | - | - | - | 0,014 | - | - |
| $UO_2$ | 0,707 | - | - | - | 0,021 | - | - | - | - | - | - | 0,045 | 0,004 | - | 0,025 | 0,027 | - | 0,016 |
| Total | 93,741 | 89,367 | 91,553 | 90,008 | 86,254 | 90,184 | 86,181 | 87,059 | 87,263 | 89,581 | 89,743 | 86,664 | 85,487 | 85,937 | 86,227 | 87,950 | 86,423 | 87,704 |
| | Number of ions (based on 14 oxygens) | | | | | | | | | | | | | | | | | |
| Si | 2,5 | 2,6 | 2,7 | 2,4 | 2,2 | 2,4 | 2,6 | 2,6 | 2,3 | 2,8 | 2,7 | 2,6 | 2,6 | 2,6 | 2,5 | 2,2 | 2,5 | 2,3 |
| $Al^{iv}$ | 1,5 | 1,4 | 1,3 | 1,6 | 1,8 | 1,6 | 1,4 | 1,4 | 1,7 | 1,2 | 1,3 | 1,4 | 1,4 | 1,4 | 1,5 | 1,8 | 1,5 | 1,7 |
| $Al^{vi}$ | 1,6 | 1,7 | 2,0 | 1,6 | 1,8 | 1,7 | 1,4 | 1,5 | 2,0 | 2,1 | 2,0 | 1,3 | 1,4 | 1,4 | 1,4 | 1,9 | 2,0 | 1,8 |
| K | tr | 0,01 | 0,08 | tr | - | tr | tr | tr | 0,08 | 0,1 | 0,08 | tr | tr | tr | - | tr | 0,09 | tr |
| Na | 2,2 | 0,02 | tr | 0,01 | 0,03 | - | - | - | 0,1 | 0,2 | 0,2 | - | - | 0,02 | tr | - | 0,02 | - |
| Mg | 2,0 | 1,8 | 1,6 | 1,4 | 1,6 | 1,4 | 2,1 | 2,0 | 0,9 | 1,1 | 1,2 | 3,1 | 3,3 | 3,3 | 3,3 | 1,2 | 1,1 | 1,3 |
| Fe | 1,3 | 2,3 | 2,0 | 2,8 | 2,6 | 2,8 | 2,3 | 2,4 | 2,6 | 2,1 | 2,2 | 1,4 | 1,2 | 1,2 | 1,2 | 2,7 | 2,3 | 2,7 |
| Zn | - | tr | tr | 0,01 | tr | tr | tr | tr | - | tr | tr | tr | tr | tr | tr | tr | tr | tr |
| Mn | 0,06 | 0,02 | 0,01 | 0,02 | 0,02 | 0,03 | 0,02 | 0,04 | 0,03 | 0,02 | 0,02 | tr | tr | tr | tr | 0,02 | 0,02 | 0,02 |
| Cr | 0,05 | 0,03 | 0,02 | 0,01 | 0,04 | - | tr | tr | 0,03 | tr | tr | 0,07 | 0,07 | 0,07 | 0,08 | 0,02 | 0,01 | 0,02 |
| Ti | 0,6 | tr | tr | tr | tr | tr | tr | tr | tr | tr | tr | tr | tr | tr | tr | tr | tr | tr |
| Ca | 0,02 | tr | - | - | - | tr | - | - | - | tr | tr | - | - | - | - | tr | - | - |
| U | 0,02 | - | - | - | tr | - | - | - | - | - | | tr | tr | - | tr | tr | - | - |

WR = Western Reefs

BF = Buffelsfontein

Table 9 cont.

| | Klerksdorp G.F. | | | | | | | | | | | | | | | | | | |
|---|---|---|---|---|---|---|---|---|---|---|---|---|---|---|---|---|---|---|---|
| Chlorite | VRS 684/1-1 | VRS 684/1-3 | VRS 685/1-1 | VRS 685/1-3 | VRE 741/1A-1 | VRE 741/1B-1 | VRE 741/2-1 | VRE 741/3-1 | VRE 750/1-2A | VRE 750/1-2B | VRE 750/1-2C | VRE 776/1-1A | VRE 776/1-1B | VRE 776/1-1C | WR 778/1A-2 | WR 788/1B-1 | WR 788/1B-2 | WR 788/1C-3 | WR 818/1-1 |
| $SiO_2$ | 22,426 | 22,189 | 23,266 | 23,764 | 22,956 | 23,556 | 23,983 | 23,717 | 23,813 | 23,653 | 23,792 | 22,684 | 21,867 | 20,298 | 25,198 | 23,778 | 24,864 | 32,256 | 25,128 |
| $Al_2O_3$ | 26,492 | 27,434 | 26,047 | 24,512 | 27,694 | 27,925 | 27,511 | 28,333 | 27,292 | 27,315 | 27,190 | 26,96 | 26,752 | 28,927 | 26,974 | 27,876 | 28,056 | 25,158 | 30,121 |
| $K_2O$ | - | 0,007 | - | 0,006 | 0,001 | 0,003 | - | -- | 0,007 | - | 0,001 | 0,023 | 0,032 | - | 0,312 | 0,001 | 0,470 | 0,874 | 0,990 |
| $Na_2O$ | 0,008 | - | 2,262 | 0,469 | - | 0,010 | 0,007 | — | 0,007 | - | - | 1,283 | 0,520 | 0,263 | 0,078 | - | 0,077 | 0,105 | 6,510 |
| MgO | 8,225 | 9,437 | 11,007 | 11,282 | 10,096 | 10,549 | 11,497 | 10,454 | 12,169 | 10,687 | 11,631 | 9,092 | 9,496 | 8,637 | 11,899 | 13,052 | 12,356 | 7,344 | 11,376 |
| FeO | 31,558 | 30,236 | 28,556 | 28,871 | 31,612 | 30,267 | 28,900 | 29,861 | 26,870 | 29,997 | 28,575 | 26,870 | 27,968 | 28,752 | 21,752 | 23,859 | 22,830 | 14,221 | 18,902 |
| ZnO | 0,229 | 1,423 | 0,040 | 0,062 | 0,078 | 0,070 | 0,080 | 0,061 | 0,047 | 0,050 | 0,076 | 0,148 | 0,091 | 0,069 | 0,104 | 0,040 | 0,118 | 0,013 | 0,041 |
| MnO | 0,257 | 0,264 | 0,257 | 0,270 | 0,286 | 0,276 | 0,287 | 0,301 | 0,276 | 0,421 | 0,319 | 0,128 | 0,146 | 0,088 | 0,263 | 0,074 | 0,093 | 0,452 | 0,119 |
| $Cr_2O_3$ | 0,081 | 0,088 | 0,289 | 0,319 | - | - | 0,013 | - | 0,917 | 0,696 | 0,872 | 0,823 | 0,619 | 0,915 | 1,324 | 0,618 | 0,587 | 0,412 | 0,600 |
| $TiO_2$ | 0,030 | 0,043 | 0,031 | 0,024 | 0,046 | 0,044 | 0,049 | 0,044 | 0,082 | 0,032 | 0,033 | 0,018 | 0,044 | 0,051 | 0,384 | 0,002 | 0,043 | 3,076 | 0,069 |
| CaO | 0,002 | 0,014 | - | - | 0,020 | 0,021 | 0,003 | 0,007 | 0,007 | 0,012 | 0,007 | - | - | - | 0,072 | 0,002 | - | 0,216 | 0,029 |
| $UO_2$ | 0,008 | 0,029 | - | - | 0,015 | - | 0,018 | - | - | 0,043 | 0,007 | - | - | 0,014 | 0,598 | 0,019 | - | 0,529 | 0,024 |
| Total | 89,316 | 91,164 | 91,755 | 89,579 | 92,804 | 92,722 | 92,348 | 92,776 | 91,487 | 92,906 | 92,503 | 88,029 | 87,535 | 88,014 | 88,958 | 89,321 | 89,494 | 84,658 | 93,909 |
| | Number of ions (based on 14 oxygens) | | | | | | | | | | | | | | | | | | |
| Si | 2,4 | 2,3 | 2,4 | 2,5 | 2,3 | 2,4 | 2,4 | 2,4 | 2,4 | 2,4 | 2,4 | 2,4 | 2,3 | 2,2 | 2,6 | 2,4 | 2,5 | 3,3 | 2,4 |
| $Al^{iv}$ | 1,6 | 1,7 | 1,6 | 1,5 | 1,7 | 1,6 | 1,6 | 1,6 | 1,6 | 1,6 | 1,6 | 1,6 | 1,7 | 1,8 | 1,4 | 1,6 | 1,5 | 0,7 | 1,6 |
| $Al^{vi}$ | 1,7 | 1,7 | 1,6 | 1,6 | 1,6 | 1,8 | 1,7 | 1,8 | 1,7 | 1,7 | 1.7 | 1,8 | 1,7 | 1,9 | 1,9 | 1,8 | 1,9 | 2,3 | 1,9 |
| K | tr | tr | - | tr | tr | tr | - | - | tr | - | tr | tr | tr | - | 0,04 | tr | 0,06 | 0,01 | 0,1 |
| Na | -- | - | 0,45 | 0,1 | - | tr | tr | - | tr | - | - | 0,26 | 0,1 | 0,05 | 0,02 | - | 0,02 | 0,02 | 1,2 |
| Mg | 1,5 | 1,5 | 1,7 | 1,8 | 1,5 | 1,6 | 1,7 | 1,6 | 1,8 | 1,6 | 1,8 | 1,4 | 1,5 | 1,4 | 1,8 | 2,0 | 1,9 | 1,1 | 1,6 |
| Fe | 2,6 | 2,6 | 2,5 | 2,5 | 2,7 | 2,6 | 2,4 | 2,5 | 2,3 | 2,5 | 2,4 | 2,4 | 2,5 | 2,6 | 1,9 | 2,0 | 1,9 | 1,2 | 1,5 |
| Zn | tr | 0,11 | tr | tr | tr | tr | tr | tr | tr | tr | tr | 0,01 | tr | tr | tr | tr | tr | tr | tr |
| Mn | 0,02 | 0,02 | 0,02 | 0,02 | 0,02 | 0,02 | 0,02 | 0,03 | 0,02 | 0,04 | 0,03 | 0,01 | 0,01 | tr | 0,02 | tr | tr | 0,04 | tr |
| Cr | tr | - | 0,02 | 0,03 | - | - | tr | - | 0,07 | 0,06 | 0,07 | 0,07 | 0,05 | 0,08 | 0,1 | 0,05 | 0,04 | 0,03 | 0,05 |
| Ti | tr | tr | tr | tr | tr | tr | tr | tr | tr | 0,02 | tr | tr | tr | tr | 0,03 | tr | tr | 0,2 | tr |
| Ca | tr | tr | - | - | tr | tr | tr | tr | tr | tr | tr | tr | - | - | tr | tr | - | 0,02 | tr |
| U | tr | tr | - | - | tr | | tr | - | - | tr | tr | - | - | tr | 0,01 | tr | - | tr | tr |

VRS = Vaal Reefs South

VRE = Vaal Reefs East

WR = Western Reefs

Table 9 cont.

| | Welkom G.F. | | | | | | | | | | |
|---|---|---|---|---|---|---|---|---|---|---|---|
| Chlorite | Pr Br 691/1-1 | Pr Br 691/1-2 | Pr Br 691/2-1 | Pr Br 691/2-2 | Pr Br 949/1-1 | Pr Br 949/1-2 | Pr Br 949/1-4 | H 665/1-1-1 | H 665/1-2 | H 665/1-3 | H 665/2-1 |
| $SiO_2$ | 25,327 | 25,760 | 24,807 | 24,757 | 22,599 | 21,978 | 22,615 | 21,900 | 22,479 | 22,27 | 22,895 |
| $Al_2O_3$ | 27,606 | 26,380 | 27,575 | 28,090 | 26,120 | 26,165 | 26,704 | 26,724 | 26,445 | 26,083 | 26,011 |
| $K_2O$ | 0,005 | 0,018 | - | 0,006 | 0,009 | - | 0,016 | - | - | - | - |
| $Na_2O$ | 0,006 | 0,022 | - | 0,046 | 0,024 | 0,034 | 0,024 | 0,006 | 0,046 | 0,013 | - |
| MgO | 14,997 | 13,191 | 15,493 | 15,315 | 6,966 | 6,930 | 7,315 | 9,885 | 10,410 | 10,020 | 10,286 |
| FeO | 22,091 | 21,542 | 22,493 | 21,928 | 32,116 | 31,937 | 31,011 | 28,146 | 27,594 | 27,605 | 27 |
| ZnO | 0,097 | 0,050 | 0,028 | 0,051 | 0,005 | 0,042 | 0,032 | 0,086 | 0,067 | 0,002 | 0,038 |
| MnO | 0,539 | 0,431 | 0,531 | 0,478 | 0,304 | 0,355 | 0,321 | 0,332 | 0,229 | 0,281 | 0,287 |
| $Cr_2O_3$ | 0,298 | 0,348 | 0,328 | 0,339 | 0,456 | 0,423 | 0,454 | 0,142 | 0,219 | 0,203 | 0,249 |
| $TiO_2$ | 0,039 | 0,045 | 0,056 | 0,025 | 0,048 | 0,026 | 0,035 | 0,023 | 0,024 | 0,04 | 0,044 |
| CaO | 0,012 | 0,064 | 0,003 | 0,005 | - | - | - | 0,010 | 0,003 | - | 0,011 |
| $UO_2$ | 0,013 | 0,79 | 0,029 | 0,006 | 0,038 | - | 0,005 | 0,016 | - | 0,028 | - |
| Total | 91,028 | 88,641 | 91,343 | 91,046 | 88,685 | 87,891 | 88,531 | 87,27 | 87,517 | 86,545 | 86,821 |
| | Number of ions (based on 14 oxygens) | | | | | | | | | | |
| Si | 2,5 | 2,6 | 2,5 | 2,4 | 2,4 | 2,4 | 2,4 | 2,4 | 2,4 | 2,4 | 2,5 |
| $Al^{iv}$ | 1,5 | 1,4 | 1,5 | 1,6 | 1,6 | 1,6 | 1,6 | 1,6 | 1,6 | 1,6 | 1,5 |
| $Al^{vi}$ | 1,7 | 1,8 | 1,7 | 1,7 | 1,7 | 1,8 | 1,8 | 1,8 | 1,7 | 1,7 | 1,8 |
| K | tr | tr | - | tr | tr | - | tr | - | - | - | - |
| Na | tr | tr | - | tr | tr | tr | tr | tr | 0,01 | tr | - |
| Mg | 2,2 | 2,0 | 2,3 | 2,3 | 1,1 | 1,1 | 1,2 | 1,6 | 1,7 | 1,6 | 1,6 |
| Fe | 1,8 | 1,8 | 1,9 | 1,8 | 2,9 | 2,9 | 2,8 | 2,5 | 2,5 | 2,5 | 2,4 |
| Zn | tr | tr | tr | tr | tr | tr | tr | tr | tr | tr | tr |
| Mn | 0,05 | 0,04 | 0,04 | 0,04 | 0,03 | 0,03 | 0,03 | 0,03 | 0,02 | 0,03 | 0,03 |
| Cr | 0,02 | 0,03 | 0,03 | 0,03 | 0,04 | 0,04 | 0,04 | 0,01 | 0,02 | 0,02 | 0,02 |
| Ti | tr | tr | tr | tr | tr | tr | tr | tr | tr | tr | tr |
| Ca | tr | tr | tr | tr | - | - | - | tr | tr | - | tr |
| U | tr | tr | tr | tr | tr | - | tr | tr | - | tr | - |

Pr Br = President Brand

H = Harmony

Table 9 cont.

| | Welkom G.F. | | | | | | | | | |
|---|---|---|---|---|---|---|---|---|---|---|
| Chlorite | H 640/1-1 | H 640/2-2-1 | H 640/2-2-2 | H 640/2-3-1 | H 640/2-3-2 | H 643/1-1 | H 643/1-2 | V 704/1-7 | V 704/2-5-1 | V 704/3-1 |
| $SiO_2$ | 23,559 | 22,539 | 22,400 | 23,097 | 22,424 | 22,154 | 22,633 | 25,427 | 23,830 | 23,118 |
| $Al_2O_3$ | 26,168 | 26,086 | 26,256 | 25,984 | 25,772 | 27,171 | 26,945 | 28,833 | 27,161 | 28,184 |
| $K_2O$ | 0,097 | 0,017 | - | - | 0,003 | - | 0,002 | 0,001 | 0,077 | - |
| $Na_2O$ | 0,380 | 0,028 | 0,029 | 0,005 | - | - | 1,668 | 0,021 | 0,006 | - |
| MgO | 10,452 | 9,907 | 10,449 | 10,037 | 10,074 | 11,828 | 12,567 | 11,426 | 12,605 | 12,383 |
| FeO | 26,024 | 26,891 | 21,570 | 26,846 | 27,113 | 24,909 | 23,464 | 22,343 | 24,572 | 25,462 |
| ZnO | 0,027 | 0,099 | 0,095 | 0,026 | 0,060 | 0,112 | 0,075 | 0,065 | 0,045 | 0,072 |
| MnO | 0,295 | 0,287 | 0,352 | 0,333 | 0,296 | 0,315 | 0,295 | 0,057 | 0,129 | 0,180 |
| $Cr_2O_3$ | 0,574 | 0,605 | 0,690 | 0,493 | 0,685 | 0,426 | 0,479 | 0,453 | 0,222 | 0,097 |
| $TiO_2$ | 0,073 | 0,039 | 0,045 | 0,035 | 0,041 | 0,048 | 0,041 | 0,026 | 0,048 | 0,018 |
| CaO | 0,006 | 0,035 | 0,012 | - | 0,04 | - | - | 0,003 | 0,025 | - |
| $UO_2$ | 0,013 | 0,025 | - | 0,034 | - | - | - | - | - | 0,003 |
| Total | 87,668 | 86,556 | 87,898 | 86,89 | 86,472 | 86,963 | 88,169 | 88,655 | 88,72 | 89,519 |
| | Number of ions (based on 14 oxygens) | | | | | | | | | |
| Si | 2,5 | 2,4 | 2,4 | 2,5 | 2,4 | 2,3 | 2,4 | 2,6 | 2,5 | 2,4 |
| $Al^{iv}$ | 1,5 | 1,6 | 1,6 | 1,5 | 1,6 | 1,7 | 1,6 | 1,4 | 1,5 | 1,6 |
| $Al^{vi}$ | 1,8 | 1,7 | 1,7 | 1,8 | 1,7 | 1,7 | 1,7 | 2,1 | 1,8 | 1,8 |
| K | 0,01 | tr | - | - | - | - | 0,34 | tr | 0,01 | - |
| Na | 0,08 | tr | tr | tr | tr | - | tr | tr | tr | - |
| Mg | 1,6 | 1,6 | 1,7 | 16 | 1,6 | 1,9 | 2,0 | 1,7 | 1,9 | 1,9 |
| Fe | 2,3 | 2,4 | 2,5 | 2,4 | 2,5 | 2,2 | 2,0 | 1,9 | 2,1 | 2,2 |
| Zn | tr | tr | tr | tr | tr | tr | tr | tr | tr | tr |
| Mn | 0,03 | 0,03 | 0,03 | 0,03 | 0,03 | 0,03 | 0,03 | tr | 0,01 | 0,02 |
| Cr | 0,05 | 0,05 | 0,06 | 0,04 | 0,06 | 0,04 | 0,04 | 0,04 | 0,02 | tr |
| Ti | tr | tr | tr | tr | tr | tr | tr | tr | tr | tr |
| Ca | tr | tr | tr | - | - | - | - | - | - | - |
| U | tr | tr | - | tr | tr | - | - | - | - | tr |

H = Harmony

V = Virginia

Table 10 Average chlorite formulae for individual gold mines

| Gold Mine | Mg* | Fe | Al | Fe+Mg+Al | Al | Si | O | OH** |
|---|---|---|---|---|---|---|---|---|
| West Rand Consolidated | 2,6 | 1,4 | 1,7 | 5,7 | 1,5 | 2,5 | 10,0 | 8,0 |
| Randfontein | 2,8 | 1,4 | 1,7 | 5,9 | 1,4 | 2,6 | 9,9 | 8,1 |
| Western Areas | 2,7 | 1,4 | 1,7 | 5,8 | 1,5 | 2,5 | 10,0 | 8,0 |
| West Driefontein | 1,5 | 2,6 | 1,7 | 5,8 | 1,5 | 2,5 | 9,9 | 8,1 |
| Blyvooruitzicht 1*** | 2,0 | 2,1 | 1,7 | 5,8 | 1,5 | 2,5 | 9,9 | 8,1 |
| Blyvooruitzicht 2 | 1,6 | 2,5 | 1,7 | 5,8 | 1,5 | 2,5 | 10,0 | 8,0 |
| Western Deep Levels 1 | 2,8 | 1,7 | 1,4 | 5,9 | 1,5 | 2,5 | 9,9 | 8,1 |
| Western Deep Levels 2 | 2,0 | 2,1 | 1,7 | 5,8 | 1,5 | 2,5 | 9,9 | 8,1 |
| Buffelsfontein 1 | 1,2 | 2,5 | 2,0 | 5,7 | 1,7 | 2,3 | 10,1 | 7,9 |
| Buffelsfontein 2 | 3,3 | 1,2 | 1,4 | 5,9 | 1,4 | 2,6 | 10,2 | 7,8 |
| Hartebeestfontein | 1,6 | 2,5 | 1 7 | 5,8 | 1,5 | 2,5 | 9,9 | 8,1 |
| Western Reefs 1 | 1,9 | 1,9 | 1,9 | 5,7 | 1,4 | 2,6 | 10,0 | 8,0 |
| Western Reefs 2 | 1,5 | 2,5 | 1,8 | 5,8 | 1,6 | 2,4 | 10,1 | 7,9 |
| Vaal Reefs East 1 | 1,1 | 2,9 | 1,8 | 5,8 | 1,5 | 2,5 | 10,0 | 8,0 |
| Vaal Reefs East 2 | 1,6 | 2,5 | 1,7 | 5,8 | 1,6 | 2,4 | 10,0 | 8,0 |
| Vaal Reefs South | 1,5 | 2,6 | 1,7 | 5,8 | 1,6 | 2,4 | 10,0 | 8,0 |
| President Brand 1 | 2,2 | 1,8 | 1,7 | 5,7 | 1,5 | 2,5 | 10,1 | 7,9 |
| President Brand 2 | 1,1 | 2,9 | 1,8 | 5,8 | 1,6 | 2,4 | 10,0 | 8,0 |
| Harmony | 1,6 | 2,5 | 1,7 | 5,8 | 1,6 | 2,4 | 10,0 | 8,0 |
| Virginia | 1,9 | 2,1 | 1,8 | 5,8 | 1,5 | 2,5 | 10,0 | 8,0 |

*) Green chlorite: Mg 2,6 to 3,3
Purple chlorite: Fe 1,8 to 2,9
No data available for orange chlorite

**) OH content by difference of total on EMP from 100%

***) 1 and 2 indicate the presence of two types of chlorite

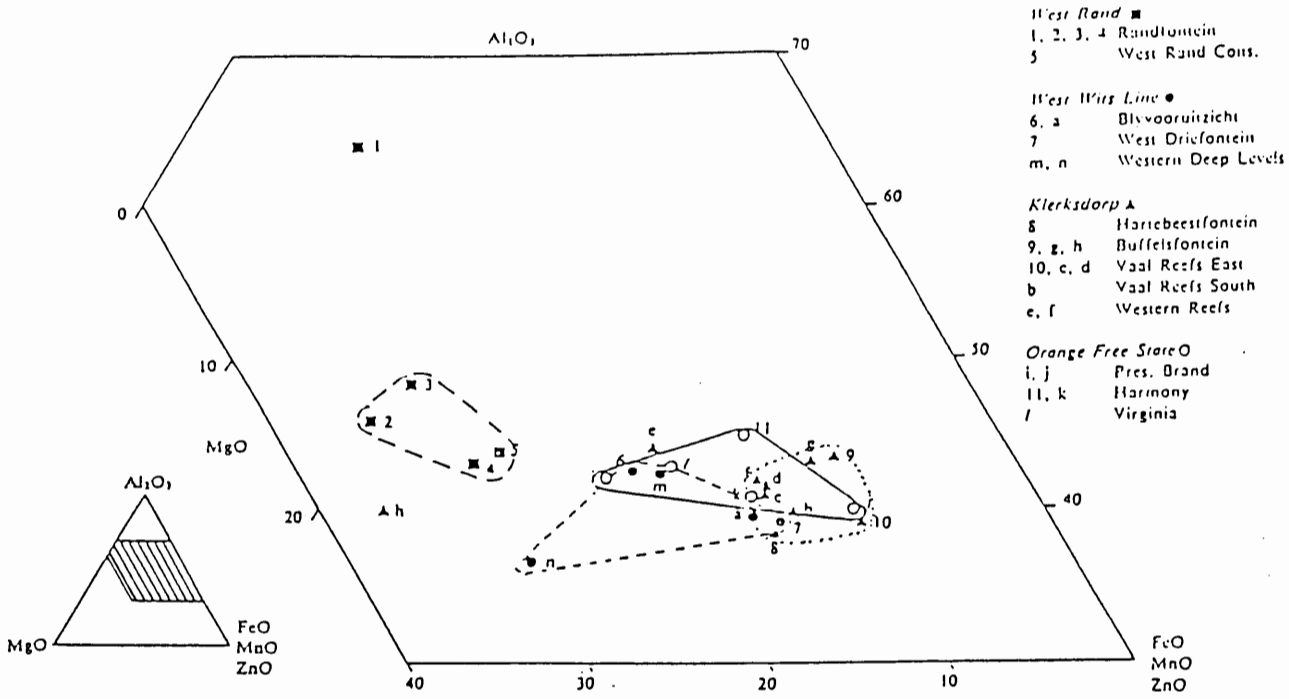



Fig. 9 Graphic representation of average compositions of chlorite in the reefs of the CRG

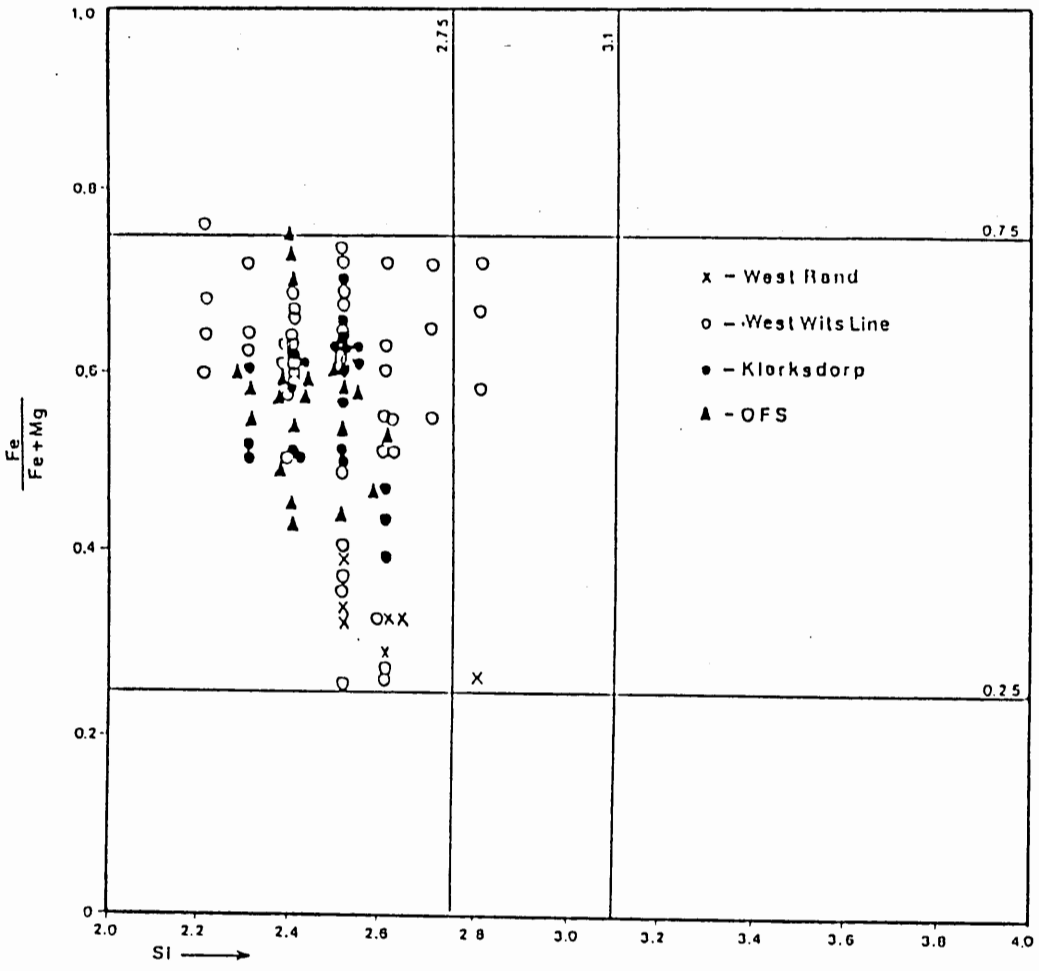



Fig. 10 Classification of chlorites in the CRG reefs according to relation between octahedral $Fe^{3+}:R^{2+}$ and tetrahedral Si:Al (Foster, 1962)

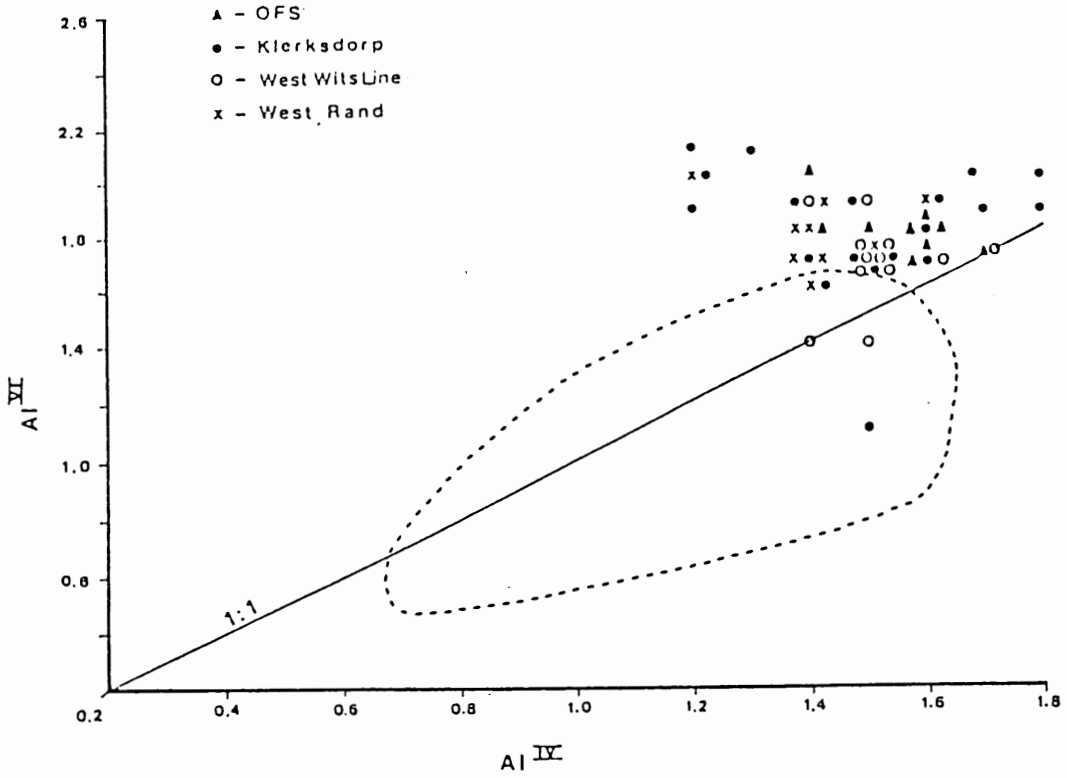



Fig. 11 Diagram showing relation between Al(IV) and Al(VI) contents of chlorites of the CRG reefs compared with those classified by Foster (1962) which fall within the area defined by the dashed line

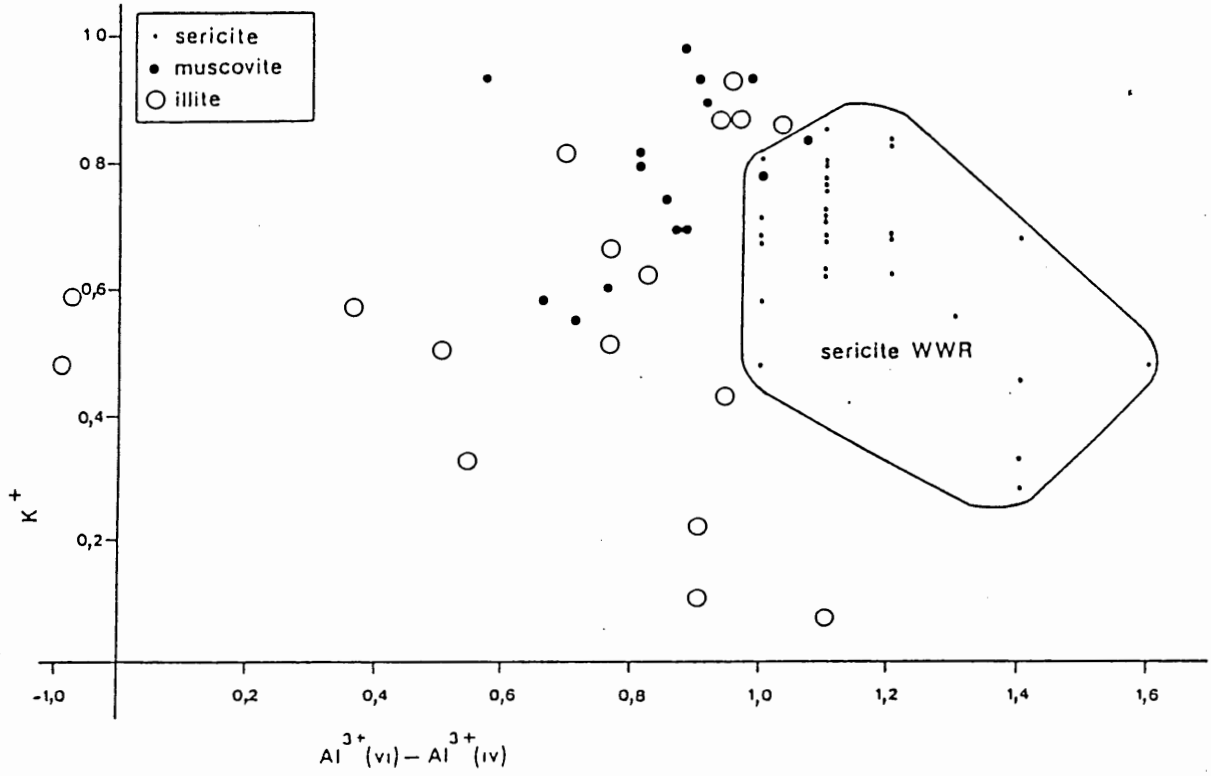



Fig. 12 Diagram showing relation between $K^+$ and $Al^{3+}(VI)-Al^{3+}(IV)$ for sericite from the Witwatersrand (this study), and muscovite and illite from other locations (Deer et al., 1962)

West Wits Line G.F.

Textural varieties of the mica and its association with other minerals are listed in Table 11, whereas the EMP analyses are presented in Table 12. The average formula calculated from these analyses is:

$$K_{0,7-0,9}Al_{1,9}(Si_{3,1}Al_{0,9})O_{10}(OH)_2.$$

When compared with analyses from Deer *et al.* (1962), it is clear that the potassium concentration of the mica in the CRG is considerably lower (Table 4; Fig. 12), and very similar to that of illite. However, illite is distinguished from muscovite by its higher (Mg+Fe) content (Velde, 1983). As is illustrated in Figure 12, the sericite of the CRG stands out by its low Al(IV), and consequently high silica content.

*3.1.3. Pyrophyllite and Chloritoid*

Pyrophyllite is intimately intergrown with sericite, but is also a constituent of the pseudomorphs after biotite (Table 13).

Chloritoid, on the other hand, occurs as discrete (Fig. A.1g), or as groups (Fig. A.1h) of twinned porphyroblasts with frayed ends up to 2 mm long. They often enclose quartz, which imparts a sieve texture to the mineral (Fig. A.1g) and rarely an hour-glass texture (Fig. A.5a). Locally the chloritoid formed at the expense of pyrite (Figs. A.5b and c), iron-bearing chromite, or arsenopyrite. The halo texture round uranous titanate described for chlorite in Table 6 (Figs. A.3g and h) also occurs in chloritoid, but less commonly (Figs. A.5d and e).

Chloritoid is relatively abundant on the West Rand and West Wits Line G.F., but uncommon in the Klerksdorp and OFS G.F. In the Green Bar and Black Bar, which occur in the hanging wall of the Carbon Leader on the West Wits Line G.F., chloritoid is a major component.

Pyrophyllite and chloritoid follow the ideal formulae (Tables 14 and 15), but like the other phyllosilicates, may incorporate trace amounts of foreign elements in their lattices (Table 5).

Table 11 Textural varieties of muscovite in CRG reefs

| Morphology | Size, mm | Distribution | Probable precursor |
|---|---|---|---|
| (1) Dense aggregates of randomly oriented shreds of ser (descriptive term for fine-grained mus) of hatched texture (Fig.A.1e). Ser frequently silicified (Fig. A.4g) and commonly intergrown with ph or associated with fine-grained chl. Minute rut crystals of acicular and geniculate habit, as a close-knit network (Fig. A.4a), or anhedral to euhedral py grains (Fig. A.4d) may occur dispersed in the ser | 0,01 to 0,10 (length) | Interstial filling in matrix of conglomerate and quartzite. Major component in Libanon Shale | Fsp, ill, or phengite. When contact of interstitial ser with q grains is straight (Fig.A.1e). it formed from ill during progressive burial. If it is strongly embayed (Fig. A.4c), the precursor required silica for its alteration to ser |
| (2) Films of ser whisps oriented parallel, or at an angle to the surface of q grains (Fig. A.4b) | <0,07 | Outlining q grains | Films initially composed of kaol, altered to ill, and via phengite to ser |
| (3) Large flakes of mus coherently or incoherently intergrown with chl and ph winding along q boundaries (Fig. A.4c). Boudinage (Fig. 6c) and kinking (Fig. A.2b) is common. For ghost textures see Table 6 (3) | <1,00 | Twisted along q grain boundaries in matrix of conglomerate or argillaceous quartzite at top of footwall quartzite | Detrital bio or bio-kaol intergrowth |
| (4) Spherules of mus or ph (Figs. A.4d and e); some composed of undeformed mus enveloped by concentric mus or ph (Fig. A.4f) | | In silicified mud- and siltstone fragments | Authigenic origin |
| (5) Undeformed mus flakes of detrital origin | <0,3 | In matrix cementing pebble fraction of reef | Inherited constituent |

Table 12

Quantitative electron-microprobe analyses of Witwatersrand sericite -

| | West Rand G.F. | | | | | | | | Carletonville G.F. | | | | | | | | | |
|---|---|---|---|---|---|---|---|---|---|---|---|---|---|---|---|---|---|---|
| Sericite | WRC 893-1 | WRC 893-2 | WRC 893-3 | WRC 900-2 | WRC 900-4 | WA 1229-2 | WA 1229-3 | WA 1229-4 | WDL 829/1-1 | WDL 829/1-2 | WDL 1231/B-3 | WDL 1231/B-4 | WDL 1231/B-5 | BV 666/1-3 | BV 666/1-4 | BV 666/1-5 | BV 666/1-6 | BV 666/2-2 |
| $SiO_2$ | 47,087 | 47,055 | 50,254 | 53,893 | 49,371 | 48,4 | 47,843 | 47,413 | 43,894 | 41,205 | 45,375 | 46,217 | 45,49 | 47,701 | 47,469 | 47,510 | 51,339 | 48,46 |
| $Al_2O_3$ | 35,336 | 34,672 | 33,799 | 34,578 | 35,391 | 35,596 | 35,712 | 36,483 | 37,673 | 35,938 | 36,761 | 36,748 | 36,535 | 39,001 | 38,592 | 38,886 | 33,168 | 37,78 |
| $K_2O$ | 7,178 | 7,871 | 7,404 | 5,525 | 8,614 | 9,795 | 9,819 | 9,532 | 7,763 | 7,332 | 9,857 | 9,034 | 9,237 | 8,10 | 8,087 | 8,24 | 7,971 | 7,564 |
| $Na_2O$ | 0,969 | 0,876 | 0,973 | 0,668 | 0,924 | 0,763 | 0,597 | 0,769 | 0,606 | 0,447 | 0,54 | 0,744 | 0,699 | 0,823 | 0,896 | 0,86 | 0,807 | 0,222 |
| MgO | 0,085 | 0,532 | 0,217 | 0,077 | 0,129 | 0,457 | 0,623 | 0,622 | 0,181 | 0,124 | 0,186 | 0,100 | 0,145 | 0,064 | 0,121 | 0,051 | 0,103 | 0,182 |
| FeO | 0,321 | 2,256 | 1,341 | 0,028 | - | 0,154 | 0,216 | 0,195 | 0,204 | 0,19 | 0,007 | 0,003 | 0,031 | 0,026 | 0,053 | 0,019 | - | 1,055 |
| ZnO | 0,019 | - | 0,015 | - | 0,06 | 0,021 | - | 0,017 | - | 0,004 | - | 0,033 | 0,004 | 0,012 | - | 0,033 | - | 0,015 |
| MnO | 0,025 | 0,038 | 0,005 | - | - | - | 0,009 | - | 0,01 | 0,012 | 0,035 | - | - | - | 0,006 | 0,009 | - | 0,020 |
| $Cr_2O_3$ | - | - | - | 0,347 | 0,308 | - | - | - | 0,892 | 1,013 | 0,118 | 0,156 | 0,006 | - | 0,011 | - | 0,045 | 0,482 |
| Total | 91,020 | 93,295 | 94,008 | 95,116 | 94,797 | 95,186 | 94,819 | 95,031 | 91,223 | 86,265 | 92,879 | 93,035 | 92,147 | 95,727 | 95,235 | 95,608 | 93,433 | 95,780 |
| | Number of ions (based on 11 oxygens) | | | | | | | | | | | | | | | | | |
| Si | 3,2 | 3,2 | 3,5 | 3,4 | 3,2 | 3,2 | 3,2 | 3,1 | 3,0 | 3,0 | 3,1 | 3,1 | 3,1 | 3,1 | 3,1 | 3,1 | 3,4 | 3,1 |
| $Al^{iv}$ | 0,8 | 0,8 | 0,5 | 0,6 | 0,8 | 0,8 | 0,8 | 0,9 | 1,0 | 1,0 | 0,9 | 0,9 | 0,9 | 0,9 | 0,9 | 0,9 | 0,6 | 0,9 |
| $Al^{vi}$ | 2,0 | 1,9 | 1,8 | 2,0 | 1,9 | 2,0 | 2,0 | 1,9 | 2,0 | 2,0 | 2,0 | 2,0 | 2,0 | 2,1 | 2,1 | 2,1 | 2,0 | 2,0 |
| K | 0,62 | 0,67 | 0,55 | 0,45 | 0,72 | 0,82 | 0,83 | 0,80 | 0,68 | 0,67 | 0,85 | 0,77 | 0,8 | 0,67 | 0,67 | 0,68 | 0,67 | 0,62 |
| Na | 0,13 | 0,11 | 0,11 | 0,08 | 0,12 | 0,1 | 0,08 | 0,1 | 0,01 | 0,06 | 0,07 | 0,1 | 0,09 | 0,10 | 0,11 | 0,11 | 0,1 | 0,03 |
| Mg | 0,01 | 0,05 | 0,02 | 0,01 | 0,01 | 0,04 | 0,06 | 0,06 | 0,02 | 0,01 | 0,02 | 0,01 | 0,01 | 0,01 | 0,01 | tr | 0,01 | 0,02 |
| Fe | 0,02 | 0,13 | 0,07 | tr | - | 0,01 | 0,01 | 0,01 | 0,01 | 0,01 | tr | tr | tr | tr | tr | tr | - | 0,01 |
| Zn | tr | - | tr | - | tr | tr | - | tr | - | tr | - | tr | tr | tr | - | tr | - | tr |
| Mn | tr | tr | tr | - | - | - | tr | - | tr | tr | tr | - | - | - | tr | tr | - | tr |
| Cr | - | - | - | 0,02 | 0,02 | - | - | - | 0,05 | 0,06 | 0,01 | 0,01 | tr | - | tr | - | tr | 0,02 |

WRC = West Rand Consolidated

WA = Western Areas

WDL = Western Deep Levels

BV 0 Blyvooruitzicht

Table 12 cont.

| | Klerksdorp G.F. | | | | | | | Welkom G.F. | | | | | | | |
|---|---|---|---|---|---|---|---|---|---|---|---|---|---|---|---|
| Sericite | WR 818/1-7 | WR 824-1 | WR 824-2 | WR 789-4 | VRE 744-4 | VRE 744-5 | VRE 744-6 | H 1226-2-3 | H 719-3 | H 719-4 | H 719-5 | H 670/3-2 | H 670/3-3 | V 702/1-1 | V 702/1-2 |
| $SiO_2$ | 42,648 | 47,548 | 47,308 | 46,700 | 47,373 | 48,164 | 48,132 | 55,922 | 47,662 | 48,457 | 49,933 | 44,596 | 45,744 | 50 | 49,054 |
| $Al_2O_3$ | 37,776 | 37,006 | 37,950 | 35,602 | 37,626 | 37,358 | 38,003 | 32,324 | 37,554 | 37,679 | 35,344 | 34,274 | 34,756 | 33,108 | 31,277 |
| $K_2O$ | 8,188 | 8,258 | 8,509 | 8,268 | 9,028 | 7,603 | 8,19 | 5,635 | 9,487 | 9,393 | 9,022 | 6,568 | 5,622 | 3,259 | 3,750 |
| $Na_2O$ | 0,543 | 0,496 | 0,607 | 1,553 | 0,323 | 0,609 | 0,409 | 0,225 | 0,700 | 0,677 | 0,734 | 0,489 | 0,492 | 0,336 | 0,349 |
| MgO | 0,212 | 0,125 | 0,115 | 0,334 | 0,126 | 0,36 | 0,192 | 0,056 | 0,244 | 0,295 | 0,239 | 1,466 | 2,829 | 0,76 | 0,606 |
| FeO | 0,630 | 0,153 | 0,041 | 0,702 | 0,140 | 0,389 | 0,149 | 0,023 | 0,084 | 0,082 | 0,098 | 4,053 | 2,914 | 1,048 | 1,348 |
| ZnO | 0,024 | 0,012 | 0,020 | 0,021 | 0,008 | 0,014 | - | 0,002 | 0,036 | 0,022 | - | 0,016 | 0,056 | 0,014 | 0,020 |
| MnO | 0,032 | 0,029 | - | 0,008 | 0,008 | 0,022 | 0,005 | 0,021 | - | 0,018 | 0,002 | 0,012 | - | - | 0,025 |
| $Cr_2O_3$ | 0,229 | - | - | - | - | - | - | - | 0,062 | 0,054 | 0,064 | 0,179 | 0,147 | 0,001 | 0,012 |
| Total | 90,282 | 93,627 | 94,548 | 93,198 | 94,632 | 94,519 | 95,08 | 94,208 | 95,829 | 96,677 | 95,436 | 92,085 | 92,560 | 88,526 | 86,841 |
| | Number of ions (based on 11 oxygens) | | | | | | | | | | | | | | |
| Si | 3,0 | 3,1 | 3,1 | 3,1 | 3,1 | 3,1 | 3,1 | 3,6 | 3,1 | 3,1 | 3,2 | 3,1 | 3,1 | 3,4 | 3,4 |
| $Al^{iv}$ | 1,0 | 0,9 | 0,9 | 0,9 | 0,9 | 0,9 | 0,9 | 0,4 | 0,9 | 0,9 | 0,8 | 0,9 | 0,9 | 0,6 | 0,6 |
| $Al^{vi}$ | 2,0 | 2,0 | 2,0 | 1,9 | 2,0 | 2,0 | 2,0 | 2,0 | 2,0 | 2,0 | 1,9 | 1,9 | 1,9 | 2,0 | 2,0 |
| K | 0,72 | 0,70 | 0,71 | 0,71 | 0,76 | 0,63 | 0,68 | 0,47 | 0,79 | 0,77 | 0,75 | 0,58 | 0,48 | 0,28 | 0,33 |
| Na | 0,07 | 0,06 | 0,08 | 0,2 | 0,04 | 0,08 | 0,05 | 0,03 | 0,09 | 0,08 | 0,09 | 0,07 | 0,06 | 0,04 | 0,03 |
| Mg | 0,02 | 0,01 | 0,01 | 0,03 | 0,01 | 0,04 | 0,02 | 0,01 | 0,02 | 0,03 | 0,02 | 0,15 | 0,28 | 0,08 | 0,06 |
| Fe | 0,04 | 0,01 | tr | 0,04 | 0,01 | 0,02 | 0,01 | tr | tr | tr | 0,01 | 0,23 | 0,16 | 0,06 | 0,08 |
| Zn | tr | tr | tr | tr | tr | tr | - | tr | tr | tr | - | tr | tr | tr | tr |
| Mn | tr | tr | - | tr | tr | tr | tr | tr | - | tr | tr | tr | - | - | tr |
| Cr | 0,01 | - | - | - | - | - | - | - | tr | tr | tr | 0,01 | 0,01 | tr | tr |

WR = Western Reefs

VRE = Vaal Reefs East

H = Harmony

V = Virginia

Table 13 Textural varieties of pyrophyllite in the CRG reefs

| Morphology | Size, mm | Inclusions | Remarks |
|---|---|---|---|
| (1) Fine-grained aggregates intergrown with ser (Fig. 6c) | <0,03 | rut, py (0,015 mm) | Fills interstices in the matrix of cementing the pebble fraction |
| (2) Whorls (Figs. A.4dand e) | <0,35 | rut, py (Fig. A.4e); 0,015 mm | In silicified aggregates of ph.sil. and in association with microstylolites |
| (3) Large flakes of pseudomorphs after bio intergrown with chl (Fig. 6c), musc, or both. Boudinage and kinking textures are common | <1,00 | po, py, rut along cleavage | Flakes flex along matrix grains subparallel to the bedding plane. Deformation due to compaction. Silicified ghost textures occur (Fig. A.1a) |

Table 14

Quantitative electron-microprobe analyses of Witwatersrand pyrophyllite

| | West Rand G.F. | | | | | | | | | | | | | | |
|---|---|---|---|---|---|---|---|---|---|---|---|---|---|---|---|
| Pyrophyllite | WRC 881-1 | WRC 881-2 | WRC 881-3 | WRC 904-1 | WRC 904-2 | WRC 904-3 | Rf 733-1 | H 604/1-1 | H 604/1-2 | H 604/1-3 | H 604/2-2 | H 604/2-3 | H 604/2-4 | WA 1215/2-2 | WA 1215/2-3 |
| $SiO_2$ | 63,933 | 63,531 | 71,408 | 64,761 | 66,510 | 66,618 | 65,272 | 66,028 | 67,547 | 61,695 | 65,925 | 67,486 | 67,392 | 65,747 | 60,600 |
| $Al_2O_3$ | 28,842 | 29,504 | 22,847 | 29,265 | 28,854 | 28,921 | 28,856 | 26,736 | 27,758 | 25,426 | 27,643 | 28,431 | 28,181 | 29,221 | 31,395 |
| $K_2O$ | 0,260 | 0,383 | 0,285 | 0,085 | 0,025 | 0,067 | 0,049 | 0,012 | 0,021 | 0,061 | 0,013 | 0,025 | 0,046 | 0,227 | 0,526 |
| $Na_2O$ | 0,299 | 0,268 | 0,287 | 0,006 | - | 0,011 | 0,085 | 0,100 | - | 0,090 | - | 0,068 | 0,13 | 0,17 | 0,230 |
| MgO | 0,198 | 0,272 | 0,248 | 0,013 | 0,140 | 0,050 | 0,160 | 0,027 | 0,040 | 0,175 | 0,016 | 0,006 | 0,067 | 0,116 | 0,287 |
| FeO | 0,373 | 0,922 | 0,510 | - | - | - | - | - | - | 0,056 | - | - | - | 0,016 | 0,290 |
| ZnO | 0,046 | 0,017 | 0,030 | 0,007 | - | - | - | - | 0,010 | 0,037 | 0,026 | - | - | - | 0,390 |
| MnO | 0,033 | - | 0,019 | 0,008 | 0,032 | 0,027 | 0,020 | - | - | - | - | 0,001 | - | 0,006 | 0,041 |
| Total | 93,984 | 94,897 | 95,634 | 94,145 | 95,435 | 95,694 | 94,442 | 92,903 | 95,376 | 87,54 | 93,623 | 96,017 | 95,816 | 95,503 | 93,408 |
| | Number of ions (based on 11 oxygens) | | | | | | | | | | | | | | |
| Si | 3,9 | 3,9 | 4,3 | 3,9 | 4,0 | 4,0 | 3,9 | 4,0 | 4,0 | 4,0 | 4,0 | 4,0 | 4,0 | 3,9 | 3,7 |
| Al | 2,1 | 2,1 | 1,6 | 2,1 | 2,0 | 2,0 | 2,1 | 1,9 | 2,0 | 2,0 | 2,0 | 2,0 | 2,0 | 2,1 | 2,3 |
| K | 0,02 | 0,03 | 0,02 | 0,01 | tr | 0,01 | tr | tr | tr | 0,01 | tr | tr | tr | 0,02 | 0,03 |
| Na | 0,04 | 0,03 | 0,03 | tr | - | tr | 0,01 | 0,01 | - | 0,01 | - | 0,01 | 0,02 | 0,02 | 0,03 |
| Mg | 0,02 | 0,02 | 0,02 | tr | tr | tr | 0,01 | tr | tr | 0,02 | tr | tr | 0,01 | 0,01 | 0,03 |
| Fe | 0,02 | 0,05 | 0,03 | - | - | - | - | - | - | tr | - | - | - | tr | 0,02 |
| Zn | tr | tr | tr | tr | - | - | - | - | tr | tr | tr | - | - | - | tr |
| Mn | tr | - | tr | tr | tr | tr | tr | - | - | - | - | tr | - | tr | tr |

WRC = West Rand Consolidated

Rf = Randfontein

H = Harmony

WA = Western Areas

Table 14 cont.

| | Carletonville G.F. | | | | | Klerksdorp G.F. | | | Welkom G.F. | | | | | | | |
|---|---|---|---|---|---|---|---|---|---|---|---|---|---|---|---|---|
| Pyrophyllite | WD 809-1 | WD 809-2 | WD 809-3 | WDL 1231/B-1 | WDL 1231/B-2 | BV 670/1-3 | BV 670/1-3-1 | WR 791/1-5 | H 1226-2-1 | H 1226-2-2 | Pr Br 1225-A-1 | Pr Br 1225-A-2 | Pr Br 1225-A-3 | Pr Br 1225-R-1 | Pr Br 1225-R-2 | Pr Br 1225-R-3 |
| $SiO_2$ | 63,795 | 64,810 | 66,505 | 67,848 | 67,033 | 54,337 | 60,988 | 61,011 | 67,396 | 67,641 | 62,881 | 63,100 | 64,733 | 62,626 | 63.428 | 62,669 |
| $Al_2O_3$ | 27,904 | 27,311 | 27,881 | 18,883 | 19,717 | 29,878 | 29,209 | 27,738 | 27,973 | 29,268 | 28,686 | 29,066 | 28,120 | 28,921 | 28,685 | 28,820 |
| $K_2O$ | 0,056 | 0,038 | 0,042 | 5,362 | 5,508 | 0,866 | 0,049 | 0,060 | 0,047 | 0,041 | 0,697 | 0,578 | 0,094 | 0,752 | 0,398 | 0,369 |
| $Na_2O$ | 0,114 | 0,014 | 0,034 | 0,561 | 0,531 | 0,306 | 0,016 | 0,036 | - | 0,084 | 0,114 | 0,072 | 0,068 | 0,182 | 0,189 | 0,077 |
| MgO | - | 0,032 | 0,123 | 0,149 | 0,083 | 0,399 | 0,035 | 0,285 | 0,005 | 0,064 | 0,121 | 0,089 | 0,061 | 0,049 | 0,067 | 0,054 |
| FeO | - | - | - | - | - | 3,175 | 0,210 | 0,488 | - | - | 0,076 | 0,047 | - | - | - | - |
| ZnO | 0,036 | 0,010 | 0,044 | 0,034 | 0,031 | 0,057 | - | - | - | - | 0,017 | 0,060 | 0,015 | 0,029 | 0,005 | 0,025 |
| MnO | 0,042 | - | 0,017 | - | 0,017 | - | 0,001 | - | - | 0,013 | 0,004 | 0,010 | 0,001 | 0,006 | 0,016 | - |
| Total | 91,947 | 92,215 | 94,646 | 92,837 | 92,92 | 89,018 | 90,508 | 89,618 | 95,421 | 97,111 | 92,596 | 93,022 | 93,092 | 92,565 | 92,788 | 92,014 |
| | Number of ions (based on 11 oxygens) | | | | | | | | | | | | | | | |
| Si | 4,0 | 4,0 | 4,0 | 4,3 | 4,3 | 3,6 | 3,8 | 3,9 | 4,0 | 4,0 | 3,9 | 3,9 | 4,0 | 3,9 | 3,9 | 3,9 |
| Al | 2,0 | 2,0 | 2,0 | 1,4 | 1,5 | 2,3 | 2,2 | 2,1 | 2,0 | 2,0 | 2,0 | 2,1 | 2,1 | 2,0 | 2,1 | 2,1 |
| K | 0,04 | tr | tr | 0,43 | 0,45 | 0,07 | tr | tr | tr | tr | 0,05 | 0,05 | 0,01 | 0,06 | 0,03 | 0,03 |
| Na | 0,01 | tr | tr | 0,07 | 0,07 | 0,04 | tr | tr | - | tr | 0,1 | 0,01 | 0,01 | 0,02 | 0,02 | 0,01 |
| Mg | - | tr | 0,01 | 0,01 | 0,01 | 0,04 | tr | 0,03 | tr | 0,01 | 0,01 | 0,01 | 0,01 | tr | 0,01 | 0,01 |
| Fe | - | - | - | - | - | 0,18 | 0,01 | 0,03 | - | - | tr | tr | - | - | - | - |
| Zn | tr | tr | tr | tr | tr | tr | - | tr | - | - | tr | tr | tr | tr | tr | tr |
| Mn | tr | - | tr | - | tr | - | tr | - | - | tr | tr | tr | tr | tr | tr | - |

WD = West Driefontein

WDL = Western Deep Levels

BV = Blyvooruitzicht

H = Harmony

Pr Br = President Brand

Table 15

Quantitative electron-microprobe analyses of Witwatersrand chloritoid

| | West Rand G.F. | | | Carletonville G.F. | | | | | | | | | | | Welkom G.F. | |
|---|---|---|---|---|---|---|---|---|---|---|---|---|---|---|---|---|
| Chloritoid | WRC 896-3 | WRC 888-3 | WRC 900-1 | WD 814-1 | WD 814-A-1 | WDL 1241-1a | WDL 1242-1b | WDL 1242-2a | WDL 1242-2b | WDL 1227-1 | WDL 1227-2 | WDL 1227-3 | BV 666/1-1 | BV 666/1-2 | BV 666/2-1 | H 1226-1-1 | H 1226-1-2 |
| $SiO_2$ | 25,003 | 25,210 | 30,531 | 25,502 | 24,602 | 24,647 | 23,448 | 25,199 | 23,622 | 26,319 | 34,371 | 27,546 | 24,742 | 24,682 | 24,706 | 24,387 | 24,734 |
| $Al_2O_3$ | 43,022 | 42,172 | 39,949 | 40,008 | 40,308 | 42,216 | 39,742 | 43,281 | 39,974 | 40,579 | 40,061 | 39,798 | 40,499 | 40,939 | 40,06 | 39,692 | 40,563 |
| $K_2O$ | - | - | - | 0,035 | - | - | - | - | - | - | - | - | - | - | - | - | - |
| $Na_2O$ | - | - | 0,025 | - | - | - | - | 0,032 | 0,004 | 0,021 | 0,068 | - | 0,022 | 0,093 | 0,014 | - | - |
| MgO | 4,312 | 2,393 | 4,285 | 1,804 | 1,688 | 1,405 | 1,434 | 2,615 | 2,557 | 3,067 | 1,818 | 2,712 | 2,304 | 2,879 | 2,84 | 1,458 | 1,762 |
| FeO | 21,907 | 24,271 | 20,268 | 25,004 | 26,373 | 27,798 | 26,182 | 26,008 | 24,285 | 22,041 | 21,906 | 22,992 | 24,438 | 23,109 | 23,5 | 24,57 | 24,476 |
| ZnO | 0,073 | 0,063 | - | 0,004 | - | 0,008 | 0,021 | 0,070 | 0,067 | 0,035 | 0,004 | - | 0,007 | 0,024 | 0,059 | 0,019 | - |
| MnO | 0,192 | 0,34 | 0,467 | 0,079 | 0,135 | 0,276 | 0,28 | 0,185 | 0,15 | 0,219 | 0,208 | 0,189 | 0,171 | 0,136 | 0,114 | 0,885 | 1,054 |
| $Cr_2O_3$ | 0,497 | - | 0,117 | - | - | 0,491 | 0,455 | 0,294 | 0,238 | - | - | - | 0,556 | 0,963 | 0,973 | - | - |
| Total | 95,006 | 94,449 | 95,642 | 92,436 | 93,106 | 96,841 | 91,562 | 97,684 | 90,897 | 92,281 | 98,436 | 93,237 | 93,739 | 92,825 | 92,266 | 91,011 | 92,589 |
| | | | | | | | Number of ions (based on 12 oxygens) | | | | | | | | | | |
| Si | 2,0 | 2,0 | 2,4 | 2,1 | 2,0 | 2,0 | 1,9 | 2,0 | 2,0 | 2,1 | 2,6 | 2,2 | 2,0 | 2,0 | 2,0 | 2,1 | 2,0 |
| $Al^{iv}$ | 2,0 | 2,0 | 1,6 | 1,9 | 2,0 | 2,0 | 2,1 | 2,0 | 2,0 | 1,9 | 1,4 | 1,8 | 2,0 | 2,0 | 2,0 | 1,9 | 2,0 |
| $Al^{vi}$ | 2,0 | 2,0 | 2,0 | 2,0 | 2,0 | 2,0 | 1,9 | 2,0 | 2,0 | 2,0 | 2,1 | 2,0 | 1,9 | 1,9 | 1,9 | 2,0 | 2,0 |
| K | - | - | - | tr | - | - | - | - | - | - | - | - | - | - | - | - | - |
| Na | - | - | tr | - | - | - | - | tr | tr | tr | 0,01 | - | tr | 0,01 | tr | - | - |
| Mg | 0,5 | 0,29 | 0,5 | 0,22 | 0,21 | 0,17 | 0,18 | 0,3 | 0,32 | 0,37 | 0,2 | 0,33 | 0,28 | 0,35 | 0,35 | 0,19 | 0,22 |
| Fe | 1,45 | 1,64 | 1,31 | 1,73 | 1,83 | 1,86 | 1,85 | 1,70 | 1,71 | 1,54 | 1,37 | 1,55 | 1,68 | 1,58 | 1,62 | 1,73 | 1,7 |
| Zn | tr | tr | - | tr | - | tr | tr | tr | tr | tr | tr | - | tr | tr | tr | tr | - |
| Mn | 0,01 | 0,03 | 0,03 | tr | 0,01 | 0,02 | 0,02 | 0,01 | 0,01 | 0,01 | 0,02 | 0,01 | 0,01 | 0,01 | 0,01 | 0,07 | 0,08 |
| Cr | 0,03 | - | 0,01 | - | - | 0,03 | 0,03 | 0,02 | 0,02 | - | - | - | 0,04 | 0,06 | 0,06 | - | - |

WRC = West Rand Consolidated

WD = West Driefontein

WDL = Western Deep Levels

BV = Blyvooruitzicht

H = Harmony

## 3.2. Sulphides and Sulpharsenides

### *3.2.1. Pyrite*

After the phyllosilicates, pyrite is the major heavy mineral in the reefs of the CRG. It occurs as:

(1) well-rounded, compact pyrite grains (Figs. A.5b and g),
(2) concretionary pyrite grains of varying texture (Figs. A.6a to e), and
(3) anhedral to euhedral, authigenic pyrite (Fig. A.6h).

In the 'mudball'type of grain of the second category (Hallbauer & Von Gehlen, 1983), the pyrite is finely intergrown with phyllosilicates, sulphides other than pyrite, and sometimes gold (Figs. A.6f to h). Detailed information about pyrite is compiled in Table 16. Major contributions to the description and classification of pyrite are made by Saager and Mihalik (1967), Saager (1968), Pretorius (1976), Utter (1978), Hallbauer and Von Gehlen (1983).

Some of the *compact pyrite* grains have been partly chloritized (Figs. A.5f, A.2f and A.9a). Together with pure, rounded chlorite grains (Fig. 7b), they occur dispersed amongst unaltered pyrite grains (Fig. A.5g), and are often coated by a 10 µm-thick layer of non-oriented crystals of brannerite (Fig. A.5g), and less commonly, uraniferous leucoxene, which caused discoloration of the adjacent chlorite (Fig. 7b). Many of the pyrite grains are covered by a slightly thicker layer (<40 µm) of uraniferous leucoxene (locally mixed with phyllosilicates) which, however, does not envelope the entire grain. This type of discontinuous uraniferous coating corroded the surface of the pyrite (Figs. A.5g and h).

The *concretionary pyrite* is made up of several pyrite generations of different composition (Figs. A.6a and e), the youngest being the purest. Hardness and reflectance of the pyrite decreases with increasing arsenic, cobalt, and nickel content (Saager & Mihalik, 1967). This type of pyrite, the textures of which resemble those of hydrothermal pyrite, has not been noticed in the Dominion Reef. In contrast with the compact pyrite, the concretionary pyrite is never chloritized.

Table 16 Textural varieties of pyrite in the CRG reefs

| Morphology | Size, mm | Inclusion or intergrowth | Distribution |
|---|---|---|---|
| **Detrital pyrite** | | | |
| (1) Well-rounded compact grains (Figs. A.5 & g). Cataclastic grains not uncommon (Fig. A.18a). Pressure fringes developed on py near shear and fracture zones (Fig. 7a) Ref.: Saager and Mihalik, 1967; Saager, 1968 Several of the grains are chloritized (Figs. A.2f and A.5f) | 0,15 to 0,35 | Round inclusions of cp, po, gn, gold (Fig. A.7a), q, rut, rare cob, sl, magn, chr, and combination of two or more of these. Grains with fracture-filling po (Fig. A.7b) and intergrowth with rut (Figs. A.7c and A.10b) are rare. | Horizons parallel to bedding plane; foresets in hanging and footwall quartzites, or quartzites interlayered with conglomerates in channel fillings |
| (2) Concretionary, also referred to as syn-sedimentary (Hallbauer, 1981; Figs. A.6a to e). Frequently made up of a framework of small granular or crystalline py (Fig. A.6b) or other minerals filling the interstices (Fig. A.7d). Several generations of py may be present in same grain (Figs. A.6a and e). Concretionary py <4 mm is called buckshot and >4 mm, pebble py*. Hallbauer and Von Gehlen further distinguish porous, oolitic (referring to the 'mineralized bacteria' of Schidlowski, 1966d), and mudball py (Figs. A.6f and g) | 0,15 to 5,00 | Angular and irregular-shaped sl, gn (Fig. A.7d), cp (Figs. A.7e and f), po, gold (Fig. A.7f), q, chlort (Fig. A.5c), ph.sil. (Fig. A.13g. Fine intergrowth with ph.sil. (Figs. A.6d, f to h, A. 13f. produces dull appearance of buckshot in handspecimen | As for compact py |
| **Authigenic pyrite** | | | |
| (1) Discrete, anhedral to euhedral, or skeletal, py particles, or encrustrations on detrital py grains (Fig. A.6h), or it cements heavy minerals (Figs. A.7g and h) | 0,01 to 0,30 | No inclusions. Authigenic sulphides or recrystallized gold may occur at the contact between allogenic and authigenic py | Associated with heavy-mineral concentrations |
| (2) Minute granular or euhedral grains | <0,03 | | Dispersed in ph.sil (Fig. A.4d) or in chert; the latter occurrence is probably inherited |

*) Pebble py is common in the Black Reef (Swiegers, 1939). The origin of these grains differs from the buckshot py in the CRG reefs

### 3.2.2. *Pyrrhotite*

Except for the small inclusions present in compact pyrite (Fig. A.7a), pyrrhotite is of post-burial origin (Table 17). It occurs as irregular-shaped grains often associated with other sulphides of similar origin or with recrystallized gold, and fills open space in kerogen (Fig. A.18b), and cracks in quartz pebbles (Fig. A.24h) where it often replaces chlorite. The association of minute laths of authigenic pyrrhotite with uraninite altered to coffinite (Fig. A.27d) or uranous titanates (Fig. A.25g) is conspicuous. In some of the pyrite foresets (Fig. A.26a) and in the younger reefs of the Turffontein Subgroup, stubby crystals precipitated in association with the alteration products of uraninite.

Pyrrhotite is particularly common in the VCR where it formed at the expense of pyrite (Viljoen, 1963).

### 3.2.3. *Other sulphides*

Except for small inclusions present in allogenic pyrite grains, galena, chalcopyrite (Fig. A.7a), and sphalerite, like pyrrhotite, are of post-burial origin and then are usually associated with quartz or enclosed by chlorite (Figs. A.3d and e).

*Pentlandite* has not been found as inclusions in pyrite, but does occur in the authigenic form, usually in association with recrystallized gold (Figs. A.13g, A.18a and b). Only once was a detrital grain noticed which contained 74 microscopic-sized particles of gold (Fig. A.17b).

The textural varieties of *galena* are listed in Table 18. A considerable portion of the galena is of radiogenic origin and occurs disseminated as ultrafine particles within radioactive minerals (Figs. A.19a and b). In contrast with the low relief and the distinctly greyish hue of the authigenic galena, the relief of radiogenic galena is high and the reflectance white. Both types of galena may contain trace amounts of silver (Viljoen, 1971).

*Chalcopyrite* is most common in the Carbon Leader (Oberthur, 1983) and in the Dominion Reef. In the latter reef, part of the chalcopyrite has been altered to covellite possibly as a result of supergene activity. In contrast with the reefs

Table 17 Textural varieties of pyrrhotite in the CRG reefs

| Morphology | Size, mm | Mineral association | Remarks |
|---|---|---|---|
| (1) Fracture fillings (Fig. A.7b) and inclusions combined with other minerals in compact detrital py. Inclusions in detrital arsenopyrite, often in association with gn | | cp, Au, gn in incl. | Inherited from source rocks. May enclose pn flames |
| (2) Filling cracks in q pebbles (Fig. A.24h) | | marc, py, chl | Of authigenic origin |
| (3) Associated with authigenic sulphides, recrystallized gold (Fig. A.18a), or chl | <0,20 | Au, cp, gn, gd | Coprecipitation with reconstituted gold is common |
| (4) Minute laths (Figs. A.25g and A.27d) or stubby crystals (Figs. A.20f and A. b) | <0,02<br><0,07 | ur. tit., cf | By product of alteration of ur to br, ulc, or cf |



Table 18 Textural varieties of galena in CRG reefs and Dominion Reef

| Morphology | Size, mm | Mineral association | Remarks |
|---|---|---|---|
| (1) Inclusions in compact and concretionary py and asp of detrital origin | <0,05 | Au, cp, po | In compact py, gn occurs combined with gold, po, or both. In concretionary py, it fills interstices on its own (Fig. A.7d) |
| (2) Inclusions in detrital asp | <0,05 | Au, po, rut, chl | Often together with po incl |
| (3) Minute particles of radiogenic gn (Figs. A.19a and b, and A.27g), which in places coalesce to larger grains (Fig. A.27d) or filled cracks (Fig. A.19c) | <0,01 | U-bearing minerals | Product of radioactive decay of uranium |
| (4) Irregular-shaped grains and crack-fillings in combination with po | <0,20 | q, cp, Au, po, sl | Coprecipitation with authigenic cp, sl, gold, po, or q. In the Dominion Reef, gn is usually associated with supertene cov, which formed from cp |

of the CRG, the workings of the Dominion Reef occur close to the surface.

Authigenic *sphalerite* is particularly common in the Vaal Reef, where its average iron content is 1,2% while, in the Basal Reef, it is 3,7% (Feather, 1976). Detrital sphalerite has only been recognized, and then rarely, in kerogen seams at the base of the Basal Reef on the OFS G.F. (Fig. A.8a). Like the other heavy minerals enclosed in that seam, the grains were boudinaged in a vertical direction, and the open space filled with quartz (Schidlowski, 1966e); (Smits, 1984a).

Authigenic *marcasite* has been found once at the base of the Leader Reef in the Harmony Complex, directly overlying the footwall quartzite (Fig. A.8b). Together with porous pyrite, it replaced pyrrhotite blades which formed *in situ*, and then was overlain again by massive neoformed pyrrhotite which encloses some galena (Fig. A.8c).

Some marcasite has also been found in the Monarch Reef, Randfontein Estates G.M., in association with pitchblende and secondary coffinite. All three components are of relatively recent supergene origin.

*Mackinawite*, $Fe_{1+x}S$ (x = 0,01 to 0,20), has been optically identified by Schidlowski and Ottemann (1966), but is rare. These authors believe that it precipitated at the same time as the other authigenic sulphides. This sulphide can form during metamorphism at a temperature of $230^0$C (Borchert, 1934), but it is also an intermediate product in the neoformation of pyrite soon after burial (Sweeney & Kaplan, 1973; Fig. 13).

*Molybdenite* (Fig. A.8d) of allogenic origin is a rare constituent of all reefs (Liebenberg 1955; Ramdohr, 1955; Van der Westhuizen & Smits, 1985).

*3.2.4. Sulpharsenides and -antimonides*

All three sulpharsenides, viz arsenopyrite, cobaltite, and gersdorffite, are constituents of the heavy-mineral assemblage (Table 19). Textural criteria indicate that the two first-named species are of detrital origin, while the last mineral formed after burial.

Gold is associated with all three sulpharsenides. In the detrital arsenopyrite (Fig. A.8e) and cobaltite (Figs. A.17a

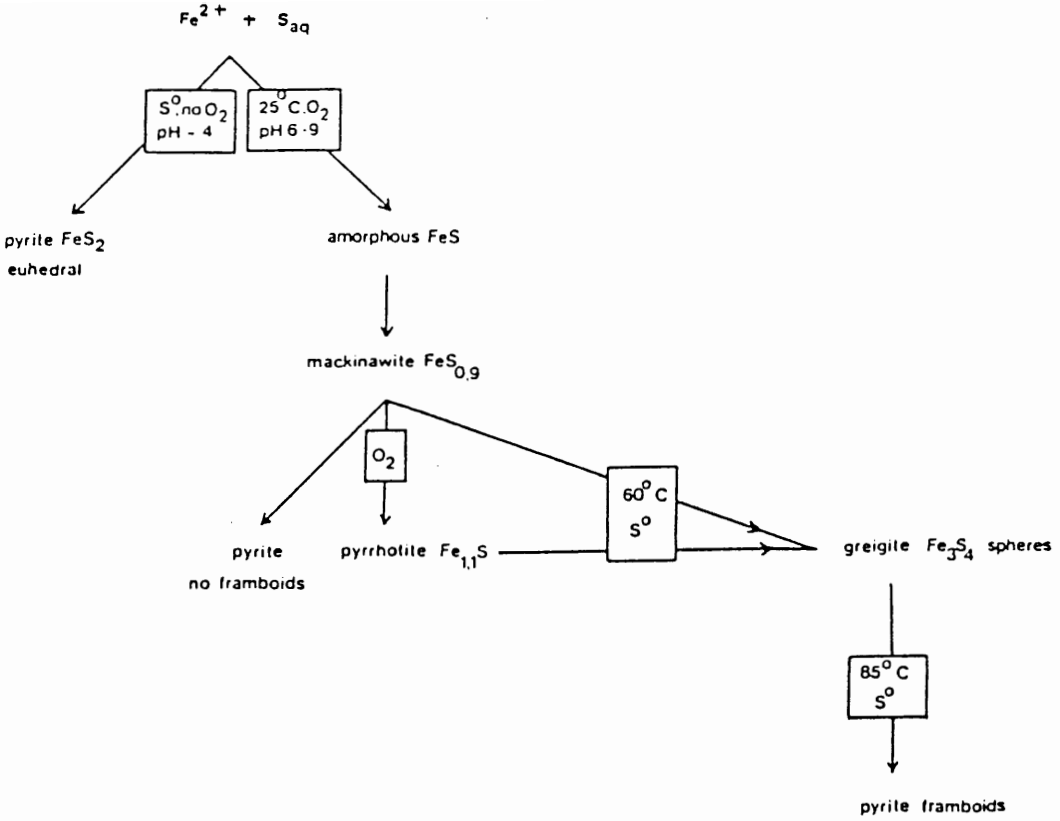



Fig. 13 Possible precipitation paths for pyrite (Sweeney and Kaplan, 1973; Berner, 1984)

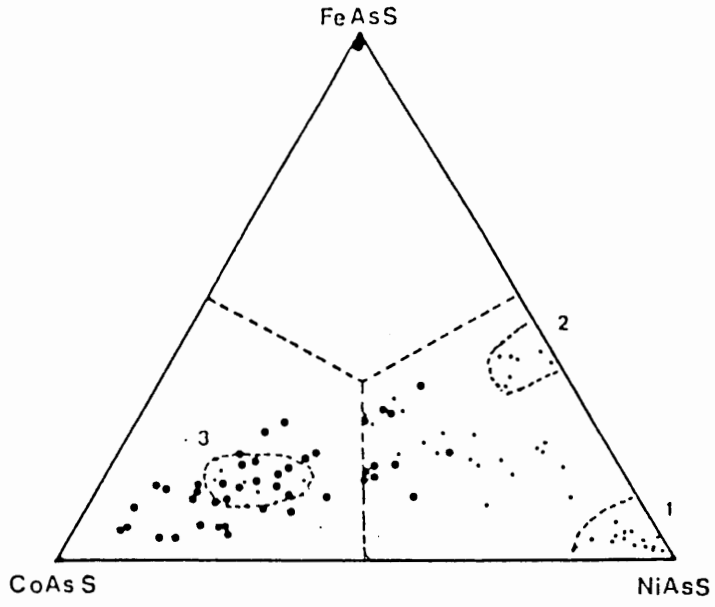



Fig. 14 Ternary diagram of compositions of detrital (•) and authigenic (•) sulpharsenides in the CRG reefs. 1. Isotropic gersdorffite in kerogen. 2. Anisotropic gersdorffite. Remaining gersdorffite is not associated with kerogen. 3. Isotropic authigenic cobaltite found in Carbon Leader only (after Saager and Oberthur, 1984)

Table 19 Textural data of sulpharsenides in CRG reefs

| Texture | Size, mm | Inclusions | Remarks |
|---|---|---|---|
| Arsenopyrite | | | |
| Well-rounded detrital grains | 0,15 to 0,25 | Au, po, gn | Slightly smaller than accompanying py. Many of the grains are partly replaced by chl, rut prisms, or both. The chloritized grains are enveloped by a film of br crystals (Figs. A.2g and A.8e) |
| Cobaltite | | | |
| Well-rounded detrital grains | 0,15 to 0,25 | Au, cp, po, sl (Fig. A.17a) | Detrital grains often overgrown by authigenic gd, less commonly cob, of different composition. The overgrowth may contain recrystallized gold (Fig. A.18d) |
| Gersdorffite | | | |
| (1) Authigenic overgrowth on detrital cob (Fig. A.18d) | | | In zoned overgrowths, Co and Ni contents vary |
| (2) Coprecipitation with recrystallized gold (Fig. A.9b), or other authigenic sulphides | <0,15 | | All type of mixed grains occur in the matrix, but in kerogen, gd is only combined with gold |
| (3) Cutans made up of minute crystals (0,01 mm) | <0,07 | | Cutans developed on detrital ur (Figs. A.9c and A.19e) and other heavy minerals (Figs. A.9a and A.25f), or kerogen nodules (Figs. A.9e and f) |
| (4) Minute euhedra (Fig. A.9g) often enclosing py, gn, or cp cores or zones | av. 0,40 | py, gn, cp | Dispersed in rare ur-ree kerogen (Fig. A.9h) or in the matrix in the vicinity of seams or in interfilamental position or in voids |

and A.18d), it occurs as minute inclusions, whereas gersdorffite precipitated commonly in the company of gold during its recrystallization (Fig. A.9b).

The composition of the sulpharsenides (Fig. 14) has been established (Feather, 1976; Oberthur, 1983) and discussed by Feather and Duggan (1974) and Saager and Oberthur (1984). These studies revealed that some of the authigenic sulpharsenide is of cobaltite composition (Fig. 14).

Although it is an inconspicuous constituent, *gersdorffite* contributes to the decoding of post-burial geochemical processes. This sulpharsenide has not been noticed in the Dominion Reef.

Like the chloritization of pyrite and chromite, that of *arsenopyrite* is a common phenomenon (Figs. A.2g and A.8e). Many of these grains are also partly replaced by oriented prisms of rutile, an alteration which is also found in chromite (Figs. A.8f and A.12a to f). As for chloritized pyrite and chromite, the shape of the chloritized grains is usually defined by a thin film of uranous titanate (Fig. A.8e).

Except for the presence of rare *tucekite* (Feather, 1976), no other antimony-bearing minerals have been identified in the reefs.

3.3. Accessory Minerals

The most common allogenic accessory minerals in the reefs of the CRG are in order of abundance: rutile-leucoxene pseudomorphs after ilmenite, zircon, and chromite, whereas rutile and tourmaline are uncommon, and xenotime, monazite, graphite, barite, and apatite rare. Magnetite is seldomly found as inclusions in compact pyrite.

A well-rounded grain of *tantalaeschynite*, $(Y,Ce,Ca)-(Ta,Ti,Nb)_2O_6$ measuring 3 mm in diameter and of cataclastic texture (Fig. A.8g), occurred in a buckshot-rich, heavy-mineral concentration at the base of the Kalkoenkrans Reef, Oryx G.M. (Van der Westhuizen & Smits, 1985). It was identified on the SEM and its presence confirmed by XRD without pre-heating. The major component contained trace amounts of uranium, calcium, iron, gadolinium, and samarium. The fractures were healed by titania which held trace amounts of niobium and tantalum. The

grain enclosed gold particles, one of which measured 0,15 mm (Fig. A.8g).

*Harmotome*, the Ba-bearing zeolite, was identified once in the Beisa Reef (Smits 1984a), and so were authigenic *apatite* in the Carbon Leader and authgenic *barite* in a kerogen seam in the Basal Reef.

The heavy-mineral assemblage of the Dominion Reef differs distinctly from that of the reefs on the CRG in that it contains significant amounts of the following detrital constituents:

> garnet (Fig. A.8h), monazite, cassiterite, euxenite, betafite, and columbite (Hiemstra, 1968), less common uranoan thorite, thorian zircon, and rare cheralite (Fig. A.10a).

### *3.3.1. Titanium-bearing Minerals*

Although the titanium oxide content of the reefs of the CRG does not exceed 0,6%, the sparsely distributed, but widespread occurrence of authigenic rutile (Table 20) is conspicuous. Authigenic anatase (Table 21) and detrital rutile are rare, the latter being slightly more common in the Dominion Reef. The rutile which replaces portions of chromite (Figs. A.11a to f) and arsenopyrite (Fig. A.8e) is considered an inherited feature from the source rocks (Smits 1984b, 1985c), as is the intimate intergrowth of pyrite and rutile (Figs. A.10b and A.7c).

Well-rounded grains composed of compact rutile and the earthy leucoxene, which are obvious pseudomorphs, are referred to as *rutile-leucoxene* (Figs. A.11b to h) to distinguish them from the detrital rutile of different shape, colour, and much smaller size. Detailed information of these detrital grains is summarized in Table 22.

Rutile-leucoxene pseudomorphs are second in importance to pyrite (Viljoen, 1963). It is a particularly common constituent of the proximal facies of the conglomerates. The leucoxenic portion of these grains is intergrown with quartz and phyllosilicates, as is indicated by many of the analyses listed in Table 23. From size, relative density, and textural

Table 20 Textural varieties of authigenic rutile in CRG reefs

| Morphology | Size, mm | Distribution |
|---|---|---|
| (1) Concentration of granular or crystalline rut in 5 to 20 mm thick layers parallel to the bedding plane (Fig.A.11a), which in places is overlain by a 2 to 3 mm-wide muddrape. The rut imparts a greyish orange colour to the quartzite | 0,05 | Locally at the top of footwall quartzites |
| (2) Single, or groups of crystals of prismatic or geniculate habit | 0,01 to 0,10 av. 0,04 | Dispersed throughout the sedimentary rocks |
| (3) Concentration in microstylolites (Fig. A.1) that wind along grain boundaries | | In quartzites and conglomerates |
| (4) Exsolution product from precursor ph.sil. (Fig.A. 1a). In chl, the titania grains are slightly larger | | In conglomerates |
| (5) Minute prisms in greyish orange to dark yellowish orange silicified mud- and siltstone clasts | 0,02 | Silicified clasts (<5 mm) are particularly common in the Basal Reef B3, Harmony Complex. In quartzites the rock fragments impart a greyish yellow colour to the rock. On the mines, these quartzites are incorrectly referred to as argillaceous; they are wackes |

Table 21 Textural varieties of anatase in CRG reefs

| Morphology | Size, mm | Remarks |
|---|---|---|
| (1) Pale pink to pale purple, granular aggregates (Fig. A.9d) | 0,15 | Recrystallization product of detrital titania. Rare in Carbon Leader, Western Deep Levels G.M. and in Leader Reef, Harmony Complex |
| (2) Greyish yellow, stubby crystals | 0,05 | Enclosed in chl and in polymineralic spheroids. Possible precursor in geode-shaped pseudomorphs after detrital ilm in Dominion Reef (Fig. A.10c) |
| (3) Yellowish grey mushy anatase (Section 3.7.4) cementing heavy minerals (Fig. 30c); in places uranium-bearing and then bluish grey | | Particularly common in Vaal Reef, Western Reefs G.M. and Main Reef, Grootvlei G.M., where it imparts a dusky yellow colour to the rock |

Table 22 Detailed information on rutile-leucoxene pseudomorphs in the CRG reefs

| | |
|---|---|
| (1) Mode of occurrence | Dimensions of grains up to 0,6 mm; slightly larger than the accompanying py. Rut forms the core (Fig.A.11b) occurs in the margin (Fig.A.11d), or as an overgrowth of minute prisms onto the grain (Fig.A.11d). It displays twinning, pleochroism, and is dark yellowish orange. Other grains consist entirely of lc. The lc is very pale orange to greyish yellow. Few particles are white to pale grey |
| (2) Shape | Rounded (Fig.A.11b and h), or indented and deformed by surrounding matrix constituents (Figs.A.11c and d) |
| (3) Composition | The lc is mixed with ph.sil. and q. Analyses (Table 23) indicate that the rut contains trace amounts of iron and manganese. Ur. tit. may fill voids (Figs.A.11e, g and h), or precipitated at the surface of the grains (Fig.A.11f) |
| (4) Alteration | Size and relative density indicate that ilm is the most likely precursor, from which iron has been removed effectively |
| (5) Distribution | Rut-lc pseudomorphs are associated with other heavy mineral concentrations in the conglomerate, but are also found on their own in one- or two-grain wide laminae within quartzite |

Table 23 Electron-microprobe analyses of titanium oxides in the CRG reefs

| Origin of sample and reference number | | MnO | ZnO | $K_2O$ | MgO | $Na_2O$ | $Al_2O_3$ | $SiO_2$ | FeO | $TiO_2$ | $Cr_2O_3$ | CaO | Total | Leucoxene, $TiO_2$, mixed with |
|---|---|---|---|---|---|---|---|---|---|---|---|---|---|---|
| CARLETONVILLE | | | | | | | | | | | | | | |
| Western Areas | 1215/2-1 | 0,073 | 0,014 | 0,019 | - | - | 0,102 | - | 0,100 | 98,345 | - | - | 98,653 | |
| KLERKSDORP | | | | | | | | | | | | | | |
| Buffelsfontein | 793/B-1 | 0,519 | - | 1,192 | 1,262 | 0,313 | 11,216 | 15,495 | 1,258 | 62,881 | 0,262 | 0,063 | 94,461 | chl, ph, ser |
| | 793/B-2 | 0,479 | - | 2,800 | 1,925 | 0,531 | 19,123 | 27,384 | 7,147 | 28,889 | - | - | 88,277 | chl, ph, ser |
| | 793/B-3 | 0,295 | 0,042 | 0,068 | 1,308 | 0,098 | 6,746 | 7,407 | 1,295 | 78,715 | 0,081 | - | 96,055 | chl, ser |
| | 793/B-4 | 0,017 | 0,003 | 0,008 | 0,064 | 0,015 | 0,291 | 0,476 | 0,572 | 97,904 | - | - | 99,350 | |
| Western Reefs | 820-1 | 0,028 | 0,020 | 0,139 | 0,035 | - | 1,227 | 1,079 | 0,020 | 95,069 | 1,021 | - | 98,638 | chl, ser |
| | 820-2 | - | 0,019 | 0,028 | - | 0,098 | 0,818 | 1,302 | 0,121 | 94,218 | 0,376 | - | 96,982 | ph, ser |
| | 820-6 | 0,028 | 0,030 | 0,044 | 0,030 | 0,010 | 1,449 | 1,994 | 0,134 | 96,681 | 0,380 | - | 100,782 | |
| | 820-7 | 0,039 | 0,003 | 1,180 | 0,153 | 0,205 | 6,770 | 11,314 | 0,423 | 78,489 | 0,348 | - | 98,924 | ph, ser, q |
| WELKOM | | | | | | | | | | | | | | |
| Harmony | | | | | | | | | | | | | | |
| Leader Reef | 663/B-1 | - | - | 0,021 | 0,015 | - | 0,057 | 76,908 | - | 23,493 | - | - | 100,495 | q |
| | 663/B-2 | 0,036 | 0,021 | 0,004 | 0,023 | - | 0,031 | 66,847 | - | 34,529 | - | - | 101,491 | q |
| | 663/B-3 | 0,003 | 0,050 | 0,005 | - | - | 0,058 | - | 0,067 | 100,206 | - | - | 100,388 | |
| | 663/B-5 | 0,325 | 0,018 | - | 7,369 | 0,009 | 18,838 | 19,781 | 21,131 | 19,825 | 0,009 | - | 87,304 | chl |
| Pyritic quartzite | 647/1-1-2 | 0,027 | - | 0,013 | 0,038 | 0,064 | 0,317 | 2,571 | 0,549 | 88,359 | 1,330 | 0,013 | 93,282 | chl, ser, ph |
| | 647/1-1-3 | 0,075 | 0,024 | 0,016 | - | 0,054 | 0,343 | 1,516 | 0,613 | 89,922 | 1,417 | 0,006 | 93,987 | chl, ser, ph |
| | 647/1-2-1 | 0,045 | 0,037 | 0,011 | - | 0,027 | 0,073 | 69,861 | - | 23,541 | - | - | 93,594 | q |
| | 647/1-2-2 | 0,038 | 0,041 | 0,013 | 1,595 | - | 3,998 | 4,960 | 1,755 | 84,202 | 1,223 | - | 97,824 | ser |
| | 647/2-3 | - | 0,217 | 0,005 | 0,190 | - | 0,128 | 0,447 | 0,442 | 96,459 | 2,128 | - | 100,017 | |

appearance, it is concluded that ilmenite is the most likely precursor (Coetzee, 1965). In contrast with the CRG reefs, ilmenite (in addition to some detrital leucoxene) was a constituent of the detrital assemblage supplied during the deposition of the Dominion Reef. It was replaced *in situ* by grains in which stubby rutile crystals line the cavity, whereas chlorite or quartz fill the core (Fig. A.10c). Aggregates of blades of mixed ilmenite-rutile of authigenic origin are fairly common in the Dominion Reef (Figs. A.28b and A.29a), and sometimes replaced the leached, detrital ilmenite grains.

Qualitative EMP analysis recorded the presence of titanium in microspherules, <2 μm in diameter (Fig. A.10d), which commonly cover the quartz grains of the matrix, but possibly occur on the surface of all matrix constituents, where they are not visible because of the opacity of the heavy minerals.

*3.3.2. Chromite*

The association with pyrite concentrations and the well-rounded shape of the chromite grains (Fig. A.10e) indicate that they are of detrital origin. The grain size ranges from 0,1 to 0,5 mm. The chromite grains are slightly smaller than the accompanying pyrite, and unlike the pyrite occur isolated. Only once was a cluster of chromite grains observed (Fig. A.10e).

Two types of chromite can be distinguished optically and chemically. The reflectance in incident light of the less common type, which is richer in magnesium and aluminium, is lower than that of the iron- and chromium-rich variety (Fig. A.10f). The respective internal reflections in thin section are moderate red and dusky brown.

The composition of the chromite is variable and falls in the category of aluminian chromite (Stevens, 1944: Eales & Reynolds, 1983). Analytical data for 89 particles (Viljoen, 1977) of different reefs at Klerksdorp G.F. were published by Utter (1978). The compositional ranges of the oxides which make up the chromite (Utter, 1978) are listed in Table 24.

Table 24. Variations in oxide composition of chromite in the Vaal Reef (Utter, 1978)

| | Mass, % | | |
|---|---|---|---|
| $Cr_2O_3$ | 39 | to | 57 |
| $Al_2O_3$ | 3 | to | 25 |
| $Fe_2O_3$ | 1 | to | 19 |
| FeO | 7 | to | 30 |
| MgO | 0,5 | to | 17 |
| MnO | 0,1 | to | 1,1 |
| $TiO_2$ | 0 | to | 1 |
| ZnO | 0 | to | 17 |
| Cr/Fe | 0,8 | to | 4 |

Utter (1978) plotted the compositions of chromite of the reefs of the CRG on two projection planes (Irvine, 1965) of a trigonal prism (Fig. 15), the conventional method to illustrate the compositions of spinels of the general formula $(Fe^{2+},Mg^{2+})(Cr^{3+},Al^{3+},Fe^{3+})_2O_4$. The composition of the chromite found in the older conglomerates of the Moodies Group in the Barberton Mountain Land, the Uitkyk Formation in northern Transvaal, and the Mozaan Group in southeastern Transvaal and Zululand (Saager *et al.*, 1982). The chromite found in ultramatic rocks of Archaean age in Lemoenfontein north of Pietersburg (Willemse, 1948) fall in the same field (Fig. 15).

Although chromite is a fairly stable mineral, the grains in the reefs underwent several pre- and post-depositional alterations (Table 25). Like pyrite and arsenopyrite, several of the detrital grains are partly chloritized (Figs. A.2h and A.7g), others are partly replaced by rutile, either earthy (Fig. A.12c) or prismatic, the prisms being oriented (Figs. 18f and A.12d) or at random (Fig. A.12b). Chromite in which zinc has been introduced are quite common (Figs. A.10g and A.12h), in particular in the Basal Reef at Harmony Complex (Table 26, analysis 647), where they occur side by side with unaltered chromite grains (Smits, 1985c). Chemical data of zinc-bearing chromite from several reefs are listed in Table 26 in order of increasing ZnO content, and are compared with unaltered

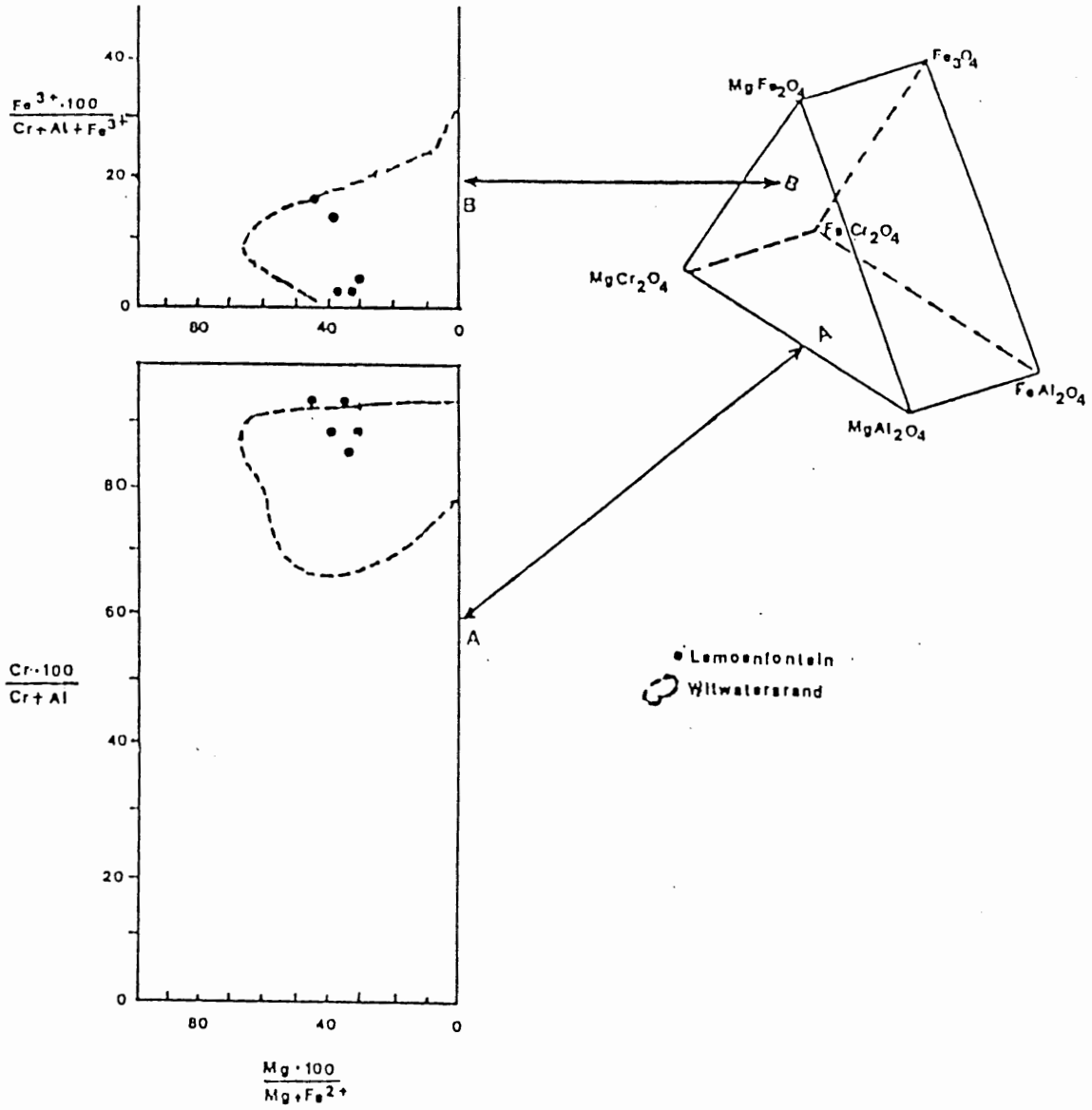



Fig. 15 Compositional field of Witwatersrand chromites (after Utter, 1978)

Table 25 Types of alterations of chromite in CRG reefs

| Alteration | Remarks |
|---|---|
| (1) Chloritization | Similar to that of py, asp, and gar; inherited feature. Shape of grain acquired during transportation is often defined by a film of br crystals (0,005 mm; Fig. A.25f) |
| (2) Rutilization | Inherited feature which starts along crystal planes (Fig.A.12a), then proceeds into grain (Figs.A.12b to d). Rut as lc (Fig.A.12c), prisms at random (Fig. A.12b), or oriented (Fig.A.12d). Some grains contain chl and rut (Fig.A.12e) |
| (3) Corrosion of surface by ur. tit. or marginal introduction of uranium with (Fig.A.12f) or without galena (Fig. A.12g) | Post-burial alteration |
| (4) Introduction of, or partial replacement by zinc | Texture: (i) dendritic (Fig.A.12h). or (ii) homogeneous distribution of zinc (Fig.A.13a and b; analyses 647, Table 20). The second type of Zn-bearing chr is found in igneous rocks in W. Australia (Groves et al., 1977) |
| (5) Marginal release of magnesium and aluminium in situ (Mihalik & Saager, 1968) | The higher reflectance of the margin (Fig.A.10) is caused by the relative enrichment of iron |

Table 26 Electron-microprobe analyses of zinc-bearing chromites listed in order of increasing zinc content

| | 1216/2B-3 UE1a | 750/2-2-1 Vaal Reef | 670/2-1 Carbon Leader | 828/1B-1-2 Carbon Leader | 647/2-5 Basal Reef Harmony | 647/4-5 Basal Reef Harmony | 647/3-1 Basal Reef Harmony | 647/4-1 Basal Reef Harmony | 647/4-4 Basal Reef Harmony |
|---|---|---|---|---|---|---|---|---|---|
| $SiO_2$ | 0,12 | 0,14 | 0,15 | 0,13 | 0,08 | 9,68 | 2,12 | 0,40 | 1,25 |
| $Al_2O_3$ | 15,32 | 12,63 | 8,97 | 10,85 | 3,37 | 13,96 | 3,89 | 6,30 | 6,94 |
| FeO | 16,70 | 17,34 | 28,95 | 33,04 | 55,39 | 19,90 | 26,81 | 37,32 | 31,59 |
| MgO | 13,55 | 13,02 | 4,50 | 0,09 | 0,02 | 4,49 | 0,63 | 0,10 | 0,38 |
| MnO | 0,32 | 0,28 | 0,45 | 0,23 | 0,79 | 0,40 | 1,02 | 1,01 | 0,84 |
| $Na_2O$ | - | - | 0,02 | 0,05 | 0,04 | 0,05 | 0,09 | 0,10 | 0,18 |
| $TiO_2$ | 0,14 | 0,17 | 0,25 | 4,67 | 0,47 | 14,20 | - | 1,88 | 2,83 |
| $Cr_2O_3$ | 54,55 | 55,80 | 56,29 | 48,06 | 36,79 | 25,57 | 55,16 | 43,26 | 42,89 |
| ZnO | 0,06 | 0,11 | 0,30 | 1,59 | 3,44 | 6,66 | 8,28 | 8,64 | 10,22 |
| Total | 100,76 | 99,49 | 99,88 | 98,71 | 100,39 | 94,91 | 98,00 | 99,01 | 97,12 |
| Cation proportions, total oxygen = 4 | | | | | | | | | |
| $Fe^{2+}$ | 0,4 | 0,4 | 0,8 | 1,0 | 0,9 | * | 0,8 | 0.8 | 0,7 |
| $Mg^{2+}$ | 0,6 | 0,6 | 0,2 | tr | tr | | tr | tr | tr |
| $Zn^{2+}$ | tr | tr | tr | 0,04 | 0,1 | | 0,2 | 0,2 | 0,3 |
| $Fe^{3+}$ | 0,1 | 0,1 | - | - | 0,7 | | - | 0,3 | 0,2 |
| $Cr^{3+}$ | 1,4 | 1,4 | 1,6 | 1,4 | 1,1 | | 1,8 | 1,3 | 1,2 |
| $Al^{3+}$ | 0,5 | 0,5 | 0,4 | 0,5 | 0,2 | | 0,2 | 0,3 | 0,4 |
| $Ti^{4+}$ | tr | tr | tr | 0,1 | tr | | - | 0,1 | 0,2 |

*) Chlorite and titania replaced part of the grain, and zircon was introduced in a dendritic manner

(Mg,Fe)-bearing chromite.

In a borehole core of Simmer and Jack G.M., the rocks bordering an intrusive body and the pyritic horizon close to the dyke, are conspicuously stained in a brilliant to moderate green. Chromium apparently migrated over a few millimetres into the bordering quartzite.

*3.3.3. Zircon*

Mineralogical details on zircon are presented in Table 27. Because zircon is generally smaller than chromite, it may occur in the extreme distal facies in the absence of the latter mineral.

The metamict zones in the zoned zircon grains may represent hydroxylated thorian zircon (Table 59), analysis no. 3). Qualitative EMP analysis by Mihalik (1968) on such a zone disclosed the presence of major yttrium, calcium, phosphorus (suggesting replacement by an Y-phosphate), less aluminium, and subordinate uranium, thorium, silicon, magnesium, iron, hafnium and zirconium.

*3.3.4. Tourmaline*

Several of the detrital tourmaline grains are overgrown syntactically in optical continuity. The mineral also precipitated as radiating prismatic aggregates, which formed at the expense of chlorite in the Booysens Shale, East Rand G.F., where it is associated with shearing and microfaulting, and in the Kalkoenkrans Reef, Oryx G.M. (Smits & Grimbeek, 1987). Optical properties and the XRD pattern fit the dravite species best.

*3.3.5. Graphite*

Except in the Kalkoenkrans Reef, Oryx G.M., graphite is extremely rare in the reefs (Table 28). The microspherulitic and fine-grained flaky textures of allogenic graphite enclosed by detrital quartz (Figs. A.15a to f) are a striking inherited feature not reported before. This type of textures has been described by Weis (1980) for graphite in Precambrian gneisses.

3.4. Polymineralic Speroids

Polymineralic spheroids (Figs. A.16a to h) are a common and conspicuous constituent in the Kimberley reefs of the Turffontein Subgroup, and occur as far apart as the OFS G.F.

Table 27 Mineralogical data of zircon in the CRG reefs

| | |
|---|---|
| (1) Mode of occurrence | Well-rounded (Fig. A.21b) or euhedral detrital grains (Figs.A.13c and d) occur in the heavy-mineral fraction and in the matrix. Grain size ranging from 0,07 to 0,50 mm |
| (2) Textural varieties | i. unzoned crystalline grains in pinkish grey or pale red purple resistant to geochemical processes Fig.A.12g)<br>ii. zoned purplish zircons in which radioactive, metamict zones alternate with unreactive zones. Radioactive zones are dull, opaque and contain minute radiogenic galena inclusions (Figs.A.13d and A.17e)<br>iii. zircons (<0,05 mm) of bipyramidal prismatic habit enclosed in q, py, rarely rut-lc, and in some of the spheroids |
| (3) Fracturing | Cataclastic zircons (Fig.A.17e) common. Fractures filled by authigenic sulphides, gold (Fig. A.17e), rut and ph.sil. In some, fracturing is due to an increase in volume as a result of metamictization (Fig.A.13d) |
| (4) Distribution | Detrital zircon present in heavy mineral concentrations; smaller grains in quartzites |

Table 28 Textural varieties of graphite in the CRG reefs

| Morphology | Size, mm | Remarks |
|---|---|---|
| (1) Flaky detrital grains | <0,15 | In Elsburg and Basal Reefs, OFS G.F. (Schidlowski, 1967) |
| (2) Intergrown with chl in microstylolites along matrix grains (Figs. A.14a to d), and as intergranular filling in quartzite pebbles (Kalkoenkrans Reef, Oryx G.M.) | <0,50 | Metamorphic product of carbonaceous matter. Minute monazite, py, and gn are dispersed in intergrowth (Figs. A.14c and d) |
| (3) Round particles and elongated fragments up to 0,3 mm long of spherulitic and flaky microtextures: | | Only in Kalkoenkrans Reef, Oryx G.M. The round particles are enclosed in detrital quartz and hence inherited from the source rocks |
| i. aggregates of minute, non-oriented flakes (Figs. A.15a and b), | | |
| ii. aggregates of spherules (0,01 mm) of radiating graphite embedded in finer-grained granular graphite. The grains are covered by a 0,01 mm wide film of columnar graphite (Fig. A.15c) | | |
| iii. flaky intergrowth of graphite and chl embedded in spherulitic graphite (Fig. A.15d) | | |
| iv. irregular-shaped particles of randomly oriented, flaky graphite grading into spherulitic texture (Figs. A.15e and f) | | A similar type of graphite is found in thin veinlets intersecting meta-greywackes in rocks of the Barberton Mountain Land (Figs. A.15g and h) |

(Smits & Grimbeek, 1987) and the East Rand G.F. They have also been noticed on rare occasions in the Vaal Reef. The spheroids, the dimensions of which range from 0,5 to 2 mm, are mainly associated with heavy-mineral concentrations, but also are found in areas devoid of pyrite. They are considerably larger than the accompanying compact pyrite. The composite particles may display a shape compatible with original crystal faces. Some exhibit a cubic habit (Figs. A.16b and c), others are six-sided (Figs. A.16d and e). The former could represent chloritized garnet, a common constituent of the Dominion Reef (Fig. A.8h); a few of the spheroids indeed enclose remnants of garnet. The six-sided grains remind of olivine crystals.

The spheroids are mainly made up of phyllosilicates, which enclose small, irregular-shaped grains <70 μm of titania, quartz, apatite, zircon, pyrrhotite, galena, sphalerite, chalcopyrite, and rarely remnants of garnet. The sulphides could be of authigenic origin, but all other inclusions were inherited. Only apatite may occur as euhedra (Fig. A.16f). In many of the spheroids, the phyllosilicate occurs in a concentric fashion around a core of a different mineral composition (Figs. A.16a, b, d, g, and h). Several possess a core enriched in light brown to pale greenish yellow rutile prisms embedded in sericite, pyrophyllite, quartz, or a mixture of these minerals (Figs. A.16g and h).

### 3.5. Gold

The *gold mineralization* has been studied by many. The most important publications are from Liebenberg (1955), Ramdohr (1955), Pretorius (1976), and Utter (1978). The modes of occurrence of the gold are listed in Table 29.

Microscopic studies clearly indicate that most of the gold occurs in the heavy-mineral concentrations that were deposited on the major unconformities before the pebble fraction of the overlying basal reef (Pretorius, 1976). Part of this gold has been captured by the microorganisms which developed in certain areas on the palaeosurfaces (Hallbauer, 1975). In the proximal facies of the midfan sector, the gold occurs in heavy-mineral concentrations enriched in buckshot pyrite and rutile-leucoxene pseudomorphs, and in the distal facies, it is less abundant and

Table 29 Mode of occurrence of gold in the CRG reefs

| Morphology | Size, mm | Mineral association | Remarks |
|---|---|---|---|
| Detrital gold | | | |
| (1) Discrete grains at q boundaries (Fig. A.13e) | 0,05 to 0,08 | | In heavy-mineral concentrations at the base of the reef unit or individual beds, less commonly in the the matrix cementing the pebble fraction |
| (2) Inclusions in compact py (Figs.A.7a and A.13f) concretionary py (Fig. A.7f), also together with gn and po, in cob (Fig. A.17a) as single inclusions with separate cp inclusions, in rare detrital pn (Fig. A.17b), and in tantalaeschynite (Fig. A.8g) | <0,05 | cp, gn, po | |
| Recrystallized gold | | | Recrystallized gold is in the Carbon Leader associated with cp or gd (Oberthur, 1983), in the West Rand G.F. with po (Tucker, 1980), in the Basal Reef with gd, in the Vaal Reef with po and gd, and in the Black Reef with sl (liebenberg, 1972). Authigenic py either younger or older than reconstituted gold |
| (1) As irregular-shaped discrete grains locally with crystal faces (Figs.A.13g and h, A.17c) | | cp, gn, sl, pn, po, gd | |
| (2) Composite grains with authigenic sulphides other than py (Figs. A.18a and b), or gd (Fig. A.9b), tucekite (Feather, 1976), or ph.sil. (Fig. A.3c) | | | |
| (3) Filling fractures or voids in detrital grains (Figs. A.17d to f) | | | |
| (4) In kerogen, it fills interfilamental space (Fig. A.17g) and other voids (Fig. A.17h); it also occurs at the surface of kerogen (Fig. A.18b). It is fibrous or platy (Fig. A.18c), spongy (Hallbauer, 1981; Utter, 1978), and frosted (A.18c) | 0,05 to 0,20 | | At the base of, or at false footwalls within the reef, a large portion of the gold is associated with kerogen |
| (5) Precipitation onto the surface of detrital cob (Fig. A.18d) or py (Fig. A.18e), followed by precipitation of gd or py resp., or enclosed in gd itself (Fig. A.9b) | | | |
| (6) When abundant, gold cements other minerals (Fig. A.18f) | | | |

associated with kerogen and uraninite. In both environments, the amount of gold in the heavy-mineral concentrations overlying the footwall quartzite exceeds that within the reef itself by far, sometimes by a hundred times or more (Table 39, last column), in particular when associated with kerogen seams.

Gold is also found in small quantities in heavy-mineral concentrations which occasionally accumulated on top of the reef, and, in larger amounts in some of the pyritic laminations and foresets in quartzites of the channel facies. Examples of the first mode of occurrence are concentrations in the U-seam overlying the UE1a Reef, West Rand G.F., and those that accumulated on top of the Upper Reef of the Dominion Reef (Fig. A.8h). Uraninite is the major component of these concentrations, the gold grade of which is very low.

Except when it occurs in association with kerogen seams, the gold is invisible in handspecimens of the conglomerates. The morphology of the grains varies greatly. The gold grains can be rounded, abraded, or display scratches and scales at the surface while, on others, crystal faces (Fig. A.13h) may have been preserved (Utter, 1978). Because of its malleable nature, grains were battered and protruding edges became bent or folded during the exogenic cycle, whereas the recrystallized gold in kerogen has a moulded texture (Fig. A.17h). The gold can be porous, and may contain microscopic inclusions of sulphide, gersdorffite, rutile, and rarely xenotime (ibid.).

Hallbauer and Joughin (1973) studied the *size distribution* of gold, and established that the grain size ranges from 5 to 500 μm, but that larger particles do occur. The majority of the grains fall in the 50 to 80 μm range, and 25% can be as large as 100 to 200 μm (Hallbauer *et al.*, 1978). The median lies in the Carbon Leader at 70 μm (Oberthur, 1983). In the Elsburg reefs in Cooke Section, the grain size ranges from 40 μm to 1,242 mm, with respective means for the UE1a Reef and the E9 Reef of 82,5 and 89 μm (Tucker, 1980). In the present study, an authigenic gersdorffite particle enclosing hundreds of gold specks of a submicroscopic size, <1 μm, has been found once in the Basal Reef.

Details on the *chemical composition* of the gold are summarized in Table 30 and the variation in fineness in Table 31, where it is compared with values of recent placers and greenstones in Zimbabwe and the Barberton Mountain Land. The silver content of the gold is fairly constant and averages about 10% (Schidlowski, 1968; Saager, 1969). Studies on the silver concentration in gold in reefs of the Klerksdorp G.F. (Utter, 1978) and the Carbon Leader (Oberthur, 1983) indicate that the fineness values range from 750 to almost silver-free gold within the reefs (Utter, 1978). Until now the variation in silver content could not be linked with any specific sedimentological or mineralogical phenomenon. The former assumption that part of the gold originates from the reworking of stratigraphically lower sediments could not be confirmed by these and other studies (Krapez, 1979; Hirdes, 1984).

3.6. Platinum Group Minerals

The Black Reef at the base of the Transvaal Sequence is by far the richest platinoid-bearing conglomerate and can be called a platinoid placer (Reimer, 1979). The combined grade of the platinum group elements (PGE) in the Kimberley Reef on Evander G.F. is about 0,1 g/t, which is comparable with recent low-grade placers. The tenor of the reefs on the Klerksdorp G.F. is the lowest. Platinum group minerals (PGM) have not been found in the Dominion Reef (ibid.).

Mineralogical data of the PGM are summarized in Table 32. Feather (1976) studied the mineralogy of the PGM in depth, whereas Koen (1964), Cousins (1973) and Reimer (1979) interpreted various features of the PGM mineralization.

Alloys of the osmium-iridium and the platinum-iron series, and sperrylite, $PtAs_2$, are the major constituents. Sperrylite and isoferroplatinum make up 15 to 20% of the platinum-bearing grains (Feather, (1976). Oberthur (1983) distinguished two types of sperrylite, one of detrital, and the other of authigenic origin. All PGM show marked deficiency in palladium.

The spread for each PGE, as indicated by the analytical data for PGM concentrates of the Main, Bird, Kimberley, Elsburg, VCR, and Black Reefs, is summarized in Table 33 (Cousins, 1973).

Table 30 Chemical composition of gold particles in the CRG reefs

| Ag* | Hg | Cu | Fe | Reference |
|---|---|---|---|---|
| 0,30 to 32,10% | | | | Viljoen, 1971 |
| | 0,27 to 4,60% | | | Erasmus et al., 1986 |
| | 1,20 to 5,90% mean: 3,10% | 75 to 2500 g/t | | Oberthur & Saager, 1986 |
| | | 75 to 2500 g/t | | Oberthur, 1983 |
| | | | 125 to 3260 g/t | Oberthur, 1983 |
| Elements less than 0,10%: Mn, Fe, Co, Ni, Zn, Pb, As, Bi, Te, Sr, Ba, Sn, and Si | | | | |
| Rare elements : Pt, Al, Cd, Ti, Se, Pd, V, and Mo | | | | |

*) Silver content of Barberton gold ranges from 3,60 to 21,60%. Variation in silver content of individual Barberton deposits is smaller than that in a single handspecimen from the Witwatersrand ores (Viljoen, 1971)

Table 31 Fineness* of gold from placers and hydrothermal veins

| Origin | Range of fineness | Reference |
|---|---|---|
| Vaal Reef | 750 to 1000 | Utter, 1978 |
| Other Witwatersrand reefs | 880 to 970 | Erasmus et al., 1982 |
| Witwatersrand reefs and recent placers | 850 to 925** | Reimer, 1984 |
| Greenstone belts in Zimbabwe and South Africa | 825 to 950** | Reimer, 1984 |
| Berberton Mountain Land | 757 to 983 | Gay, 1968 |

*) Fineness: 1000 x Au/Au+Ag
**) Median values

Table 32 Data on platinum group minerals in the CRG reefs

| | |
|---|---|
| (1) Mode of occurrence | PGM occur chiefly as detrital grains 0,01 to 2,00 mm in diameter (Pretorius, 1976); average size 0,058 mm (Cousins, 1973). Rarely as authigenic sperrylite, PGE-sulphides and -arsenides, which formed from less stable tellurides and antimonides (Feather, 1976) |
| (2) Shape of grains | Well-rounded, spherical, hexagonal, dumbell-shaped, and irregular-shaped (Koen, 1964) |
| (3) Inclusions | Sulphides, silicates, phosphates (Reimer, 1979) and most commonly gold |
| (4) Type of PGM | Alloys (Koen, 1964; Cousins, 1973; Barras, 1974; Feather, 1976), sulphides, and composite sulphides combined with alloys (Reimer, 1979). Grains usually combined with two or more minerals, some of which are zoned. Most common zoned species made up of Os-rich core surrounded by an (Ir,Pt)-rich outer zone, mixed with exsolution lamellae of a (Pt,Fe)-alloy (Feather, 1976) |

Table 33. Compositional range of PGE from Main, Bird, Kimberley, Elsburg, VCR, and Black Reefs (Cousins, 1973)

| Element | Mass, % |
|---|---|
| Os | 28 to 45 % |
| Ir | 28 to 41 % |
| Ru | 9 to 22 % |
| Pt | 5 to 23 % |
| Rh | 0,5 to 1,3% |
| Pd | trace amounts |

## 3.7. Uranium-bearing Minerals

Major contributions to the mineralization of the uranium-bearing minerals have been made by Liebenberg (1955), Ramdohr (1955, 1958a), Schidlowski (1966a to c), Hiemstra (1968), Feather (1976), and Smits (1984a and b, 1985a to c).

In the present study, the following uranium-bearing minerals were identified in reefs mined for gold and uranium:

uranium oxide, as
*uraninite*, $(U,Th)O_2$:
discrete grains in the matrix, or
enclosed by kerogen
*pitchblende*, $UO_2$

uranous titanate, $(U,Th)_{1-x}Ti_{2+x}O_6$, as
*uraniferous leucoxene* ($UO_2/TiO_2$ <1), and
*brannerite* ($UO_2/TiO_2$ >1)

anhydrous, $(U,Th)SiO_4$, and hydrated (U,Th)-silicates.
$(U,Th)SiO_4.nH_2O$ (n<4), as
*hydrated uranoan thorite* and *thorogummite*, and
*anhydrous* and *hydrated thorian coffinite*

*(Zr,Th)-silicates*, $(Zr,Th)(SiO_4)_{1-x}(OH)_{4x}.nH_2O$
(x=0,2 to 0,8) as *hydrated thorian zircon*.

Detrital uraninite and authigenic uranous titanates are the major uranium carriers today found in the reefs of the CRG. They occur in approximate equal amounts in most reefs exploited for uranium, but if kerogen seams are absent, the volume of the uranous titanates may exceed that of uraninite. Except for the thorogummite, which has only been identified in the Dominion Reef, and the rare uranoan thorite grains in reefs of the CRG and the Dominion Reef, the (U,Th)-silicates are of authigenic

origin. Zoned zircons, the metamict zones of which are usually hydrated (Zr,Th)-silicates mixed with an Y-phosphate, are common detrital constituents of the reefs of the CRG and the Dominion Reef, whereas the detrital thorian zircon has only been identified in the Dominion Reef.

Pitchblende and secondary coffinite of relatively recent supergene origin have been found in the Monarch Reef on the East Champ d'Or G.M.

Hydrated uranyl minerals are absent in the reefs but, in places, fill hairfine cracks in the rocks. Schoepite, $UO_3.2H_2O$, is the most common species.

All uranium-bearing minerals are pigmented by minute particles of galena on average <10 μm in diameter which formed from radiogenic galena released in the course of geologic time during autooxidation. Hence, small specks of galena occurring anywhere in the rock suggest the presence of uranium or thorium. In many instances the specks of galena coalesced to larger-sized grains (Fig. A.19a) or accumulated in cracks (Figs. A.19c and A.22c) or at the surface of the grains (Figs. A.19b and A.28b).

*3.7.1. Uraninite*

In reefs of the carbon-seam type, a large portion of the detrital uraninite is encapsulated by kerogen which, up to this date, shielded the grains from their environment. The uraninite also occurs in large, well-packed clusters in the absence of kerogen and other heavy minerals in the gritty facies of the Monarch Reef, West Rand G.F. (Figs. A.19c and A.28a), and in thin heavy-mineral concentrations which, as was mentioned earlier, overlie the Upper Reef of the Dominion Reef (Fig. A.8h) and the UE1a Reefs on the West Rand G.F.

Mineralogical information about uraninite is summarized in Table 34, and the analyses done by Mintek in 35. In Table 36, range and average values of various parameters for $UO_2$, $ThO_2$, and $PbO_2$ of uranium-bearing conglomerates of the Elliot Lake District, Canada, and the reefs in the Witwatersrand are compared.

The cell size of the uraninite from the Vaal Reef is 5,4683A (Grandstaff, 1976), that of the Dominion Reef 5,46A

Table 34 Mineralogical data of uraninite in the CRG reefs and the Dominion Reef

| | |
|---|---|
| (1) Mode of occurrence | Single, isolated particles (Fig. A.19a), groups of 5 to 50 grains (Fig. A.19b), or large clusters of 500 or more grains (Fig. A.19c);<br>i. in the matrix (Figs. A.19a to c), or<br>ii. enclosed by ker (Figs. A.19d and A.21a, e to h) |
| (2) Morphology | Rounded (Fig. A.19a), muffin-shaped (Fig. A.17f), ot sub- to euhedral (Fig. A.14e). Grain size <0,35 mm; average in CRG reefs 0,075 mm, and in Dominion Reef 0,1 mm |
| (3) Texture and mineral association | Some ur grains show cataclastic habit (Figs. A.19f to h); others are leached along crystal planes. Open space filled by q (Figs. A.19g and A.20a), gold (Fig. A.17f), ur. tit. (Fig. A.20 ), cf (Fig. A.19f), or sulphides (Fig. A.19a). |
| (4) Alteration | Partly or entirely leached grains in the matrix, referred to as relict uraninite (Figs. A.20d and e); replacement by authigenic ur. tit. (Figs. A.15c and d), thorian cf (Figs. A.27d and g), or sulphides (Fig. A.20f); supergene alteration to pitchblende and cf (Fig. A.28c). Shape of original detrital ur from which uranium was leached is defined by cutans of gd (Figs. A.23a, A.20d and e), or ur. tit. (Fig. A.17f). |
| (5) Distribution | Ur enclosed by ker occurs at the base of, or at false footwalls within the reef before deposition of the pebble fraction of the conglomerate. Ur also occurs dispersed throughout the reef, following the distribution pattern of heavy minerals. In places, ur-rich layers up to 1 cm thick overlie the reef, e.g. the Upper Reef of the Dominion Reef (Fig. A.8h; Hiemstra, 1968) and the UE1a Reef, Cooke Section (Tucker, 1980). Large clusters (Fig. A.19c) are common in the Monarch Reef, West Rand Consolidated G.M. |

Table 35 Electron-microprobe analyses of uraninite in the CRC reefs

| Reference | $UO_2$ | $ThO_2$ | PbO | $SO_3$ | $Y_2O_3$ | $P_2O_5$ | $SiO_2$ | $Al_2O_3$ | FeO | $TiO_2$ | CaO | Total |
|---|---|---|---|---|---|---|---|---|---|---|---|---|
| Bv conct.• | 71,40 | 3,30 | 14,20 | 2,00 | 0,60 | n.d. | 1,30 | 1,20 | 2,30 | n.d. | 0,80 | 97,10 |
| Bv conct. | 75,95 | n.d. | 18,41 | 2,24 | 0,77 | 0,09 | 0,41 | 0,06 | 0,95 | 0,24 | 0,35 | 99,47 |
| Bv conct. | 80,12 | n.d. | 13,22 | 0,42 | 0,64 | 0,10 | 0,53 | 0,04 | 0,86 | 0,20 | 0,94 | 97,07 |
| Bv conct. | 79,15 | n.d. | 15,55 | 2,01 | 0,52 | 0,11 | 1,04 | 0,09 | 1,00 | 0,59 | 0,66 | 100,72 |
| VRE | 59,38 | n.d.† | n.d. | 0,60 | n.d. | n.d. | 1,15 | 1,78 | 1,15 | 0,79 | 0,65 | 65,50‡ |
| VRE | 65,82 | n.d. | n.d. | 1,38 | n.d. | n.d. | 4,01 | 5,87 | 1,41 | n.d. | 0,71 | 79,20‡ |
| Rf 605 | 66,88 | n.d. | 3,62 | 0,79 | 1,73 | 1,22 | 4,45 | 0,37 | 1,03 | – | 1,64 | 81,73§ |

conct. Concentrate n.d. Not determined – Not detected Bv Blyvooruitzicht VRE Vaal Reefs East Rf Randfontein

• From chemical analysis of the Blyvooruitzicht concentrate

† The average thorium oxide content of uraninite is 2,7 per cent

‡ Totals are low because the contents of galena and thorium oxide were not determined; together they amount to approximately 20 per cent

§ Trace amounts of coffinite and churchite are present

Table 36 Compositional data on uraninite in sediments of Early Proterozoic age (values in percentages)

| | Blind River, Canada | Witwatersrand, South Africa | | | | | | |
|---|---|---|---|---|---|---|---|---|
| | | | | | Simpson and Bowles , 1977 | | | |
| | Grandstaff 1974 | Liebenberg 1955 Main Reef and Carbon Leader resp. | Grandstaff 1974 Vaal Reef | Feather 1976 average of several U-bearing reefs | Uraninite, Dominion Reef* | Uraninite, Vaal Reef | Pitchblende† intercolumnar carbon, Vaal Reef | Pitchblende in kerogen, Carbon Leader |
| $UO_2$ | 58,0 to 69,0 | 66,7 to 74,1 | 55,0 to 77,0 | 61,0 to 77,0 | 63,3 | n.d. | n.d. | n.d. |
| $ThO_2$ | 4,0 to 9,0 | 1,6 to 2,7 | 0,8 to 11,0 | 0,4 to 10,2 | 5,4 to 8,4 | 0,9 to 9,1 | 3,2 to 6,9 | 1,1 to 2,9 |
| Median $ThO_2$ | n.d. | n.d. | n.d. | n.d. | 6,6 | 3,5 | 6,3 | 2,0 |
| $UO_2$-$ThO_2$ | 8,0 to 12,0 | 40,9 to 27,4 | 10,0 to 40,0 | 6,4 to 47,4 | 6,4 to 10,9 | 8,3 to 48,0 | 6,2 to 12,2 | 25,0 to 69,0 |
| Median $UO_2$-$ThO_2$ | n.d. | n.d. | n.d. | n.d. | 8,5 | 19,0 | 9,0 | 33,0 |
| $PbO_2$ | n.d. | 18,1 to 15,5 | n.d. | 9,8 to 30,4 | 7,0 to 24,0 (PbO) | n.d. | 10,0 to 25,0 (PbO) | 7,0 to 10,7 (PbO) |

* Data from Hiemstra (1968)
† Pitchblende refers to poorly crystalline uraninite of low thorium content
n.d. = Not determined

(Hiemstra, 1968). For sedimentary uraninite devoid of thorium, it is 5,406A, and for hydrothermal, thorium-poor uraninite 5,437A (Berman, 1957). The high thorium content of the Witwatersrand uraninite is responsible for the high cell parameters.

The composition of uraninite ranges from $UO_2$ to $U_3O_8$ ($UO_{2,67}$). Oxidation above this limit is caused by autooxidation. During the process, each $UO_2$ unit disintegrates to radiogenic PbO and releases an oxygen atom which becomes available for the oxidation of one $UO_2$ unit to $UO_3$ (Berman, 1957). The information available on the $UO_3$ content in percentage of Witwatersrand concentrates is presented in Table 37.

Table 37. $UO_2$, $UO_3$, and PbO contents of uraninite concentrates of the Dominion, Main, Vaal, and Carbon Leader Reefs

| Reef | $UO_2$ | $UO_3$ | PbO |
|---|---|---|---|
| Dominion Reef | | | |
| Hiemstra (1968) | 17,10 | 46,29 | 14,85 |
| Laxen (1972) | 46,99 | 11,14 | 15,88 |
| | 41,50 | 9,30 | n.d. |
| Main Reef | | | |
| Laxen (1972) | 57,05 | 0,68 | n.d. |
| Vaal Reef | | | |
| Grandstaff (1974) | 23,20 | 46,90 | 21,00 |
| Carbon Leader | | | |
| This study | 59,40 | 12,80 | 14,20 |

n.d. - not determined

The analytical data done at Mintek (analyses from Laxen and this study) differ from those done by Hiemstra (1968) and Grandstaff (1974). The wide range in values cannot be explained.

The thorium content of the uraninite in the reefs of the CRG varies, but the variation is the same, whether it occurs in

the matrix or in the kerogen (Grandstaff, 1974). The respective average $UO_2$ contents as calculated by Feather (1976) from EMP analyses, are 69,5 and 67,2%, which is lower than the chemical and EMP analyses done at Mintek on the concentrate from Blyvooruitzicht G.M. (Table 35).

The uraninite grains in the matrix, which are not mantled by kerogen, were evidently exposed to surficial processes, as is indicated by the abundant presence of grains that were leached. In this thesis, this type of grain is referred to as *relict uraninite* (Figs. A.20d to f, A.23a and b). Part of, or all the uranium was removed from the precursor uraninite, the shape of which was preserved by cutans composed of gersdorffite or uranous titanate (Smits, 1984a and c, 1986). The term cutans was introduced by Brewer (1960) for coatings on grains, aggregates and walls of voids, which form in the lower portion of the soil horizon in weathering profiles. They precipitate *in situ* from downwards percolating, supersaturated solutions or from upward evaporation of such solutions through capillary activity. Unrestricted circulation is required for the formation of cutans.

In most of the relict uraninite grains some uranous titanates precipitated just inside or outside the cutan, whereas the inner portion was filled by quartz or chlorite (Figs. A.23a and b).

*3.7.2. Uraninite-bearing Kerogen*

Hallbauer and Van Warmelo (1974) have shown convincingly that the kerogen represents fossilized remains of primitive life. Zumberge *et al.* (1978) established that the organic matter had formed from ancient algal or bacterial colonies which had been subjected to thermal degradation under the influence of progressive burial and irradiation through radioactive decay of the enclosed uraninite.

The kerogen contains 60 to 70% carbon, 7 to 9% oxygen, and 3,5 to 4% hydrogen (Liebenberg, 1955; Snyman, 1965). These figures fall in the category of coal, the oxygen content of which varies between 7 and 30%, and that of hydrogen between 2 and 5% (Vassilou & Kerr, 1972).

Uraninite-bearing kerogen occurs as nodules, the 'fly speck' carbon, in both subgroups of the CRG on all goldfields (Table 38), and as seams, which are only found at the base of the following reefs in the Johannesburg Subgroup in the western portion of the Witwatersrand Basin, i.e. the Basal Reef and Leader Reef on the OFS G.F., the Vaal Reef on the Klerksdorp G.F., and the Carbon Leader on the West Wits Line G.F. The sedentary type of kerogen - the seams - developed before the pebble fraction of the overlying reef was deposited at major unconformities or at false footwalls within the reef unit. This process was contemporaneous with the concentration of the heavy minerals, which preceded the sedimentation. The two nodular varieties (Table 38) occur dispersed throughout the reef. The one represents single uraninite grains overgrown by organic matter (Fig. A.21a), the other fragments of seams that were broken up probably during periods of reworking of older sediments (Fig. A.21b).

The kerogen nodules in the reefs of the Turffontein Subgroup and the VCR have been altered after final deposition. The uranium present in the uraninite fragments enclosed by the kerogen reacted and reprecipitated in (Fig. A.22g), or just outside the nodule as coffinite (Fig. A.27h) or uranous titanate (Fig. A.22e). The authigenic coffinite may also occur in the kerogen nodules as minute wavy laths (Fig. A.24b) often elongated in the direction of apparent growth of the organic matter (Fig. A.24f). In the UE1a and E9 Reefs, West Rand G.F., the alteration was so severe that most of the kerogen was replaced by quartz and fine-grained phyllosilicate (Figs. A.24c to e). This type of relict kerogen nodules has not been noticed elsewhere in the basin. When kerogen is exposed to the atmosphere, it loses its specific optical characteristics and becomes homogeneously black in colour, a feature which is found in the reefs of the Turffontein Subgroup (Fig. A.24a).

The uraninite grains and fragments enclosed by the kerogen are responsible for the conspicuous optical properties of the latter. The undulose extinction resembles that of graphite, but the light olive grey reflecting colour differs from the typical silky, light brown reflectance of graphite. XRD patterns

Table 38 Mineralogical data of uraninite-bearing kerogen in the CRG reefs

| | Sedentary kerogen | Nodular kerogen |
|---|---|---|
| (1) Morphology | Ker seams (Figs. 5b and A.20g) of a thickness ranging from hairline to 12 cm (av. 5 mm) cover areas of a few mm² to m². The ker rarely cements pebbles at the base of the conglomerate | Discrete nodules <1 mm (Figs. A.21a and b). Liebenberg (1955) referred to them as 'fly speck' carbon |
| (2) External structure | Curved columns (Figs. A.20g and A.21c) perpendicular to bedding planes impart a fibrous appearance in handspecimen. Under the SEM, the ker is finger-shaped (Fig. A.21d; Hallbauer, 1975). In Beisa Reef (Fig. 5b) layers of curved, filamentous texture, <2 cm thick, are stacked and separated by a thin film of clay ( 0,05 mm). | Two types of nodules are distinguished:<br>i. ker enclosing single ur grains (Fig. A.21a), and<br>ii. fragments of ker seams that were broken up, in which the grain boundary intersects the fragmented ur (Fig. A.21b) |
| (3) Microscopic texture | Under the microscope the ker is segmented. In crossection the columns are oval (Figs. A.21e to h). Boudinage in vertical direction is displayed by;<br>i. minerals enclosed by ker such as, sl (Fig.A.8a), zr (Fig. A. 8a), authigenic q infilling space in ker (Fig. A.24g), in which the void was filled with authigenic chl, or ker (Fig. A.24g), and<br>ii. neighbouring minerals or pebbles: py (Fig. A.24h), refilled by q, zr refilled by py (Fig. A.25a), q pebble (A.24h) refilled by po or by ker (Fig. A.25b) | |
| (4) Enclosed mineral | Ur was the only mineral which became encapsulated by the organic matter. It is usually fragmented (Figs.A.19d, A.15a and g) but, at bottom and top of the seams, they are less fragmented (Fig. A.19d). | Fragmented ur common (Figs. A.21a and b) |
| (5) Intergrowths and intercolumnar filling | Ur-bearing ker is intimately intergrown with ph.sil. (Figs. A.22a and b). Gold (Figs. A.17g and h), in places associated with gd, pn, or po (Fig.A.18b), mobilized radiogenic gn (Fig. A.22c), authigenic ur. tit. (Fig. A.22d), and rarely other detrital constituents (Fig. A. 8a) occur in interfilamental spaces or voids in the ker. Sometimes segmented columns alternate with ker of fibrous texture enclosing minute particles of ur, py, or gold (Fig. A.22d) | Ker intergrown with ph.sil. |
| (6) Cleats | Cleats measuring 0,01 by 0,15 mm developed locally parallel to the bedding plane (Figs. A.21e and A.23g) | |
| (7) Alteration | Some of the enclosed ur grains were replaced by authigenic ur. tit. (Figs. A.22e and f) or cf (Figs. A.22g and h); both precipitated at the expense of ker. Locally the ker was subjected to temperatures higher than the metamorphic one; it acquired an anthracitic reflectance (Figs. A.22e and A.23g). In the Elsburg Reefs, West Rand G.F., the ker precipitated at the expense of py (Fig. A.24b) | In some reefs the ker nodules have have been oxidized (Fig. A.24a) as is indicated by the black colour. In the UE1a Reef, West Rand G.F., ker nodules were partly or almost completely replaced by q and ph.sil. (Figs. A.24c to e) |

confirm that the kerogen did not reach the final maturation state, i.e. graphite. The reflectance values of the kerogen ranges from 8,1 to 10,5%, whereas kerogen near a dyke may attain values up to 25% (Fig. A.23g). The reflectance of kerogen in contact with uranous titanate is usually much lower (Fig. A.22d). In the Elliot Lake deposits, they range from 3,5 to 6%.

The kerogen in contact with the uraninite it envelopes is usually of smooth optical appearance and forms a radiating fibrous aureole around the fragments (Fig. A.21e), a feature which imparts a segmented texture to the sedentary kerogen (Fig. A.21e to h). If the uraninite particles are very small and numerous, the kerogen extinction is of mottled appearance (Figs. A.22c and d).

The residue of sedentary uraninite-bearing kerogen, which has been ashed to 300$^0$C, consisted of (1) greenish-grey to medium-grey phyllosilicate of platy habit (Fig. A22a), (2) equant fragments of black uraninite (Fig. A.22b), (3) gold in thin scales (Fig. A.18c) or fibres, which were moulded by the organic matter (Fig. A.17h), and (4) rarely pyrite oxidized to hematite or other heavy minerals.

Chemical data of uraninite-bearing kerogen are listed in Table 39, and those of kerogen itself in Table 40.

Kerogen which does not enclose uraninite fragments is extremely rare (Figs. A.23c to f). It is structureless and homogeneous. Its reflectance is much lower than that of the uraninite-bearing kerogen, but higher than the non-uraniferous carbon present in the much younger Black Reef at the base of the Transvaal Sequence. In contrast with the fairly smooth, rounded top and bottom surfaces of the seams (Figs. A.21c and d), the surface of the non-uraniuferous kerogen is spongy (Fig. 23d) or frayed (Fig. 23f). It occurs on its own (Figs. 23c and e), or as an overgrowth on uraninite-bearing kerogen (Fig. 23f) or on detrital minerals (Figs. 23h and 29g), and hence is younger than the kerogen which encapsulates uraninite. As mentioned in Section 3.2.4., it often encloses minute crystals of authigenic gersdorffite, <40 $\mu$m (Fig. A.9h), or is covered by a film of gersdorffite crystals (Figs. A9e and f).

Table 39 Chemical analyses of uraninite-bearing kerogen in CRG reefs

| Constituent | mass. % | | |
|---|---|---|---|
| | Bf | VRS | PB |
| $SiO_2$ | 62,22 | 43,03 | 67,42 |
| $Al_2O_3$ | 3,55 | 3,03 | 2,83 |
| $Fe_2O_3$ | 6,99 | 2,26 | 3,04 |
| MnO | 0,01 | 0,03 | 0,02 |
| MgO | 0,85 | 0,34 | 0,80 |
| CaO | 0,10 | 0,11 | 0,12 |
| $K_2O$ | 0,64 | 0,44 | 0,34 |
| $Na_2O$ | tr | tr | tr |
| $TiO_2$ | 0,36 | 0,11 | 0,11 |
| $P_2O_5$ | 0,12 | 0,17 | 0,05 |
| $Cr_2O_3$ | 0,01 | 0,01 | 0,01 |
| $ZrO_2$ | 0,05 | 0,04 | 0,02 |
| $H_2O^+$ | 2,20 | 3,00 | 2,10 |
| $H_2O^-$ | 0,06 | 0,23 | 0,11 |
| $U_3O_8$ | 1,84 | 2,62 | 1,55 |
| $ThO_2$ | 0,21 | 0,25 | 0,11 |
| S | 4,60 | 1,20 | 2,10 |
| L.O.I. | 13,20 | 41,60 | 13,60 |
| | mass, p.p.m. | | |
| Value | Bf | VRS | PB |
| Au | 623 | 482 | 3 940 |
| Cu | 155 | 88 | 95 |
| Ni | 585 | 837 | 273 |
| Co | 376 | 250 | 194 |
| Zn | 2 479 | 124 | 297 |
| Ag | 92 | 41 | 448 |
| Pb | 4 732 | 3 710 | 4 791 |
| As | 1 887 | 1 980 | 703 |

Bf Buffelsfontein VRS Vaal Reefs South
PB President Brand L.O.I. Loss on ignition

Table 40 Chemical analyses of kerogen in the CRG reefs

| | 1 | 2 | 3 | 4 | 5 | 6 | 7 | 8 | 9 | 10 | 11 | 12 |
|---|---|---|---|---|---|---|---|---|---|---|---|---|
| Relative density | 2,60 | 2,60 | - | | 1,96 | 1,51 | 1,30 | 1,63 | | 1,63 | 1,68-2,30 | |
| Moisture at 110°C, % | 1,44 | 0,73 | 2,14 | 0,43 | 0,76 | 3,70 | 3,84 | 4,00 | 1,00 | 1,28 | 1,09 | |
| Volatiles, % | 13,17 | 8,51 | 14,36 | | 9,12 | 22,65 | 16,82 | 18,76 | 17,90 | 12,34 | 9,29 | 13,50 |
| Fixed carbon, % | 45,88 | 36,26 | 43,56 | 25,18 | 36,28 | 52,35 | 61,84 | 65,34 | 61,90 | 61,05 | 44,00 | 53,10 |
| Ash, % | 39,51 | 54,50 | 39,94 | 71,90 | 53,84 | 21,30 | 17,50 | 11,90 | 19,20 | 25,33 | 45,62 | 26,06 |
| Sulphur, % | | | | 1,90 | 1,22 | 1,04 | 2,32 | 2,50 | | 1,91 | 2,18 | |
| Calorific value, B.t.u. | | | | | 5 110 | 11 280 | 11 710 | 12 700 | | 12 300 | 9 090 | |
| $U_3O_8$, % | 6,88 | 6,39 | 5,93 | | | | | | 1,89 | | | |
| Gold, g/t | | | | | 369 | 9 103 | 32 | 1 073 | | | | |

B.t.u. British thermal units

1, 2 Basal Reef, resp. President Steyn and St. Helena G.M. (Liebenberg, 1955)
3 VCR, Western Reefs G.M. (Liebenberg, 1955)
4 Vaal Reef, Vaal Reefs South G.M. (Hintek, 1985)
5, 6 Carbon Leader, resp. Doornfontein and West Driefontein G.M. (de Kock, 1964)
7 Monarch Reef, Luipaardsvlei G.M. (De Kock, 1964)
8, 9 Main Reef, resp. Vogelstruisbult G.M. (De Kock, 1964) and Van Dyk G.M. (Liebenberg, 1955)
10, 11 May Reef, Vogelstruisbult G.M. (De Kock, 1964)
12 Witwatersrand (Vassilou, 1980)

### 3.7.3. *Uranous Titanates*

Uranous titanates are common in all uranium-bearing reefs of the CRG. They are virtually absent in the Dominion Reef, except for the occasional overgrowth on uraninite, the major components of which are niobium, titanium, and uranium (Mihalik, 1968; Fig. A.29a). Detrital grains of brannerite have only once been found in the Leader Reef, Harmony Complex (Figs. 29b and c). Textural data of brannerite and uraniferous leucoxene are presented respectively in Tables 41 and 42.

Liebenberg (1955) referred to the brannerite as 'secondary uraninite', whereas Ramdohr (1955) used the German term 'Uranpecherz' for both uraninite and brannerite grains. Since the uranous titanates are metamict, the two authors were not able to establish their identity. Schidlowski (1966a) established on the EMP that these minerals are (U,Ti)-bearing oxides.

The two types of uranous titanate can be distinguished by their optical properties and chemical composition. The one in which the $UO_2$ to $TiO_2$ mass ratio is less than unity is referred to as *uraniferous leucoxene* (Smits, 1984a and b, 1985a to c; Fig. 29d), the term originally used by Liebenberg (1955). Like leucoxene, these species are earthy and do not reflect in incident light, but their internal reflection varies with the increase in uranium content from yellowish grey to pale blue and medium bluish grey, whereas that of non-uraniferous leucoxene is very pale orange to dark yellowish brown. Both types of leucoxene are intergrown with phyllosilicate and quartz, and the uraniferous leucoxene can be readily recognized from the presence of specks of radiogenic galena. The uranium-rich species, the $UO_2$ to $TiO_2$ mass ratio of which lies above unity, are *brannerite* (Fig. 29e). The mass ratio for the end member $UTi_2O_6$ is 1,69. The internal reflection of these species is a striking dusky red. The $UO_2/TiO_2$ values of the Canadian uranous titanates range from 0,65 to 1,65 (Theis, 1976, 1979), whereas those found in other deposits in the world display values between 0,72 and 1,74 (Table 46).

Table 41 Textural data of brannerite in the CRG reefs

| Morphology | Size, mm | Remarks |
|---|---|---|
| (1) Spindle-shaped crystals of authigenic origin | <0,1 | Br replaced ur (Figs. A.25c and d) and rut-lc. (Fig. A.25e), q filling open space. It also formed 0,01 mm-wide films of randomly oriented prisms coating and outlining detrital chloritized py or detrital chl (Fig. g), asp* (Fig.A.8e), and chr (Fig. A.25f) |
| (2) Cryptocrystalline br of authigenic origin | | Replaced rut-lc ( 0,7 mm; Figs. A.25g and h), ur in situ (<0,1 mm; Fig. A.26a), or reprecipitated outside original grain (Fig. A.26b). Filled voids in rut-lc (Figs.A. 11f and A.26c) Formed at q grain boundaries (Fig. A.26d) |
| (3) Detrital cryptocrystalline br of authigenic origin | <0,2 | Found only in Leader Reef, Harmony Complex, close to site where reef overlies Basal Reef to form a composite reef (Figs. A.23b and c). Composition of these grains is listed in Table 45 (Har 1346) |

Table 42 Textural data of uraniferous leucoxene in the CRG reefs

| Morphology | Size, mm | Mineral association | Remarks |
|---|---|---|---|
| (1) Pseudomorphs after ur (Fig. A.26a) | <0,15 | gn, cf | Associated with:<br>i. minute specks of radiogenic gn<br>ii. small laths of po (<0,05 mm) |
| (2) Pseudomorphs after rut-lc (Fig. A.26f) | <0,50 | gn, br, lc, po | As for (1) |
| (3) Outlining detrital grains in reefs (Fig. A.26h) | | gn | As for (1) |
| (4) Coatings on detrital heavy minerals (Fig. A.17f), py in particular (Figs. A. 5h and A.7g), and ker nodules (Fig. A.27a) | | | |
| (5) Intergrowth with ph.sil. (Figs.A.27band c) | | | |

Uytenbogaardt and Burke (1971) report for brannerite a reflectance value in air of 'about 17%' as compared to 17,1% for uraninite (at a wavelength of 515 nm) and 10 to 15% for pitchblende. However, the reflectance of brannerite in the CRG is distinctly lower than that of uraninite and varies with the uranium content from about 13 to 15%.

Additional optical and physical properties of brannerite from deposits of various localities are listed in Table 43. X-ray diffraction data are listed in Table 44.

The brannerite in the Witwatersrand has been dated at 1810 Ma (Feather, 1976), against an age of 2000 Ma for the brannerite in the Blind River deposits (Mair *et al.*, 1960).

The uranium-bearing substance, which occurs at grain boundaries and in hair-fine cracks as indicated by autoradiographs or Lexan prints, is submicroscopic and hence is difficult to detect in the polished sections. Its presence is indirectly manifested when in contact with pyrite (Fig. A.5h), arsenopyrite, and chlorite, which have been corroded (Section 3.2.1.) or discoloured (Figs. 8b and c; Section 3.1.1) by the uranous titanate. Other uranium-bearing minerals in contact with pyrite, arsenopyrite, or chlorite did not cause such reactions.

Brannerite and uraniferous leucoxene are only rarely noticed in kerogen (Figs. A.22d and A.29f) and then formed at the expense of kerogen. In the reefs of the Turffontein Subgroup, the uraninite fragments enclosed in the kerogen nodules reacted and the leached uranium reprecipitated as uranous titanates (rarely as coffinite) at the surface of the kerogen nodules (Fig. A.22e). Minute particles of brannerite may also be enclosed by the younger generation of non-uraniferous kerogen (Fig. A.23f).

A phenomenon, which provides evidence with regard to the time of precipitation of the uranous titanates is noticed in some of the rutile-leucoxene pseudomorphs (Figs. A.23h and A.29g), detrital chlorite (Fig. A.30g) or chloritized pyrite, arsenopyrite, or chromite grains, and kerogen nodules (Fig. A.9f). These grains were first coated by uranous titanate, and then overgrown by the younger generation of kerogen. Another

Table 43 Properties of brannerite of occurrences elsewhere in the world

| Locality | Type of deposit | Relative density | Hardness Moh's | Crystallographic system | cell constants a° | b° | c° | Reflectance | Refractive index |
|---|---|---|---|---|---|---|---|---|---|
| Kelly Gulch, Idaho<br>Hess and Wells, 1920 | placer | 4,5-5,43 | 4,5 | tetragonal or orthorhombic | | | | | 2,26-2,30 |
| Cordoba, Spain<br>George, 1949 | pegmatite | 5,17 | | monoclinic | | | | | 2,21<br>2,39 * |
| Vosges, France<br>Branche et al., 1951 | quartz vein | 4,82 | | | | | | | |
| Mono County, California<br>Pabst, 1954 | quartz vein | 5,43 | | | | | | | |
| Bernadino County, California<br>Hewett et al, 1954 | granite gneiss | 4,76 | 5,0 | | | | | | 2,20-2,30 |
| Ontario, Canada<br>Moddle, 1957 | metasediments | 4,85 | 4,0 | | | | | | |
| Russia (mineral named Iodochnikite)<br>Soboleva and Pudovkina, 1958 | | 5,48<br>5,55 * | 5,0-6,0 | | | | | | 2,16<br>2,19 * |
| Unknown<br>Bowie and Taylor, 1958 | | | 710-730 | | | | | 13,7-16,0 | |
| Synthetic brannerite<br>Schröcke, 1958 | | | | monoclinic | 6,1 | 14,2 | 5,7 | | |
| Synthetic brannerite<br>Ostunali, 1959 | | 6,10 | | | 5,27 | 3,54 | 6,31 | | |
| Rajastan, India<br>Karkhanavala, 1959 | pegmatite | | | triclinic $P_1$ or $P_{\bar{1}}$ | 10,689 | 13,248 | 10,258 | | |
| Synthetic brannerite at 2000°C<br>Patchett and Nuffield, 1960 | | 6,36 | | monoclinic $C_{2h}^3$-C2/m | 9,87 | 3,76 | 6,95 | | |
| Crocker Wells, Australia | metasediments | 4,0-4,2 | 5,0 | | | | | | 1,95-1,96 |
| Bou Azzer, Morocco | vein | | | | | | | | 2,22 |
| Florence, Montana | placer | | | | | | | | 2,26 |
| Elk City, Idah | placer | | | | | | | | 2,26 |
| Adler and Puig, 1961 | | | | | | | | | |
| Wölsendorf, Germany<br>Seeliger and Strunz, 1965 | | | | | 9,89 | 3,70 | 6,87 | | 2,00-2,20 |
| USSR<br>Gotman et al., 1968 | hydrothermal<br>low T, 200°C | 4,32 | 5,1 | | | | | 13 - 15% | 2,06-2,11 |
| Carbon County, Pennsylvania<br>Finkelman and Klemic, 1976 | sandstone | | | monoclinic | | | | | |
| Orthobrannerite, Szechun Prov., China<br>Peking Inst., 1978 | syenite, alkali lamprophyre | 5,44 | 515-532 VHN | | 7,37 | 11,67 | 6,33 | 15 - 17% | 2,33 |
| Sierra Pintada, Argentine<br>Nicolli, 1980 | sandstone | | | | | | | | |
| France<br>Ruhlmann, 1980 | metasediments | | | | | | | | |
| Synthetic brannerite<br>Szymanski and Scott, 1982 | | 6,37 | | monoclinic C2/m | 9,8123 | 3,7697 | 6,9253 | | |
| Bohemian Massif, Germany<br>Dill, 1980 | unconformity-type deposit | | 420-680 VHN | | | | | 14% | |
| Bohemian Massif, Germany<br>Dill, 1985 | hydrothermal | | | | | | | | |
| Baviaanskrantz, South Africa<br>This study | hydrothermal | | | monoclinic | | | | 13-15% | |

* Refractive index after heating

For additional occurrences see Ferris and Ruud (Table 1, 1971)

Table 44 X-ray diffraction data for several brannerites

| 1 | | 2 | | 3 | | 4 | | 5 | | 6 | | 7 | | 8 | |
|---|---|---|---|---|---|---|---|---|---|---|---|---|---|---|---|
| d, Å | I | d, Å | I | d, Å | I | d, Å | I | d, Å | I | d, Å | I | d, Å | I | d, Å | I |
| 6,04 | 3,5 | 6,07 | 3 | 6,08 | 4 | 6,10 | 1 | 6,08 | 3 | 6,10 | 2 | 6,02 | 1 | 6,08 | 5 |
| 4,74 | 9,5 | 4,70 | 5 | 4,76 | 7 | 4,72 | 5 | 4,73 | 8 | 4,74 | 6 | 4,74 | 3 | 4,71 | 9 |
| 4,29 | 2 | 4,31 | 2 | 4,27 | 4 | 4,36 | 1 | 4,33 | 3 | 4,33 | 3 | 4,28 | 3D | 4,28 | 3 |
| 3,44 | 10 | 3,42 | 10 | 3,43 | 10 | 3,44 | 10 | 3,44 | 10 | 3,44 | 8 | 3,41 | 4B | 3,44 | 10 |
| 3,35 | 10 | 3,32 | 5 | 3,32 | 6 | 3,36 | 4 | 3,27 | 7 | 3,33 | 5 | 3,33 | 1 | 3,34 | 7 |
| 3,28° | 1,4 | | | | | | | | | 3,23 | 3° | | | 3,25° | |
| 3,02 | 3,5 | 3,02 | 3 | 3,03 | 5 | 3,05 | 5 | 3,08 | 5 | 3,03 | 3 | 3,05 | 10 | 3,01 | 3 |
| 2,90 | 3,5 | 2,91 | 3 | 2,91 | 9 | 2,91 | 5 | 2,85 | 8 | 2,93 | 10 | 2,91 | 5 | 2,91 | 4 |
| 2,77 | 3 | 2,76 | 4 | 2,76 | 6 | 2,76 | 4 | 2,79 | 5 | 2,77 | 5 | 2,76 | 3 | 2,77 | 4 |
| 2,53 | 3 | 2,51 | 4 | 2,53 | 5 | 2,49 | 6 | 2,56 | 7 | 2,53 | 6 | 2,57 | 1 | 2,57 | 1 |
| 2,47 | 3 | 2,45 | 7 | 2,45 | 5D | | | 2,49° | 8 | 2,46 | 5 | 2,49 | 4 | 2,52 | 5 |
| 2,41 | 1,8 | 2,43 | 2 | | | | | | | | | 2,46 | 4 | 2,46 | 3 |
| 2,303 | 0,8 | | | 2,34 | 1 | | | | | | | 2,35 | 1 | 2,42 | 2 |
| 2,292 | 2,5 | 2,276 | 7 | 2,285 | 5 | 2,29° | 5 | 2,287 | 7 | 2,279 | 4 | 2,279 | 5 | 2,274 | 4 |
| 2,276 | 1,2 | | | | | | | | | | | | | 2,189 | 1 |
| 2,144 | 1 | 2,151 | 2 | 2,154 | 2 | 2,196 | 4 | | | 2,159 | 1 | 2,193 | 2 | 2,146 | 1 |
| 2,080 | 0,8 | 2,080 | 1 | 2,079 | 3 | 2,040 | 3B | 2,052 | 3B | 2,085 | 1 | 2,083 | 5 | 2,072 | 1 |
| 2,043 | 3,5 | 2,029 | 4 | 2,021 | 4D | | | | | 2,034 | 4 | 2,013 | 3 | 2,036 | 1 |
| 2,015 | 2,5 | 2,017 | 2 | | | | | | | | | 1,982 | 3 | 2,014 | 1 |
| 1,911 | 0,6 | | | 1,947* | 1 | 1,914 | 5 | 1,914 | 3 | 1,909 | 5 | 1,920 | 7 | | |
| 1,903 | 2 | 1,903 | 8 | 1,905 | 7 | | | | | | | | | 1,901 | 3 |
| 1,881 | 2,5 | 1,861 | 6 | 1,866 | 4 | 1,870 | 3 | 1,875 | 3 | 1,872 | 4 | 1,872 | 6 | 1,874 | 2 |
| 1,798 | 0,4 | 1,776 | 1 | 1,771 | 3 | 1,776 | 1 | | | 1,794 | 6 | 1,789 | 5 | | |
| 1,749 | 0,8 | | | | | 1,745 | 1 | | | 1,740 | 1 | 1,728 | 2 | 1,737 | 1 |
| 1,732 | 0,6 | 1,729 | 3 | | | | | | | | | | | 1,713 | 2 |
| 1,723 | 0,4 | | | | | | | | | | | | | | |
| 1,709 | 2 | 1,700 | 4 | 1,703 | 4 | | | | | 1,704 | 2 | | | | |
| 1,675 | 0,6 | | | | | | | 1,683° | 3 | | | 1,671 | 1 | | |
| 1,642 | 0,8 | | | 1,649 | 5 | 1,647 | 1 | 1,631 | 3 | | | | | 1,630 | 2B |
| 1,630 | 2 | 1,623 | 6 | | | | | | | 1,620 | 5D | 1,623 | 1 | | |
| 1,609 | 1,8 | 1,609 | 4 | 1,612 | 2 | 1,622 | 4 | | | | | 1,605 | 3 | 1,613 | 1 |
| 1,597 | 0,6 | 1,585 | 2 | | | | | | | | | | | 1,600 | 1 |
| 1,578 | 1 | | | | | | | 1,577 | 2 | | | | | | |
| 1,569 | 0,8 | 1,569 | 5 | 1,567 | 5D | 1,569 | 3 | 1,568 | 2 | 1,567 | 4D | | | 1,559 | 1B |
| 1,561 | 0,6 | | | | | | | | | | | | | | |
| 1,558 | 0,6 | 1,557 | 3 | 1,530 | 4 | | | 1,530 | 1 | 1,530 | 5 | | | | |
| 1,493 | 0,2B | 1,489 | 1 | 1,488 | 1 | 1,483 | 2 | 1,481 | 1 | | | | | 1,481 | 1 |
| 1,486 | 0,4 | | | | | | | | | | | | | | |
| | | 1,481 | 2 | | | | | | | | | | | 1,452 | 2B |
| 1,45 | 0,4 | 1,461 | 1,7 | | | | | | | | | | | | |
| | | 1,440 | 2,3 | 1,438 | 1 | | | | | | | | | | |
| | | 1,411 | 0,7 | 1,414 | 1 | | | | | | | | | | |
| more lines occur below 1,41 | | | | | | | | | | | | | | | |

° possibly rutile line
* possibly uraninite line
1 Synthetic brannerite, Patchett and Nuffield, 1960
2 Mono County, USA, Pabst, 1954
3 Heated brannerite from Baviaankrantz, South Africa
4 Heated altered brannerite from ditto
5 ditto; less sharp lines
6 Brannerite of Baviaankrantz heated after leaching
7 Detrital brannerite, Leader Reef, Harmony Complex (not heated)
8 Authigenic brannerite, Vaal Reef, Vaal Reefs East G.M. (heated)

feature indicative of the precipitation of uranous titanates soon after burial is the presence of brannerite in microstylolites (Fig. A.29h).

Tables 45 and 46 present chemical compositions of brannerite in the CRG reefs and elsewhere in the world respectively. A few of the analyses are of uraniferous leucoxene composition (Table 45: 639-2, VRE 750, WR 823-1 and -2; bottom section Table 46).

In addition to the titanium and uranium, which could be present in the tetra- as well as the hexavalent state, the uranous titanates contain thorium, calcium, iron, silicon, and water. All variants fit the general formula given at the beginning of the section on uranium-bearing minerals (Section 3.7).

*3.7.4. (U-Th)-silicates*

From the (U,Th)-silicates found in the Witwatersrand and elsewhere in the world, it was established in this study that two series exist, i.e. one of anhydrous, the other of hydrated species (Smits, 1987, 1989). On the basis of existing names, the end members are respectively:

*anhydrous coffinite* and *thorite*, and
*coffinite* and *thorogummite*.

For the intermediate uranium-bearing silicates the respective names *uranoan thorite* and *thorian coffinite* have been proposed (Smits, 1989). The term uranoan was introduced by Palache *et al.* (1944), while the use of thorian was advised by Nickel and Mandarino (1987). These names are preceded by *anhydrous* or *hydrated* depending on the presence of water (Smits, 1987, 1989).

Detrital grains of *uranoan thorite* and *thorogummite* are fairly common in the Dominion Reef (Hiemstra, 1968), but very rare or absent in the CRG Reefs (Figs. A.30a and b). Both are three to four times larger in size than the accompanying detrital uraninite. The thorogummite, which is often referred to as orangite (Table 49), is moderate reddish brown to very pale orange in thin sections. Hydrated uranoan thorite which, in contrast with thorogummite, is metamict, occasionally replaces detrital uraninite in the Dominion Reef.

Table 45 Electron-microprobe analyses of brannerite in the CRG reefs

| Sample | $UO_2$ | $TiO_2$ | $ThO_2$ | PbO | $SO_3$ | $Y_2O_3$ | $P_2O_5$ | CaO | FeO | $SiO_2$ | $Al_2O_3$ | Total | $UO_2/TiO_2$ | Other minerals |
|---|---|---|---|---|---|---|---|---|---|---|---|---|---|---|
| Synthetic brannerite | 62,80 | 37,20 | – | – | – | – | – | – | – | – | – | 100,00 | 1,69 | |
| WDL 1244-1 | 46,85 | 37,35 | 1,10 | 1,40 | 0,02 | 0,50 | 0,04 | 0,58 | 0,74 | 5,17 | 1,56 | 95,31* | 1,25 | |
| WDL 1244-2 | 41,59 | 41,35 | 2,06 | 1,46 | 0,10 | 1,28 | 0,08 | 0,39 | 0,45 | 5,63 | 1,91 | 96,30 | 1,01 | |
| Rf 1306-1 | 49,75 | 21,90 | 2,99 | 4,58 | 0,71 | 3,08 | 2,95 | 0,84 | 0,23 | 10,94 | 1,12 | 99,09 | | cf, chur, gn |
| Rf 1306-2 | 46,75 | 29,35 | 4,34 | 1,79 | 0,19 | 2,92 | 2,92 | 0,92 | 0,32 | 10,64 | 1,29 | 101,43 | | cf, chur |
| Har 1346-1 | 48,41 | 41,83 | 2,01 | 0,13 | 0,09 | – | 0,01 | 0,55 | 1,59 | 5,31 | 1,35 | 101,28 | 1,16 | |
| Har 1346-2 | 38,32 | 40,97 | 3,20 | 0,04 | – | 0,73 | – | 1,30 | 0,39 | 8,39 | 0,76 | 94,10 | 0,93 | |
| Har 1346-3 | 42,45 | 42,28 | 3,14 | 0,10 | – | 0,75 | – | 1,36 | 0,45 | 8,86 | 0,81 | 100,20 | 1,00 | |
| Bv 676 | 39,31 | 37,88 | n.d. | 1,86 | 0,63 | 0,84 | – | 2,14 | 1,50 | 4,97 | 0,93 | 90,06 | 1,00 | |
| Bf 615 | 34,69 | 38,28 | n.d. | 6,61 | 2,96 | 1,06 | 0,12 | 0,45 | 1,13 | 4,63 | 1,40 | 91,33 | 0,91 | gn |
| Har 639-1 | 41,51 | 36,72 | n.d. | 0,59 | 0,12 | 0,07 | 0,03 | 0,93 | 0,65 | 9,88 | 1,50 | 92,00 | 1,13 | |
| Har 639-2 | 31,97 | 38,69 | n.d. | 2,37 | 0,86 | 2,76 | 0,03 | 0,71 | 0,85 | 7,71 | 1,44 | 87,39 | 0,83 | |
| WDL 659-1 | 44,17 | 33,03 | n.d. | 2,72 | 0,90 | 0,47 | 0,27 | 0,70 | 1,97 | 8,83 | 1,14 | 94,20 | 1,34 | |
| WDL 659-2 | 43,39 | 37,76 | n.d. | 1,40 | 0,16 | 0,87 | 0,10 | 0,85 | 1,35 | 6,25 | 1,36 | 93,49 | 1,15 | |
| WR 818 | 38,86 | 35,15 | n.d. | n.d. | 0,05 | n.d. | n.d. | 0,83 | 1,13 | 8,21 | 1,85 | 86,08 | 1,11 | |
| VRE 750 | 25,65 | 50,41 | n.d. | n.d. | 0,53 | n.d. | n.d. | 0,53 | 1,65 | 6,03 | 3,65 | 88,45 | 0,51 | |
| WR 823-1 | 20,21 | 42,22 | 1,70 | 1,34 | – | 2,14 | 1,46 | 0,61 | 1,02 | 14,75 | 5,94 | 91,39 | 0,48 | ph.sil, an, cf, chur |
| WR 823-2 | 16,85 | 31,14 | 1,58 | 1,00 | 0,04 | 1,29 | 1,13 | 0,42 | 1,43 | 21,96 | 11,71 | 88,55 | 0,54 | |
| GV 1345-1 | 57,25 | 8,07 | 1,58 | 0,66 | 0,45 | 1,21 | 2,34 | 1,42 | 1,63 | 14,95 | 2,17 | 91,73 | | cf, br, ph.sil, chur |

– Not detected; n.d. Not determined

WDL Western Deep Levels Rf Randfontein, Cooke Section Har Harmony Bv Blyvooruitzicht
Bf Buffelsfontein WR Western Reefs VRE Vaal Reefs East GV Grootvlei

* The low totals are due to the presence of varying amounts of water

Table 46 Compositions of brannerite and uraniferous leucoxene from various localities in the world

| Locality | $UO_2$ | $UO_3$ | $ThO_2$ | $TiO_2$ | PbO | REE | FeO | CaO | $SiO_2$ | $H_2O$ | other elements | Total | $UO_2/TiO_2$ |
|---|---|---|---|---|---|---|---|---|---|---|---|---|---|
| Brannerite | | | | | | | | | | | | | |
| 1. Kelly Gulch, USA | 10,30 | 33,50 | 4,10 | 39,00 | 0,20 | 3,90 | 2,90 | 2,90 | 0,60 | 2,00 | 0,80 | 100,20 | 1,08 |
| 2. Cordoba, Spain | $U_3O_8$: 51,76 | | 1,20 | 32,45 | 2,34 | 1,10 | 3,11 | 2,74 | 0,16 | 2,35 | 0,02 | 97,23 | 1,53 |
| 3. Vosges, France | $U_3O_8$: 43,30 | | 0,30 | 35,20 | 3,20 | 2,20 | 5,40 | 2,70 | 3,30 | 3,70 | 1,30 | 100,60 | 1,18 |
| 4. Mono County, USA | 8,20 | 32,00 | 5,00 | 32,90 | n.d. | 6,50 | 2,40 | 2,80 | 0,50 | 2,60 | 5,60 | 98,50 | 1,17 |
| 5. San Bernadino County, USA | tr. | 26,74 | 9,15 | 39,60 | 1,75 | 9,75 | 3,98 | 2,70 | 2,25 | 2,40 | 2,06 | 100,38 | 0,72 |
| 6. Crocker Wells, Australia | $U_3O_8$: 31,83 | | 12,81 | 35,13 | 2,79 | 5,14 | 1,23 | - | - | 9,95 | 1,69 | 100,57 | 0,86 |
| 7. Unknown locality, USSR | 33,48 | 13,54 | 0,03 | 30,65 | 0,40 | 0,49 | 0,70 | 3,64 | 1,80 | 7,83 | 7,44 | 100,00 | 1,56 |
| 8. Unknown locality, USSR | 16,45 | 35,41 | 3,96 | 42,05 | 0,13 | - | 0,24 | - | 0,21 | 0,04 | 1,61 | 100,10 | 1,28 |
| 9. Blind River, Canada | 32,55 | n.d. | 1,25 | 34,57 | 1,82 | 2,66 | 1,56 | 2,86 | 6,34 | n.d. | 16,38 | 99,99 | 0,91 |
| Ditto | 41,08 | n.d. | 0,30 | 36,13 | 1,68 | 1,84 | 2,11 | 5,46 | 3,30 | n.d. | 6,85 | 98,75 | 1,14 |
| 10. Witwatersrand, South Africa | 36,00 | n.d. | 2,70 | 31,90 | 12,54 | n.d. | 4,10 | 0,50 | 8,00 | n.d. | n.d. | 94,90 | 1,13 |
| 11. Yunnan and Szechuan, China | 28,75 | 31,08 | 1,03 | 35,35 | 0,17 | 0,28 | 0,38 | 0,44 | 0,65 | 1,87 | 0,20 | 100,10 | 1,74 |
| 12. Novoveska Huta, Slovakia | 53,40 | n.d. | n.d. | 36,00 | n.d. | n.d. | 1,70 | 0,50 | 4,10 | n.d. | n.d. | 95,70 | 1,48 |
| 13. Pongola Basin, South Africa | 34,00 | n.d. | 1,04 | 38,33 | 4,62 | n.d. | 1,20 | 2,29 | 7,75 | n.d. | n.d. | 89,23 | 0,89 |
| Uraniferous leucoxene | | | | | | | | | | | | | |
| 9. Blind River, Canada | 30,45 | n.d. | - | 46,85 | 0,91 | 2,66 | 1,25 | 0,65 | 3,94 | n.d. | 11,42 | 98,13 | 0,65 |
| 14. Blind River, Canada | 14,38 | n.d. | 1,34 | 66,49 | 1,71 | n.d. | 1,26 | 0,88 | 5,81 | n.d. | n.d. | 91,79 | 0,22 |
| 13. Pongola Basin South Africa | 12,82 | n.d. | 0,36 | 62,85 | 4,16 | n.d. | 2,96 | 0,77 | 6,66 | n.d. | n.d. | 90,58 | 0,20 |
| 10. Witwatersrand, South Africa | 26,60 | n.d. | 2,30 | 45,10 | 0,32 | n.d. | 1,60 | 0,30 | 13,70 | n.d. | n.d. | 89,90 | 0,59 |

n.d. not determined; - not detected

References:


1. Hess et al., 1920
2. George, 1949
3. Branche et al., 1951
4. Pabst, 1954
5. Hewett et al.. 1954
6. Adler and Puig, 1961
7. Gotman et al., 1968
8. Soboleva and Pudovkina, 1958
9. Theis, 1973
10. Feather, 1976
11. Peking Inst. of Uranium Geol., 1978
12. Rojkovic and Boronichin, 1982
13. Saager and Stupp, 1983
14. Saager and Stupp, 1983

Optical and physical properties of thorium-bearing silicates established by various investigators are listed in Table 47. Data on the composition of these silicates in the Witwatersrand and elsewhere in the world are presented in Table 48, and of those in the Dominion Reef in Table 49. The analytical data from this study (Table 48) differ from those of Glatthaar and Feather (1985; Table 49), in particular with respect to the yttrium concentration and the elements not accounted for in the analyses.

The incomplete chemical analysis of 'uranothorite' grains from a gravity concentrate (Ortlepp, 1962) is compared here below with the average EMP analysis of uranothorite (Table 49) given by Glatthaar and Feather (1985).

Table 50. Comparison of analytical data of uranothorite

| | Ortlepp, 1962 | Glatthaar & Feather, 1985 |
|---|---|---|
| $UO_2$ | 9,14 | 9,97 |
| $ThO_2$ | 34,90 | 12,88 |
| $PbO_2$ | 16,05 | 13,29 |
| $SiO_2$ | 10,00 (est.) | 17,85 |
| Other oxides | 10,00 (est.) | 13,97 |
| Total | 80,09 | 67,96 |
| Not accounted for | 19,91 | 32,04 |

After addition of an estimated 20% of silica and other oxides, the unidentified portions of the two analyses can be compared. Porosity and microcrystallinity may partly be responsible for the significant differences between the chemical and EMP analyses. The composition of the partly analyzed grains by Ortlepp (1962) indicates that they represent detrital uranoan thorite.

Authigenic *thorian coffinite*, which replaces uraninite, is a common constituent of the UE1a and E9 Reefs in the West Rand G.F. (Smits, 1984a and b, 1985a to c, 1986, 1987, 1989) and in the Dominion Reef (Hiemstra, 1968). The mineral is rarely found in other reefs of the CRG, where it also occurs as the alteration product of uraninite. Details on the texture of

Table 47 Optical and physical properties of thorium-bearing silicates

| Property | | Thorite | Thorogummite | Huttonite |
|---|---|---|---|---|
| Hardness | | 4.5 to 5.0 | 5.5 | n.d. |
| Relative density | | 6.7 | 4.4 to 4.5 | 7.1 |
| Reflectance, % | | 5 to 7 | - | n.d. |
| Refractive index | $n_\alpha$ | 1.818 to 1.825 | | 1.898 |
| | $n_\beta$ | - | 1.54 to 1.74 | 1.900 |
| | $n_\gamma$ | 1.839 to 1.840 | | 1.926 |
| Crystal system | | Tetragonal | Tetragonal | Monoclinic |
| Cell dimensions, Å | a° | 7.12* | 7.068 | 6.80 |
| | c° | 6.32 | 6.26 | 6.54 |
| Colour of mineral | | Black, light olive to olive-grey, moderate light brown to light brown, often mottled | Ligth brown to moderate reddish brown, dusky yellow-green very pale orange | Colourless to very pale orange |

n.d. not determined

*)

| | a° | c° | |
|---|---|---|---|
| Natural thorite | 7.03 | 6.25 | (Bonatti and Gallitelli, 1951) |
| Synthetic thorite | 7.128 | 6.314 | (Fuchs and Gebert, 1958) |
| Thorite heated at 1100°C for 8 hrs | 7.16 | 6.319 | (Keller, 1963) |

Data are from Frondel (1953, 1958), except for cell dimensions of thorite (a uranoan thorite from New Zealand), which are from Pabst (1952), and the data on huttonite, relative densities and refractive indices of thorite, which are from Hutton (1950), and the reflectance values, which are from Uytenbogaardt and Burke (1971). The refractive indices for metamict thorite vary from 1.68 to 1.78. For synthetic huttonite, the cell dimensions are 6.78 and 6.50 A at 1250°C, and 6.77 and 6.51 A at 1400°C (Keller, 1963),

Table 48 Compositions of thorium silicates from the Witwatersrand and elsewhere

| Constituent | 1 | 2 | 3 | 4 | 5 | 6 | 7 | 8 | 9 | 10 | 11 |
|---|---|---|---|---|---|---|---|---|---|---|---|
| $ThO_2$ | 81.46 | 67.33 | 41.44 | 45.30 | 57.79 | 21.20 | 62.60 | 56.80 | 34.90 | 30.31 | 44.59 |
| $UO_2$ | | | 21.16 | 22.40 | 2.81 | 17.57 | 11.50 | 25.40 | 9.14 | 21.59 | 30.51 |
| $SiO_2$ | 18.54 | 15.32 | 13.09 | 13.90 | 15.77 | 14.43 | 19.50 | 17.30 | | 12.80 | 17.62 |
| $PbO^2$ | | | 2.16 | 3.74 | 1.25 | 0.17 | 0.51 | | 14.98 | 8.94 | 2.86 |
| $REE_2O_3$* | | | 6.69 | 1.86 | 0.97 | 9.55 | 1.10 | | | 1.64 | 2.06 |
| $Fe_2O_3$ | | | 0.85 | | | 2.84 | 2.30 | | | 1.42 | 0.57 |
| CaO | | | 0.41 | 0.59 | 1.65 | | 0.30 | | | 1.12 | 1.21 |
| MgO | | | | 0.10 | 0.60 | | 0.30 | | | | |
| $Al_2O_3$ | | | 0.97 | | 0.88 | 8.84 | | | | | |
| $P_2O_5$ | | | 1.19 | 0.67 | 1.33 | 2.62 | | | | 3.28 | 1.22 |
| $H_2O$ | | 17.35 | 9.11 | 4.81 | 15.18 | 13.43 | 1.93 | | | | |
| LOI | | | | | 1.50 | | | | | | |
| Others | | | | 5.38 | | 8.33 | | | | 4.01 | 1.80 |
| Total | 100.00 | 100.00 | 97.07 | 98.75 | 99.73 | 98.99 | 100.04 | 99.50 | | 85.11 | 102.44 |
| $(UO_2+ThO_2)/SiO_2$ | 4.39 | 4.39 | 4.78 | 4.87 | 3.84 | 2.69 | 3.80 | 4.75 | | 4.06 | 4.26 |
| Relative density | 6.7 | 3.2 to 5.4 | 4.4 | 5.4 | | | 6.25 | 4.4 to 4.8 | | | |

LOI Loss on ignition *) Mainly yttrium and cerium

1 Ideal thorite
2 Ideal hydrated thorite
3 and 4 Beringer Hill, Texas
5 Wodgina, W. Australia
6 South Manchuria
coloured thorogummite (Frondel 1958)
7 Uranoan thorite from beach sand, New Zealand (Hutton 1950)
8 Uranoan thorite from alkali rhyolite, Utah (Foord et al. 1985)
9 Uranoan thorite from Dominion Reef, South Africa (Ortlepp 1962)
10 Uranoan thorite, Orange Free State G.F., South Africa
11 Altered uraninitem Dominion Reef, South Africa

Table 49 Average electron-microprobe analyses of radioactive minerals in the Dominion Reef (Glatthaar & Feather, 1985)

| Constituent | Uraninite (7) | Altered uraninite (10) | Brannerite type mineral (11) | Coffinite (11) | Coffinite-uranothorite group (41) | Uranothorite (30) | Orangite (17) | Euxenite (15) | Monazite (32) | Zircon (94) | Allanite (6) |
|---|---|---|---|---|---|---|---|---|---|---|---|
| $UO_2$ | 63,95 | 53,68 | 31,68 | 38,79 | 16,86 | 9,97 | 2,27 | 6,73 | 0,42 | 0,34 | 0,12 |
| $ThO_2$ | 2,60 | 2,38 | 1,55 | 3,06 | 10,68 | 12,88 | 14,88 | 0,78 | 1,57 | 0,14 | 0,05 |
| $PbO_2$ | 9,73 | 19,26 | 7,63 | 14,83 | 10,12 | 13,29 | | | | 0,60 | |
| FeO | 0,81 | 1,24 | 2,36 | 0,38 | 0,76 | 0,97 | 9,74 | | | | |
| $TiO_2$ | 0,20 | 0,36 | 14,95 | 0,32 | 0,51 | 0,45 | 0,25 | 24,28 | | | |
| CaO | 1,20 | 1,66 | 0,49 | 0,90 | 0,94 | 1,04 | 1,76 | 3,06 | 0,79 | | 9,94 |
| $SiO_2$ | 1,90 | 8,15 | 17,43 | 12,96 | 14,33 | 17,85 | 10,09 | 9,78 | 1,28 | 31,66 | 29,23 |
| $MnO_2$ | 0,64 | 0,43 | | | | 0,06 | | | | | |
| $Al_2O_3$ | 0,93 | 1,63 | 0,51 | 0,93 | 1,23 | 2,08 | 1,46 | | 0,24 | 1,16 | 17,29 |
| $P_2O_5$ | 0,58 | 0,51 | 0,39 | 1,39 | 2,16 | 1,46 | 5,78 | | 29,67 | | |
| $Fe_2O_3$ | | | | | | | | 1,88 | 0,65 | 1,24 | 13,56 |
| $Y_2O_3$ | 3,47 | 5,51 | 11,07 | 11,17 | 11,42 | 7,91 | 14,13 | 16,89 | 1,80 | 2,45 | |
| $La_2O_3$ | | | | | | | | | 17,64 | | 6,95 |
| $Ta_2O_3$ | | | | | | | | 3,83 | | | |
| $Nb_2O_3$ | | | | | | | | 14,62 | | | |
| $Ce_2O_3$ | | | | | | | 0,61 | | 27,28 | | 10,43 |
| $Pr_2O_3$ | | | | | | | | | 2,87 | | 1,15 |
| $Nd_2O_3$ | | | | | | | 0,73 | | 11,05 | | 4,14 |
| $Sm_2O_3$ | | | | | | | | | | | 0,48 |
| $Eu_2O_3$ | | | | | | | | | | | 0,06 |
| $ZrO_2$ | | 0,14 | | | | | | | | 60,60 | |
| $HfO_2$ | | | | | | | | | | 1,28 | |
| Total | 86,01 | 94,95 | 88,06 | 84,73 | 69,01 | 67,96 | 61,70 | 81,85 | 95,26 | 99,47 | 93,40 |

The figures in parentheses refer to the number of analyses carried out in each case

coffinite and its association with other minerals are presented in Table 51.

Physical and optical characteristics of coffinite, as established by others, are listed in Table 52. XRD data are presented in Table 53. (U,Th)-silicates, zircon, and xenotime, whether anhydrous or hydrated, are isostructural, and hence their XRD patterns alike.

The Witwatersrand thorian coffinite is porous and of a microcrysstalline nature, and mixed with impurities such as, sulphide, gold, kerogen, and gangue minerals. Their presence hampers the determination of the chemical and physical properties of this silicate. Its reflectance in air ranges from 5 to 7%, and in oil, the value lies below 1,5% (Ramdohr, 1961).

Chemical compositions of coffinite in the Witwatersrand and elsewhere in the world are summarized in Tables 54 and 55 respectively. When compared with the data in Table 49, the yttrium concentrations reported in this table are much higher and the totals distinctly lower. Although never identified positively by XRD, the presence of an Y-phosphate in some of the coffinite grains in the UE1a Reef is suggested by the EMP analyses (Table 56). The low total of these analyses is not necessarily due to the presence of water only. It is possible that other REE, e.g. cerium and lanthanum for which the Y-phosphate was not analyzed, are present.

The EMP analyses of Table 54 (analyses 1306 and 1216) indicate that, in the UE1a and E9 Reefs, the silicate is an *anhydrous thorian coffinite*. This mineral has been reported only once before in metamorphosed sandstones of Permian age (Kurat *et al.*, 1977), where it coexisted with pitchblende (Table 55, analysis 15).

The compositions of (U,Th)-silicates of the Witwatersrand and other deposits have been plotted in ternary diagrams for the (U+Th)-Si-$H_2O$ (Fig. 16) and U-Th-Si (Fig. 17) systems. For most of the silicates from elsewhere, water has been determined by wet chemistry. (U,Th)-silicates of the Witwatersrand were analyzed on the EMP, which cannot determine the water content. Ignoring the possible presence of minor amounts of organic matter, the water content was in this instant determined by

Table 51 Textural varieties of thorian coffinite in the CRG reefs and the Dominion Reef

| Morphology | Size, mm | Mineral association | Distribution |
|---|---|---|---|
| (1) Pseudomorphous after ur (Fig. A.28a). Some grains are well rounded (Figs. A.27d and g). Frequently in groups of clogged grains enveloped by a 0,02 mm-wide film of ur.1c mixed with ph.sil. and q (Fig. A.27e) | <0,3 | Minute specks and larger inclusions (<0,05 mm) of radiogenic gn; po laths 0,03 mm | Common in-situ transformation product of ur in UE1a and E9 Reefs and Dominion Reef (Fig. A.28b). Replacement started along cracks and crystal planes (Fig. A.20c) |
| (2) Amoeboid-shaped grains (Fig. A.27f) | <0,3 | Au, po, radiogenic gn, ur, ur. tit. Intergrown with ph.sil., q, and Y-phosphates | Common in UE1a and E9 Reefs |
| (3) Irregular-shaped inclusions in ker replacing ur fragments (Figs. A.22g, A.24b and f), or cf enveloping ker ((Fig. A.27h) | | po, radiogenic gn | Noticed in UE1a and E9 Reefs, Beisa Reef (Fig. A.22h), other reefs of the Turffontein Subgroup and the VCR |
| (4) Pseudomorphs after ur (Fig. A.28c) and agglomerations of colloform cf, ur, and py of recent supergene origin (Figs. A.28d and e) | <0,1 | Recrystallized gn. Supergene cf and ur are devoid of gn | Monarch Reef, East Champ d'Or G.M. |

Table 52 Optical and physical properties of coffinite

| Investigators | Hardness, Moh's scale | Relative density | Reflectance in air, %* | Refractive index | Cell dimensions, Å a° | c° |
|---|---|---|---|---|---|---|
| Gruner and Smith (1955) | | | | | 6,92 | 6,22 |
| at 25°C | | | | | 6,85 | 6,15 |
| at 500°C | | | | | | |
| Stieff et al. (1956) | 5 to 6 | 5,1 | | | 6,94 | 6,31 |
| Hoekstra and Fuchs (1956) | | | | 1,83 to 1,85 | 6,937 | 6,285** |
| | | | | at 1000°C 1,88 | 6,977 | 6,307 |
| Filipenko (1958) | 2,9 to 3,1 | | 5,6 to 7,5 | | 7,01 | 6,26 |
| Fuchs and Gebert (1958) (synthetic cf) | | 7,15 | | | 6,981 | 6,250 |
| Moench (1962) | | | 7,5 | 1,73 to 1,75 | | |
| Arribas (1966) | 3 to 4 | 4,54 | 9,2 | 1,674 | | |
| at 1300°C | | 3,40 | | 1,528 | 6,98 | 6,22 |
| Ludwig and Grauch (1980) | | | 7,0 to 8,6 | | | |

*) Uytenbogaardt and Burke (1971) report reflectance values for cf from 7 to 10%
**) Values for natural cf and synthetic $USiO_4$ respectively

For intermediate synthetic species the values are, (Hoekstra and Fuchs, 1956):

| | | |
|---|---|---|
| $3USiO_4.ThSiO_4$ | 7,021 | 6,288 |
| $USiO_4.ThSiO_4$ | 7,033 | 6,307 |
| $USiO_4.3ThSiO_4$ | 7,085 | 6,327 |

Table 53 X-ray diffraction data for thorium and uranium silicates

Thorium silicates

| 1 d, Å | 1 I | 2 d, Å | 2 I | 3 d, Å | 3 I | 4 d, Å | 4 I | 5 d, Å | 5 I | 6 d, Å | 6 I | 7 d, Å | 7 I |
|---|---|---|---|---|---|---|---|---|---|---|---|---|---|
| 4,69 | 9 | 4,73 | 8 | 4,695 | 9 | 4,75 | 10 | 4,74 | 10 | 4,67 | 10 | 4,72 | 10 |
| 3,56 | 10 | 3,56 | 10 | 3,537 | 10 | 3,58 | 10 | 3,55 | 10 | 3,55 | 10 | 3,55 | 10 |
| 2,84 | 7 | 2,84 | 7 | 2,821 | 4 | 2,824 | 5 | 2,85 | 2 | 2,84 | 5 | 2,82 | 2 |
| 2,66 | 8 | 2,68 | 8 | 2,653 | 6 | 2,665 | 8 | 2,65 | 8 | 2,65 | 5 | 2,64 | 3 |
| 2,52 | 5 | 2,52 | 7 | 2,499 | 3 | 2,516 | 2D | 2,53 | 1 | | | 2,47 | 1 |
| | | | | 2,336 | 0,5 | | | | | | | | |
| 2,22 | 1 | 2,22 | 8 | 2,203 | 4 | 2,207 | 4 | 2,212 | 4 | 2,210 | 2 | 2,205 | 2 |
| 2,01 | 5 | 2,02 | 4 | 2,000 | 4 | 2,004 | 4 | 1,999 | 2 | 1,981 | 1 | 1,992 | 1 |
| 1,89 | 6 | 1,874 | 6 | 1,869 | 3 | 1,884 | 2 | 1,892 | 1 | 1,890 | 1 | 1,865 | 1 |
| 1,84 | 10 | 1,834 | 10 | 1,818 | 6 | 1,829 | 6 | 1,823 | 4 | 1,819 | 2 | 1,809 | 2 |
| 1,787 | 5 | 1,780 | 8 | 1,767 | 1 | | | 1,783 | 2 | | | 1,783 | 2 |
| 1,749 | 6 | 1,757 | 6 | 1,740 | 1 | 1,740 | 1 | | | | | | |
| 1,672 | 3 | 1,667 | 6 | 1,653 | 1 | 1,655 | 1 | 1,667 | 1 | | | | |
| 1,599 | 5 | 1,592 | 7 | | | 1,591 | 1B | | | | | | |
| 1,571 | 4 | 1,580 | 4 | 1,582 | 1 | | | | | | | | |
| 1,486 | 6 | 1,576 | 4 | 1,565 | 1 | 1,567 | 1 | | | | | 1,567 | 1 |
| 1,438 | 7 | 1,482 | 5 | 1,481 | 3 | 1,481 | 2 | 1,481 | 2 | | | 1,481 | 1 |
| | | 1,444 | 5 | | | 1,454 | 3 | | | | | | |
| 1,396 | 6 | 1,440 | 4 | 1,431 | 3 | | | 1,430 | 2 | | | 1,426 | 1 |
| 1,336 | 8 | | | 1,379 | 2 | | | 1,390 | 1 | | | | |
| 1,282 | 7 | | | 1,326 | 3 | 1,330 | 3 | | | | | | |
| + | | | | 1,267 | 2 | 1,278 | 3 | | | | | | |
| 24 lines | | | | + | | | | | | | | | |
| | | | | 16 lines | | | | | | | | | |

Uranium silicates

| 1 d, Å | 1 I | 2 d, Å | 2 I | 3 d, Å | 3 I | 4 d, Å | 4 I | 5 d, Å | 5 I |
|---|---|---|---|---|---|---|---|---|---|
| 4,64 | 9,5 | 4,66 | s | 4,62 | 7 | 4,65 | 10 | 4,67 | 10 |
| 3,48 | 10 | 3,47 | s | 3,49 | 10 | 3,49 | 10 | 3,46 | 10 |
| 2,79 | 4,5 | 2,78 | w | 2,78 | 4 | 2,79 | 5 | 2,78 | 4 |
| 2,64 | 9,5 | 2,64 | m | 2,62 | 5 | 2,645 | 6 | 2,64 | 8 |
| 2,46 | 2,5 | 2,46 | f | 2,47 | 3 | 2,493 | 3 | 2,455 | 2 |
| 2,326 | 0,4 | | | | | 2,337 | 0,5 | | |
| 2,177 | 3 | 2,18 | w | 2,178 | 6B | 2,178 | 3 | 2,167 | 3 |
| 1,996 | 3 | 2,01 | f | 1,974 | 1,5 | 2,000 | 3 | 1,995 | 3 |
| 1,849 | 3,5 | 1,841 | w | 1,848 | 3B | 1,843 | 1 | 1,838 | 3,5 |
| 1,803 | 7 | 1,801 | m | 1,789• | 6B | 1,800 | 5• | 1,792 | 6 |
| 1,738 | 3,5 | 1,737 | w | 1,743 | 3 | 1,736 | 2 | 1,726 | 3,5 |
| 1,633 | 1,5 | 1,629 | f | 1,629 | 1 | | | 1,627 | 1 |
| 1,561 | 2,5 | 1,556 | f | 1,561 | 1 | 1,556 | 3 | 1,549 | 2 |
| 1,456 | 2,5 | 1,451 | f | 1,483 | 1 | 1,452 | 2 | 1,446 | 2 |
| 1,427 | 2,5 | 1,435 | f | | | 1,434 | 1 | 1,421 | 1 |
| 1,419 | 0,5 | | | 1,406 | 0,5 | | | | |
| 1,362 | 1,5 | | | 1,359 | 1B | 1,367 | 2 | 1,355 | 2 |
| 1,320 } 1,315 } | 2,5 | | | 1,326 | 0,5 | 1,330 | 2 | 1,316 | 1 |
| 1,270 | 0,7 | | | | | | | | |

1. Synthetic thorite (Frondel, 1958)
2. Uranothorite, ASTM card 18-395 (calculated)
3. Thorogummite, ASTM card 8-440
4. President Brand G.M., Basal Reef (thoroan coffinite?)
5. Western Reefs G.M., Vaal Reef
6. Orangite, Dominion Reef (broad lines)
7. Altered portion of uraninite (thoroan coffinite?), Dominion Reef

• galena included
1 Synthetic coffinite
2 Natural coffinite (Stieff et al., 1956)
3 Cooke Section, UEla Reef
4 Secondary coffinite, Monarch Reef, East Champ d'Or G.M.
5 Secondary coffinite, Monarch Reef, Randfontein Estates G.M.

Table 54 Electron-microprobe analyses of coffinite from the Witwatersrand

| Reference | $UO_2$ | $ThO_2$ | $SiO_2$ | PbO | $SO_3$ | $Y_2O_3$ | $P_2O_5$ | CaO | FeO | $TiO_2$ | $ZrO_2$ | Total | $UO_2+ThO_2/SiO_2$* |
|---|---|---|---|---|---|---|---|---|---|---|---|---|---|
| Coffinite: | | | | | | | | | | | | | |
| $USiO_4$ | 81,80 | | 18,20 | | | | | | | | | 100,00 | 4,50 |
| $USiO_4.2H_2O$ | 73,75 | | 16,41 | | | | | | | | | 90,16 | 4,49 |
| Thorite; | | | | | | | | | | | | | |
| ThSiO | | 81,46 | 18,54 | | | | | | | | | 100,00 | 4,39 |
| $ThSiO_4.2H_2O$ | | 73,31 | 16,68 | | | | | | | | | 89,99 | 4,40 |
| Rf 602-1 | 45,89 | n.d. | 14,33 | 5,92 | 1,77 | 5,02 | 4,73 | 0,51 | 0,40 | - | n.d. | 78,57 | |
| 2 | 62,58 | n.d. | 12,87 | 5,50 | 2,16 | 1,14 | 1,68 | 0,83 | 0,96 | 1,77 | n.d. | 89,49 | |
| 3 | 63,08 | n.d. | 13,68 | 3,73 | 1,27 | 0,53 | 1,60 | 1,17 | 0,81 | 0,27 | n.d. | 86,14 | |
| 4 | 39,60 | n.d. | 9,45 | 14,78 | 3,63 | 7,95 | 7,90 | 1,41 | 0,60 | - | n.d. | 85,32 | |
| 1306-1 | 56,02 | 15,94 | 11,20 | 3,57 | 0,49 | 4,67 | 6,01 | 1,87 | 0,20 | 0,26 | n.d. | 100,23 | 6,43 |
| 2 | 47,03 | 11,13 | 9,66 | 15,70 | 1,90 | 3,20 | 4,31 | 1,20 | - | 2,04 | n.d. | 96,17* | |
| 1308-1 | 32,70 | 25,43 | 22,58 | 5,06 | 0,54 | 1,23 | 2,50 | 0,69 | 0,19 | 1,34 | n.d. | 92,36* | |
| 2 | 32,97 | 19,10 | 20,75 | 9,00 | 0,94 | 0,89 | 1,69 | 0,21 | 0,52 | 4,80 | n.d. | 90,87* | |
| WA 1216-1 | 60,24 | 9,71 | 18,91 | 0,19 | - | 3,12 | 4,60 | 2,24 | - | 0,14 | n.d. | 99,15 | 3,70 |
| 2 | 62,80 | 9,98 | 14,85 | 6,02 | 0,63 | 1,97 | 2,02 | 1,03 | - | 0,06 | n.d. | 99,36 | 4,90 |
| 1211/2-2 | 54,43 | 8,00 | 18,61 | 2,77 | 0,39 | 1,38 | 0,90 | 0,59 | 0,13 | 0,01 | 0,18 | 87,39 | 3,36 |
| 3-1a | 54,33 | 11,82 | 16,24 | 6,89 | 1,39 | 0,80 | 0,50 | 0,35 | 0,14 | 0,20 | 0,31 | 92,98 | 4,07 |
| 3-3 | 48,18 | 8,27 | 18,02 | 5,23 | 1,20 | 1,69 | 1,34 | 0,34 | 0,04 | 0,03 | 0,18 | 84,52 | 3,13 |
| PB 833/1a-1 | 58,47 | 7,95 | 13,65 | 5,88 | 1,16 | 1,73 | 1,22 | 1,04 | 0,02 | 0,13 | 0,27 | 91,50 | 4,87 |
| 1b-edge | 57,72 | 3,03 | 12,48 | 0,11 | 0,06 | 1,58 | 1,07 | 0,89 | 0,33 | 14,52** | 0,17 | 91,95 | 4,87 |
| 1b-2 | 60,17 | 12,33 | 12,52 | 0,85 | 0,20 | 1,81 | 1,48 | 1,15 | 0,03 | 0,12 | - | 91,67 | 5,79 |
| 2a-3 | 67,03 | 5,62 | 10,99 | 1,60 | 0,27 | 1,47 | 1,23 | 1,15 | 0,09 | 0,35 | 0,66 | 90,54 | 6,61 |
| Vir 705/1-1 | 21,58 | 30,31 | 12,80 | 8,94 | 3,51 | 1,64 | 3,28 | 1,12 | 1,28 | 0,07 | 0,43 | 84,97 | 4,05 |
| Beisa 1020-1 | 63,56 | 8,67 | 14,27 | 0,83 | 0,09 | 1,97 | 2,00 | 2,15 | - | 0,97 | n.d. | 94,51 | 5,06 |
| 2 | 62,61 | 9,74 | 13,70 | 1,44 | 0,29 | 1,67 | 1,94 | 2,60 | - | 0,02 | n.d. | 94,01 | 5,28 |
| DR 1446/1a-1 | 46,26 | 14,90 | 13,91 | 13,94 | 2,31 | 0,34 | 0,03 | 0,75 | 0,47 | 0,78 | 0,48 | 94,16 | 4,40 |
| 1a-5 | 46,06 | 9,64 | 12,53 | 11,22 | 3,84 | 2,30 | 0,59 | 0,51 | 0,37 | 0,31 | 0,50 | 87,87 | 4,43 |
| 1b-1 | 48,33 | 1,60 | 11,33 | 19,91 | 5,01 | 1,98 | 0,31 | 0,11 | 0,37 | 0,25 | 0,67 | 89,88 | 4,40 |
| 3a-2 | 46,39 | 8,91 | 8,36 | 12,40 | 3,20 | 0,98 | 0,34 | 0,30 | 0,51 | 0,40 | 0,37 | 82,16 | 6,61 |
| 3a-4 (boundary) | 29,71 | 10,81 | 23,95 | 3,65 | 0,38 | 0,16 | 0,31 | 0,99 | 1,81 | 9,62** | 2,10 | 83,48 | 1,69 |
| 3b-1 | 52,98 | 19,11 | 13,57 | 4.08 | 1,54 | 0,24 | 0,21 | 1,10 | 0,72 | 0,42 | 0,64 | 94,60 | 5,31 |
| 3b-2 | 30,51 | 44,59 | 15,62 | 2,86 | 0,86 | 2,06 | 1,22 | 1,21 | 0,51 | 0,14 | 0,80 | 100,38 | 4,81 |
| GV 1345-1 | 58,61 | 5,15 | 9,30 | 13,45 | 2,41 | 1,07 | 1,90 | 1,00 | - | 0,43 | n.d. | 93,32 | 6,85 |
| 2 | 62,06 | 5,36 | 11,28 | 8,27 | 1,15 | 1,22 | 2,99 | 1,51 | - | 0,30 | n.d. | 95,04 | 5,97 |
| 3 | 67,43 | 6,39 | 8,75 | 8,31 | 0,97 | 0,99 | 1,88 | 1,08 | 0,01 | 0,59 | n.d. | 96,40 | 8,44 |

n.d. not determined; - not detected

* In analyses showing ratios above 4,50, coffinite is mixed with uraniite; those below 4,50 are mixed with silica

* All coffinites contain $Al_2O_3$ below 1,5%, but in samples 1306-2, 1308-1 and 1308-2, the values are respectively 2,59, 5,57 and 7,62. The alumina is present as phyllosilicates

** Uraninite grains are often coated by titania; this explains the high titania of the analysis at the boundary of the particles

Rf Randfontein Estates G.M., Cooke Section; WA Western Aareas G.M.; PB President Brand G.M.; Vir Virginia G.M.; DR Dominion Reef; GV Grootvlei G.M.

Table 55 Composition of coffinites occurring in other deposits in the world*

| | ideal-coffinite | | 1 | 2 | 3 | 4 | 5 | 6 | 7 | 8 | 9 | 10 | 11 | 12 | 13 | 14 | 15 | 16 |
|---|---|---|---|---|---|---|---|---|---|---|---|---|---|---|---|---|---|---|
| | anhydrous | hydrated | | | | | | | | | | | | | | | | |
| $UO_2$ | 81,80 | 73,75 | 68,29 | 46,37 | 58,60 | 71,33 | 25,05 | 27,66 | | 67,49 | 73,50 | 88,60 | 77,90 | 52,40 | 63,14 | 70,01 | 81,50** | 69,80 |
| $UO_3$ | | | | | | | 17,63 | 9,50 | | | | | | | | | | |
| $U_3O_8$ | | | | | | | | | 45,50 | | | | | | | | | |
| $SiO_2$ | 18,20 | 16,41 | 5,20 | 7,40 | 8,50 | 29,20 | 26,92 | 31,17 | 24,09 | 15,24 | 15,80 | 8,50 | 17,42 | 42,50 | 14,60 | 10,84 | 14,20 | 15.40 |
| $P_2O_5$ | | | | 2,69 | | | | | 2,10 | 2,18 | | | | | 0,09 | | | |
| CaO | | | | | 2,00 | | 1,91 | 1,47 | 3,72 | 2,34 | 3,00 | 1,75 | 1,18 | 2,51 | 1,58 | 1,69 | 0,26 | 2,03 |
| PbS | | | | | | | | | | 0,38 | | 0,83 | | | | | 0,37 | |
| PbO | | | 0,12 | 0,52 | 0,15 | | | | | | | | | | | | | |
| S | | | | 0,80 | | | 3,00 | 3,79 | 5,82 | | | | | | 0,39 | 0,14 | | |
| $Fe_2O_3$ | | | 1,24 | 1,57 | 4,44 | | 2,51 | 6,34 | 8,29 | 0,30(FeO) | | | | | 0,33 | 0,47 | | |
| $As_2O_5$ | | | 4,35 | 1,44 | 1,22 | | | | | | | | | | | | | |
| $V_2O_5$ | | | 2,85 | 18,90 | 3,25 | | | | 1,61 | 0,79 | | | | | | | | |
| MgO | | | | | | | 1,34 | 1,94 | 0,95 | | | 0,42 | 0,17 | 0,24 | | | 0,85 | 0,15 |
| $Al_2O_3$ | | | 3,87 | 6,80 | 10,12 | | 12,88 | 12,53 | | | | | | | | | | |
| LOI | | | 8,49 | 10,04 | 14,00 | | | | | | | | | | 4,05*** | 3,66*** | | |
| $H_2O$ | | 9,84 | | | | | 7,86 | 5,91 | 6,52 | 10,65 | | | | | | | | |
| Total | 100,00 | 100,00 | 94,41 | 96,53 | 102,28 | 100,53 | 99,10 | 100,31 | 96,50 | 99,37 | 92,30 | 100,10 | 96,67 | 97,65 | 84,18 | 86,81 | 97,18 | 87,38 |
| $UO_2/SiO_2$ | 4,50 | 4,49 | 13,13 | 6,27 | 6,89 | 2,44 | 1,55 | 1,17 | 1,82 | 4,43 | 4,65 | 10,42 | 4,47 | 1,23 | 4,32 | 6,46 | 5,74 | 4,53 |

1, 2, 3 Stieff et al., Colorado (1956)
4 Fuchs and Hoekstra, Colorado (1959)
5, 6 Filipenko, USSR (1958)
7 Arribas, Spain (1966)
8 Kim (1978); average of 10 samples of New Mexico
9 Ludwig and Grauch (1980); average of 7 samples of Colorado
10, 11, 12 Simova, Yugoslavia (1981); average of 2
13, 14 Smits and Uiterwijk, Karoo (1983)
15, 16 Kurat et al. (1977); resp. Austria and Yugoslavia.

* All coffinites are from sandstone-type uranium deposits, except 4 and 7, number 4 being a synthetic coffinite and number 7 a major constituent of several hydrothermal deposits in Spain

** $ThO_2$ less than 0,02%; $TiO_2$ 0,18%; BaO 0,59%; $K_2O$ 1,28%

*** Carbon

Table 56 Electron-microprobe analyses of Y-phosphates

| Reference | $UO_2$ | $ThO_2$ | PbO | $SO_3$ | $Y_2O_3$ | $P_2O_5$ | $SiO_2$ | CaO | FeO | $TiO_2$ | Total | $UO_2/P_2O_5$ |
|---|---|---|---|---|---|---|---|---|---|---|---|---|
| Xenotime | | | | | 61,40 | 38,60 | | | | | 100,00 | 1,59 |
| Churchite | | | | | 55,92 | 35,16 | | | | | 91,08 | 1,59 |
| Bf 923 | 3,64 | n.d. | 1,36 | 0,34 | 32,14 | 27,89 | 1,67 | 0,58 | 0,51 | n.d. | 68,13 | 1,15 |
| Rf 602-1 | 2,79 | n.d. | 1,59 | 0,41 | 36,66 | 32,35 | 1,38 | 0,24 | 0,29 | n.d. | 75,71 | 1,15 |
| Rf 602/1-1 | 3,19 | 0,81 | 0,90 | 0,27 | 30,18 | 26,88 | 0,97 | 0,65 | 0,09 | 0,06 | 64,00 | 1,27 |
| Rf 602/1-3 | 1,74 | 0,45 | 1,04 | 0,12 | 33,18 | 27,88 | 0,71 | 0,40 | 0,15 | 0,04 | 65,71 | 1,19 |
| Rf 602/2-6 | 7,85 | 0,25 | 2,90 | 0,50 | 30,44 | 26,66 | 1,66 | 0,74 | 0,12 | 0,05 | 71,17 | 1,14 |
| WA 1211/2-1 | 0,13 | 0,25 | 0,66 | - | 34,12 | 31,96 | 0,22 | 0,05 | 0,10 | 0,03 | 67,52 | 1,07 |

n.d. not determined - not detected

Bf Buffelsfontein G.M.; Rf Randfontein Estates G.M., Cooke Section; WA Western Areas G.M.

Table 57 Diffraction data of coffinite patterns from mushy anatase in the Witwatersrand

| 1 | | 2 | | 3 | | 4 | |
|---|---|---|---|---|---|---|---|
| d, Å | I | d, Å | I | d, Å | I | d, Å | I |
| 4,66 | s | 4,60 | 6 | 4,64 | 8 | 4,63 | 10 |
| 3,47 | s | 3,49 | 6 | 3,48 | 10 | 3,48 | 10 |
| 2,78 | w | 2,781 | 4 | 2,80 | 3 | 2,80 | 3 |
| 2,64 | m | 2,638 | 5 | 2,64 | 6 | 2,63 | 6 |
| 2,46 | f | 2,473 | 4 | 2,479 | 3 | 2,464 | 2 |
| | | | | 2,306 | 1 | | |
| 2,18 | w | 2,187 | 3 | 2,174 | 4 | 2,179 | 2 |
| 2,01 | f | 1,996 | 4 | 1,982 | 3 | 1,987 | 2 |
| 1,841 | w | 1,841* | 1 | 1,850 | 3 | 1,841 | 2 |
| 1,801 | m | 1,813 | 5 | 1,797 | 7° | 1,791 | 6° |
| 1,737 | w | 1,741 | 3 | 1,743 | 1 | 1,740 | 1 |
| 1,629 | f | 1,635 | 2 | 1,637 | 2 | 1,623 | 1 |
| 1,556 | f | 1,555 | 2 | 1,555 | 2 | 1,554 | 1 |
| 1,451 | f | | | 1,451 | 2 | 1,450 | 2 |
| 1,435 | f | | | | | | |
| | | | | 1,414 | 1* | | |
| | | | | 1,360 | 4* | 1,374 | 2 |
| | | | | 1,326 | 4 | 1,328 | 2 |
| | | | | 1,314 | 3 | | |

* quartz included ° galena included

1 Natural coffinite (Stieff et al., 1956)

2 Grootvlei G.M., Kimberley Reef

3 Vaal Reefs East G.M., Vaal Reef

4 West Rand Consolidated G.M., White Reef

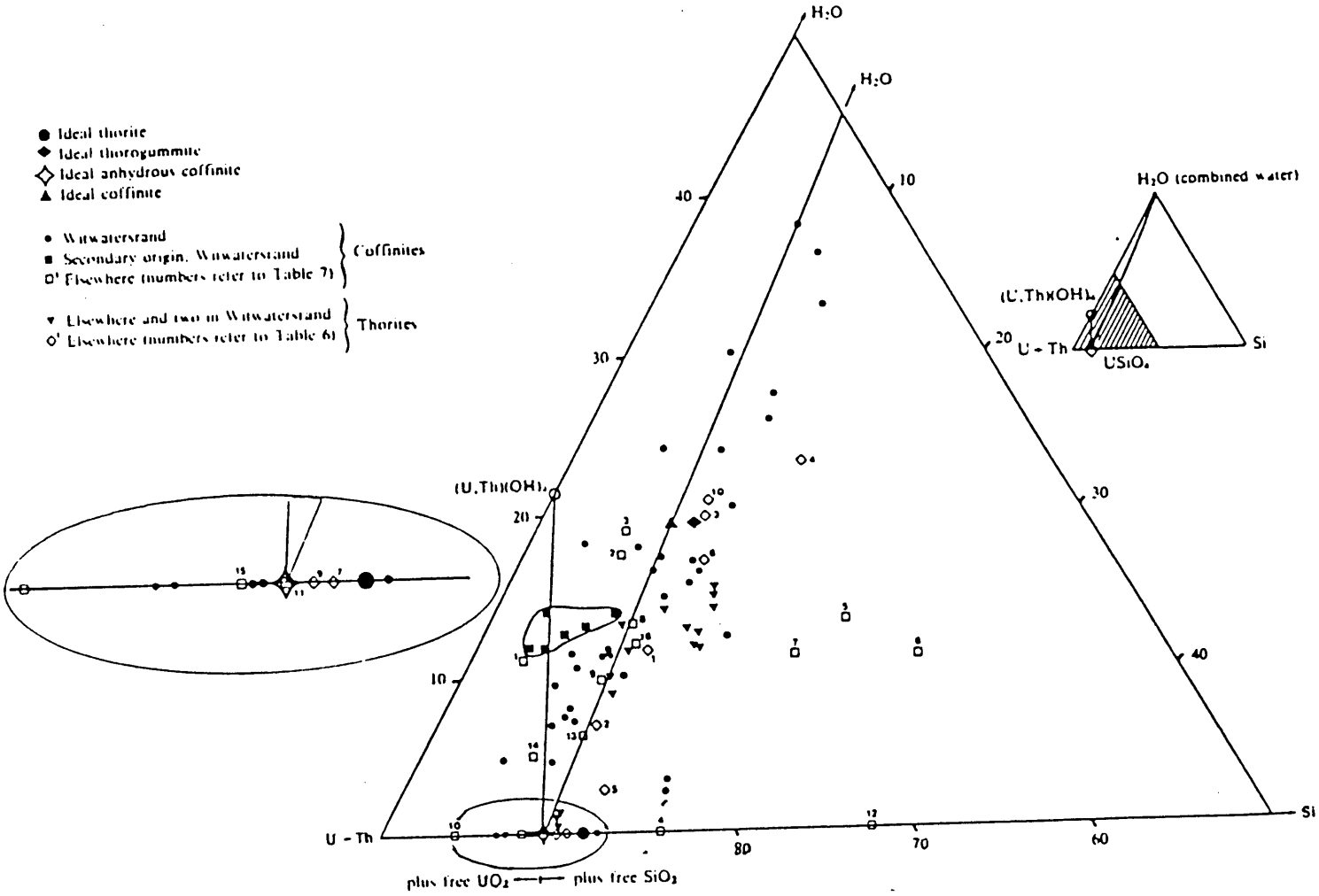



Fig. 16 Composition of (U,Th)-silicates in the (U+Th)-Si-$H_2O$ system in mass per cent ($H_2O$ combined water)

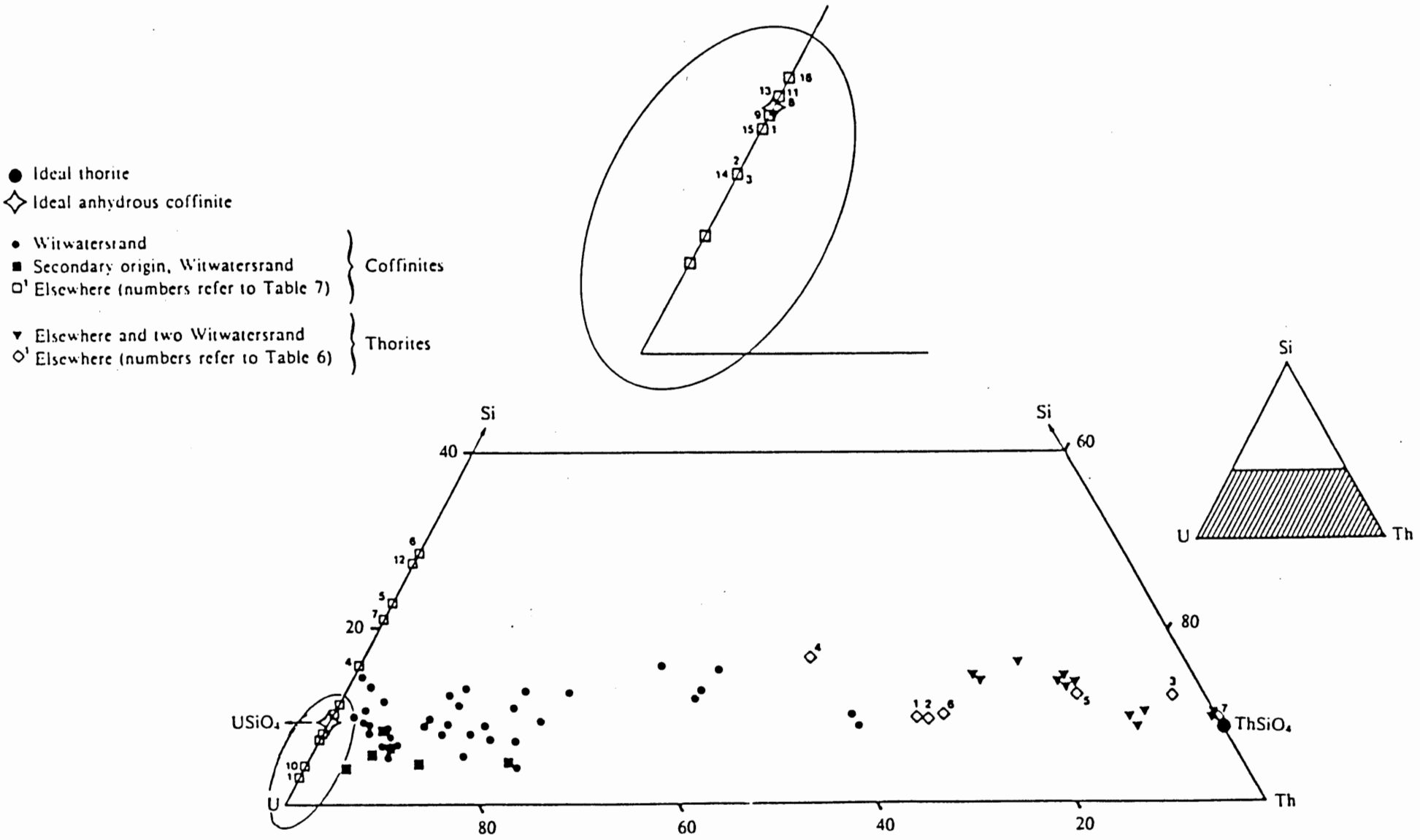



Fig. 17 Composition of (U,Th)-silicates in the U-Th-Si system in mass per cent

difference. Figure 16 shows that the compositions are mostly distributed on either side of the tie line between $H_2O$ and ideal $(U,Th)SiO_4$, and that the concentration of compositions along the tie line between $(U,Th)(OH)_4$ and $(U,Th)SiO_4$ is not a distinct one. Furthermore, the silica content is fairly consistent in comparison with those of water and (U+Th), which fluctuate considerably. No specific concentration of composition is found along the tie line between $(U,Th)OH_4$ and $(U,Th)SiO_4$.

The presence of coffinite has also been indicated by XRD (Table 57) in a leucoxenic substance of anatase composition, which cements detrital minerals, including rutile-leucoxene pseudomorphs (Fig. A.30c). Because of its appearance and the presence of anatase, the product of earthy texture is referred to as *'mushy' anatase*, to distinguish it from the non-uraniferous leucoxene cement, which is composed of rutile. Like the leucoxene, the mushy anatase is mixed with quartz and phyllosilicates, but the mushy anatase encloses also radioactive patches as is indicated by the presence of minute spots of radiogenic galena, and the bluish tint of its internal reflection. EMP analyses (Table 58) record the presence of major titanium, silicon, and uranium (but no thorium), some lead (in the form of galena) and small amounts of yttrium, which could occur as an Y-phosphate. The back scattered electron (BSE) and X-ray distribution images for uranium, titanium, and silicon of the mushy anatase (Fig. 18) show that it is composed of a submicroscopic intergrowth of several phases in dimensions <1 μm, which lies below the X-ray spatial resolution capability of the EMP of <2 μm. In the BSE image, where the grey-tone contrasts indicate differences in atomic number of the elements, galena stands out as bright specks (Fig. A.30d). The molecular masses of (U,Si)- and (U,Ti)-bearing components of variable compositions approach or overlap each other, so that they can barely be distinguished in the BSE. Because of the submicroscopic size of the individual particles, it was not possible to establish the identity of the mineral constituents of which the anatase mush is made up. The presence of coffinite as indicated by XRD is not confirmed

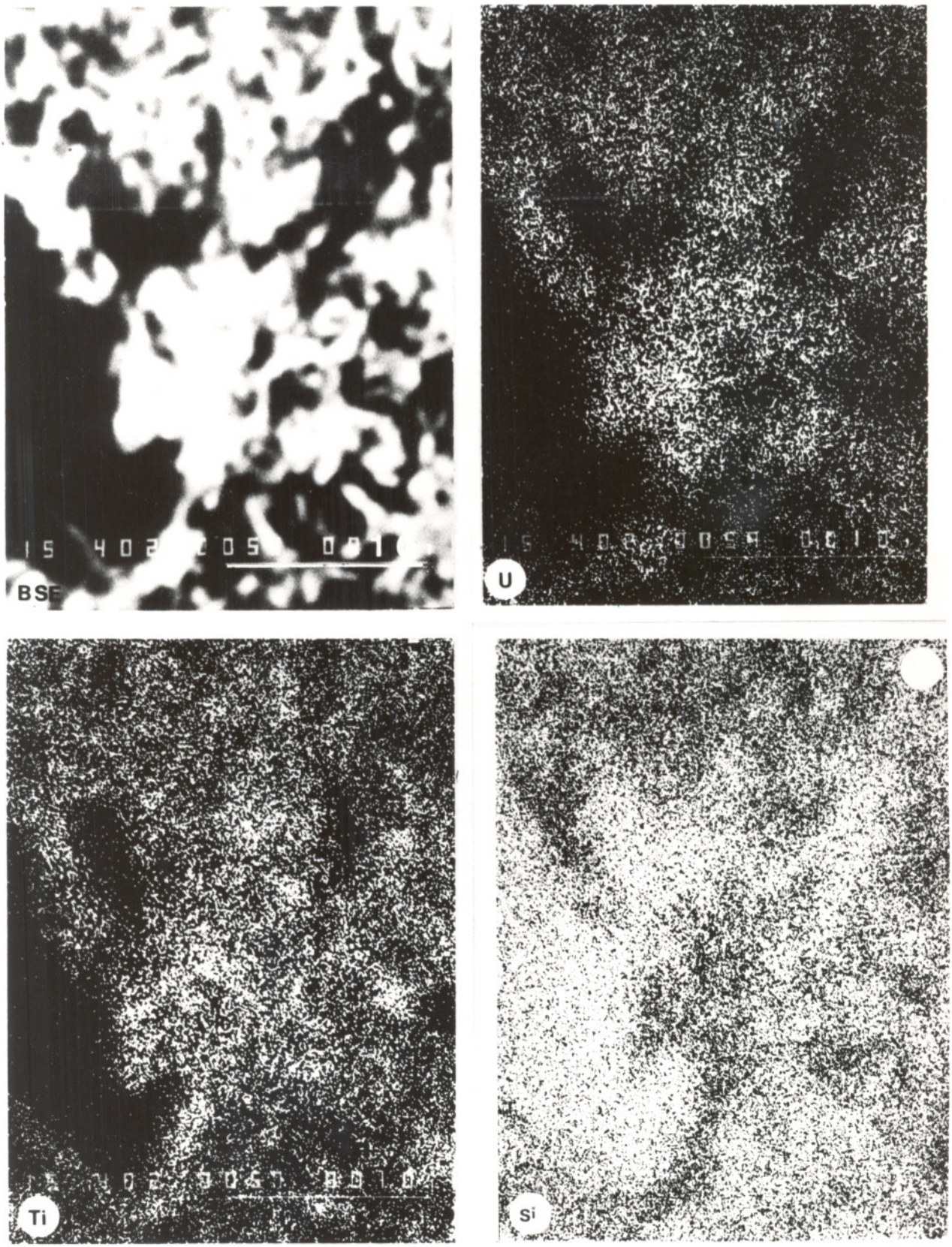



Fig. 18 Backscattered electron and X-ray distribution images for uranium (U), titanium (Ti), and silicon (Si), In BSE, quartz is black and mushy anatase white. The individual constituents of the mushy anatase cannot be distinguished in these images. Scale: 1$\mu$m = 2,6 mm

Table 58 Electron-microprobe analyses of coffinite associated with mushy anatase

| Reference | $UO_2$ | $ThO_2$ | $SiO_2$ | PbO | $SO_3$ | $Y_2O_3$ | $P_2O_5$ | CaO | FeO | $TiO_2$ | $ZrO_2$ | Total | $UO_2+ThO_2/SiO_2$ |
|---|---|---|---|---|---|---|---|---|---|---|---|---|---|
| Rf 602/2-edge | 40,94 | 4,09 | 8,02 | 4,53 | 0,82 | 3,83 | 3,47 | 0,54 | 1,11 | 22,35 | 0,28 | 89,98 | 5,61 |
| Bv 1415/2-1a | 40,85 | 1,80 | 9,41 | 1,65 | 0,15 | 0,89 | 0,57 | 0,16 | 0,36 | 16,48 | 0,22 | 72,54 | 4,53 |
| Bv 1415/2-2 | 24,13 | 0,42 | 8,54 | 2,65 | 0,62 | 0,51 | 0,34 | 0,57 | 1,01 | 47,81 | 0,04 | 86,64 | 2,87 |
| Bv 1415/2-2a | 37,71 | 1,19 | 12,59 | 3,32 | 0,57 | 0,44 | 0,30 | 0,62 | 0,54 | 27,89 | 0,11 | 85,28 | 3,09 |
| WR 824/1-1 | 48,48 | 1,98 | 12,95 | 1,04 | 0,20 | 1,08 | 1,07 | 0,68 | 0,52 | 22,00 | 0,66 | 90,66 | 3,90 |
| WR 824 | 38,43 | 2,18 | 11,69 | 0,56 | 0,17 | 1,12 | 0,99 | 0,64 | 0,83 | 33,86 | 0,62 | 91,09 | 3,47 |

Rf Randfontein Estates G.M., Cooke Section; Bv Blyvooruitzicht G.M. ; WR Western Reefs G.M.

Table 59 Electron-microprobe analyses of uraninite and coffinite of primary and secondary origin in the Monarch Reef, West Rand Goldfield

| Reference | $UO_2$ | $ThO_2$ | $SiO_2$ | PbO | $SO_3$ | $Y_2O_3$ | $P_2O_5$ | CaO | FeO | $TiO_2$ | $ZrO_2$ | Total | $UO_2+ThO_2/SiO_2$ |
|---|---|---|---|---|---|---|---|---|---|---|---|---|---|
| Bv uraninite conc. | 71,40 | 3,30 | 1,30 | 14,20 | 2,00 | 0,60 | n.d. | 0,80 | 2,30 | n.d. | n.d. | 95,90 | |
| Detrital uraninite clusters | | | | | | | | | | | | | |
| WRC 1456/1-1 | 63,83 | 7,89 | 2,45 | 22,33 | 2,31 | - | 0,86 | 0,18 | 0,15 | 0,27 | 0,13 | 100,40 | |
| 1-2 | 74,20 | 2,60 | 1,14 | 15,64 | 1,25 | 1,21 | 0,01 | 2,27 | 0,62 | 0,02 | 0,01 | 98,97 | |
| Alteration product of clustered uraninite | | | | | | | | | | | | | |
| WRC 1456/1-3 | 38,00 | 10,63 | 5,02 | 29,65 | 5,58 | 0,57 | 2,22 | 0,45 | 0,38 | 0,18 | 0,91 | 93,59 | |
| 1-3 | 47,22 | 6,42 | 4,25 | 25,00 | 4,63 | 0,63 | 1,18 | 0,64 | 0,64 | 0,27 | 0,52 | 91,40 | |
| Secondary colloform pitchblende | | | | | | | | | | | | | |
| ECh 1457/1-1 | 67,66 | 0,24 | 1,81 | 0,05 | 0,32 | 0,09 | 0,56 | 0,70 | 0,81 | 0,69 | 0,56 | 73,49 | |
| 1-3 | 71,35 | 0,26 | 2,00 | 0,61 | 0,69 | 0,16 | 0,45 | 0,50 | 1,34 | 0,47 | 0,50 | 78,33 | |
| 1-3a | 74,00 | 0,28 | 0,82 | 0,65 | 0,02 | 0,47 | 0,36 | 0,70 | 1,23 | 0,55 | 0,21 | 79,29 | |
| Remnant of detrital uraninite | | | | | | | | | | | | | |
| ECh 1457/1-2 | 60,65 | 2,96 | 1,48 | 7,83 | 1,01 | 0,17 | 0,46 | 0,43 | 0,47 | 0,53 | 0,25 | 76,24 | |
| Secondary colloform coffinite | | | | | | | | | | | | | |
| Rf 1452/1-1 | 65,09 | 4,52 | 13,54 | 0,25 | 0,17 | 1,44 | 2,04 | 0,97 | 0,17 | 0,19 | 0,36 | 88,74 | 5,14 |
| 1-2 | 63,88 | 5,88 | 10,95 | 1,63 | 2,38 | 0,96 | 1,78 | 0,81 | 0,71 | 0,33 | 0,45 | 89,76 | 6,37 |
| 1-3 | 67,86 | 4,96 | 9,03 | 2,58 | 0,86 | 0,90 | 1,55 | 0,91 | 0,40 | 0,25 | 0,42 | 89,67 | 8,06 |
| 1-4 | 72,68 | 3,85 | 6,14 | 3,28 | 0,73 | 0,51 | 0,97 | 0,84 | 0,36 | 0,30 | 0,26 | 89,92 | |

n.d. not determined; - not detected
Bv Blyvooruitzicht G.M.; WRC West Rand Consolidated G.M.; ECh East Champ d'or G.M.; Rf Randfontein Estates G.M., Randfontein Section

optically, neither is there unambiguous evidence for the presence of uraniferous leucoxene, which is metamict.

*3.7.5. Pitchblende and Secondary Coffinite*

In the Monarch Reef, East Champ d'Or, uraninite has been mobilized to reprecipitate as pitchblende and hydrated thorian coffinite (Figs. A.28c to e). The colloform texture (Figs. A.28d and e), difference in reflectance, and their composition (Table 59) suggests that the mobilization took place close to the water table in a supergene environment relatively recently.

*3.7.6. Thorian Zircon*

Hydroxylated thorian zircon of dimensions between 0,2 to 1 mm is an uncommon detrital constituent of the Dominion Reef. The radioactive and metamict zones in the zoned zircon (Figs. A.13c and d, A.19f), which are dark grey, porous, and pigmented by radiogenic galena, are of a similar composition (Table 60, analyses 3 and 4). The detrital thorian zircon in the Dominion Reef optically resembles the detrital uranoan thorite, but is finer-grained and contains moderate reddish patches enriched in iron (Table 60, analysis no. 6).

Thorite and zircon form a complete series (Frondel, 1953). Natural metamict zircon is hydroxylated, contains fluorine, and is enriched in radioactive elements, which destroy the zircon. The general formula as proposed by Caruba *et al.* (1985) is: $(Zr,Th,U,REE)(SiO_4)_{1-x}(OH,F)_{4x}.nH_2O$, in which x varies from 0,2 to 0,8.

The analytical data for zircon, its hydrated counterparts in the Dominion Reef, and cyrtolite, a mineral name which has been discredited, are in Table 60 compared with those for metamict zones in zircon of the reefs in the CRG. The hydrated thorian zircon contains significant amounts of yttrium, and some calcium and phosphorus, which probably substituted for zirconium and silicon respectively. The composition of the thorian zircon in the Dominion Reef (Table 60, analysis no. 7) is similar to that of the 'cyrtolite' (analysis no. 5) of Ellsworth (1928). When the black thorian zircon was heated to $1000^0C$ for 3 minutes, a translucent greyish pink zircon was left (Smits, 1987, 1989).

Table 60. Compositions of minerals of the thorite-zircon group

| Constituent | Zircon 1 | Hydrated zircon 2 | Metamict zircon | | Cyrtolite* 5 | Dominion Reef | | |
|---|---|---|---|---|---|---|---|---|
| | | | Bv 3 | WA 4 | | Orange 6 | Black 7 | Black 8 |
| $ZrO_2$ | 67,20 | 50,79 | 38,72 | 56,33 | 43,03 | 30,44 | 35,72 | 21,02 |
| $SiO_2$ | 32,80 | 23,08 | 22,13 | 30,16 | 22,86 | 19,53 | 22,57 | 13,83 |
| $UO_2$ | | | 1,63 | 0,12 | 1,40 | 2,37 | 1,16 | 11,31 |
| $ThO_2$ | | | 0,46 | – | 0,66 | 4,63 | 4,22 | 5,99 |
| PbO | | | 0,75 | 0,26 | n.d. | 1,37 | 2,75 | 7,76 |
| $SO_3$ | | | 0,41 | 0,12 | n.d. | 0,56 | 0,85 | 8,58 |
| $Y_2O_3$ | | | 8,11 | 0,01 | 6,76 | 6,13 | 7,37 | 5,31 |
| Other rare-earth elements | | | n.d. | n.d. | 0,34 | n.d. | n.d. | n.d. |
| FeO | | | 0,30 | 0,51 | 4,62 | 14,03 | 2,26 | 3,87 |
| MnO | | | n.d. | n.d. | 3,12 | n.d. | n.d. | n.d. |
| CaO | | | 1,50 | 0,27 | 1,58 | 0,62 | 1,22 | 1,12 |
| $P_2O_5$ | | | 5,66 | 0,19 | 3,53 | 1,20 | 1,52 | 1,36 |
| LOI | | 26,13 | n.d. | n.d. | 12,54 | n.d. | n.d. | n.d. |
| Total | 100,00 | 100,00 | 79,67 | 87,97 | 100,44 | 80,88 | 79,64 | 80,15 |
| Elements not accounted for | – | – | 20,33 | 12,03 | – | 19,12 | 20,36 | 19,85 |

*) Analysis from Ellsworth (1928); cyrtolite is a discredited name for metamict zircon
LOI – loss on ignition Bv – Blyvooruitzicht G.M.
WA – Western Aareas G.M. n.d. – not determined
– not detected

# 4. INTERPRETATION AND DISCUSSION OF MINERALOGICAL OBSERVATIONS IN THE REEFS OF THE CENTRAL RAND GROUP

The information provided by the mineral assemblages in the reefs of the CRG and the Dominion Reef have been carefully analyzed and compared with the response of minerals in the modern oxidizing environment. The minerals that hold important clues with regard to the physicochemical conditions which prevailed at the earth's surface during the sedimentation of the CRG can be subdivided in three major groups:

(1) minerals which are commonly found in igneous rocks, but were destroyed before or after deposition
(2) allogenic constituents that were preserved, some of which even remained unaffected during the final metamorphic stage attained by the sedimentary rocks of the CRG, and
(3) minerals that were altered or neoformed after deposition and burial.

Table 6 lists the minerals which fall in these three categories.

## 4.1. Minerals that are Absent

Since the Witwatersrand sediments are of Archaean age, the provenance was most probably dominated by rocks of the granite-greenstone terrane of the Kaapvaal Craton and old metamorphic complexes like that of the Limpopo. Remnants of the greenstone belts are, for example, found in the Barberton Mountain Land or the Murchison Range. Sediments older than those of the Witwatersrand Supergroup also contributed to the detrital supply.

The minerals, which have not been noticed in the heavy-mineral assemblage of the reefs (Table 61, first column), are common constituents of the supracrustal rocks of the Barberton Mountain Land and the surrounding granites as was established by Liebenberg (1972).

Fuller (1958) reported the presence of albite, magnetite, calcite, and less commonly epidote and apatite in the older sedimentary rocks of the WRG. They could have been eliminated when the proximal facies of the sediments of the WRG were reworked and redeposited in the sediments of the CRG.

Table 61 Genetic classification of heavy minerals in the CRG reefs and the Dominion Reef

| Minerals that are * | | |
|---|---|---|
| missing | inherited | neoformed and altered |
| silicates | compact pyrite | kerogen |
| carbonates | rutile-leucoxene | Diagenetic produts: |
| sulphates | chromite | uranous titanates |
| ilmenite | zircon | relict uraninite |
| magnetite | uraninite | cutans |
| detrital sulphides; | arsenopyrite | (U,Th)-silicates |
| galena | cobaltite | crystalline rutile |
| sphalerite | gold | leucoxene |
| pyrrhotite | PGM | crystalline gersdorffite |
| chalcopyrite | sericite | alteration of biotite |
| apatite | fuchsitic sericite | to kaolinite, illite, |
| ferrihydrite? | polymineralic spheroids | chlorite |
| hematite? | tourmaline | intermediate diagenetic |
| | xenotime | clay minerals |
| | graphite | Metamorphic products: |
| | molybdenite | chloritoid |
| | Products of hydrothermal activity: | pyrophyllite |
| | concretionary pyrite | chlorite IIb |
| | chloritized pyrite | sericite/muscovite $2M_1$ |
| | chloritized chromite | alteration of biotite to |
| | chloritized arsenopyrite | pyrophyllite, chlorite, |
| | chloritized garnet | muscovite |
| | detrital chlorite | galena |
| | In Dominion Reef: | sphalerite |
| | monazite | pyrrhotite |
| | garnet | chalcopyrite |
| | uranoan thorite | gersdorffite |
| | thorian zircon | recrystallized gold |
| | euxenite | overgrowth tourmaline |
| | cheralite | Supergene products: |
| | | pitchblende |
| | | secondary coffinite |
| | | marcasite |

*) Minerals are listed in approximate order of abundance in each group

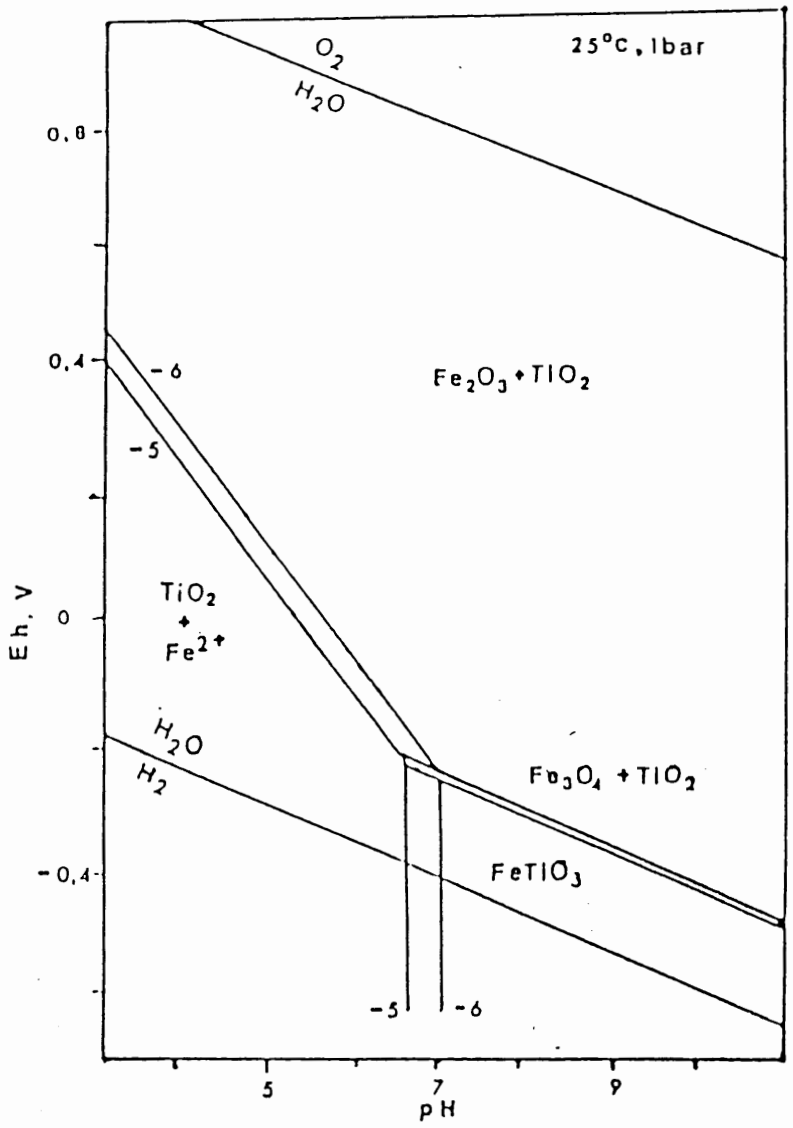



Fig. 19 Stability fields for ilmenite, magnetite + rutile, and hematite + rutile in natural waters at total dissolved $Fe^{++}$ of $0^{-5}$ and $10^{-6}$ (Dimanche & Bartholomé, 1976)

The absent minerals provide indirect information about the geochemical activity at the earth's surface. Most of the minerals listed in the first column of Table 61 dissolve in an acid envorinment, whereas amphibole, pyroxene, and olivine are unstable at the earth's surface in an acid or alkaline environment (Loughnan, 1969). Hence, the absence of these minerals could be an indication that acid conditions prevailed at some stage before or after deposition on the alluvial fan.

*4.1.1. Ilmenite, Magnetite, Hematite, and Ferrihydrite*

The absence of ilmenite, magnetite, hematite, and ferrihydrite is an important geochemical aspect which contributes to the decoding of the physicochemical environment at the earth's surface during the Archaean. Of these minerals, only ilmenite survived the exogenic cycle in the form of *rutile-leucoxene* pseudomorphs (Section 4.2.6).

In the modern oxidizing environment *magnetite* may survive modern weathering conditions even though it is out of equilibrium, and, like ilmenite, is a common constituent of beach sands. *Ilmenite* reacts in an oxidizing as well as a reducing environment. As is illustrated in the pH-Eh diagram (Fig. 19), the dissolved ferrous iron can follow three paths (Dimanche & Bartholome, 1976):

(1) at pH values below 7, it remains in solution and can migrate, whereas
(2) at pH values above 7, it reprecipitates in an oxidizing or reducing environment as limonite, which matures to hematite or is incorporated in illite or ML illite/smectite, and
(3) in a reducing, weakly acid to alkaline environment, it is sulphidized if sufficient sulphur is available, otherwise it precipitates as magnetite or chlorite.

In an oxidizing environment, the ferrous iron is removed in a stepwise fashion to form rutile via the intermediate product pseudorutile, $Fe_2Ti_3O_9$, in the following way (Temple, 1966):

$$3FeTiO_3 + 2H^+ + 1/2O_2 \longrightarrow Fe_2Ti_3O_9 + Fe^{2+} + H_2O \quad (1)$$

$$Fe_2Ti_3O_9 + 4H^+ \longrightarrow 3TiO_2 + 2Fe^{2+} + 2H_2O + 1/2O_2 \quad (2)$$

Under reducing conditions, iron is leached progressively, and rutile is the immediate end product (Dimanche & Bartholome, 1976):

$$FeTiO_3 + 2H^+ \longrightarrow TiO_2 + Fe^{2+} + H_2O \quad (3)$$

The total absence of remnants of ilmenite in the rutile - leucoxene pseudomorphs indicates that the mechanism responsible for the dissolution of ferrous iron was extremely effective. Since the rate of oxidation of ilmenite and magnetite is extremely slow, it is virtually impossible that oxidation was responsible for the thorough removal of ferrous iron from ilmenite and the complete eradication of magnetite. The release of ferrous iron from these minerals in a neutral to acid environment which, with an increase in the oxidation potential, have to be more acid (Fig. 19), is a much more effective geochemical process. This type of reaction takes place in diagenetic and supergene environments if the iron concentration of the intrastratal solutions is sufficiently low (Dimanche & Bartholome, 1976). Ilmenite would dissolve incongruently and produce residual titania. Pure *magnetite* would be completely destroyed in an acid-reducing environment, leaving no sign of its existence, but titaniferous magnetite would produce a skeletal titania residue after the removal of iron. The delicate remnants, including some of the leucoxene with unfilled pores could have disintegrated during transportation. This type of residue was then deposited as leucoxenic cement and mushy anatase in the more remote areas of the depositional surface. Because pyrite, hematite, or siderite are not found in close association with the rutile-leucxoxene pseudomorphs, most of the ferrous iron could have remained in solution, unless it was taken up by neoformed chlorite.

The study of palaeosols on Archaean rocks onto which the Dominion reef was deposited confirms that the dissolution of ferrous iron was a common near-surface phenomenon at that time (Grandstaff *et al.*, 1986).

Hydrothermal solutions could have infiltrated and affected certain areas in the provenance. These fluids could have been responsible for the eradication of part of the ilmenite. In that case, unaltered ilmenite should also have been a constituent of the detritus, as is the case with the unaltered and the chloritized iron-bearing minerals, which occur side by side. The pseudomorphs after ilmenite in the Dominion Reef,

which were leached *in situ*, suggest that, at the time of the deposition of the first reef on the Archaean floor of the Witwatersrand Basin, ilmenite had not been completely eliminated in the source rock.

Hutchinson and Viljoen (1988) recently advanced the following hypothesis for the source of gold in the Witwatersrand deposit. In analogy with the modern black 'smokers' on the ocean floor, primary pyritic and auriferous exhalites could have formed very early in the history of the basin along the tectonically active northern and western margin of the basin. After subsidence of the basin floor and marginal down-faulting at the western and northern edge, these vents became the source of hydrothermal fluids. The authors propose that magnetite would have been converted to pyrite and ilmenite to pyrite and a relict titanium oxide. However, there is no evidence for such a pyritization process in the reefs or in the magnetic shales in the WRG (Coetzee, 1965).

Dimroth (1979) and Clemmey (1981) also believe that *pyritization of magnetite and ilmenite* was an important process during the Witwatersrand sedimentation. The sulphur required for the process was of volcanic origin, or was released during the oxidation of pyrite (ibid.).

The following features contradict general sulphidation of ilmenite- and magnetite-rich sands or recrystallization of compact and concretionary pyrite:

(1) the preservation of inherited features such as, sulphide and gold inclusions (Fig. A.7a), fracture fillings (Fig. A.7b), and textures typical for hydrothermal pyrite (Figs. A.6a to d, A.7d and e).
(2) the virtual absence of relicts of magnetite or ilmenite within pyrite,
(3) the etch textures of detrital pyrite (Fig. A.6e), which do not show characteristic replacement textures,
(4) the variable composition of the pyrite (Hallbauer and Von Gehlen, 1983; Fig. A.6e),
(5) the presence in compact detrital pyrite of highly saline fluid inclusions comprising a variety of daughter minerals (Hallbauer, 1983), and
(6) the narrow spread of $\delta^{34}S$ values of detrital pyrite around 0‰, the value for sulphur of the mantle (Table 62).

Table 62 Isotopic composition of kerogen, sulphides and sulphates

| | $\delta^{13}C$, ‰ | $\delta^{34}S$, ‰ |
|---|---|---|
| WITWATERSRAND | | |
| Basal Reef President Brand, Free State Geduld, Western Holdings G.M. | -30,3 to -32,8[1] | +1,8 to + 4,0[2] |
| 'B' Reef | -27,1 and -30,5[1] | +1,9 to + 3,2[2] |
| Basal Reef, Virginia G.M. | -22,4 and -22,9[1] | +1,0[2] |
| Carbon Leader | -27,4 to -37.2[3] | |
| Elsburg A3 Reef | | +0,2 to +5,6[4] |
| West Rand Group, marine shales | | 0,0 to +4,5[5] |
| ELLIOT LAKE DISTRICT, CANADA | | |
| Lower Huronian Supergroup conglomerate | ? to -38,8[6] | -1,5 to +1,2[7] |
| Upper Huronian Supergroup sandstones | | -20,4 to +3,2[7] |
| BARBERTON MOUNTAIN LAND | | |
| Barites | | +3,1 to +3,8[8] |
| Pyrites | | -0,9 to +1,6 |
| Fig Tree Group | -25,0 to -33,0[9] | |
| Theespruit Formation | -14,7 to -19,5[8] | |

Data from (1) Hoefs and Schidlowski (1967), (2) Hoefs et al. (1968), (3) Hoering (1967), (4) Jensen and Dechow (1964), (5) Cameron (1982), (6) Eichmann and Schidlowski (1974), (7) Hattori et al. (1983), (8) Perry et al. (1971), and (9) Oehler et al. (1972)

The $\delta^{34}S$ values for the pyrite in the reefs of the CRG are close to that of the earth's mantle (0‰ ), whereas the low spread of these values indicates that little isotopic fractionation took place (Table 62).

At the appropriate pH, *hematite* and *ferrihydrite* may precipitate at oxygen pressures as low as $10^{-65}$ (White and Yee, 1985), but if conditions become too acid, these minerals will dissolve (Figs. 19 and 20). Ferric iron species were not identified in any of the reefs or at the top of footwall quartzites, which were exposed to the atmosphere for a long period, neither was there textural evidence for their earlier presence. One can say with fair confidence that large-scale oxidation of iron-bearing minerals did not take place. The preservation of the detrital constituents uraninite (Section 4.2.1.), pyrite (Section 4.2.4.), chlorite (Section 4.2.5.), and biotite (Section (4.2.7.) during transportation also suggests that oxidation at the earth's surface was not as rapid as today.

*4.1.2. Carbonates, Sulphates, and Silicates*

Carbonates, sulphates, and silicates are common constituents of the supracrustal rocks in South Africa (Liebenberg, 1972). These minerals could have become unstable before or after deposition in the sediments of the CRG. A high carbonic acid concentration of ground- and surface waters would generate acid conditions, in which these minerals are eliminated. For example, it would drive the following reaction to the right:

$$CaCO_3 + H_2CO_3 \rightleftharpoons Ca^{2+} + 2HCO^-_3 \qquad (4)$$

If *calcite* formed after burial, it would anyhow have disappeared at a depth of burial >3700 m (Hower *et al.*, 1976). The mineralogical modification of sediments in the depth interval between 2000 and 3700 m is marked by the loss in CaO (ibid.). The fabric of the sediment does not provide unquestionable textural evidence for the earlier occurrence of detrital carbonate or cement. Pressure fringes on minerals are usually filled with carbonate or quartz, but those in the reefs of the CRG contain chlorite (Fig. 7a) and less commonly quartz.

*Sulphates* would undergo the same fate as the carbonates, and would be eliminated in an acid environment.

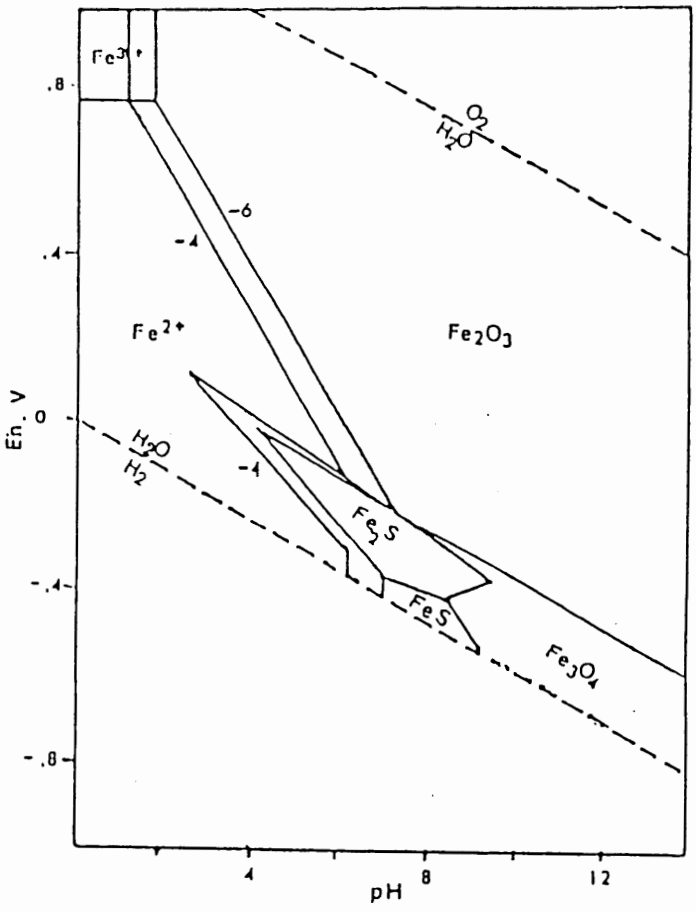



Fig. 20 Eh-pH diagram showing stability fields of iron oxides and sulphides in water at 25°C, 1 atm and $S_{tot}=10^{-6}$ (after Garrels & Christ, 1965)

Recurrent sedimentary activity could have been responsible for the absence of *feldspar*. But even if it survived the sedimentary cycle, potassium feldspar, like calcite, disappears at a depth >3700 m, the potassium being taken up by neoformed illite (Hower *et al*, 1976). After a depth of 3700 m, no significant depth-dependent mineralogical changes are detected (ibid.).

Except for possible chlorite pseudomorphs after *amphibole* or *pyroxene* in the Vaal Reef (Fig. 6b), and the common pseudomorphs after biotite in all reefs of the CRG, there is no textural evidence which can be used for the identification of other allogenic silicate precursors. All silicates today present in the CRG reefs are products of metamorphism and are the major metamorphic indicators (Section 4.3.4.).

*4.1.3. Apatite*

Notwithstanding its slow chemical reaction, for which acid conditions are required, apatite is conspicuously absent. The complete disappearance of apatite, which is slightly more resistant to present-day surface processes than ilmenite (Loughnan, 1969), is difficult to explain because in modern weathering conditions, apatite reacts only very slowly in an acid environment as follows:

$$ap + 3H^{+} \rightarrow 5Ca^{2+} + 3HPO_4^{2-} \qquad (5)$$

As for ilmenite, magnetite, and the minerals discussed in the preceding section, the thorough destruction of this phosphate is an indication that persistent acid conditions must have prevailed at the earth's surface. Post-depositional conditions were obviously not favourable for its reprecipitation. As for the chloritized iron-bearing minerals, if hydrothermal activity in the source rocks was responsible for its dissolution, some unaffected apatite is expected to occur in the reefs. The apatite crystals which occur in the polymineralic spheroids of possible volcanic origin (Reimer, 1983) could have been preserved, because they were enclosed by phyllosilicates, or they are of authigenic origin.

The presence of authigenic yttrium phosphate in association with the *in situ* transformation of uraninite to coffinite in the UE1a and E9 Reefs, West Rand G.F., in an alkaline-reducing environment indicates that dissolved phosphate ions were present after burial.

*4.1.4. Framboidal Pyrite*

In the modern oxidizing environment at the earth's surface, minute crystals or framboids of pyrite commonly form in the upper few centimetres below the water-sediment interface in the presence of sulphate (Fig. 13). Because this type of pyrite requires oxygen for its formation, its absence at the unconformities could be an indirect indication of the lack of free oxygen in the primitive atmosphere. In the quartzites overlying the basal conglomerate of a cycle, rapid sedimentation would have inhibited the precipitation of this type of pyrite.

Instead of the minute pyrite crystals and framboids, gersdorffite crystals of similar size (<40 μm), sometimes enclosing a core of pyrite, chalcopyrite, or galena (Fig. A.9g) precipitated together with the younger uraninite-free kerogen generation in the environment which was suitable for the growth of microorganisms (Figs. A.9e, f, and h).

*4.1.5. Sphalerite, Galena, Chalcopyrite, Pyrrhotite, and Pentlandite*

Although sphalerite, galena, chalcopyrite, pyrrhotite, and pentlandite are common constituents of hydrothermal origin in the supracrustal rocks of the Barberton Mountain Land (Liebenberg, 1972) and most likely in other greenstone remnants, they do not occur as allogenic constituents in the reefs of the CRG, except for rare detrital sphalerite present in kerogen seams of the Basal Reef (Fig. A.8a). The detrital sulphides must have been eliminated at some stage before or after arrival at the final site of deposition. For nickel, lead, and zinc to dissolve, the pH has to drop below 6,5 at a partial pressure of carbon dioxide of $10^{-2}$ atm (Garrels and Christ, 1965). For the dissolution of copper as $Cu^{2+}$, the environment should be acid and weakly oxidizing, but when conditions are acid and reducing, dissolved copper may occur in

the lower oxidation state $Cu^{+}$ (Pourbaix, 1963).

In the modern oxidizing environment, hydrous oxides of iron and manganese serve as a sink for metal ions. In the absence of these hydrous oxides, the cations could have remained in the ionic state dispersed in the sediment, or they were adsorbed onto clay minerals.

The sulphides and gersdorffite of authigenic origin precipitated after burial together with quartz and fairly commonly with gold, which recrystallized at the same time (Section 4.3.4.).

## 4.2. Minerals that were Preserved

Several of the constituents in the reefs of the CRG, including the rutile-leucoxene pseudomorphous after ilmenite (Section 4.1.1.), arrived unaltered at the final site of deposition, and remained so after burial (Table 61, column 2).

A large part of the detrital uraninite and gold, but only insignificant amounts of other detrital minerals, were entrapped by the microbial communities. These microorganisms supposedly grew in shallow pools of stagnant water (Hallbauer, 1975) on some of the major unconformities and on palaeosurfaces of hiatuses of much shorter duration between individual conglomerate pulses within the Johannesburg Subgroup in the western half of the Witwatersrand Basin.

Both the heavy-mineral concentrations and the microbial mats formed on the major unconformities prior to the deposition of the pebble fraction of the basal conglomerate. Because of the syngenetic sedimentary nature of the process, the kerogen is discussed in the section on neoformed and altered minerals (Section 4.3.1.).

### *4.2.1. Uraninite*

Uraninite is the most informative constituent of all heavy minerals with regard to pre- and post-burial geochemical conditions at, and close to the surface.

From the unaltered state of the uraninite encapsulated by the kerogen, it is obvious that the uraninite arrived at the depositional plane in the unoxidized state and remained so up to this date when associated with organic matter (Smits, 1986).

This feature tells us that the microbiota did not produce metabolic oxygen while they entrapped the uraninite (Section 4.3.1).

The low uranium concentration of the quartzites over- and underlying the reefs, which is <10 g/t compared with about 200 g/t of the reefs, indicates that uranium was not present in the dissolved state before the debris were deposited.

The large agglomerates solely composed of uraninite grains in the Monarch Reef, East Champ d'Or G.M. (Fig. A.19c), are not associated with kerogen. They could have accumulated in areas unsuitable for the growth of microbiota and also the oxidation of the uraninite. For example, the water could have been too deep or too turbulent. After burial, the uraninite in these concentrations was partly or entirely altered to coffinite (Fig. A.28a).

In contrast with the uraninite encapsulated by kerogen, the grains that formed part of the heavy-mineral concentrations in the matrix in which the pebble fraction was set, reacted after burial. This reaction is evident from the common occurrence in all reefs of relict uraninite grains from which the bulk of the uranium was released (Figs. A.20d to f, A.23a and b). The characteristic pegmatitic composition of the uraninite in the Witwatersrand including the oldest uranium-bearing conglomerate, the Dominion Reef, suggests that pegmatites must have existed in the provenance (Pretorius, 1976; Grandstaff, 1976). However, the rocks which supplied the uraninite and other pegmatitic minerals have nowhere been preserved so that there is no unequivocal evidence what type of rocks supplied these minerals.

Uraninite of pegmatitic origin is known to occur in large lumps (Frondel, 1958). Occasionally, cataclastic aggregates of uraninite up to ten times larger than the discrete grains, which on average are 80 μm in diameter, were noticed in the polished sections (Fig. A.19f to h, A.20b). The cracks in these aggregates, which frequently follow crystal planes, are sometimes healed by authigenic uranium-bearing minerals or an yttrium-phosphate. If such a fragmented grain is broken up, the individual particles could possess a sub- to euhedral shape

(Figs. A.19d and e) or one flat side (Figs. A.17f and A.19a). Schidlowski (1966b) referred to the latter type as muffin-shaped grains.

*4.2.2. Gold*

Several investigators (Hallbauer, 1975; Reimer, 1984; Mossman & Dexter-Dreyer, 1985) believe that at least part of the gold arrived in the depository in the colloidal state, organically bound or in the form of gold complexes. But the distinct relationship which exists between the concentration pattern of the gold and the depositional environment is clear evidence for its *detrital origin* (Coetzee, 1965; Von Gehlen, 1983). This is confirmed by the age of gold and sphalerite particles in the Basal Reef, which was determined at 3200 Ma (Giusti *et al.*, 1986).

However, it is generally accepted that the gold was *reconstituted* during metamorphism at about 250$^{0}$C (Liebenberg, 1955; Saager, 1969). The introduction of magmatic matter along faults could have influenced the gold recrystallization on a local scale. The recrystallization is indicated by:

(1) the change in shape of the detrital gold, in particular when enclosed by kerogen,
(2) the association with the authigenic sulphides, gersdorffite, and quartz, and
(3) the homogeneous distribution of silver and mercury within each gold grain.

The gold was mobilized during its reconstitution over microscopic distances, so that the sedimentary distribution pattern was retained (Pretorius, 1976; Hallbauer & Von Gehlen, 1983).

The *size* of the gold grains in the reefs is comparable with that of the gold found in rocks of the Barberton Mountain Land, where it is mainly associated with pyrite, pyrrhotite, and arsenopyrite, or occurs as discrete grains in the gangue of the veins or in the wall rock. In view of the microscopic grain size, Nami (1982) postulated that the bulk of the Witwatersrand gold was transported in suspension. Because suspended particles are buoyed upwards by turbulence and seldomly touch each other, they are not subjected to the same mechanical abrasion as particles dragged along the stream bed (ibid.).

Although the *composition* of individual gold grains is homogeneous (Utter, 1978; Oberthur, 1983), it differs from one grain to another in the same handspecimen of a reef or kerogen seam. The variation in gold composition, even of neighbouring grains, rules out the general dissolution of the gold at any stage before or after deposition, including a general homogenization during metamorphism (Von Gehlen, 1983).

Because of the long time span between denudation in the source rocks and deep burial in the depositional area, it is very unlikely that the present, extremely variable *fineness* values of the gold would represent those that were inherited from the source rocks. Nevertheless, the variation in fineness of the gold generally reflects their origin and can be used to discriminate between source rocks (Utter, 1978; Krapez, 1979; Oberthur, 1983; Hirdes, 1984). The distribution pattern of fineness values of the Vaal Reef (Utter, 1978) confirmed the existence of two separate entry points, which gave rise to the Witkop and Stilfontein Facies (Minter, 1972). Two entry points have also been recognized from the gold composition on the West Wits Line G.F. (Oberthur, 1983) and on the East Rand G.F. (Hirdes, 1984). The inheritance of gold through reworking of underlying reefs appears to be much less common than was previously assumed (Utter, 1978; Krapez, 1979; Hallbauer, 1983).

The *variation in fineness* values of the detrital gold in the sediments as a whole (Table 31) is very similar to that of gold from the Barberton Mountain Land (Gay, 1968: Viljoen, 1971), which is assumed to be comparable with greenstones in the provenance of the Witwatersrand. The low average fineness value of the gold in the Black Reef, viz 800, could then be explained by stratigraphic inversion of the source rocks during sedimentation (Viljoen *et al.*, 1970), because the silver concentration in the gold occurring near the contact of granite and greenstone rocks in the Barberton Mountain Land is high (Gay, 1968).

The *mercury content* (Table 31) of the gold of the Witwatersrand, <3,1% is higher than that of the rocks in the Barberton Mountain Land, <0,3%, but in concert with that of the

rocks of the Murchison Belt (another preserved remnant of greenstones) where the mean is 4,6% (Erasmus *et al.*, 1982).

The *geochemical response* of gold to various natural conditions has been studied by several investigators. This information is summarized in Table 63 and pictured in Figure 21. Mechanisms which could have led to the dissolution of gold after burial are a change in pH, the presence of dissolved arsenic, a decrease in sulphur activity as a result of the precipitation of sulphides, and an increase in temperature and pressure with the increase in depth of burial (Seward, 1973). The simultaneous precipitation of recrystallized gold with the authigenic sulphides and gersdorffite suggests that the decrease in sulphur activity could have played a role. The common association of the detrital or recrystallized gold with sulpharsenides of both allogenic and authigenic origin accentuates the affinity of gold for arsenic.

The three following phenomena observed in the present study indicate indirectly that gold did not occur in the dissolved state before, or on arrival at the final site of deposition.

Firstly, if complexed gold was present at the time of the dissolution of ferrous iron, the gold complex would have been reduced by the iron, so that the gold would have reprecipitated in the vicinity of the rutile-leucoxene. However, no specific relation has been noticed between gold and the rutile-leucoxene pseudomorphs.

Secondly, nugget formation, a common near-surface process in the modern environment, is rare or did not take place at all. It is possible that conditions were not oxidizing enough for the mobilization of gold because of the assumed deficiency of free oxygen in the atmosphere.

Thirdly, the gold enclosed by kerogen is never associated with the phyllosilicate enclosed by the kerogen. If gold would have occurred in the dissolved state when entrapped by the microbiota, the clay mineral present at that time would have absorbed the gold complex. However, gold organic-complexes could well have formed after the gold had been entrapped by the microorganisms.

Table 63 Geochemical response of gold in different natural environments

| Environment | Geochemical behaviour |
|---|---|
| Natural water | Gold complexes with strong ligands, e.g. chloride, sulphide, thiosulphate, or cyanide. Major species are: $Au(OH)_3^-$, $AuO^{2-}$, $AuCl_4^-$, $Au(S_2O_3)_2^{3-}$, $Au(CN)_2^-$, $Au(CNS)_4^-$, $AuS^-$, and $Au_2(HS)_2S^{2-}$ (Boyle et al., 1975). $Au(CN)^{2-}$ is stable over the full pH range in the stability field of natural waters (Fig. I.12b) Concentration of gold in natural water about 0.03 µg/l (ibid.) |
| Acid water | At 25°C, 1 atmosphere, pH > 5, Eh > 0,9V, concentrations of Au = $10^{-5}$, and $Cl^-$ = $10^{-3,2}$, in the presence of an oxidant, gold is oxidized to $AuCl_4^-$ (Mossman and Harron, 1983; equation 1). In weakly acid to alkaline solutions, the gold is transported as an organic protected colloid |
| Presence of organic matter and bacteria | Solid organic acid is able to reduce gold complexes at very low pH (Ling Ong and Swanson, 1974). Humic acids and microbes can dissolve, absorb, and enrich gold. $Au(CN)_2^-$, which is produced in soils in the presence of organic matter, may be absorbed by some plants; when decomposed gold precipitates (Lakin et al.,1974; equation 2). Living bacteria actively precipitate gold, but dead organisms do not (Dexter-Deyer-Grosovsky, 1983). Decay of organic matter by anaerobic bacteria in acid, reducing environment promotes dissolution of gold (Pares et al, 1965; Korobushkina et al., 1976) |
| Lateritic horizons | At low pH and high $Cl^-$ concentration, gold occurs as $AuCl_4^-$; in the presence of $Fe^{2+}$, the complex is reduced to native gold (Mann, 1984; equation 3). $Mn^{2+}$ plays a similar role |
| Present day tidal flats in northwest Sri Lanka (Dissanayaka and Kritsotakis, 1984) | Au and Pt precipitate in peat and algal mats; they are associated with clay minerals, and iron and manganese oxides |
| Oxidizing | At pH 5 to 8, $S_2O_3^{=}$ will dissolve gold (Lakin et al., 1974; equation 4). Removal from solution by absorption on humic acids, clays (Goleva et al., 1970), and ferrihydrites. Precipitation of particulate gold by recurring redox reactions |
| Supergene | Gold transported by ferric sulphate solution as chloride or sulphur complexes (Fig I.12a); gold will precipitate if pH or Eh changes, e.g. at water table, to form nuggets (Mossman and Harron, 1975) |
| Reducing | $AuS^-$ is dominant species at about pH 7 and low temperature |
| Hydrothermal | Complexes present at 300°C low pH: $HAu(HS)^\circ$ (Seward, 1984) (Fig. I.12c) neutral pH: $Au(HS)_2^-$ and alkaline pH: $Au_2(HS)_2S^{2-}$ (Seward, 1973) Gold precipitation results from drop in temperature and pressure, change in pH and Eh, and decrease in activity of ligands. If FeO is present, gold and pyrite precipitate (equation 5) |

Equations:

(1) $Au^\circ + 4Cl^- \rightleftharpoons AuCl_4^- + 3e^-$

(2) $Au(CN)_2^- + e^- \rightleftharpoons Au^\circ + 2CN^-$

(3) $AuCl_4^- + 3Fe^{2+} + 6H_2O \rightleftharpoons Au^\circ + 3FeOOH + 4Cl^- + 9H^+$

(4) $Au^\circ + 2S_2O_3^{2-} \rightleftharpoons Au(S_2O_3)_2^{3-} + e^-$

(5) $2Au(HS)_2^- + 2H^+ + FeO \rightleftharpoons 2Au^\circ + 2H_2S + FeS_2 + H_2O$

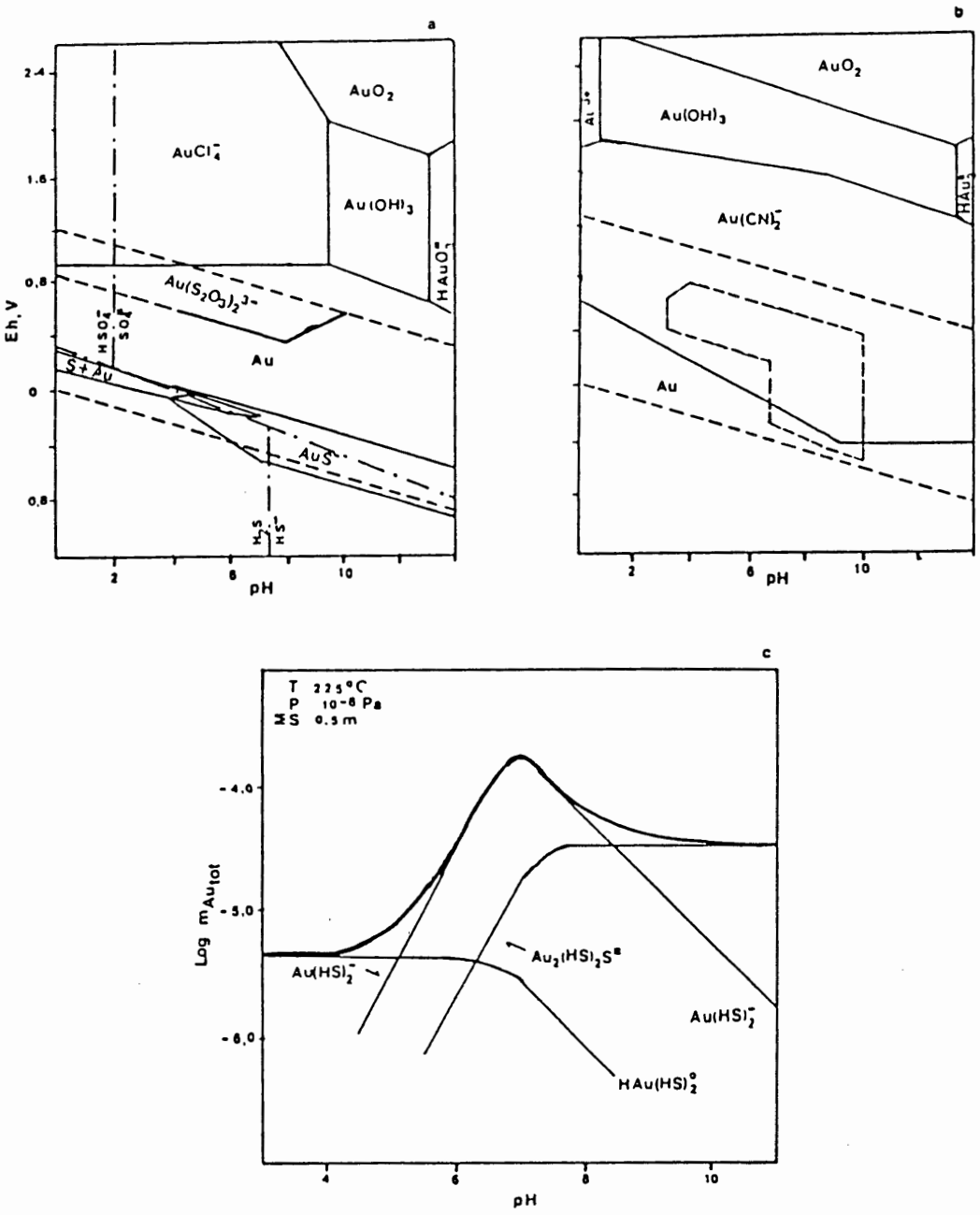



Figure 21 a Eh-pH diagram for Au-Cl-S-$H_2O$ system at 25°C, 1 atm, $Cl^-$=10 M, S=$10^{-1}$ M. The fields for aqueous sulphur species are defined by stripe-point line (Garrels and Christ, courtesy J. Phillips, 1965)

b Eh-pH diagram for Au-CN-$H_2O$ system at 25°C, 1 atm. Au=$10^{-4}$, CN=$10^{-3}$ (Finkelstein, 1972). The area defined by interrupted line within the stability field of water represents the natural aqueous environment (Baas Becking *et al.*, 1960)

c Solubility curves for three thio-gold complexes compared with experimentally determined solubility isotherm (heavy line) for 225°C, $10^{-8}$ Pa, $S_{tot}$=0,5 m/l (after Seward, 1984)

Recrystallization of the gold during metamorphism could be responsible for the moulded texture of the gold tightly filling open space in the kerogen.

*4.2.3. Platinum Group Minerals*

The same controversy as for the gold existed between hydrothermalists and placerists on the origin of the PGM. But today, it is generally accepted that almost all PGM are of detrital origin. They must have derived from mafic and ultramafic rocks of the Archaean greenstone belts, in which platinum and palladium were the major platinoid elements (Cousins, 1973).

Compared with the other PGE, palladium, the most unstable element amongst the platinoids (Table 64), is deficient in the reefs of the CRG (Feather, 1976). The rare occurrence of secondary Pt-minerals in the reefs of the CRG indicate that small amounts of platinum were dissolved and, after burial, reduced to give rise to authigenic species (ibid.).

The grain size of the PGM is noticeably smaller than the PGM found in recent placers, and accretion of PGE to form larger-sized nuggets, a common process in modern placers, has not been noticed in the Witwatersrand. As for gold, a lack of free oxygen could have hindered such a process.

The removal of two of the platinoids during sedimentation complicates the assessment of the PGE that were originally supplied by the source rocks. As pointed out by Reimer (1979), the figures available from beneficiation concentrates represent about 50 to 60% of the total platinoid content, and therefore might not reflect the correct distribution pattern of the PGE.

The greater abundance of PGM in the East Rand and Evander G.F. in reefs of the Turffontein Sugroup suggests that at the time of their deposition, the source rocks consisted of mafic or ultramafic rocks. The occurrence of Mg-rich chlorite in the sediments of this subgroup and the low fineness value of the gold in the Black Reef (Gay, 1968) confirm that, in that period, rocks at the base of the greenstone belt must have supplied the debris for the eastern portion of the basin.

Table 64 Some properties of platinum group elements (Pourbaix, 1963)

| Sequence of resistance* | Ir | Os | Ru | Rh | Pt | Pd |
|---|---|---|---|---|---|---|
| Most inert PGE | x | x | | | | |
| Do not dissolve in aqua regia | | x | x | x | | |
| Resists oxidation, not attacked by acids | x | | | | | |
| Corroded by alkalic oxidants | | x | x | | | |
| Reacting in strong acidic, oxidizing environment | | | | x | x | x |
| Most unstable | | | | | | x** |
| Not in native state on its own; alloyed with iridium and other platinoids | | x | | | | |
| Rare in nature | | | x | | | |

*) Cousins, 1973
**) May be remobilized by groundwatersand dispersed within rock. Soluble in nitric and sulphuric acid at moderate temperature.

*4.2.4. Pyrite*

Unlike the uraninite grains that occurred in the matrix unprotected by organic matter, pyrite did not oxidize after final deposition. In the modern oxidizing environment, this iron sulphide is unstable and readily reacts when exposed to the atmosphere in a temperate and warm climate. But unoxidized pyrite and uraninite have been found in rivers in India (Zeschke, 1960) and the United States (Steacy, 1953). Chemical reaction of the two minerals is delayed because of the very low temperature which prevailed in the provenance. High rates of erosion and sedimentation would have a similar effect, and so would the lack of, or a deficiency in oxygen.

The preservation of pyrite at the time that ferrous iron was dissolved from ilmenite and other iron oxides limits the conditions for the dissolution of iron, to the dotted field in Figure 29. This implies that the pH did not drop below 4 at, or close to the earth's surface.

*4.2.5. Chloritized iron-bearing Minerals and Chlorite Pseudomorphs*

Well-rounded grains of pure chlorite (Figs. 7b and A.5g) and of chloritized iron-bearing minerals, i.e. pyrite (Fig. A.5f), chromite (Fig. A.2h), arsenopyrite (Fig. A.8e), and in the Dominion Reef also garnet (Fig. A.8h), are found in all reefs. Since they occur amongst their unaltered counterparts, the chloritization is a replacement which was inherited from the source rock.

Robb and Meyer (1985) established that the Archaean granites west and northwest of Klerksdorp G.F. were subjected to hydrothermal activity, which caused sericitization and chloritization of the wall rocks bordering the veins. In view of these findings, the following two hypotheses are here advanced.

Firstly, the chloritization of pyrite, arsenopyrite, chromite, and garnet stems from hydrothermal activity in the source rocks prior to their denudation.

Secondly, the equally well-rounded concretionary pyrite represents hydrothermal pyrite. In contrast with the compact pyrite, the concretionary variety is never chloritized.

Furthermore the following mineralogical features of the concretionary pyrite are typical for hydrothermal pyrite:

(1) the variable textures,
(2) the presence of several generations of pyrite of different composition in the individual grains (Fig. A.6e), and
(3) the association with chalcopyrite (Fig. A.7e), galena (Fig. A.7d), sphalerite (Fig. A7d), gold (Fig. A.7f), and gangue minerals (Figs. A.6c and d).

A hydrothermal origin in the source rocks implies that the concretionary pyrite was subjected to the same mechanical processes as the compact pyrite and, for that reason, it is equally well-rounded.

*4.2.6. Rutile-leucoxene Pseudomorphs*

Shape, size, and textural appearance strongly suggest that ilmenite is the most likely precursor for the bulk of the iron-free rutile-leucoxene pseudomorphs (Coetzee, 1965; Smits, 1984a and b). This type of allogenic pseudomorphs and insignificant amounts of detrital ilmenite and magnetite have been noticed in the older conglomerate of the Uitkyk Formation (Muff & Saager, 1979), and in weathering profiles in the upper part of the Archaean granite basement (Robb & Meyer, 1985; Grandstaff, 1986; Section 4.2.7). They are also a common constituent of the quartz-pebble conglomerates in the Elliot Lake-Blind River district in Canada (Theis, 1976).

Leucoxene pseudomorphs of an unknown precursor mineral also occur in the Dominion Reef. In some of these grains, minute specks of radiogenic galena indicate the presence of radioactive matter. Because uranous titanates did not form in the Dominion Reef, these leucoxene grains could be the alteration product of euxenite, which is a constituent of the reef, davidite, $(Fe^{2+},Ce_3U)_2(Ti,Fe^{3+},V,Cr)_5O_{12}$ or betafite, $(Ca,Fe^{2+},U)_2(Nb,Ti,Ta)_2O_6(OH,F)$. In addition to the leucoxene grains, titania-bearing, geode-shaped particles occur in the Dominion Reef (Fig. A.10c), which obviously represent detrital ilmenite, which was leached *in situ*. Their occurrence implies that conditions for the dissolution of ferrous iron not only prevailed in the source rocks but also after burial of the detritus in the Dominion Reef. Some of the dissolved ilmenite

grains in the Dominion Reef have been replaced by laths of mixed, authigenic ilmenite and rutile (Fig. A.28b). The geode-shaped pseudomorphs after ilmenite in the absence of magnetite are also a common characteristic of Phanerozoic uranium deposits of the sandstone-type all over the world, including those in the Karoo (Smits & Uiterwijk, 1983).

Primary *ilmenite* occurs in igneous and metamorphic rocks as pure ilmenite, or as intergrowths with hematite or magnetite. Depending on the predominant phase, they are called hemo-ilmenite, ilmeno-hematite (Fig. A.7c), or ilmeno-magnetite (Dimanche & Bartholome, 1976). If the hematite is dissolved from the ilmenite-hematite intergrowths, the remaining titania will display relict cleavage, a common texture of the rutile-leucoxene pseudomorphs of the Witwatersrand (Fig. A.11h). Release of iron from the ilmeno-magnetite intergrowths would produce a cloth or a trellis texture (ibid.). The latter texture is extremely rare in the Witwatersrand. Because of its ultrafine nature, the grains with a cloth texture will not show a specific relict texture after the release of iron. Hence, the homogeneous leucoxene pseudomorphs could well represent pure ilmenite or ilmeno-magnetite which possessed a cloth texture.

The release of iron causes porosity in the ilmenite and consequently a decrease in relative density, even if the pores were refilled by quartz and phyllosilicates. Because the rutile-leucoxene pseudomorphs in the reefs of the CRG are larger than the accompanying pyrite and chromite (the relative densities of the three minerals are roughly the same), the iron must have been removed and replaced from most of the grains prior to their arrival at the depositional plane. The open space has been filled by quartz or phyllosilicates (Table 23), and if dissolved uranium was available, also uranous titanates. The pseudomorphs are well-rounded (Figs. A.11b and h) or were moulded by the neighbouring matrix constituents (Figs. A.11c and d). The rounded grains must have been solid when they left the provenance, whereas the deformed pseudomorphs could represent grains in which the pores were not completely or only partly filled (Smits, 1985a). The solidified pseudomorphs have been noticed in the sericitized profile in the upper part of

the Archaean granite floor of the Witwatersrand Basin (Robb & Meyer, 1985), and in conglomerates older than those of the Witwatersrand Supergroup (Muff & Saager, 1977; Saager *et al.*, 1982).

*4.2.7. Sericite, Muscovite,* and *Pseudomorphs after Biotite,*

Some of the *sericite,* all the *fuchsitic sericite,* and the *undeformed muscovite* are considered detrital in origin. They probably were deposited as the $2M_1$ polytype, which is the final, stable metamorphic form of the mica.

The *pseudomorphs after biotite,* indicate that conditions at the earth's surface were not favourable for their oxidation, which involves the alteration to vermiculite via hydrobiotite, i.e. ML biotite/vermiculite (Wilson, 1970). Instead, the biotite has been replaced after burial by the intergrowth of two or three of the following phyllosilicates: muscovite $2M_1$, chlorite II*b*, and pyrophyllite. Because of their alteration, these pseudomorphs are discussed in Section 4.3.4.

*4.2.8. Zircon, thorian Zircon, and Tourmaline*

Because of its resistance to physical and chemical processes, *zircon* is a common constituent of all reefs of the CRG. It also occurs less commonly in the quartzites in a smaller size. As a result of the broad range in grain size in which it occurs, it was noticed in this study that it is present over a long distance down the palaeoslope of the fan.

The rare occurrence of detrital grains of *thorian zircon* in the Dominion Reef, which like many of the detrital constituents in this reef is of pegmatitic origin, is conspicuous.

Like zircon, the presence of *tourmaline,* and rutile as well, in the absence of silicates, is an indication of the maturity of the sediments in the CRG. Minerals of the zircon-rutile-tourmaline group together with quartz are the most stable minerals during sedimentary processes.

The scarcity of rutile and tourmaline point to their paucity in the source rocks.

*4.2.9. Chromite*

Most of the chromite grains underwent pre- and post-depositional alterations (Section 3.3.2). The introduction of

zinc and the partial replacement of chromite by rutile are both conspicuous features which have been inherited, since the altered grains occur side by side by side with unaltered grains. The zinc is either homogeneously distributed throughout the grain (Figs. A.13a and b)., and then could be of magmatic origin (Groves *et al.*, 1977), or is of a dendritic nature (Fig. A.10g and A.12h), and then was introduced after its formation. The entire or partial replacement by rutile (Figs. A.12a to d) is an unknown phenomenon and no tenable explanation can be provided for their origin.

The marginal leaching of chromite grains (Fig. A.10f), and the corrosion of the surface by uranous titanates (Figs. A.12f and g), similar to that of pyrite, are of post-depositional origin. However, hydrothermal activity in the source rock is considered to be responsible for the chloritization of chromite (Section 4.2.5).

*4.2.10. Sulpharsenides*

Two of the three (Ni,Co,Fe)-bearing sulpharsenides, arsenopyrite and cobaltite, are of detrital origin. Both may enclose gold. Some of the *arsenopyrite* grains are chloritized (Section 4.2.5.) and then, the grain is usually covered by a film of brannerite crystals (Fig. A.8e). In addition, arsenopyrite is partly replaced by oriented prismatic rutile.

*Cobaltite* has not been subjected to alteration. Often it is coated by a layer of authigenic gersdorffite, which may enclose recrystallized gold (Fig. A.18d). This type of coating did not form on arsenopyrite.

*4.2.11. Polymineralic Spheroids*

The polymineralic spheroids noticed in Kimberley reefs and less commonly in the Elsburg Reef on Western Reefs G.M., Klerksdorp G.F. (Fig. A.16) have never been reported before.

Spheroids of diverse mineral composition are commonly found in the Barberton Mountain Land in chert horizons present in the Onverwacht, Fig Tree, and Moodie Groups (Lowe & Knauth, 1978; Reimer, 1979, 1983; Paris, 1984). Their dimensions range from 1 to 10 mm with a mean of 2 mm (Reimer, 1983). Most of these spheriods are silicified carbonate ooids, but some consist of a nucleus of silica or a mixture of other minerals,

which is surrounded by an outer rind of fibrous minerals that grew either at right angles or concentrically to the core (Reimer, 1983). Lowe and Knauth (1978) noticed a resemblance between the spheriods in the chert horizons and accretionary lapilli. This type of lapilli forms from matter suspended in a gaseous medium in, or thrown from volcanic vents, and is made up of volcanic clasts enveloped by fine-grained ash.

The description of the spheroids in the Barberton Mountain Land fits the polymineralic spheroids in some of the reefs of the CRG closely. They survived the sedimentological processes remarkably well, and their resistance to corrosion, abrasion, and compaction is conspicuous. The well-preserved shape suggests that the matrix, in which the spheroids were set after their deposition, was not lithified, or it was dissolved or disintegrated during the exogenic cycle. The morphology of the polymineralic spheroids, their distribution within the reefs, and their association with heavy-mineral concentrations leave no doubt about their detrital origin. However, the constituents of which the spheroids are made up could be of pre- or post-depositional origin.

The spheroids which are composed of remnants of garnets set in chlorite remind of the chloritized garnets in the Dominion Reef. Chloritized garnets have been found in the peraluminous granite west and northwest of the Klerksdorp G.F., which was subjected to hydrothermal activity and associated wall-rock alteration (Robb & Meyer, 1985).

*4.2.12. Rare accessory Minerals*

*Molybdenite*, *graphite*, and *xenotime* are rare detrital minerals which are found in some of the reefs of the CRG - so are *uranothorite*, *cheralite* and *euxenite* in the Dominion Reef. Locally *monazite* is a quite common constituent in the latter reef. Their preservation is of no specific interest with respect to the geochemical activity which took place before and after deposition of the detritus.

## 4.3. Altered and Neoformed Minerals

Rapid accumulation of the quartzites overlying the basal conglomerate must have prevented the formation of a soil zone at the hiatuses of relatively short duration between individual layers of quartzite. On the other hand, the time interval during which the major unconformities were exposed to the atmosphere must have been long enough for pedochemical weathering. At certain sites, the top 5 to 30 mm of the footwall quartzite is argillaceous (Figs. 5a and A.1f). The quartz grains in this horizon have been strongly corroded. The corrosion could have resulted from leaching by alkaline solutions, a pedogenic feature characteristic for an arid environment, or from the alteration of clay minerals to sericite and pyrophyllite, a process which requires silica.

Another possible pedologic feature on the major unconformities is the local near-surface enrichment of authigenic titania (Fig. A.11a). Today this type of rutile concentration is diagnostic for soils which develop in the absence of vegetation, and in a climate characterized by alternating wet and dry seasons. Such climatic conditions enhance periodic capillary activity (Walker *et al.*, 1969, Fitzpatrick *et al.*, 1978; Milnes & Hutton, 1974). The titania may originate from the breakdown of unstable silicates, which released titanium in the form of orthotitanic acid, $Ti(OH)_4$. In modern soils, this acid is present at a pH below 5,5 (Fig. 22; Loughnan, 1969; Fitzpatrick *et al.*, 1978).

### *4.3.1. Kerogen*

Because the kerogen seams formed on the major unconformities before the deposition of the pebble fraction of the conglomerate at the base of a cycle, it is discussed in this section as a neoformed product.

Sharpe (1949) was the first to point out that the occurrence of carbonaceous matter in the reefs of the CRG was restricted to certain horizons, and to suggest that, because of its specific location, it represented fossilized bacteria or algae. Snyman (1965) then proposed that the structure of the thucholite resembled the algal structures of boghead coals. The alpha-irradiation from the enclosed uraninite caused dehydro-

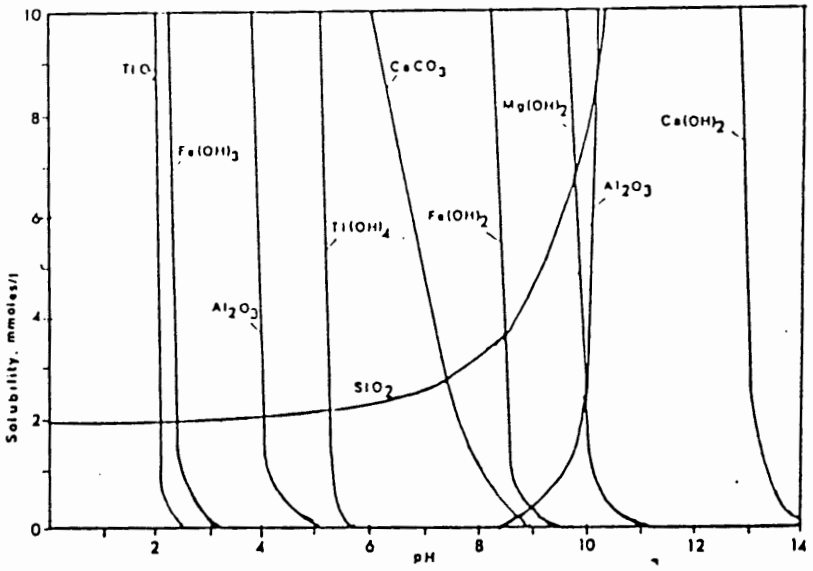



Fig. 22 Solubility of components released during weathering in relation to pH (after Loughnan, 1969)

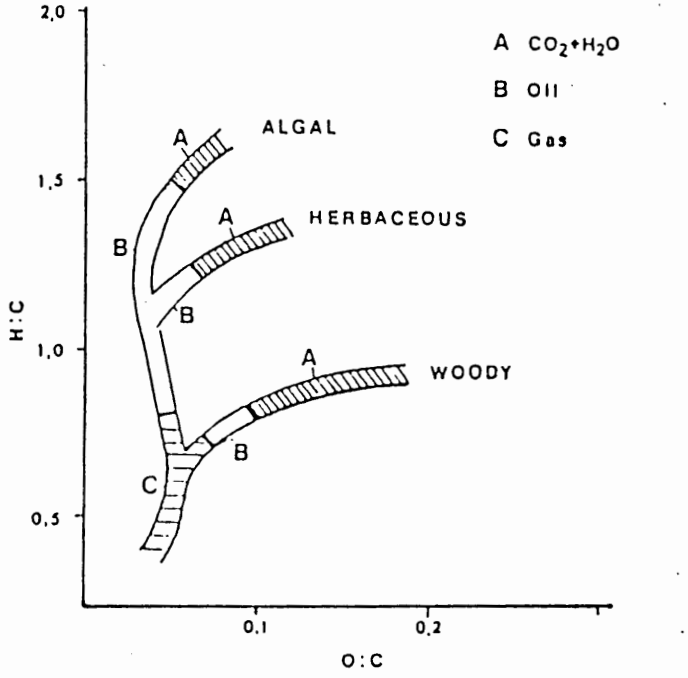



Fig. 23 Van Krevelen diagram illustrating the diagenetic pathways for different types of organic matter (after Schmidt and McDonald, 1979)

genation of the organic matter and structural changes to produce a high-rank boghead coal. Hallbauer and Van Warmelo (1974) postulated that the kerogen represents the fossil remains of symbiotic fungi and algae, similar to the modern lichens, which grew in water-filled depressions on the fans (Hallbauer, 1975). However, lichens only appeared in the Late Proterozoic (Grandstaff, 1980). It is assumed that the only creatures which could have lived during the Archaean and Early Proterozoic were prokaryotic cyanobacteria (Schidlowski, 1985).

Kerogen could have formed abioligically by polymerization of methane through the irradiation from the uraninite grains. However, the patchwise occurrence of stratiform kerogen (Table 38) on major unconformities, which separate two cycles, and on false footwalls between individual conglomerate horizons within the reef makes it unlikely that the organic matter formed abiologically. Zumberge *et al.* (1978) determined the organic geochemistry of the carbonaceous matter, the composition of which confirmed its biogenic origin. So does the isotopic composition of the kerogen (Table 62).

The kerogen seams are restricted to the small pebble conglomerates, the Basal, Leader, Steyn, and Vaal Reefs, and the Carbon Leader, whereas the nodular type of kerogen (Table 38) continues to occur in the reefs of the Turffontein Subgroup and in the VCR. The appearance of the carbon in the much younger Black Reef is structureless and black, and it does not enclose minerals.

The distribution pattern of the kerogen in the reefs of the CRG indicates <u>firstly</u>, that the environment required for the growth and the preservation of microbial colonies only occurred on certain unconformities in the western portion of the basin during the time that the sediments of the Johannesburg Subgroup were deposited, and <u>secondly</u>, that in the younger reefs, the conditions were such that only the nodular type (Fig. A.21a), i.e. the first stage of the growth of microorganisms onto uraninite grains, was able to form or was preserved. If larger microbial communities did form in the time that the sediments of the Turffontein Subgroup were deposited, they could have been broken up during periods of reworking of

the surficial sediment, as is suggested by the occurrence of nodules of the fragmented type.

The relative densities of gold and uraninite are 19 and 10 respectively, while those of the remaining heavy minerals is less than 6. This large gap in the values of the relative densities could have been responsible for the segregation by sedimentary processes of the two heaviest minerals and hence, their exclusive association with organic matter in the virtual absence of other heavy minerals. Moreover, the small grain size of the gold and uraninite could have enhanced their entrapment by the microbial mats, which, once they were captured, also inhibited their dislodgment. These assumptions (Smits, 1986) are emphasized by the following observation. In the Vaal Reef on Buffelsfontein G.M., laminae of kerogen 1 to 5 mm wide, which enclose gold and uraninite, alternate with layers in which heavy minerals of a relative density below 6 are concentrated. This alteration confirms that sedimentary conditions for the simultaneous deposition of gold and uraninite differed from those for the less dense heavy minerals.

With progressive burial, organic matter follows a definite, irreversible path of *maturation*, in which $H_2$, $H_2O$, $CH_4$, and some $CO_2$ are released, resulting in the systematic increase in carbon. Graphite and methane are the ultimate end products (Harrison, 1979; Durand, 1985), a stage which is reached in the amphibolite facies at about $450^0$C and 2 to 6 kbar (Landis, 1971; Harrison, 1979). Different types of organic matter follow different maturation pathways, which is best illustrated in a Van Krevelen diagram in which the relationship of H/C and O/C atomic ratios are expressed (Fig. 23). The organic matter in the Witwatersrand must have followed the path of the alganites.

The *radiochemical degradation of organic matter* is accompanied by the release of methane and hydrogen. It therefore becomes relatively enriched in oxygen, while the alpha-radiation accelerates the induration of the organic matter (Breger, 1974).

It is suggested here that the earlier discussed boudinage of (1) enclosed detrital heavy minerals (Fig. A.8a) - with the exception of the malleable gold (Fig. A.18b) -, (2) authigenic

interfilamental quartz (Fig. A.24g), and (3) detrital constituents alongside (Fig. A.24h), and in the same plane as the kerogen (Figs. A.25a and b) could have been caused by the release of methane and hydrogen. The process must have taken place fairly soon after burial when pore solutions saturated with dissolved elements were able to circulate freely.

Since the *reflectance* of the two types of kerogen nodules (Table 38) is similar to that of the seams, their post-depositional history is the same. An exception are the nodules found at Grootvlei G.M. and some of those on West Rand Consolidated G.M. (Fig. A.24a), which are black. Recurrent, intensive reworking could be responsible for the change in appearance. Once buried, organic matter resists reaction with fluids and solids, and is not subject to retrograde alteration (Bostick, 1979).

The reflectance of the kerogen cannot be used as a parameter of the degree of *coalification*, since the degradation of the organic matter was greatly influenced by the uraninite it encloses. This is evident from the extremely immature appearance of uraninite-free kerogen (Fig. A.23c), the reflectance of which lies below 3%. It is possible that, when the stage of petroleum generation within the high bituminous volatile coalification stage (referred to as the 'oil window') was reached, the precursor of the uraninite-free organic matter migrated along permeable zones as a wet gas or liquid. Such a process would explain the conspicuous scarcity of this type of kerogen. If the petroleum did not migrate, it would have indurated *in situ* at 200$^{0}$C (Stach *et al.*, 1982). The uraninite-free kerogen noticed locally at the base of the Leader Reef, Harmony Complex, which is indented by the surrounding authigenic quartz (Fig. 23e), could represent a remnant of such solidified bitumen.

4.3.1.1. Kerogen-Uraninite Association

Virtually all the kerogen in the reefs encloses detrital uraninite grains (Figs. A.21a to c, e and f) and kerogen devoid of uraninite is rare (Figs. A.23c and e). The *non-uraniferous kerogen* is featureless and dark grey (Figs. 23c to f), and does not display the filamentous texture of the uraninite-bearing

kerogen, nor does it reflect the extent of maturation expected of carbonaceous matter which was subjected to low-grade metamorphism.

In the past, it has been assumed that the uraninite enclosed by kerogen reacted in an unspecified manner with the organic matter. Terms like 'assimilation', 'digestion', 're-placement', and 'resorption' have been used to express the relationship between the two (Liebenberg, 1955; Ramdohr, 1955; Schidlowski, 1966c; Feather & Koen, 1975). If a reaction between uraninite and microorganisms would have taken place, some sort of replacement texture should have developed, as is, for example, quite distinct at the contact between microbiota and quartz or pyrite (Fig. A.24b). This kind of texture has not been noticed between uraninite and kerogen. Furthermore, the kerogen in direct contact with the uraninite grains or fragments does not contain any uranium.

The following hypotheses are here advanced about the kerogen, its relation with uraninite, its morphology and maturation.

The *preferential growth of microbiota onto uraninite* could have resulted from a certain affinity between the two, or from a physical property of the uraninite, e.g. its porous surface could have promoted this association.

At the start, the microbiota enveloped single uraninite grains and penetrated the particles along cracks or crystal planes, forcing the fragments apart (Figs. A.21a and e). In a similar, but less common fashion, the microbiota also wedged fractures in quartz and pyrite (Fig. A.24h). In the kerogen seams, that display an early stage of the biological fragmentation of uraninite, the angular pieces are close enough to reconstruct the original grain when viewed in a polished surface (Figs. A.21e and g). With the advance in the growth of the organisms, the angular fragments of each grain became smaller in size and increased in number. They were pushed apart in all directions and to different extents. At that stage, it becomes less easy to fit the pieces together (Figs. A.21f and h). In certain localities, the microbiota captured fine-grained abrasion particles of uraninite, <5 μm in diameter, which

resulted in a continuous mottled texture (Fig. A.22d).

Initially, a kerogen seam would have been composed of interconnected individually encapsulated uraninite grains (Fig. A.19d). Once such a cohesive layer was established, the colony was able to continue to capture the two densest components of the mineral assemblage, i.e. gold and uraninite, and to prevent them from being dislodged (Smits, 1984a).

The actual *morphology of the original microorganisms*, if their shape was at all defined, became distorted because of the incorporation of uraninite and clay minerals - the size of which was several orders of magnitude larger than that of the microbes. Each segment encloses a single fragmented uraninite grain and stacked segments make up a column. Viewed in three dimensions on the SEM, the kerogen is composed of finger-shaped columns (Fig. A.21d, photograph from Hallbauer & Van Warmelo, 1974). The gold filled available open space in the carbonaceous matter.

When the kerogen is volatilized at $300^0$C, a residue mainly composed of metamorphosed clay minerals of platy habit (Fig. A.22a), uraninite fragments, and gold particles remains. The interfilamental quartz and gold, and the clay mineral and uraninite enclosed by the microorganisms must have formed a rigid, supporting framework which prevented the collapse of the organic matter during compaction (Smits, 1984a). The uraninite and the clay mineral enclosed by the organic matter determine the volume of segments and columns in the kerogen, and mask the actual morphology of the primitive creatures. Their soft tissue of non-rigid structure would in any case be readily distorted. Hence, it is unlikely that structural features of the microbiota that produced the mats and nodules would have been preserved.

The kerogen protected the uraninite against chemical attack, and since the uranium oxide was not oxidized, the microbiota could not have produced metabolic oxygen. The conditions in the stagnant pools in which the microorganisms supposedly grew must have been reducing, an environment favourable for the growth of anaerobic microorganisms.

The close relationship suggests that the uranium oxide could have been beneficial for the growth of the micro-organisms, and might have prevented its destruction by microbes or chemical activity. The extreme paucity of uraninite-free kerogen of spongy or ragged habit (Figs. 23d and f) suggests that the organic matter was not preserved if it did not enclose uraninite. If at all present, the latter is a younger generation of organic matter.

Today, organic matter is destroyed in the soil zone by microbes. A similar process could have been responsible for the destruction of the kerogen nodules, which have only been noticed in the UE1a and E9 Reefs on the West Rand G.F., where the organic matter was replaced by quartz and phyllosilicates (Figs. A.24c to e).

The authigenic uranous titanate, which rarely infiltrated the kerogen, usually subdivided the carbonaceous matter in small, more or less globular fragments of dimensions between 0,05 and 0,10 mm (Figs. A.22f and A.29f), which distinctly differ from the filamental texture of the seams.

4.3.1.2. Kerogen-Gold Association

The concentration of gold associated with kerogen frequently exceeds that in the matrix by far (Table 39). Visible gold is only found in kerogen seams, and very rarely in quartz veins.

The relationship between gold and kerogen differs distinctly from that between uraninite and kerogen. The detrital gold was entrapped mechanically, and for that reason filled available open space in the mats, whereas detrital uraninite was captured biologically since the latter served as a substrate for the growth of microbiota. Recrystallization of the gold at the time that the organic matter solidified could be responsible for the moulded texture of the gold in kerogen.

The originally detrital origin of the gold associated with kerogen is indicated by the variation in the silver and mercury concentrations of the individual gold particles occurring at short distance of each other in the same handspecimen (Von Gehlen, 1983).

4.3.1.3. Kerogen-Gersdorffite Association

The minute crystals of gersdorffite (<30 μm) closely associated with seams and nodules of kerogen, precipitated after the growth of the microorganisms which entrapped uraninite and gold, but before the younger non-uraniferous generation of organic matter. The period of neoformation of these crystals is well-defined by the modes of its occurrence and is a phenomenon which took place during early-burial. It is indicated by its precipitation (1) onto uraninite grains in the matrix from which uranium was leached (Figs. A.30e and g), (2) in the open space in the kerogen seams usually together with amorphous silica (Fig. A.30f), (3) onto the surface of kerogen nodules (Fig. A.9e), sometimes before the overgrowth of the second generation of organic matter (Fig. A.9f), and (4) within the non-uraniferous kerogen (Fig. A.9h).

As mentioned in Section 4.1.4, the gersdorffite precipitation could represent a process similar to the neoformation of minute pyrite crystals and framboids which today commonly form from dissolved sulphate and iron just below the water-sediment interface. Some of the gersdorffite crystals possess cores of pyrite, galena, or chalcopyrite. The absence of authigenic pyrite suggests that (1) sulphate was not present at all or only in limited amounts, as is indicated by the occasional pyrite core in a gersdorffite crystal (Fig. A.9g), and that (2) conditions close to the surface of the unconformities where sedentary kerogen developed were more favourable for the precipitation of gersdorffite than for that of pyrite.

*4.3.2. Authigenic Uranium-bearing Minerals and Cutans*

*Relict uraninite* (Figs. A.23a and b) and pervasively distributed *uranous titanates* (Figs. A.27b and c, A.29g) are noticed in all reefs throughout the Witwatersrand Basin, except for the Dominion Reef, but are particularly prominent in the reefs of high uranium concentration. Their occurrence in the presence of unoxidized uraninite when mantled by kerogen (Figs. A.21a to c, e to h) is conspicuous. It means that, once deposited, the unprotected grains in the matrix reacted.

In the UE1a and E9 Reefs on the West Rand G.F. (Figs. A.27d to g) and in the Dominion Reef (Fig. A.28b), the

uraninite was directly transformed *in situ* to hydrated and anhydrous *thorian coffinite* of varying composition (Table 54) through the addition of silica. On the West Rand G.F., uranous titanates and coffinite are both present.

In the eastern portion of the Witwatersrand Basin, the uranium grade of the reefs that were, and still are mined for gold is low, and so is the grade of the uranium-poor reefs of the Turffontein Subgroup recently mined in the southern corner of the OFS G.F. In these reefs, seams of kerogen are absent and, with the exception of some altered kerogen nodules, uraninite was chiefly a matrix constituent, so that it freely reacted during the periods that it was exposed to the atmosphere. But even the uraninite enclosed in kerogen nodules was leached to reprecipitate just outside the nodule as uranous titanate (Fig. A.22e) or coffinite (Fig. A.27h). Part of the dissolved uranium must have been carried away in solution. In view of the preceding observations, the low uranium grade in the above-cited reefs does not necessarily imply a low supply of uraninite from the source rocks. The absence of organic matter could well be responsible for the loss in uranium, because as a matrix constituent, uraninite was subject to oxidation.

The *pitchblende* and *secondary coffinite* of colloform habit (Figs. A.28c to e) observed in East Champ d'Or G.M. on the West Rand G.F., formed relatively recently in a supergene environment close to the present-day surface. Their occurrence has not been reported before by other investigators. This type of texture has nowhere been noticed in the reefs of the CRG, indicating that supergene activity near the watertable prompted by the oxidation of sulphides above it did not take place during deposition of the sediments of the CRG.

The *geochemical behaviour* of uranium and uranium-bearing minerals at $25^{0}$C and 1 atmosphere has been studied by several investigators (Hostetler & Garrels, 1962; Garrels & Christ, 1965; Schmidt-Collerus, 1969; Langmuir, 1978; Hemingway, 1982). In nature, uranium is found in the tetra-, penta- and hexavalent state, whereas thorium only occurs in the tetravalent state. The stability fields of various types of uranous

ions and hydroxy complexes are pictured in Figure 24a, and that for uraninite in Figure 24b. The stability field of coffinite is assumed to overlap the field of uraninite (Langmuir, 1978).

The uranyl ion, $UO_2^{2+}$, which is the exclusive form of hexavalent uranium in aqueous solution, will combine with carbonate, phosphate, sulphate, or silicate at definite pH-Eh limits. Today, dissolved and solid phases of iron exert control upon the uranium mobility in most natural waters in the following manner:

$$UO_2 + 2Fe^{3+} \rightleftharpoons UO_2^{2+} + 2Fe^{2+} \qquad (6)$$

In an arid to semi-arid climate, capillary activity promoted by evaporation will lead to the precipitation of hydrated uranyl minerals of which, up to now, about 160 have been identified (Fleischer, 1983). In the presence of a reductant, e.g. $HS^-$, $S^{2-}$, or organic matter, the uranyl ion is reduced to the tetravalent state.

The mobility of uranium and thorium is also changed if colloidal sorbents are present. Clays, humic acids, hydrous iron and manganese oxides, zeolites, and titanium hydroxide are effective concentrators of uranyl ions, particularly the last-named phase (Davies *et al*, 1964).

4.3.2.1. Relict Uraninite and Cutans

Many of the uraninite grains in the matrix were covered by a *cutan* of gersdorffite (Figs. A.20d to f) or uranous titanate (Fig. A.17f), which preserved the shape of the leached grain. Size, shape, and the presence of uranous titanate (Fig. A.30e) clearly indicate that these grains represent leached uraninite. For that reason, they are here referred to as 'relict uraninite' (Figs. A.20d and e, A.23a and b, A.25d; Smits, 1986). The formation of coatings on grains, aggregates, and walls of voids, for which Brewer (1960) has coined the term cutan, is one of the characteristics of the transition zone between weathering and diagenesis (Brewer, 1964). These cutans indicate in which elements the pore solutions were saturated in this zone. Grains which were not covered by a cutan must have been dissolved completely without leaving a trace of their pre-existence.

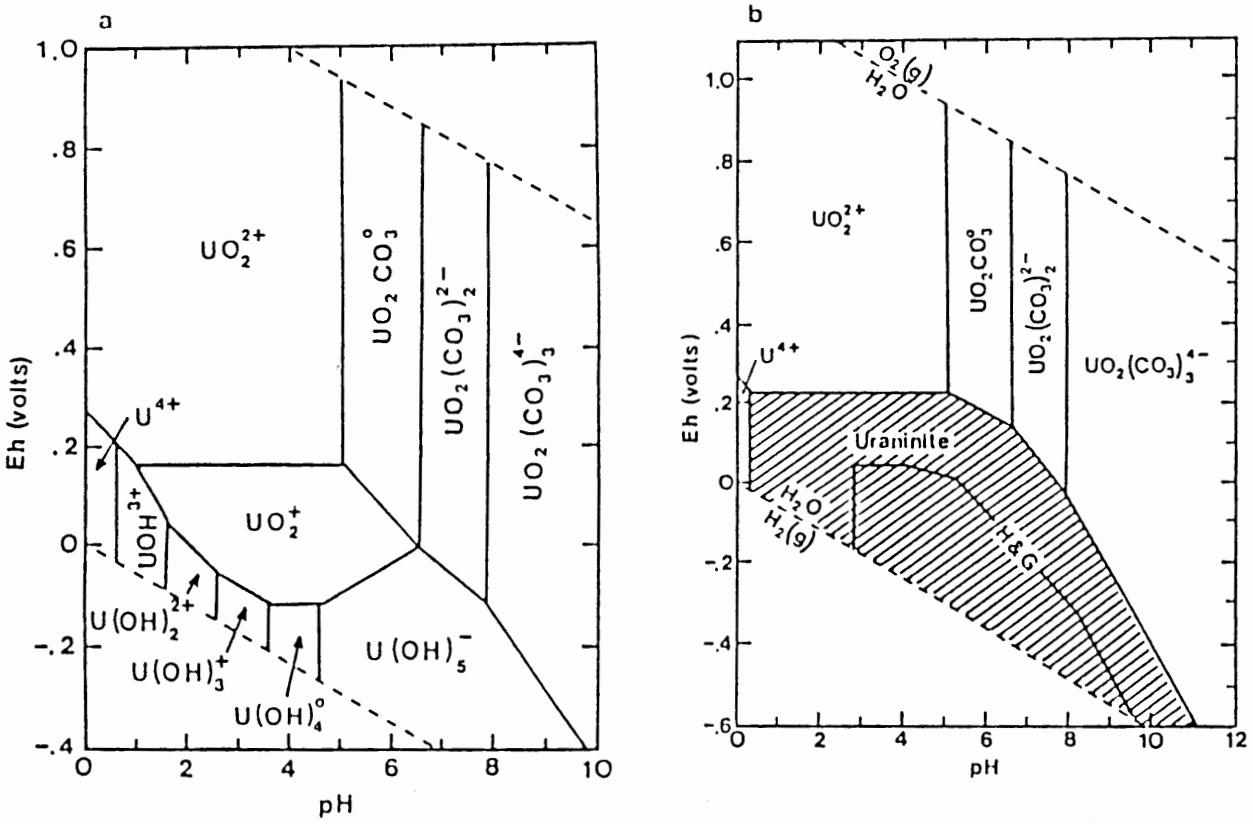



Fig. 24 Eh-pH diagrams in the $U-O_2-CO_2-H_2O$ system at 25°C and a typical groundwater $CO_2$ pressure of $10^{-2}$ atm, and $U_{tot}=10^{-6}$ M (0,24 mg/ℓ) dissolved uranium species

a Stability fields for tetra-, penta-, and hexavalent species

b Stability field for uraninite, $UO_2$ (c). H & G outlines stability field as defined by Hostetler and Garrels in 1962 (after Langmuir, 1978)

The thickness of the gersdorffite cutans on some of the uraninite (Fig. A.19e) or brannerite grains pseudomorphous after uraninite (Fig. A.30e) and relict uraninite suggests that the cutans continued to grow from saturated pore solutions which stagnated round the grain after the circulation became restricted because of a decrease in porosity towards early diagenesis. The uninterrupted films must have formed in open space which became available by preceding chemical interaction of the uraninite or the surrounding matrix with the pore solutions. The nickel required for the formation of the gersdorffite cutans could initially have been incorporated at low concentrations in primary, ferromagnesian silicates, from which it was released during post-depositional weathering, or it was supplied by detrital Ni-bearing sulphides, which were dissolved before burial.

Some of the uraninite grains not covered by a cutan display incipient leaching along the crystallographic planes, while open space was then filled by quartz (Fig. A.20a). Others were replaced *in situ* by brannerite crystals and quartz (Fig. A.25c). In Figure A.23a, a relict uraninite and uraninite grain replaced by uranous titanate occur side by side.

Much thinner cutans made up of minute brannerite crystals formed on detrital chlorite and chloritized pyrite (Fig. A.5g), arsenopyrite (Fig. A.2g), chromite (Fig. A.10h), and leucoxene grains (Fig. A.23h) with the exclusion of the corresponding grains which were not chloritized. These <10 $\mu$m-wide films discoloured the neighbouring chlorite (Fig. 7b) and marginally lowered the intensity of the anistropy of arsenopyrite, but no visible evidence is found for the interaction between gersdorffite cutans and uraninite. A chemical affinity must have existed between the chlorite and the uranoan-titano gel, from which the uranous titanates eventually precipitated. This type of cutans would also have formed on partially chloritized garnets in the Dominion Reef, but, with the exception of rare coatings on a few uraninite grains which, in addition to niobium and a number of trace elements, also contain uranium and titanium, intensive mobilization of uranium and titanium has not been noticed in this reef.

In contrast with the uninterrupted brannerite cutans on uraninite and chloritized iron-bearing minerals, the *coatings on pyrite*, made up of uraniferous leucoxene frequently mixed with phyllosilicates, only cover part of the grains (Fig. A.5h). The portion covered by, or in contact with any type of uraniferous leucoxene or brannerite (Figs. A.25c and e) has been corroded by the uranous titanate.

In view of the two following facts, <u>firstly</u>, that uraninite appeared to be the preferred substrate for the growth of microbiota and <u>secondly</u>, that gersdorffite precipitated in close association with the microorganisms (Fig. A.30f), it is here postulated that the incipient growth of microorganisms on uraninite grains could have provided conditions suitable for the precipitation of gersdorffite at its surface, which then stopped further growth of the microbiota.

Kerogen is extremely rare in the Dominion Reef and gersdorffite has not been noticed. Furthermore, there is no evidence for the dissolution or migration of uranium in this reef. These three aspects could mean that the heavy minerals were covered by water when deposited, or that the physico-chemical conditions during the deposition of the Dominion Reef, the oldest reef, differed from those when the reefs in the CRG were deposited.

Note that the precipitation on gersdorffite in association with gold (Fig. A.9b) is considered to have taken place at a higher temperature during very-low-grade metamorphism (Winkler, 1979).

4.3.2.2. Uranous Titanates

Ramdohr (1955) and Liebenberg (1955) were the first to describe the uranous titanates in the reefs of the CRG, but in the absence of an EMP, the authors were not able to establish the actual identity of the metamict species. When comparing the Witwatersrand deposit with that of Blind River, Ramdohr (1957) realized that these radioactive constituents were related to brannerite. He proposed that they formed from: "...the reaction between uraninite and rutile...". Ramdohr (1957) referred to this reaction as the 'Pronto' reaction:

$$UO_2 + 2 \text{ to } 3TiO_2 \rightarrow UTi_{2-3}O_{6-8} \qquad (7)$$

It was Schidlowski (1966a) who first identified and analyzed the minerals on the EMP. Today a great number of analyses are available from Blind River (Theis, 1976, 1979; Table 46) and the Witwatersrand (Feather, 1976; Smits, 1984a and b, 1985a to c; Table 45).

In the Elliot Lake deposits, the bulk of the brannerite occurs in ovoid composite grains of brannerite, rutile, and quartz, 0,25 to 1,50 mm in diameter (Theis, 1979). These grains display the familiar trellis texture of altered ilmenite and titaniferous magnetite. The branneritization advanced from the surface towards the centre of the grains. Theis (1976) concluded from microscopic observations that the brannerite replaced rutile in pseudomorphs after ilmenite. In the Witwatersrand reefs, on the other hand, the ilmenite was leached and mainly replaced by leucoxene and only small amounts of rutile (Figs. A.11b to d) before deposition on the fan (Section 4.1.1.). The uranous titanates then selectively replaced the leucoxenic portion (Figs. A.25h and A.29e) and never the rutile, precipitated in voids (Figs. A.11e, g and h), or at the surface of these grains (Fig. A.11f). They also replaced many of the detrital uraninite grains in the matrix (Figs. A.30e and A.26a). In some of the brannerite pseudomorphs after leucoxene, uranium seems to have been removed from the margin after the replacement of leucoxene by uranous titanate (Fig. A.11g).

The following postulations are advanced with respect to the conditions which led to the *precipitation* and subsequent *maturation of uranous titanates*, their variation in *composition*, and the *nomenclature* of the two major types.

The common occurrence of uranous titanates in all reefs of the CRG in the basin indicates that intensive mobilization of uranium and titanium took place shortly after burial, probably at the time that the porosity was still significant enough to allow free circulation of the intrastratal solutions. The simultaneous presence of dissolved uranium and titanium led to the neoformation of uranous titanate species of variable composition. It also caused the dispersion of submicroscopic radioactive matter along grain boundaries and hairfine cracks

as is indicated by autoradiographs and Lexan prints made from polished rock slabs. Taking the pervasive distribution of uranous titanate species into consideration, this ultrafine radioactive matter, the size of which lies below the detection limit of the EMP, most likely represents submicroscopic specks of brannerite or uraniferous leucoxene, rather than uraninite, as was proposed by Simpson and Bowles (1978) and Thiel *et al.* (1979).

Uranyl ions are the most likely ionic species in which the dissolved uranium occurred (Fig. 24a). If uranyl carbonate or phosphate complexes would have been present, coprecipitation of carbonates or phosphates at the time of the conversion of hexavalent uranium to the tetravalent state is expected.

Titania is practically insoluble under natural conditions. However, the neoformation of anatase in modern soils from orthotitanic acid, $Ti(OH)_4$ has been established (Fitzpatrick *et al.*, 1978) and confirmed experimentally (Deelman, 1979). This acid is known to be an effective concentrator of uranyl ions (Davies *et al.*, 1964), and can even be used for the extraction of uranium from natural water (Laskorin *et al.*, 1956). Enrichment of titanium oxide in the form of anatase is also found in modern indurated horizons that develop in the absence of vegetation when subjected to seasonal wet and dry periods (Walker *et al.*, 1972; Hutton *et al.*, 1972; Summerfield, 1983). These occurrences confirm that titanium is not entirely immobile at low temperature and pressure.

It is proposed that the reaction between uranyl ions and orthotitanic acid and that of the uranyl with leucoxene (Fig. 29e; Table 65) and orthotitanic acid with uraninite (Figs. A.30e and A.26a; Table 65) at first resulted in the formation of an amorphous colloidal substance, a uranoan-titano gel, which with the increase in depth of burial, gradually matured to the uranous titanate species found in the present reefs (Smits, 1984a and b).

Depending on the amounts of dissolved uranium and titanium that were locally available, uraniferous leucoxene or brannerite formed. The $UO_2/TiO_2$ ratios of the two minerals lie below and above unity respectively. In the absence of uranium, rutile

Table 65 Modes of precipitation of uranous titanates*

| Reaction between: | Mineralogical and textural features |
|---|---|
| (1) Uraninite and dissolved titanium | Ur entirely replaced by ur. tit. in situ (Fig. A.20a) or a mixture of br crystals and q (Figs. 19a and b). Br also precipitated just outside the original ur (Figs. 23g and A.20b) forming 'uraninite ghosts' (Ramdohr, 1955), while ur was replaced by q or sulphides (Fig. A.15f). When a cluster of ur grains was cemented by lc, the two reacted to form massive patches of ur. tit. (Figs. A.20e and g) |
| (2) Leucoxene and dissolved uranium | Only the leucoxenic portion of the rut-lc pseudomorphs (Fig. A.20f) reacted with dissolved uranium (Figs. A.19g and h). Ur. tit. also precipitated in voids present in the pseudomorphs (Figs. A.20c and d) |
| (3) Dissolved uranium and dissolved titanium | Ur. tit. which precipitated from the interaction of dissolved uranium and titanium, is tenuously dispersed in the interstices of the matrix of the conglomerate (Fig. A.20d) and forms ill-defined streaky or cloudy accumulations of irregular shape (Fig. 22d); sometimes it is intergrown with ph.sil. (Figs. A.21b and c) |

*) Whether br or ulc would form depended on the relative amounts of uranium and titanium that were available. Microscopic observations indicate that dissolved titanium exceeded dissolved uranium

crystals precipitated (Smits, 1984a and b). From the distribution of the uranous titanates and the authigenic rutile, it is concluded that dissolved titanium was more abundant than dissolved uranium.

Like the formation of cutans, this process must have taken place close to the transition zone between weathering and diagenesis (Smits 1984b). Evaporation and capillary activity could have played a role in the mobilization of titanium and uranium and the subsequent precipitation of uranous titanates relatively close to the surface.

The conclusion that the uranous titanates must have formed soon after burial at shallow depth is supported by the following textures. Some of the detrital leucoxene (Figs. A.23h and A.29g) and detrital chlorite grains (Fig. A.30g) were first covered by a film of brannerite, and then overgrown by the younger generation of non-uraniferous organic matter. A similar feature is noticed in some of the kerogen nodules in which the uraninite fragments were first replaced by uranous titanate and the nodule covered by gersdorffite crystals, and then by the younger generation of non-uraniferous organic matter (Fig. A.9f). The non-uraniferous kerogen frequently encloses uranous titanate (Figs. A.23e and f) indicating that, like the gersdorffite crystals, it precipitated before the growth of the younger generation of microorganisms. Another texture, which provides evidence for the precipitation of uranous titanate soon after burial is found in the Carbon Leader which is mined at depths greater than any of the other reefs. In this reef, brannerite is a common component in microstylolites which wind along quartz boundaries (Figs. A.1g and A.29h). The stylocumulate, usually one grain wide, represent thin films of mud (Fig. A.30h) or of minute detrital grains, which during compaction became stylolitic. The presence of brannerite indicates that interaction between dissolved uranium and titanium took place before this compactional feature developed.

Although not impossible, the synthesis of brannerite in the laboratory has proved to be difficult, even at high temperature (Schroeke, 1958; Oztunali, 1959; Kaiman, 1959; Patchett & Nuffield, 1960). Its formation at low temperature

and pressure in the reefs of the CRG is therefore unexpected.

*Detrital brannerite* has been noticed only once in the Leader Reef, where this reef directly overlies the Basal Reef in the Harmony Complex. The texture of some of the composite grains suggests that it is of sedimentary origin. This implies that the source-rock sediment was lithified. The brannerite could have originated from older reefs or from the much older sediments of the Swazian Era, although such a type of brannerite has as yet not been found in the sediments of the greenstone belts.

The absence of uranous titanates and relict uraninite in the Dominion Reef, the gradual increase in an upward stratigraphic direction in the dissolution of uranium from uraninite in the matrix, and in the Turffontein Subgroup also from uraninite enclosed by kerogen nodules, suggest that, in the course of time, the conditions at the earth's surface became increasingly more favourable for the oxidation of uraninite (Smits, 1986).

4.3.2.3. (U,Th)-silicates

Because the optical properties of coffinite and thorite are identical, the uranium silicate has been overlooked for a long time in many deposits, including the Witwatersrand. It was first recognized in the unoxidized ores of the Colorado Plateau, USA, by Stieff *et al.* (1955, 1956), and has since been identified in similar (including those west of Beaufort West in the Karoo; Smits & Uiterwijk, 1983) and other types of uranium deposits. Anhydrous and hydrated coffinite have also been recognized in recent years in the quartz-pebble conglomerate deposits (Hiemstra, 1968; Robinson & Spooner, 1982; Smits, 1984a).

The *synthesis* of (U,Th)-silicates from its oxides was undertaken by several investigators, i.e. Hoekstra and Fuchs (1956), Frondel and Colette (1957), Fuchs and Gebert (1958), Fuchs and Hoekstra (1959). The temperature limits for the precipitation of anhydrous coffinite in nitrogen lie between 200 and 360$^0$C, whereas the pH ranges from 8 to 10,5 (Fuchs & Hoekstra, 1959). Langmuir (1978) assumed that the stability field of coffinite overlaps that of uraninite, and both

minerals continue to be stable in a weakly oxidizing environment.

Coffinite and its thorium-bearing counterpart thorogummite both contain water. From thermal studies, Frondel (1953) proposed for thorogummite the formula $Th(SiO_4)_{1-x}(OH)_{4x}$, and in analogy, Stieff *et al.*, (1956) suggested for coffinite a similar one: $U(SiO_4)_{1-x}(OH)_{4x}$. However, Abdel-Gawad and Kerr (1961) established that the water associated with the coffinite represents absorbed water, which is confirmed by the distribution of the compositions of (U,Th)-silicates pictured in the ternary diagram (Fig. 16) constructed from data from this study and from elsewhere in the world. Since no specific concentration of coffinite species occurs along the tie line between $(U,Th)SiO_4$ and $(U,Th)(OH)_4$, it is proposed that the correct formula for hydrated (U,Th)-silicates is (Smits, 1989):

$$(U,Th)SiO_4.nH_2O.$$

The available chemical data indicate that $n$ is less than 4 (Fig. 16).

The ternary diagram, in which the relation between U, Th, and Si is illustrated (Fig. 17), shows that the Witwatersrand coffinite contains a significant thorite component. Although the compositions of known (U,Th)-silicates in this diagram are concentrated towards the uranium-bearing end of the series, the spread of compositions suggest that a continuous series exists between the hydrated species coffinite and thorogummite. Fuchs and Gebert (1958) established the existence of such a series for the synthetic anhydrous minerals.

Nord (1977) established on the TEM-SEM and the EMP that the coffinite in the sandstone-type uranium deposits in the Colorado coexists with amorphous silica and uraninite of a composition ranging from $UO_2$ to $UO_{2,08}$. Brookins (1975) proposed that the following reversible reaction for coffinite and uraninite

$$USiO_4(c) + 2H_2O \rightleftharpoons UO_2(c) + H_4SiO_4^0 \qquad (8)$$

is at equilibrium, when dissolved silica exceeds $10^{-6,9}$ M (8 $\mu$g/l $SiO_2$). The silica concentration in groundwater ranges from 19 to 120 mg/l $SiO_2$ (resp. $10^{-3,5}$ and $10^{-2,7}$ M; Langmuir, 1978).

Hemingway (1982) postulated that coffinite would only form when uranyl ions are adsorbed on the surface of a silica gel, and when the prevailing conditions are unfavourable for rapid dehydration and alteration of the gel. The precipitation of coffinite depends on the amount of amorphous silica available. In the absence of amorphous silica, uraninite will precipitate so that zones of coffinite and uraninite may alternate. This type of alteration is observed in the recent supergene mobilization of uranium in the Monarch Reef in East Champ d'Or G.M. (Figs. A.28c and d).

The *association of titanium with coffinite* in rocks of the Massif Central in France has led Ruhlmann (1980) to suggest the existence of (U,Ti)-silicates, which would form a solid solution series between $U(TiO_4)_{1-x}(OH)_{4x}$ and $U(SiO_4)_{1-x}(OH)_{4x}$. Because the difference in the ionic radii of $Ti^{4+}$ and $Si^{4+}$ (0,68 and 0,29 A respectively) well exceeds the excepted 15% limit, substitution of silica by titanium is unlikely. Moreover, if such a series would exist, the cell-size dimensions and the XRD patterns would differ substantially from those of pure coffinite. In the UE1a and E9 Reefs, the coffinite is sometimes coated by a uraniferous leucoxene-bearing film (Figs. A.27e and f), which merely indicates that the conversion of uraninite to coffinite preceded the precipitation of uranous titanate. For the adequate dissolution of silica and titanium near the surface, different acidities are required, i.e. pH values of respectively 9 and 5,5 and this implicates that the one precipitated after the other.

In the Witwatersrand, (U,Th)-silicates are only found in the Dominion Reef and in the reefs of the Turffontein Subgroup. It is evident from the textural relationship between uraninite and coffinite in these reefs, that the transformation took place *in situ* through the addition of silica. In the Dominion Reef, where authigenic uranous titanate did not form at all, the uraninite was partly or entirely replaced *in situ* by hydrated (U,Th)-silicates usually of thorian coffinite composition (Table 54, DR1446). In contrast with the reef of the CRG, the Dominion Reef occurs close to the present surface. Many of the (U,Th)-silicates in the UE1a and E9 Reefs are anhydrous

thorian coffinites (Table 54, RF1306 and 1308). Initially, the coffinite reefs could have been of the hydrated type which, with the increase in depth of burial, must have gradually lost the water.

In contrast with the uranous titanates, (U,Th)-silicates are very rare in the reefs of the Johannesburg Subgroup in the western portion of the basin, but are fairly common in the reefs of this subgroup in the eastern part of the basin. The silicates increase in abundance in the reefs of the Turffontein Subgroup throughout the basin. In the latter subgroup, kerogen only occurs in the nodular form, so that uraninite was mainly a constituent of the matrix. After final deposition the uraninite enclosed by kerogen and in the matrix both reacted to form uranous titanates or less commonly coffinite. The general transformation *in situ* of uraninite to coffinite in the reefs mined on Cooke Section and Western Areas G.M. is therefore conspicuous.

From his study on these reefs, Tucker (1980) concluded that the depositional setting differed from that of the other reefs of the CRG. The debris were transported across a scoured pediment at the foot of highlands and then deposited beyond the pediment on an alluvial outwash plain upon which a braided river system developed. In contrast with the clastic wedge of a fan, the sediments increase in thickness away from the entry point.

The following environment and process for the formation of coffinite in the UE1a and E9 Reefs is here suggested. If the climate was arid, alkaline conditions could have existed on the pediment and on the outwash plain. Such an environment would have been favourable for the dissolution of silica and the transformation of uraninite to coffinite, which requires reducing conditions. The well-rounded coffinite grains could have formed on the scoured pediment, and acquired its shape (Fig. A.27d) on its way to, or through reworking on the outwash plain, whereas the less irregular-shaped grains (Fig. A.27g) and amoeboid-shaped aggregates (Fig. A.27f) would have formed on the plain itself. Silica has been mobilized within the UE1a and E9 Reefs at various stages after burial. However, the

quartz in the pressure fringes on pyrite grains precipitated after the authigenic coffinite, and so did the quartz which is associated with authigenic sulphides.

The substantial increase in volume of the coffinite pseudomorphs in the West Rand G.F. is evidence for the transformation of the uraninite at a time that pore solutions could circulate freely, and expansion of the original grain was possible, i.e. soon after deposition. As for the precipitation of uranous titanates and the formation of cutans and relict uraninite, it is concluded that this process took place at an early stage after burial.

The following *chemical changes* took place during the transformation of uraninite to coffinite. The high thorium content of the coffinite (Table 54) indicates that thorium remained *in situ* and became relatively enriched, so that some of the uranium must have migrated. The radiogenic galena was redistributed within the coffinite. The iron was not taken up by the coffinite, but the coffinite grains are usually accompanied by minute laths or pyrrhotite (Figs. A.27d and h), which also commonly precipitated within (Fig. A.25g) or in the vicinity of authigenic uranous titanates. Since this iron sulphide is not known to occur in the acicular habit, the crystals could represent sulphidized hematite. For the precipitation of hematite, the conditions have to be less reducing than for pyrrhotite (Figs. 20 and 29). Pyrrhotite laths did not precipitate during the transformation of uraninite to coffinite in the Dominion Reef, where pyrrhotite has not been found at all. The absence of this type of iron sulphide implicates that physicochemical conditions were generally unfavourable for its precipitation.

In pyrite-rich foresets of the Johannesburg Subgroup and in the Elsburg Reefs generally (Fig. A.20f), the branneritization of uraninite is associated with coarser pyrrhotite crystals of a stubby habit (Figs. A.26a and b), which precipitated onto the surface of the altered uraninite and of some of the pyrite grains in the immediate vicinity. Their neoformation suggests that pyrite itself could have been incipiently oxidized if excess oxygen was available, so that

more dissolved ferric iron became available over and above that which was leached from the uraninite. A subsequent change in the oxidation potential after burial must have led to the reprecipitation of the dissolved ferric iron as pyrrhotite in the area where the uraninite which was oxidized.

The EMP analyses of coffinite from Cooke Section (Table 54) indicate that the silicate usually contains yttrium and phosphorus, usually in the proportions of an Y-phosphate (Table 55). The X-ray distribution images for uranium, silicon, yttrium and phosphorus in coffinite overlap each other. Since yttrium may substitute for uranium, and phosphorus for silicon, they can form an integral part of the coffinite, and in that case, the general formula would read $(U,Th,Y)(Si,P)O_4$. As the uptake of yttrium and phosphorus is probably not unlimited, some of the yttrium and phosphate could have combined and precipitated as a discrete mineral intergrown with coffinite. A discrete, transparent yttrium phosphate which could not be identified, has been noticed in many of the grains. Leaching tests on polished sections with dilute sulphuric acid, have confirmed their presence. The hydrated yttrium phosphate churchite has been recognized in weathered rocks (Milton *et al.*, 1944; Claringbull & Hey, 1953), but has also been reported from a supergene environment (Podporina *et al.*, 1983).

It is noteworthy that the phosphate ions did not react with uranium to form the uranium phosphate *ningyoite*, a mineral which has been identified in sedimentary rocks in Japan, where it precipitated from uranium-bearing groundwaters together with uraninite and coffinite (Kajitani, 1970).

XRD suggests that coffinite is also a component of the *mushy anatase* which cements heavy minerals and is composed of leucoxene, quartz, and phyllosilicates (Figs. A.26h and A.30c). The mush could represent accumulations of dust-sized abrasion particles of eroded leucoxene and the residue of titaniferous magnetite from which ferrous iron was dissolved. The EMP analyses of the anatase much (Table 58) fail to provide unambiguous information on the constituents present, and optically there is no evidence for the presence of coffinite, although minute specks of radiogenic galena indicate the

presence of radioactive matter, which also could point to the presence of metamict uraniferous leucoxene.

4.3.2.4. Pitchblende and Secondary Coffinite

The pitchblende found in the Monarch Reef, West Rand G.F., practically formed *in situ* in a supergene environment together with secondary coffinite, pyrite, galena, and marcasite (Smits, 1985c, 1987). The term 'secondary' coffinite is used to distinguish the silicate from the much older authigenic species in the UE1a and E9 Reefs and the Dominion Reef.

The absence of radiogenic galena in the pitchblende confirms that the redistribution of uranium occurred in relatively recent times. The relationship between the secondary tetravalent uranium minerals and the detrital uraninite differs distinctly from that found between the same minerals in the UE1a and E9 Reefs (cf Figs. A.28c with A.27g) and in the Dominion Reef (cf Figs. A.28c with A.28b). In contrast to the coffinite that formed *in situ* at the expense of uraninite, uranium was mobilized over microscopic distances (Fig. A.28d) during the precipitation of the supergene products.

The composition of the pitchblende and secondary coffinite (Table 59) again differs from that of the detrital uraninite (Table 35) and the coffinite respectively that formed directly from uraninite *in situ* (Table 54, Rf1306). The low chemical totals imply high water contents, whereas the pitchblende contains only trace amounts of thorium. On the other hand, the thorium content of the secondary coffinite is similar to that of the primary uraninite (Smits, 1987, 1989).

*4.3.3. Rutile and Leucoxene of authigenic Origin*

Although the $TiO_2$ concentration of the reefs does not exceed the 0,6%, the sparse but pervasive distribution of minute authigenic rutile crystals and grains (Table 20) throughout the sediments is conspicuous, particularly in view of the fact that detrital rutile is rare.

The solubility of titanium oxide in pure water is virtually nil (Deelman, 1979), but there is ample evidence for its dissolution in recent soils when certain conditions are met. In the uranium-bearing reefs, the sparsely dispersed minute rutile crystals and possibly some of the dispersed

leucoxene present throughout the reefs confirm the post-depositional mobilization of titanium. Its occurrence after burial in the dissolved state is also revealed by the common occurrence of non-uraniferous, titanium-bearing microspherules (Fig. A.10d), <2 μm in diameter, which are only visible in the polished sections on the transparent quartz grains, but probably cover all grains. These microspherules could have formed through dehydration of a liquid titanium-bearing pellicle which adhered to the particles. A large part of the dissolved titanium was taken up by the authigenic uranous titanates.

*4.3.4. The Metamorphic Assemblage*

The entire original phyllosilicate assemblage of the sediments of the CRG has been stabilized during metamorphism, and is at the present made up of:

chloritoid-pyrophyllite-chlorite II*b*-muscovite/sericite $2M_1$.

*Pyrophyllite* and *chloritoid* are the best indicators for the establishment of the maximum metamorphic stage reached by the sedimentary rocks of the CRG. *Sericite* and *chlorite* acquired their final stable polytype structures, i.e. muscovite $2M_1$ and chlorite II*b*, for which lower temperatures and pressures are required than for the formation of pyrophyllite and chloritoid. The two last-named minerals disclose that the metamorphic conditions to which the sedimentary rocks were subjected lie just beyond the lower limit of the low metamorphic grade (Winkler, 1979), previously referred to as the greenschist facies (Sections 4.3.4.3 and 4.3.4.4). Minerals diagnostic for the higher limit of this grade, viz biotite, garnet, staurolite, and cordierite are absent. The rare occurrence of *kyanite* in the Orange Grove Quartzite at Northcliff and in pre-Transvaal faults at West Rand Consolidated G.M. in Krugersdorp (Schreyer & Bischoff, 1982) resulted from local changes in pressure and temperature. In both instances, the presence of kyanite is not representative of the regional metamorphic grade attained by the sediments in the Witwatersrand Basin.

The parageneses of the very-low and the low metamorphic grade are pictured in Figures 25a and b respectively (Winkler, 1979) and that for the Witwatersrand in Figure 26, whereas the

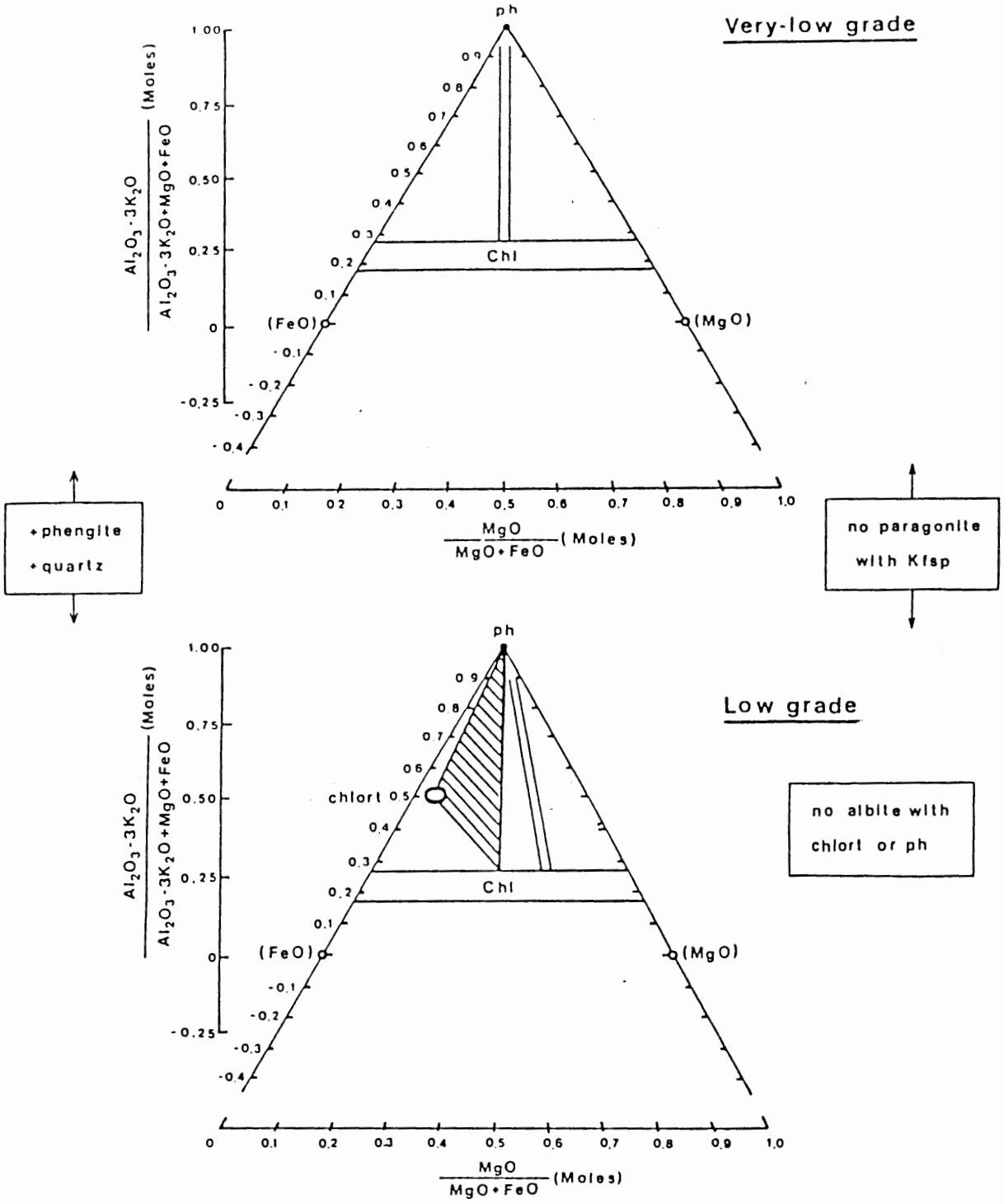



Fig. 25 Parageneses of very-low and low metamorphic grades illustrated in an AMF projection plane (Winkler, 1979)

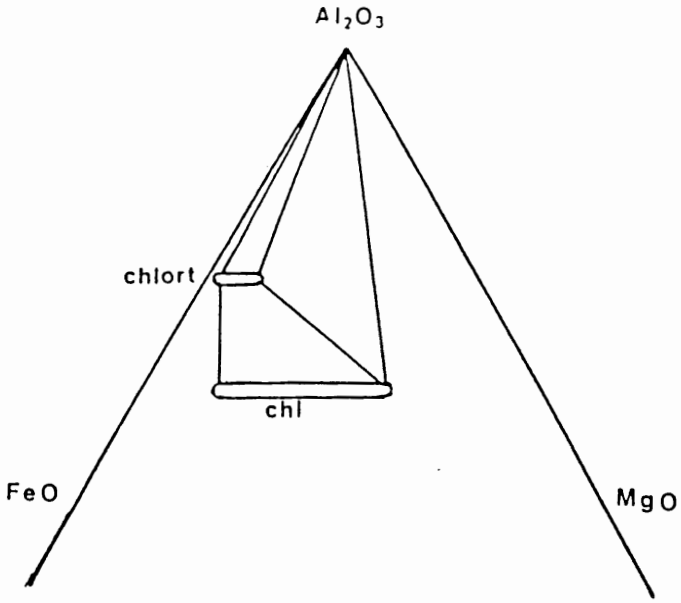



Fig.26 Graphic representation in an AFM projection plane of parageneses and compositional ranges of chloritoid and chlorites found in the uranium-bearing CRG reefs.
MgO/(MgO+FeO) ratios for:
chloritoid 0,03 to 0,16, and
chlorite 0,17 to 0,62

petrogenetic grid in Figure 27 indicates the area in which the metamorphic reactions of the Witwatersrand sediments most likely took place, i.e. around 400$^0$C at 3 to 4 kbar. The metamorphic grade was attained through normal regional progressive burial, and no additional event is required to explain the metamorphic activity.

The maximum metamorphic temperature of about 400$^0$C is indicated by two other phenomena, viz (1) the *homogenization temperature* of secondary inclusions in quartz pebbles from Krendelev *et al.* (1973) and (2) the degree of maturation attained by the kerogen in the reefs of the CRG.

Krendelev *et al.* (1973) recorded the following homogenization temperatures for primary and secondary, two-phase inclusions in quartz pebbles:

| Reef | Primary inclusions | Secondary inclusions |
|---|---|---|
| Dominion Reef | 130 to 320$^0$C | 300 to 400$^0$C |
| Main Reef | 110 to 280$^0$C | 300 to 360$^0$C |
| Basal Reef | 80 to 290$^0$C | 270 to 350$^0$C |

The homogenization temperatures of the secondary inclusions from Krendelev *et al.* (1973) agree with the peak metamorphic temperature as indicated by the silicate assemblage. They are considerably higher than those measured by Hallbauer (1983), which did not exceed 250$^0$C.

The kerogen in the reefs of the CRG did not attain the ultimate stable state of graphitization, which is achieved in the medium-metamorphic grade between 450 and 500$^0$C (Miyashiro, 1973).

The degree of maturation of organic matter can be correlated with diagenetic and metamorphic mineral assemblages as follows (Murchison *et al.*, 1985; Fig. 28):

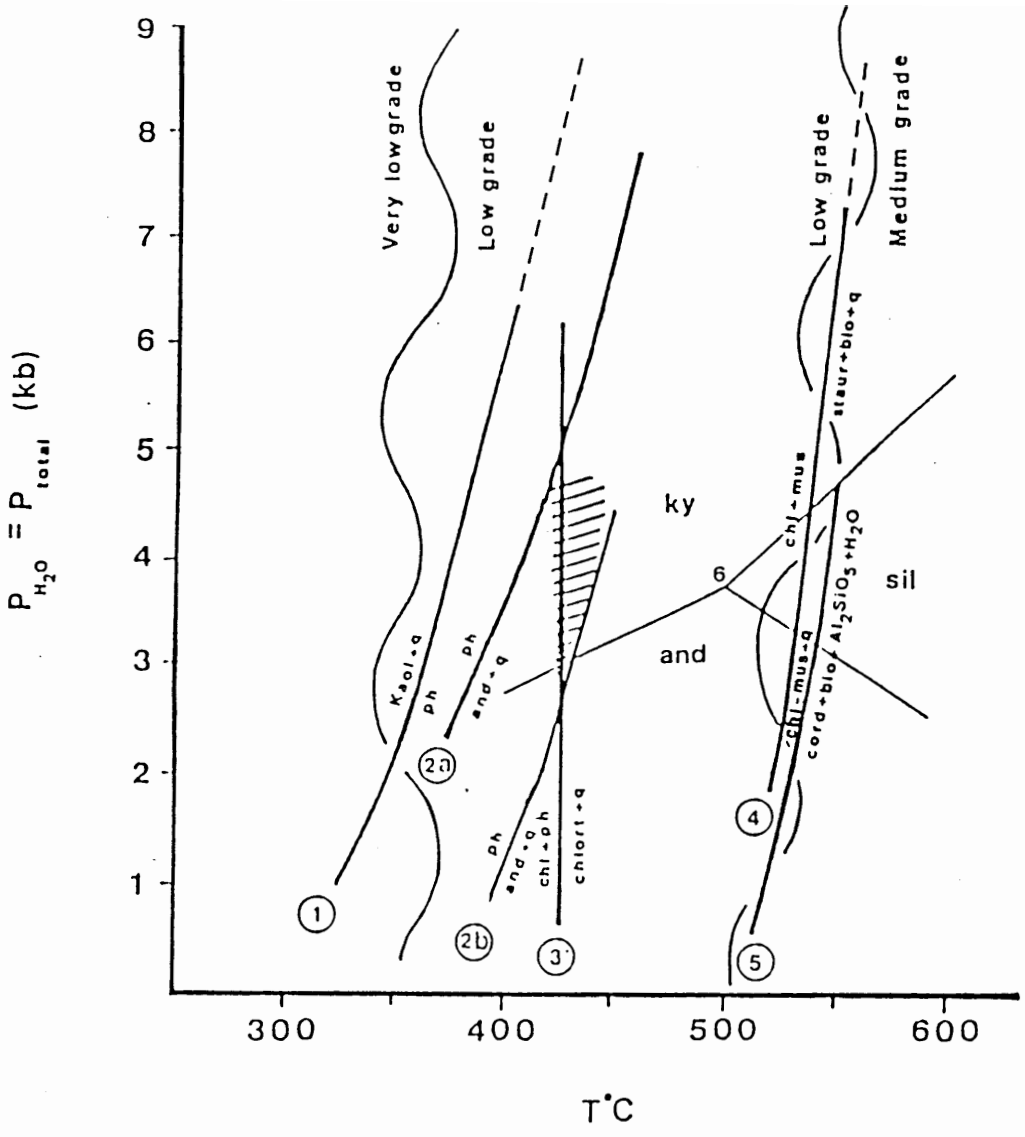
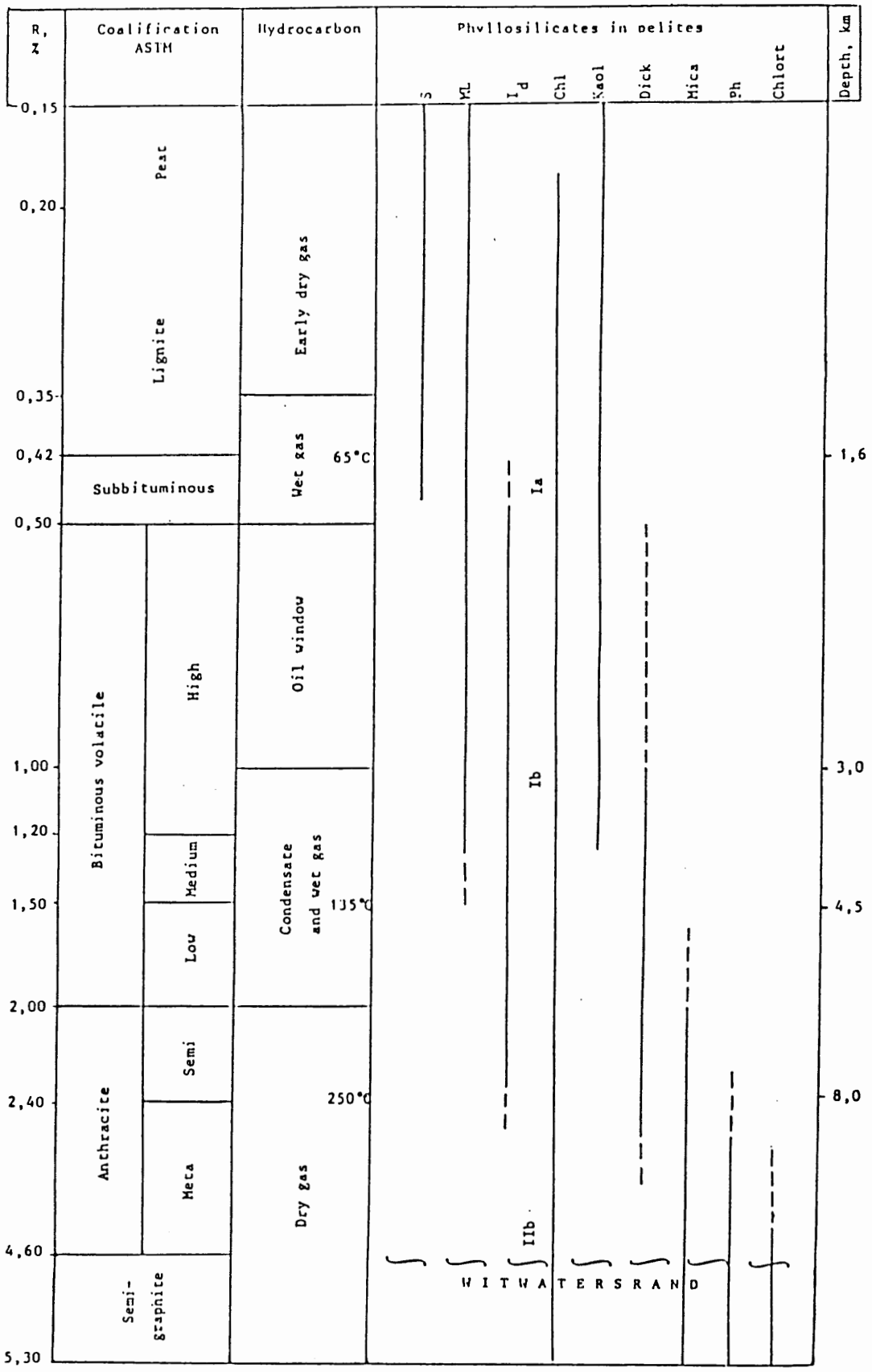



Fig. 27 Petrogenetic grid of metamorphic reactions relevant to Witwatersrand rocks

| | | |
|---|---|---|
| (1) | kaol+q = ph+$H_2O$ | (Thompson, 1970 |
| (2a) | ph = and+q+$H_2O$ | (Haas & Holdaway, 1973) |
| (2b) | ph = and+q+$H_2O$ | (Kerrick, 1968) |
| (3) | ph+chl = chlort+q+$H_2O$ | (Hoschek, 1969) |
| (4) | chl+mus = staur+bio+q+H2O | (Hoschek, 1969) |
| (5) | chl+mus+q = cor+bio+$Al_2SiO_5$+$H_2O$ | (Hirschberg and Winkler, 1968) |
| (6) | ky - and - sil | (Holdaway, 1971) |

Hatched area outlines field for estimated metamorphic conditions for the bulk of the CRG reefs




R - reflectance in oil  S - smectite  ML - ML clay minerals
$I_a$ - disordered illite  Dick - dickite

Fig. 28 Correlation between thermal indicators for coal hydrocarbon, and minerals (after Heroux *et al.*, 1979; Stach *et al.*, 1982; Hower *et al.*, 1976)

| Coal stage | Metamorphic facies |
|---|---|
| bituminous | zeolite |
| low rank anthracite | prehnite-pumpellyite, pumpellyite-actinolite |
| high rank meta-anthracite | greenschist |

As is illustrated in Figure 28, the mineral assemblage of the sediments of the CRG reefs falls in the last-mentioned coalification stage.

From his study on sediments of the WRG in the Heidelberg Area, Camden Smith (1980) established that some of the shales reached the very-low grade metamorphic stage. However, chloritoid and pyrophyllite have been found in conglomerates within the WRG in the Central Rand (Fuller, 1958) and in the western portion of the basin (Meyer & Tainton, 1986). Phillips (1987) studied several pelitic rocks in the Witwatersrand Supergroup and concluded that the metamorphic temperature lies at about 350 + 50$^0$C, at a pressure between 1 and 2 kbar.

Going back in geologic time, it is possible to make predictions for the *immediate precursors* of the present metamorphic phyllosilicate assemblage (Table 66).

Table 66. Possible precursor minerals of present metamorphic phyllosilicate assemblage

| Metamorphic mineral | Precursor: immediate | earlier |
|---|---|---|
| chloritoid | pyrophyllite, | see pyrophyllite |
| | chlorite II*b* | see chlorite II*b* |
| pyrophyllite | kaolinite, chlorite I*b* | kaolinite ML chl/smect |
| chlorite II*b* | chlorite I*b* | ML chl/smect |
| musccovite $2M_1$ | phengite or illite of high crystallinity | ML ill/smect |

The last diagenetic phyllosilicate assemblage was most likely composed of kaolinite, chlorite I*b*, and phengite or illite, whereas the ultimate precursor for illite and chlorite

(preceding the ML species) could be smectite. The common association of pyrite concentrations with chlorite, which in the Carbon Leader has been replaced by chloritoid, suggests that smectite, which then would have precipitated in stagnant water, could have been the ultimate precursor.

From the present composition, it is here inferred that the *detrital biotite* was first partly altered to kaolinite, while the remaining portion was transformed *in situ* during diagenesis to a mixture of illite and chlorite. The potassium from the biotite is incorporated in illite, and the magnesium and iron in chlorite (Kisch, 1983; Aldahan & Morad, 1986). The titanium and some of the iron released during the alteration process, recrystallized as rutile and pyrite along the cleavage. With the increase in depth of burial, the kaolinite was converted to pyrophyllite, chlorite recrystallized to the stable polytype chlorite II*b*, and illite altered to the stable polytype muscovite $2M_1$.

*4.3.4.1. Chlorite*

Theoretically trioctahedral chlorite can occur in six polytypes of different structure, of which four have been recognized in nature (Brown & Bailey, 1962). In sedimentary rocks, they precipitate according to the following stability sequence (Hayes, 1970):

I*a* ($\beta=97^0$), I*b* ($\beta=97^0$), I*b* ($\beta=90^0$), and II*b*($\beta=97^0$).

The polytypes can be distinguished by their *h0l* intensities on XRD patterns (ibid.). The formation of a particular polytype of chlorite depends on temperature, but the composition of the chlorite is a reflection of that of the precursor mineral, and chemical activities in the environment where it occurs (Hayes, 1970), and does not influence the structural stability (Frey, 1987). The polytypes I*a* and I*b* are diagenetic species. For the I*b* ($\beta=90^0$) to be converted to the most stable II*b* structure, the conditions should approach that of the very-low metamorphic grade (Curtis *et al.*, 1985). Chlorite II*b* is fully established at 200 to 230$^0$C (Evarts & Schiffman, 1983). XRD patterns of *chlorite* in the *sediments of the CRG* confirm that all the chlorites are of the stable II*b* type.

The composition of these chlorites shows the following distribution pattern. The chlorite of the reefs of the Turffontein Subgroup on the West Rand G.F. is rich in magnesium (i.e. the 'green' variety), and in the older Vaal Reef, Basal Reef, and Carbon Leader, the chlorites are of the iron-rich variety (i.e. the 'purple' chlorite), although occasionally they enclose cores of green chlorite. Chloritoid is on the West Rand G.F. associated with green chlorite, but in the Carbon Leader with the purple variety. In the Vaal reef and Basal Reef, where the chlorite is of the 'purple' or 'orange' variety, chloritoid is much less common.

With regard to the *evolution of the composition of chlorite* during metamorphism, the following suggestions have been made. White *et al.* (1985) noticed that in sediments of the very-low metamorphic grade, chlorite ranges from Mg-rich to Fe-rich ripidolite, whereas in the schistose rocks, it is mostly Fe-rich. Wybrecht *et al.* (1985) conclude from a study on greywackes that chlorite loses silicon and aluminium, so that it becomes richer in (Fe+Mg) with increasing metamorphism, and that, in the sample of the highest metamorphic grade, the chlorite is richer in magnesium. Hirschberg and Winkler (1968) and Hoschek (1969) determined that the upper stability for chlorite lies at 4 kbar at approximately 540$^0$C (Fig. 27 curves 4 and 5), while Fawcett and Yoder (1966) established that Mg-chlorite persists to higher temperatures (762$^0$C at 3,5 kbar). Burnell and Rutherford (1984) demonstrated experimentally that in the presence of excess muscovite and quartz, chlorite of intermediate Fe/Mg ratio persists to a higher grade than do the Mg and Fe end-members, and that chlorite will disappear at 4 kbar at 640$^0$C, and at 2 kbar at 612$^0$C.

The observations on the evolution of the composition of chlorite during metamorphism, cited in the preceding paragraph, are contradictory. It is here suggested that factors such as, (1) the bulk composition of the rocks in the provenance, (2) the composition of the precursor chlorite or clay mineral, or (3) the distance between the mouth of the river and the site of final deposition in the basin, which therefore is related to the grain size of the clay minerals, could have influenced the

composition of the metamorphic chlorite in the reefs. It is concluded that the Fe/Mg ratios of chlorite cannaot be regarded as a reliable parameter for the metamorphic grade.

4.3.4.2. Muscovite-Sericite

In the reefs of the CRG, sericite is the ubiquitous potassium-bearing mica, which fills interstices and outlines quartz boundaries, while muscovite mainly occurs in the distorted, detrital phyllosilicate intergrowths. The much less common undeformed muscovite flakes and part of the sericite $2M_1$ are considered to have been inherited as the stable $2M_1$ polytype from the source rocks. The scarcity of allogenic muscovite indicates that it was much less common than biotite. The muscovite in the pseudomorphs after biotite and the remaining portion of the interstitial sericite acquired the stable $2M_1$ state after burial. The low-temperature, disordered illite $1M_d$ polytype slowly evolves between 200 and 350$^0$C at about 2 kbar water pressure via phengite, or directly to the metamorphic muscovite $2M_1$ polytype (Velde, 1983).

4.3.4.3. Pyrophyllite

Pyrophyllite forms in argillaceous rocks devoid of albite and K-feldspar. In the presence of the last-named minerals, paragonite or muscovite would form respectively (Hemley & Jones, 1964).

Pyrophyllite has a rather narrow stability field with respect to temperature, but the pressure range is much wider. At low $H_2O$ pressure, it forms within the range of very-low-grade metamorphism (Fig. 25a), but at higher pressure, it appears in the low metamorphic grade, (Fig. 27 curve 1). Thompson (1970) established that at 1 kbar, pyrophyllite forms at 325+20$^0$C, and at 4 kbar (equivalent to an approximate depth of 12 km) at 375+15$^0$C (Fig. 27). The latest data from Frey (1987) indicate that at 4 kbar and $a_{H2O}$ = 1, the temperature ranges from 310 to 410$^0$C.

Several investigators (Ianovici *et al.*, 1981; Kisch, 1983; Frey, 1987) have found that pyrophyllite and chloritoid formed locally at lower pressure and temperature, but these occurrences are rare.

Zen (1960) proposed the following reaction for the formation of pyrophyllite:

$$kaol + H_4SiO_4 \rightleftharpoons ph + H_2O \qquad (9)$$

However, kaolinite usually becomes unstable before the temperature has reached the level at which it would be transformed to pyrophyllite (Dunoyer de Segonzac, 1970). In the presence of alkaline solutions, it will alter to illite between 150 and 200°C, or to dickite above 200°C (ibid.).

For reaction (9) silica is required. The strongly embayed quartz grains in argillaceous rocks cemented by a sericite-pyrophyllite mixture (Figs. A.1f and A.4c) indicate that silica was here supplied by the quartz grains.

Pyrophyllite can also form from chlorite (Zen, 1960):

$$chl + H_4SiO_4 \rightleftharpoons ph + 5(Mg,Fe)^{2+} + 10(OH)^- \qquad (10)$$

In the sedimentary rocks of the CRG, pyrophyllite and chlorite of varying composition may occur together in the pseudomorphs after detrital biotite, which twist along quartz grains of the matrix (Fig. 6c), so that reaction (10) could not have taken place.

With a further increase in temperature, pyrophyllite will be transformed to chloritoid (equation 12) at the required chemical conditions, or it is broken down to andalusite and quartz (Fig. 27 curves 2a and 2b):

$$ph \rightleftharpoons and + q + H_2O \qquad (11)$$

The upper stability limit for pyrophyllite was established experimentally by various investigators. The equilibrium data from Haas and Holdaway (1973) are given by curve 2a and for Kerrick (1968) by curve 2b in Figure 27. The temperature range for the stability field of pyrophyllite extends at 3,5 kbar respectively from 360 to 380°C (curve 2a) and 360 to 440°C (curve 2b).

The metamorphic assemblages in the CRG sediments show that the pressure conditions must have exceeded the point at which the curves representing the dehydration of pyrophyllite (Fig. 27 curves 2a and 2b; equation 11) intersect the one representing the formation of chloritoid (equation 12) from chlorite and pyrophyllite (Fig. 27 curve 3). According to the equilibrium data established by Hoschek (1969), the pressure

would be 2,5 kbar or more at a temperature of 430°C, whereas the data determined by Haas and Holdaway (1973) indicate that chloritoid starts to form at a temperature and pressure of respectively 420°C and 5 kbar.

4.3.4.4. Chloritoid

Although chloritoid is an index mineral for pelitic rocks subjected to low-grade metamorphism, it is not diagnostic for this grade since the following specific chemistry of the sediments is required for its formation (Halferdahl, 1961):

(1) low alkali and calcium, and
(2) moderately high alumina contents, and
(3) a high FeO/FeO+MnO ratio.

Because of this particular chemistry, the following minerals cannot coexist with chloritoid:

biotite, stilpnomelane, and as for the precipitation of pyrophyllite, albite, and K-feldspar.

The incompatibility of biotite with regard to the precipitation of chloritoid indicates that the biotite was altered to the muscovite, chlorite, and pyrophyllite intergrowth prior to the formation of chloritoid. The last transformation of biotite indeed took place during late diagenesis and the very-low metamorphic stage.

Zen (1960) suggested the following reaction for the lower stability limit of chloritoid:

$$ph + chl \rightleftharpoons chlort + q + H_2O \qquad (12)$$

of which Hoschek (1969) determined the equilibrium data (Fig. 27 curve 3). Frey (1972) established that this reaction occurs above 450°C. Baltatzis (1980) postulated that if non-ideal solutions are present, chloritoid will start to form at 400°C at a pressure of 3 kbar, which is higher than that required for the breakdown of pyrophyllite to andalusite and quartz (Fig. 27 curve 2b). If the pressure gradient is taken at 300 bar/km, pyrophyllite would form at a depth of about 11 km at 370°C (Fig. 27 curve 1). Chloritoid would then have formed at greater depth, but probably well below 4,5 kbar (Fig. 27 triple point 6).

The following alternative reaction at a slightly higher temperature was proposed by Thompson and Norton (1968):

$$\text{hem} + \text{Fe-chl} \rightleftharpoons \text{chlort} + \text{magn} + \text{q} + H_2O \qquad (13)$$

However, metamorphic magnetite has not been noticed in the reefs.

Textural relationships indicate that chloritoid formed indiscriminately from any type of chlorite. In the reefs mined on the West Rand and West Wits Line G.F., chloritoid acquired iron from pyrite (Figs. A.5b and c), arsenopyrite, and the iron-bearing chromite species.

The paucity of chloritoid in the sediments of the Klerksdorp and Welkom G.F. is conspicuous, for which the following factors could be responsible.

(1) the bulk composition of the pelitic portion of the sedimentary rocks did not satisfy the chemical requirements for the formation of chloritoid,
(2) the absence or scarcity of pyrophyllite or chlorite,
(3) the common silicification of phyllosilicates, in the Vaal Reef particularly, or
(4) the lesser depth of burial.

#### 4.3.4.5. Authigenic sulphides and gersdorffite and recrystallization of gold

In contrast with the extremely rare occurrence of detrital sulphides, that of authigenic sphalerite, galena, pyrrhotite, pentlandite, chalcopyrite is fairly common, so is the presence of authigenic gersdorffite. Some of the authigenic sulphides occur within the reefs, others in quartz veins which are usually of small extent and represent low or high temperature fault fillings. These minerals often precipitated together with recrystallized gold, which implies that the two processes occurred at the same time. Recrystallization of gold takes place at about 250°C (Liebenberg, 1955; Saager, 1969), a temperature which prevails during the very-low-grade metamorphic stage (Winkler 1979).

It has been suggested that the magmatic matter, which was introduced along the fault system across the sediments, could be responsible for the precipitation of the sulphides (Pretorius, 1976). This would not explain the common association with the gold, unless the intrusives also caused the remobilization of the gold. No specific studies have as yet

been done on the source of the metal ions for the authigenic sulphides, their distribution within the reefs, and a possible association with the intrusives which intersect the sedimentary sequence of the Witwatersrand Supergroup.

4.3.4.6. Tourmaline Overgrowth

The author considers the syntaxial overgrowth on detrital tourmaline in the Witwatersrand a metamorphic phenomenon, although it has never generally been regarded as a diagnostic metamorphic feature.

4.3.4.7. Other metamorphic Parameters in the Witwatersrand

Parameters other than diagnostic metamorphic minerals have been used by various investigators in an attempt to establish the metamorphic grade of the Witwatersrand sediments.

Feather and Duggan (1974) used the chemical composition and the crystal structure of *authigenic cobaltite* and *gersdorffite* and concluded that the peak metamorphic temperature achieved lies between 400 and 600$^{0}$C. They based their conclusion on diagrams of Bayliss (1969) and Klemm (1965). The reliability of the chemical isotherms determined by Klemm (1965) was first questioned by Skinner (in discussion of paper from Saager & Oberthur, 1984) and is now generally disputed.

Heating experiments on a gold grain (Erasmus *et al.*, 1982) disclosed that at atmospheric pressure, the *mercury in the gold* starts to volatilize at approximately 350$^{0}$C. It varies for different grains from 350 to 450$^{0}$C. Higher pressures would raise the starting temperature of volatilization slightly. The authors propose that the metamorphic temperature did not exceed 400$^{0}$C, which is in accordance with the indications provided by the metamorphic mineral assemblage.

# 5. THE PALAEOENVIRONMENT AT THE EARTH'S SURFACE DURING WITWATERSRAND TIMES

## 5.1. Geologic Setting

Archaean granite-greenstone rocks and pre-Witwatersrand sediments suplied the detritus for the Witwatersrand deposit. Because of the substantial erosion that must have taken place, the portion of the Archaean provenance which has been preserved cannot be considered representative for the original source rocks. The conglomerates of the Uitkyk Formation of the Pietersburg Group (Muff & Saager, 1979), and the Mozaan Group of the Pongola Sequence (Smits, 1978; Saager *et al.*, 1982), which are found in the centre and in the east of Transvaal and in Natal are older than those of the CRG (Hegner *et al*, 1984). In strong contrast, with the remarkable concentration of gold and uraninite in the reefs of the CRG, which gave rise to a deposit of unique and unequalled magnitude, the older conglomerates do not contain gold or uranium in economic concentrations.

The debris for the sediments of the CRG not only originated from the hinterland of the basin, but also from the proximal facies of the WRG and, on the Klerksdorp G.F., possibly also from the Dominion Reef. Viljoen *et al* (1970) suggested that the detritus suplied directly by the Archaean rocks was deposited in a stratigraphic order reversed to that of the rocks in the provenance. This assumption implies that the source rocks of the sediments of the Dominion Group were made up of Archaean rocks of a higher stratigraphic level than those of the sediments of the CRG.

The types of igneous rocks from which the major detrital constituents could have been inherited are listed in Table 67.

Table 67 Indicator minerals for the type of source rocks of the reefs of the CRG and the Dominion Reef

| Mafic and ultra-mafic rocks | Acid rocks | Pegmatites | Rocks affected by hydrothermal activity |
|---|---|---|---|
| chromite | zircon | uraninite | gold |
| PGM | garnet* | uranoan thorite | cobaltite |
| pyrite | | arsenopyrite | |
| rutile-leucoxene | | thorian zircon** | concretionary pyrite |
| biotite | | monazite** | chloritized Fe-bearing minerals |

*) from peraluminous granite (Robb & Meyer, 1985)
**) the mineral assemblage of the Dominion Reef is of typical pegmatitic origin (Hiemstra, 1968)

The complete eradication of the rocks which supplied the approximately 11000 m thick-pile of sediments that filled the basin (Pretorius, 1976) indicate that large volumes of continental crust were stripped off from a vast area. The cyclic sedimentation at sites of major fluvial influx into the basin during CRG times, was a response to tectonically controlled erosion and aggradation (ibid.). In the absence of an effective vegetative cover in the mountainous hinterland, the weathered debris were readily washed down the slopes, so that sediment yields must have been substantial.

The constituents of the reefs indicate that sedimentological and geochemical processes during denudation, transportation, and periods of reworking caused the almost total disintegration of rock fragments into monomineralic grains. The high degree of sorting, the predominance of quartz, and the roundness of the detrital constituents, particularly that of the pebble fraction, are measures of the extreme maturity, and therefore a long history of recycling of the sediments of the CRG. The presence of indented and well-rounded mud- and siltstone clasts, which are particularly common on the OFS G.F., is evidence for the reworking of incipiently, or well-lithified, older sediments on the depositional plane.

The duration of the break in sedimentation at the end of a cycle, after the peneplanation of the provenance had been completed until tectonic activity restarted, must have exceeded

by far the time required for the deposition of the next cycle in response to renewed tectonic activity in the provenance (Smits, 1984b). This is indicated, firstly, by the absence of evidence for geochemical activity at hiatuses within the quartzites in each cycle and, secondly, even more by the sedimentary, geochemical, and biological activities that took place on the major erosional unconformities which separate the cycles. During this prolonged period of quiescence, microbial communities grew in waterlogged shallow pools (Hallbauer & Van Warmelo, 1974; Hallbauer, 1975), while, at the same time a thin layer of heavy minerals accumulated on the palaeosurface. The microbiota played a major role with regard to the distribution of gold and uraninite, which they entrapped selectively together with clay minerals. The heavy minerals were intensely reworked and concentrated on the major unconformities until sedimentation restarted as a result of renewed uplift of the hinterland.

5.2. The primitive Atmosphere and Biosphere

From the description and understanding of the behaviour of the detrital constituents, one can go a step further and speculate on the composition of the atmosphere in the early history of the earth's crust, and draw conclusions about the influence it had on the geochemical conditions at the surface.

The time-bound concentration of gold and uraninite in quartz-pebble conglomerates of Archaean and Early Proterozoic is believed to reflect the start of the evolution of the composition of the atmosphere from oxygen-poor and carbon dioxide-rich to the present one where the two gases have reached an equilibrium which is maintained and controlled by the biological system (Schidlowski, 1985; Cloud, 1988).

The stromatolitic structures, which are assumed to represent microbial communities and have been traced back to about 3,5 Ga (Walter, 1983), indicate that the earth was habitable during the Archaean. Isotopic data of sediments of the Isua Complex in Greenland, suggest that biological activity could even date as far back as 3,8 Ga ago (Schidlowski, 1985, 1988).

The existence of life and its subsequent evolution is of decisive significance for the evolution of the composition of the atmosphere. The microbiota adapted for their energy requirements to photosynthesis, which triggered off the production of oxygen and the simultaneous decrease in carbon dioxide (Cloud, 1988). They initiated the interaction of the lithosphere with the atmosphere and hydrosphere, which is marked by a continuous and irreversible change in surface conditions and consequently surface processes. The cycles of carbon, sulphur, and oxygen played a key role in the oxygenation of the atmosphere (Schidlowski, 1985).

The oxygen could not accumulate in the atmosphere until the reduced gases and oxygen-consuming minerals at the earth's surface were saturated with oxygen (Cloud, 1988). From the sudden global appearance of red beds about 2,2 Ga ago, it is evident that, at that time, free oxygen was available in unlimited quantities (Nisbet, 1987; Cloud, 1988). The constant composition of today's atmosphere was achieved in the Phanerozoic about 400 m.y. ago and since has been maintained within a level tolerable for life (ibid.).

The microorganisms which developed in shallow water depressions on the unconformities in the CRG did not produce free oxygen. This is evident from the uraninite mantled by kerogen, since the enclosed, fragmented grains remained in the unoxidized state in which it was captured. Except for the precipitation of gersdorffite crystals and the boudinage parallel to the plane of deposition of minerals enclosed by the kerogen (Fig. A.8a), or present in the same plane as the kerogen seam (Figs. A.24h and A.25a), there is no tangible indication of their possible geochemical influence on heavy minerals.

From the geochemical changes that are recorded by the heavy-mineral assemblage of the reefs of the CRG, it is concluded that, during the exogenic cycle and before final deposition, the minerals were not subjected to oxidation (Sections 4.2.1, 4.2.4, and 4.2.7). However, the relict uraninite and the pervasive distribution of uranous titanates in the reefs of the CRG is indisputable evidence for the large-

scale, post-depositional mobilization of uranium, which implies that a certain amount of oxygen was present. The uraninite grains not protected by organic matter reacted with the available oxygen probably during periods of reworking when they were exposed to the atmosphere, and did so before the other oxygen-consuming minerals.

The chief volatile components that were released during the early degassing stages of the aggregated earth were carbon gasses and water vapor, which initially could have escaped into space, but eventually formed the primary atmosphere and hydrosphere (Nisbet, 1987). It is believed that the primitive atmosphere contained considerably more *carbon dioxide* than the present one (Schidlowski *et al.*, 1983), the partial pressure of which is $10^{-3,5}$ atm, while that of the groundwater is $10^{-2}$ atm. The high carbon dioxide level created a greenhouse effect, which kept the temperature on earth in the stability range of liquid and solid water, which is the optimum for life. The subdued temperatures ensured that water did not escape from the lower atmosphere (Nisbet, 1987).

The partial pressure of the carbon dioxide in the primitive atmosphere is estimated to have ranged from $10^{-2}$ to $10^{-1}$ atm. Above a partial pressure of $10^{-1}$ atm, the growth of microorganisms would have been inhibited (Holland, 1978). The high carbon dioxide level of the primitive atmosphere would have increased the acidity of the rain, ground- and surface waters, and hence the palaeoenvironment at the surface in general. Pure water which contains carbon dioxide at the present level of the atmosphere, i.e. $10^{-3,5}$ atm, attains a pH of 5,7 (Carroll, 1970). At a partial pressure of 0,012 atm, the pH of the rain could be as low as 4,9 (Martini, 1986) and at $10^{-2}$ atm, which is the partial pressure of carbon dioxide in today's ground water, the value would drop to about 4,5 (Carrol, 1970).

In an acidic environment, $Fe^{2+}$, $Ti^{4+}$, $Al^{3+}$, $Mn^{2+}$, $Cu^{+}$, $Pb^{2+}$, $Zn^{2+}$, and $Ni^{2+}$ would be mobilized (Pourbaix, 1963; Loughnan, 1969; Fig. 22). Carbonic acid would also cause the breakdown of silicates. However, the dissolution of silicates, for example, is expected to lead to the concurrent precipita-

tion of carbonate, so that equilibrium between consumption and supply of carbon dioxide is restored. The fate of the hydrogen carbonate ion produced during the dissolution of certain minerals is unknown and inferences in that respect are speculative (Schidlowski *et al.*, 1983).

Grandstaff (1980) estimated that the *oxygen* level of the primitive atmosphere was between $10^{-2}$ and $10^{-2}$ of the present atmospheric level (PAL). It is possible that at these low levels, the distribution of the oxygen was not uniform and varied from one locality to another (Schidlowski *et al.*, 1983). The narrow range in $\delta^{34}S$ values around zero (Table 62) for detrital and authigenic pyrite in the reefs of the CRG is further evidence for the lack of oxygen.

Kasting *et al.* (1985) proposed that early photochemical processes could have affected the oxidation potential of rain water through the presence of dissolved $H_2O_2$ at an oxygen level not exceeding $10^{-3}$ PAL and a high partial pressure of carbon dioxide.

*5.2.1. Influence of Climate*

The effect of climate in recent times on the geochemical activity in rocks can be considerable because it influences the pH and Eh conditions at the earth's surface (Carroll, 1970). Chemical decomposition is most effective in *humid tropical* areas. The high rainfall enhances chemical activity and today may produce monomineralic profiles, e.g. of bauxite or kaolinite. In *arid* areas, physical disintegration may be pronounced (Siever & Woodford, 1979), and new minerals may form as a result of evaporation and capillary activity. In *temperate* and *semitropical* regions, chemical weathering is less rapid (Carroll, 1970).

Seasonal alternation of *wet and dry* conditions cause the watertable to fluctuate so that redox conditions change periodically (Carroll, 1970). This type of environment could have enhanced the formation of uranous titanates and cutans in the thin veneers of heavy minerals which were concentrated on the major erosional surfaces in the CRG in the absence of vegetation (Smits, 1984b).

On the basis of their high aluminium content, Wiebols (1961) proposed that the chloritoid shales, i.e. the Booysens Shale, Black Bar and Green Bar, are the weathering products of *glacial* material, probably till. The chemical composition of these shales is comparable with that of the fire clays overlying the Dwyka tillite in the East Rand (ibid.). It is here pointed out, that the pebbles in the Witwatersrand conglomerates could have been inherited from eskers and outwash fans which formed in a glacio-fluviatile environment in the provenance. However, permanent glacial conditions would have hindered geochemical activity and erosion in the source rocks. The complete dissolution of iron from ilmenite, magnetite, and possible other iron oxides and hydroxides, a process which took place in the provenance, is difficult to reconcile with permafrost conditions. In such an environment, the drop in temperature below freezing point would prevent the flow of water and consequently inhibit the geochemical reaction of minerals. It is more likely that rugged terrane in the provenance and recurrent reworking of the debris was responsible for the formation of the well-rounded gravel-size fraction.

The climatic conditions on the palaeosurfaces was probably less severe than in the mountainous hinterland, but it is more likely that the oxidation of uraninite not mantled by organic matter was promoted by the thorough reworking of the heavy minerals over a long span of time on the major unconformities before the deposition of the pebble fraction of the conglomerate at the base of the next cycle (Smits, 1984a).

5.3. Geochemical Aspects

The mature character of the sediments is not only reflected in the physical properties of the mineral assemblage, but also in the low concentration of all major elements other than silica (Table 68). The range and the average of whole-rock analyses from the four goldfields in the western portion of the basin illustrate that chemical activity led to the elimination of calcium, sodium, and manganese, and the depletion in aluminium, iron, magnesium, and probably phosphorus. The combined, pre-depositional mechanical and chemical processes

Table 68 Range and average of total rock analyses of reefs on the OFS, Klerksdorp, West Wits Line, and West Rand G.F.

| In % | OFS G.F. (6)* | | Klerksdorp G.F. (5) | | West Wits Line G.F. (8) | | West Rand G.F. (7) | |
|---|---|---|---|---|---|---|---|---|
| | Range | Av. | Range | Av. | Range | Av. | Range | Av. |
| $SiO_2$ | 68,5 - 88,4 | 80,5 | 73,9 - 85,1 | 77,4 | 85,5 - 93,3 | 88,8 | 70,1 - 70,8 | 82,1 |
| $Al_2O_3$ | 1,4 - 2,6 | 1,9 | 3,5 - 8,4 | 5,2 | 1,1 - 7,8 | 2,7 | 1,1 - 11,6 | 4,0 |
| $Fe_2O_3$ | 5,2 - 14,2 | 9,0 | 4,9 - 11,0 | 8,7 | 2,1 - 6,0 | 3,9 | 2,3 - 16,8 | 7,8 |
| MgO | 0,1 - 0,7 | 0,3 | 0,2 - 0,6 | 0,4 | 0,1 - 0,6 | 0,3 | 0,1 - 1,0 | 0,3 |
| CaO | ‹0,1 | ‹0,1 | ‹0,1 | ‹0,1 | ‹0,1 | ‹0,1 | ‹0,1 | ‹0,1 |
| $Na_2O$ | ‹0,1 | ‹0,1 | 0,1 - 0,2 | 0,1 | 0,1 - 1,0 | 0,2 | 0,1 - 0,5 | 0,1 |
| $K_2O$ | 0,1 - 0,3 | 0,2 | 0,3 - 1,8 | 1,0 | 0,1 - 0,6 | 0,4 | 0,1 - 0,3 | 0,2 |
| $TiO_2$ | 0,1 - 0,6 | 0,2 | 0,2 - 0,5 | 0,3 | 0,1 - 0,2 | 0,1 | 0,1 - 0,5 | 0,2 |
| $P_2O_5$ | ‹0,1 | ‹0,1 | 0,1 - 0,2 | 0,1 | ‹0,1 | ‹0,1 | 0,1 - 1,0 | 0,1 |
| MnO | ‹0,1 | ‹0,1 | ‹0,1 | ‹0,1 | ‹0,1 | ‹0,1 | ‹0,1 | ‹0,1 |
| $H_2O$ | 0,8 - 1,5 | 1,0 | 0,8 - 2,5 | 1,4 | 0,3 - 1,3 | 0,7 | 0,4 - 2,7 | 1,1 |
| S | 4,0 - 9,6 | 6,0 | 1,9 - 8,0 | 5,6 | 1,0 - 4,1 | 2,2 | 1,5 - 9,0 | 4,0 |
| $C_{org}$ | 0,1 - 5,7 | 1,6 | 0,1 - 4,1 | 0,9 | 0,1 - 0,8 | 0,2 | 0,1 - 1,1 | 0,2 |

*) (6) Number of analyses

reduced the number of minerals and changed the composition of certain constituents, while post-burial chemical activity was responsible for the moblization of uranium and titanium, and the precipitation of post-burial products, viz uranous titanates, coffinite, relict uraninite, cutans, and gersdorffite crystals. The increase in temperature and pressure with the increase in depth of burial led to the metamorphic recrystallization of gold and silicates, and the neoformation of the sulphides and gersdorffite.

Certain inferences about the geochemical processes, which must have operated at the earth's surface during the Archaean can be made from the mineralogical changes and these can be used for the reconstruction of the geochemical environment at the surface of the earth during the Witwatersrand sedimentation.

*5.3.1. Pre-depositional Mineral Modifications*

The following mineralogical features of detrital constituents in the reefs of the CRG are regarded as inherited from hydrothermal activity in the source rocks (Section 4.2.5.):

(1) the textures of concretionary pyrite, and
(2) the chloritization of some of the detrital grains of the iron-bearing minerals, pyrite, chromite, arsenopyrite, less commonly rutile-leucoxene pseudomorphs and, in the Dominion Reef, of garnet.

An inherited hydrothermal origin explains their well-rounded habit and sporadic, irregular distribution amongst and alongside their unaltered counterparts.

Another pre-depositional process, which is a significant source of information is the dissolution of ferrous iron from magnetite, ilmenite and, if they were ever present, other iron oxides and hydroxides. It eliminated magnetite completely, whereas the removal of iron from ilmenite produced rutile-leucoxene pseudomorphs. The dissolution of iron from ilmenite has also been noticed in conglomerates older than the Witwatersrand (Muff & Saager, 1979; Saager *et al.*, (1982) and in the weathering profiles (Section 5.3.2.2) which developed in the upper part of the Archaean floor onto which sediments of the Dominion Group (Grandstaff *et al.*, 1986) and Witwatersrand

Supergroup (Robb & Meyer, 1985) were deposited. For the release of ferrous iron from ilmenite and magnetite (Section 4.1.1), the environment should be neutral to acid, and with an increase in the oxidation potential, has to be more acid (Figs. 19 and 29). In the absence of an oxidant, the dissolved iron and, if present, manganese will also remain mobile and, if not taken up by other minerals, will be carried away.

*5.3.2. Weathering Profiles*

In tectonically active areas, mechanical weathering is intensive whereas, in areas of low topographic relief, chemical weathering predominates, which may lead to the development of palaeosols and palaeoregoliths.

Today subsurface weathering is greatly affected by biota and phytoclasts. Microbial and chemical decay of organic matter in the upper surface accelerates the rate of weathering. The organic matter controls the acidity of the soil water and the intensity of leaching through the release of organic acids and carbon dioxide during metabolism and decay (Blatt, 1982).

5.3.2.1. Palaeosols in the Central Rand Group

Rapid accumulation of the sediments must have prevented the formation of palaeoprofiles within the sedimentary cycles of the CRG. In the absence of vegetation and humus, pedochemical weathering and soil formation were anyhow at a minimum, and when sediments were covered by water, these processes could not take place at all. However, in the waterlogged shallow depressions that developed on the depositional surface, smectite could have precipitated which, with the increase in depth of burial, could have been altered via ML chlorite/smectite to chlorite. The heavy-mineral concentrations that underlie the basal conglomerate are frequently cemented by chlorite.

Conditions for soil formation could have locally been favourable on the major palaeosurfaces during the prolonged breaks in sedimentation. At certain sites, the top 5 to 30 mm of the footwall quartzite is *argillaceous* while, in others, it is enriched in *authigenic titania* (Fig. A.11a). The presence of biotite pseudomorphs (Fig. A.1f) oriented parallel to the plane of deposition in the argillaceous zones, which do not display

particular zonation or other pedogenic structures, indicates that this horizon most likely formed from the fine-grained, suspended mud which settled out at the end of a sedimentary cycle. The local concentration of authigenic rutile in laminae parallel to the unconformity plane (Fig. A.11a) is more convincing evidence for the surficial alteration of the footwall quartzite (Smits, 1984b). The titania enrichment in recent soils is a diagnostic pedological feature during subaerial exposure of the surface in areas of seasonal alternation of wet and dry periods, where capillary activity is periodically enhanced. Modern examples are titania-rich indurated horizons which, in Hawaii, develop on basalt when vegetation is absent (Walker *et al.*, 1969), duricrusts in Western Australia (Hutton *et al.*, 1972), and silcretes in the Cape Province (Frankel, 1952). In duricrusts and silcretes, the titania occurs as anatase. The dissolved titanium, which may stem from the breakdown of unstable silicates, produces orthotitanic acid, $Ti(OH)_4$, which in modern soils occurs at a pH below 5,5 (Fig. 22; Loughnan, 1969; Fitzpatrick *et al.*, 1978; Deelman, 1979). Dehydration after burial through evaporation or ageing leads to its crystallization. On the palaeosurfaces of the CRG, the periodic fluctuation in the water supply could have resulted from a change in the sedimentation pattern or from variations in the water influx in the fluvial system.

5.3.2.2. Palaeosols in the Archaean Granite Basement

Weathering profiles in the upper part of the Archaean granite floor have been studied by Robb and Meyer (1985) and Grandstaff *et al.* (1986). The profiles may attain thicknesses of as much as 30 m and are of regional extent, which suggests that they developed on a surface of negligible relief. In addition to diagenetic and metamorphic processes, the influx of extraneous fluids could have influenced the rock alteration. At renewed tectonic activity in the provenance, the altered profile would be eroded before the actual granite.

The weathering profiles of the granite are characterized by:

(1) a homogeneous and structureless fabric,

(2) the change in composition relative to the parent rock,
(3) the reduction in mineral constituents, and
(4) the vertical redistribution of certain elements.

Sericite, for which illite could be the precursor, is the predominant mineral in the profiles. As in the reefs of the CRG, magnetite and ilmenite are absent, but leucoxene pseudomorphs have been noticed (Robb & Meyer, 1985; Grandstaff *et al.*, 1986). Magnesium, iron, sodium, and calcium were removed from the profile, whereas the top part became enriched in alumina, titania, potassium, gold, and uranium relative to the parent rock. With depth, chlorite increases in importance, and the rock gradually passes into its original fabric (ibid.). The enrichment in gold in these profiles is too insignificant to account for the unusual gold concentration in the reefs of the CRG. Trace amounts of uranium are associated with leucoxene (ibid.), and this type of uranium-bearing leucoxene could be the precursor of the mushy anatase in the reefs of the CRG (Section 3.7.4), but not that of the uranous titanates, which are distinctly of post-depositional origin.

The three cores of the palaeosol in the granite underlying the Dominion Reef, showed respective iron losses of 20, 70, and 80% (Grandstaff *et al.*, 1986). This substantial loss in iron confirms that the dissolution of ferrous iron must have been a common surficial process in the source rocks. The behaviour of iron and manganese in soils is controlled by the availability of an oxidant. In modern soils, these elements are oxidized and retained as oxides or hydroxides.

### 5.3.3. *Geochemical Indicators in the Reefs of the Central Rand Group*

In the modern environment, reactions at the earth's surface take place at pH values between 4 and 9 at oxidation potentials between 0,53 and 0,99 V (Baas Becking *et al.*, 1960). The subsurface activity is considerably accelerated by biota. If sulphides are present, their oxidation strongly increases the acidity of the oxidation zone, the pH of which may drop as low as 2. Carbonates and silicates are destabilized in such an environment and usually replaced by clay minerals and hydrous

iron oxides (Curtis *et al.*, 1985). No microscopic evidence whatsoever has been found for a large-scale oxidation of pyrite in subaerial parts of the palaeosurfaces of the CRG.

In the absence of vegetation and possibly bacteria as well, the chemical activity at the surface and the formation of soil must have been considerably less effective during the Archaean. Although the chemical activity at, and below the depositional palaeosurface differed distinctly from that of today, the attack by saturated solutions has been significant as is evident from the following near-surface processes in the reefs of the CRG.

(1) the formation of cutans, mainly of gersdorffite and uranous titanate composition, which resulted in
(2) the formation of relict uraninite,
(3) the dissolution of titanium and of uranium from uraninite not protected by microbiota, and
(4) the concurrent neoformation of uranous titanates and reprecipitation of excess titania,
(5) the transformation *in situ* of uraninite to coffinite,
(6) the neoformation of gersdorffite in association with the microbiota, and
(7) that of pyrrhotite (which could have formed from hematite) in association with the alteration of uraninite to uranous titanates and coffinite.

The dispersed nature of the geochemical activity indicates that there were no barriers to prevent the flow of solutions close to the surface. The size of the constituents of the matrix and the fabric of the reef controlled the porosity and permeability of the unconsolidated sediment. Both the extensive lateral continuity and the original porosity of the reefs enhanced the circulation of the solutions and hence the distribution of the authigenic minerals.

In the Dominion Reef, much of the uraninite has been replaced *in situ* by coffinite, whereas uranous titanates are virtually absent. It is possible that the debris were deposited in a subaqueous environment, which prevented the dissolution of uranium. However, the apparent increase in the precipitation of uranous titanates and the less common coffinite in an upward stratigraphic direction in the CRG suggests that the geochemical conditions became increasingly more favourable for the redistribution of titanium and uranium close to the palaeo-

surface. For uranium to dissolve, oxygen has to be available because uraninite is the stable mineral under reducing conditions in the 4 to 9 pH range of the present natural environment. A possible gradual increase in free oxygen in the atmosphere in the course of the sedimentation of the CRG could have been responsible for a concurrent increase in the dissolution and loss of uranium.

From the response of the minerals such as, the absence of carbonates, silicates, sulphates, detrital sulphides other than pyrite, and apatite, the removal of ferrous iron from ilmenite and magnetite, and the dissolution of uranium, it is concluded that the geochemical conditions during sedimentation at, or close to the earth's surface must have been neutral to acid.

The detrital constituents that did not react during the exogenic cycle indicate that oxidation only occurred after final deposition and then was restricted to uraninite not mantled by organic matter. The uranium oxide was apparently more susceptible to the access of oxygen than pyrite, biotite, and chlorite, which in the modern environment, like uraninite, are chemically unstable and readily oxidized. In the present-day surface environment, the rate of breakdown of uraninite and pyrite is determined by the duration of the exposure to the atmosphere, and the acidity and composition of the solutions that are present.

The only, but undisputed evidence for the presence of oxygen is provided by the dissolution of uranium from uraninite grains not encapsulated by microorganisms. The oxidation of uraninite with the exclusion of other oxygen-consuming minerals suggests that the amount of oxygen available was limited and that it was consumed by the mineral that reacted most rapidly, which was obviously uraninite. During the exogenic cycle, the dissolution of uranium could have been inhibited because of low surface temperatures or the rapid dumping of the debris. Hence its preservation before deposition is not evidence *per se* for a lack of oxygen before deposition.

The conditions that prevailed close, or at the surface as deduced from the information provided by the geochemical behaviour of certain minerals is summarized in the pH-Eh diagram of Figure 29. The fields that are marked represent the conditions for:

(1) the dissolution of uranium and titanium and the subsequent precipitation of uranous titanates,
(2) the removal of ferrous iron from ilmenite, magnetite, and, if they were present, the dissolution of other iron oxides or hydroxides, and
(3) the formation of coffinite.

The dissolution of the many ealier-mentioned missing minerals falls in the same field as that for the dissolution of ferrous iron from ilmenite and magnetite. Because pyrite remained stable before and after burial, the pH did not fall below 4. Two different sets of alkaline conditions are suggested for the neoformation of coffinite, i.e. weakly reducing if the pyrrhotite laths formed from hematite, and strongly reducing, if pyrrhotite precipitated directly from the iron release from uraninite.

It is concluded that the mechanism behind the acid conditions which existed during the exogenic cycle and the final deposition of the detritus can only be explained in a speculative manner. These acid conditions appear to have occurred in the provenance for the Witwatersrand deposit all along the western and northern edge of the basin and for the pre-Witwatersrand conglomerates (Saager *et al.*, 1982), and in weathering profiles which developed in the granite floor. It means that these conditions were of regional, and could even have been of global extent, as is suggested by the replacement of ilmenite by rutile and brannerite in the quartz-pebble conglomerates in the Elliot Lake District in Canada (Theis, 1979). The generation of acid conditions at the edge of the Witwatersrand Basin by an exhalative source as proposed by Hutchinson and Viljoen (1988) would be of local significance, and then, for example, unaltered ilmenite grains are expected to be present amongst the pseudomorphs.

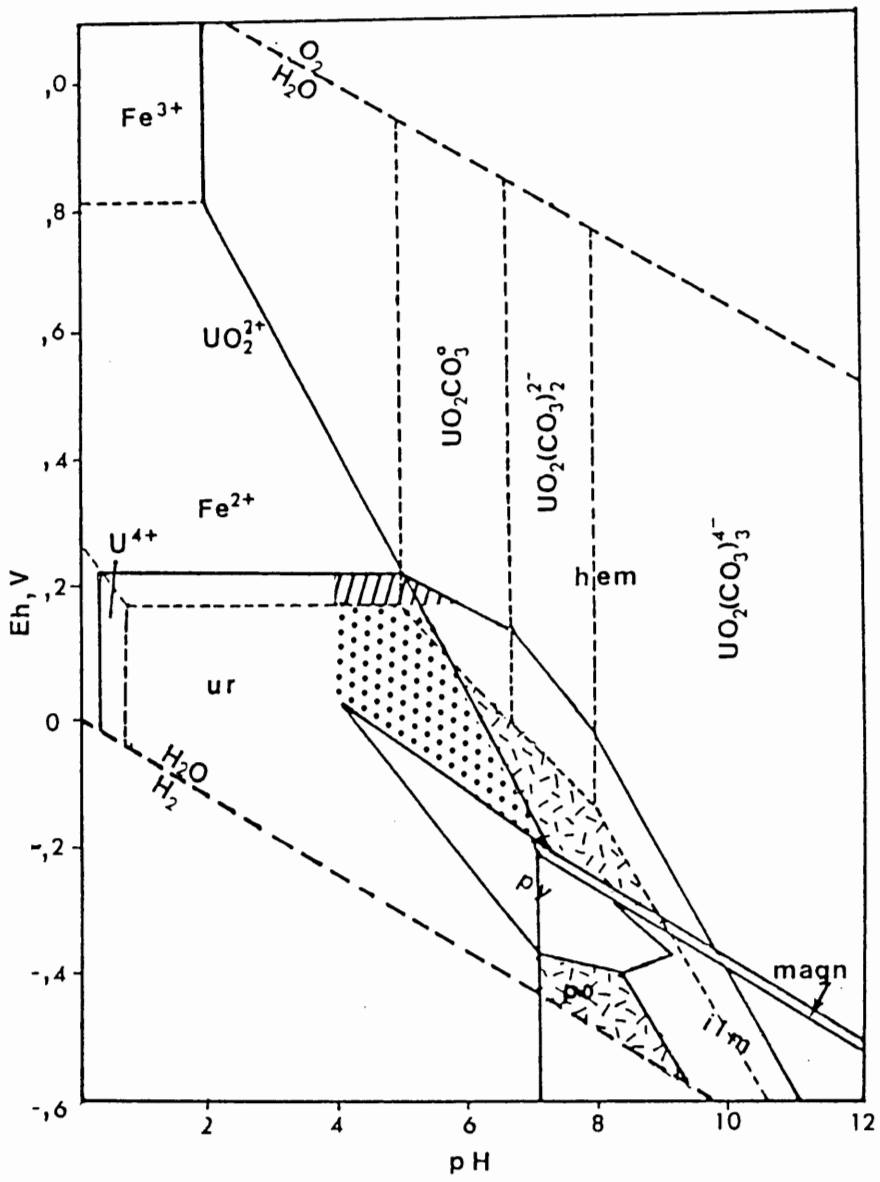



Fig. 29 Eh-pH diagram at 25°C and 1 atm on which the conditions are indicated that prevailed during leaching of uraninite (striped), dissolution of iron (dotted), and in situ transformation of uraninite to coffinite (cross-hatched) with pyrrhotite or hematite. Interrupted lines define stability fields of dissolved uranium and iron species and the solid lines those for uraninite, pyrite, hematite, pyrrhotite, magnetite, and ilmenite. Sulphur, iron, and uranium activities: $10^{-6}$ M, $CO_2$ pressure: $10^{-2}$ atm (after Garrels & Christ, 1965; Langmuir, 1978; Coipel & Dimanche, 1981)

If the acid environment was indeed of global extent, its occurrence was most likely related to the composition of the early atmosphere, a topic which is loaded by uncertain assumptions and speculative, conflicting interpretations, on which as yet no general agreement has been reached.

## 6. CONCLUSIONS

From critical microscopic observations of the heavy-mineral assemblage of the reefs of the Central Rand Group, certain inferences - some of a speculative nature -, can be made about the geochemical conditions which prevailed at the Archaean earth's surface during the Witwatersrand sedimentation. Detailed analysis of the response of the mineral assemblage revealed the following.

The sedimentary rocks attained the lower stage of the low metamorphic grade at a peak temperature of less than $400^0$C and a pressure of 3 kbar, as is indicated by the paragenetic assemblage:

chloritoid-pyrophyllite-chlorite II*b*-muscovite $2M_1$.

Normal progressive burial metamorphism is responsible for the formation of the silicates and no other source of heat is required to explain the acquired metamorphic grade. The metamorphic silicate assemblage does not provide direct information about the silicates originally deposited on the palaeosurfaces.

The well-rounded chlorite and chloritized pyrite, chromite, arsenopyrite, and garnet - all detrital in origin -, which occur amidst and alongside unaltered detrital counterparts, and concretionary pyrite, are considered to have been inherited from rocks that were subjected to hydrothermal activity.

The detrital rutile-leucoxene grains represent pseudomorphs after ilmenite, from which the iron was removed in a remarkably efficient way. Their occurrence explains the absence of magnetite and other iron oxides and hydroxides. This type of pseudomorphs is also found in the altered upper profile of the Archaean granites underlying the Witwatersrand sediments (Robb & Meyer, 1985) and in pre-Witwatersrand conglomerates (Muff & Saager, 1979; Saager *et al.*, 1982). In addition, Grandstaff *et al.* (1986) established that palaeosols in the granite underlying the Dominion Reef are strongly depleted in iron. These features indicate that the dissolution of ferrous iron was a common weathering process during the Archaean. The presence of similar pseudomorphs in the quartz-pebble con-

glomerates of the Elliot Lake District, Canada (Theis, 1979), suggests that the process could even have been of global extent and hence, must be related to the composition of the atmosphere. The dissolution of iron requires neutral to acid conditions, and the required level of acidity increases with an increase in oxidation potential (Fig. 29). Other minerals commonly found in igneous rocks but absent in the reefs such as, carbonates, sulphates, sulphides other than pyrite, gersdorffite, silicates, and apatite, would also have been destroyed in such an acid environment.

In some of the reefs of the Johannesburg Subgroup in the western portion of the basin, a substantial part of the detrital uraninite and gold was captured by algal colonies which grew in stagnant pools on the major unconformities that developed between sedimentation cycles in the Central Rand Group. Low surface temperatures, rapid erosion and accumulation of debris, and a lack of oxygen could have delayed the reaction of uraninite during the exogenic cycle. The unaltered state of the uraninite enclosed by kerogen tells us firstly, that it arrived at the site of final deposition in the unoxidized state and remained so up to this date if protected by organic matter, and secondly, that the microorganisms did not generate metabolic oxygen. On the other hand, the grains that escaped entrapment by microbiota were leached after deposition as is indicated by the common presence of relict uraninite, in which the shape of the original grain was preserved by a cutan of gersdorffite or uranous titanate that precipitated onto their surface during the removal of uranium. The dissolved uranium was recaptured by dissolved titanium, which resulted in the precipitation of uranous titanates, i.e. brannerite and uraniferous leucoxene of variable composition. Textural criteria indicate that cutans and uranous titanates precipitated shortly after burial. Because the synthesis of brannerite has proved to be difficult, the neoformation of uranous titanates at low temperature and pressure, which is unique for the uranium-bearing quartz-pebble deposits of Archaean and Early Proterozoic, is unexpected.

Uranous titanate has not been noticed in the Dominion Reef. Instead, many of the uraninite grains were transformed *in situ* to coffinite through the addition of silica. This process is rare in all other reefs, except for the Elsburg Reefs on the West Rand G.F. where coffinite and uranous titanates occur in about equal amounts. Alkaline conditions are required for the dissolution of adequate amounts of silica and the coffinite formed under alkaline-reducing conditions which must have prevailed in waterlogged depressions on the unconformities.

No tangible indication is found in the reefs of the Central Rand Group for the action of ascending hydrothermal solutions *in situ* as was postulated in the past (Graton, 1930; Davidson & Bowie, 1951), a hypothesis which recently has been revived by Hutchinson and Viljoen (1988) who propose a shallow, exhalative source for the gold at the tectonically active northern and western periphery of the basin. However, there is ample evidence for the detrital origin of the bulk of the constituents, including the ore minerals. Although the gold lost its detrital character and primary compositional properties during metamorphic recrystallization, its distribution pattern in the reefs is decisively sedimentary (Pretorius, 1976). The variation in composition of the gold even in the same handspecimen, also indicates that the gold did not arrive at the final site of deposition in the dissolved state (Nami, 1982; Von Gehlen, 1983).

The response of the minerals after exposure to the atmosphere indicates that surface conditions during the Archaean must have been neutral to acid and reducing to weakly oxidizing (Fig. 29). It is generally assumed that the primitive atmosphere contained carbon dioxide at levels 5 to 30 times higher than that of the present atmosphere, and oxygen between $10^{-2}$ and $10^{-1}$ PAL (Grandstaff, 1980). The high partial pressure of the carbon dioxide could have been responsible for the leaching of iron from ilmenite and iron oxides and the dissolution of the earlier-mentioned range of missing minerals.

The presence of partly or entirely leached relict uraninite provides unquestionable evidence for the presence of oxygen at the palaeosurfaces, since tetravalent uranium is

practically immobile under reducing conditions. The inert behaviour of minerals, which are unstable in an acid-oxidizing environment such as, pyrite, chlorite, and biotite, suggests that the amount of free oxygen was limited.

The apparent increase in the formation of uranous titanates and coffinite at the expense of uraninite in an upward stratigraphic direction could indicate a gradual increase in the oxygen content of the atmosphere in the course of the Witwatersrand sedimentation.

In summary:

(1) Like today, the geochemical response of the minerals at, or close to the Archaean earth's surface depended on the composition of the atmosphere.
(2) Acid conditions prevailed at the surface, for which the high carbon dioxide content of the primitive atmosphere could be responsible.
(3) It is evident from the geochemical response of the mineral constituents that the oxygen level of the early atmosphere was well below that of the present atmosphere.

## ACKNOWLEDGEMENTS

The author wishes to express her sincere thanks and appreciation to the following institutions and persons.

The Council for Mineral Technology (Mintek), Randburg, for its permission to use the information that was obtained during an investigation carried out on the extraction of uranium from the Witwatersrand ores in the period from 1980 to 1985.

The Atomic Energy Corporation of South Africa, Pelindaba, for its permission to publish the information on the uranium mineralogy of the Witwatersrand deposits.

Gencor Ltd, Johannesburg, for its permission to use some of the information obtained in a study on the Kalkoenkrans Reef, Welkom G.F.

Prof. S.A. de Waal and Prof. J. Markgraaff for supervising this study and for their valuable assistance and advice to improve the manuscript, and Prof. N.J. Beukes from the Randse Afrikaanse Universiteit, Johannesburg, for his greatly appreciated comments and suggestions.

Mrs C.W. Stafleu for the translation of the Synopsis in Afrikaans.

Mrs J.A. Russell for her work on the electron microprobe.

Mrs M. Mastanjevic of the Mintek Library for obtaining copies of publications.

Mrs J.D. Pyne-Mercier and Mrs M.C. Furney for their assistance in the typing of the manuscript.

Mr J.P. de Sousa for the photographic printing work.

Mr I.G.E. Cumming for his assistance in the printing of the thesis.

## REFERENCES


ABDEL-GAWAD, A.M. & KERR, P.F., 1961. Urano-organic mineral association. *Amer. Miner.*, 46:402-419.

ADLER, H.H. & PUIG, J.A. 1961. Observations on the thermal behaviour of brannerite. *Amer. Miner.*, 46:1086-1096.

ALDAHAN, A.A. & MORAD, S. 1986. Chemistry of detrital biotites and their phyllosilicate intergrowths in sandstones. *Clays and Clay Miner.*, 34:539-548.

ALLSOPP, H.L. 1964. Rubidium-strontium ages from the western Transvaal. *Nature*, 204:361-363.

ALLSOPP, H.L., EVANS, I.B., GIUSTI, L., HALLBAUER, D.K., JONES, M.Q.W. & WELKE, H.J. 1986. U-Pb dating and isotopic characterization of carbonaceous components of the Witwatersrand reefs. (*In* Extended Abstracts Geocongress '86. Johannesburg: Geol. Soc. S. Afr. p.85-88.)

ARMSTRONG, R.A. 1987. Personal communication to author. Cape Town: University of Cape Town.

---------, COMPSTON, W., RETIEF, E.A. & WELKE, H.J. 1986. Ages and isotopic evolution of the Ventersdorp volcanics. (*In* Extended Abstracts Geocongress '86. Johannesburg: Geol. Soc. S. Afr. p.89-92.)

ARRIBAS, A. 1966. Nuevos datos sobre la coffinita. *Estudios Geologicos*, 22:47-59.

BAAS BECKING, L.G.M., KAPLAN, I.R. & MOORE, D. 1960. Limits of the natural environment in terms of pH and oxidation-reduction potentials. *J. Geol.*, 68:243-284.

BAILEY, A.C., LAW, J.D.M., CADLE, A.B. & PHILLIPS, G.N. 1989. The Zandfontein Quartzite Formation, a marine deposit in the Central Rand Group, Witwatersrand Supergroup. Johannesburg: Univ. Witwatersrand. Econ. Geol. Res. Unit, Inf. Circ. 212:18p.

BAILEY, S.W. 1980. Summary of recommendations of AIPEA nomenclature committee on clay minerls. *Clays and Clay Min.*, 28:73-78.

BALTATZIS, E. 1980. Chloritoid-forming reaction in the eastern Scottish Dalradian: a possibility. *N. Jb. Miner. Mh.*, 7:306-313.

BARRAS, P.F. 1974. Platinoid minerals in the gold reefs of the Witwatersrand Basin. England. (Dissertation (Ph.D.) - Durham Univ.)

BARTON, E.S., BARTON, J.M., CALLOW, M.J., ALLSOPP, H.L., EVANS, I.B. & WELKE H.J. 1986. Emplacement ages and implications for the source region of granitoid rocks associated with the Witwatersrand Basin. (*In* Extended Abstracts Geocongress '86. Johannesburg: Geol. Soc. S. Afr. p.93-97.)

BAYLISS, P. 1969. X-ray data, optical anisotropism, and thermal stability of cobaltite, gersdorffite, and ullmanite. *Miner. Mag.*, 37:26-33.

---------- 1975. Nomenclature of the trioctahedral chlorites. *Can. Miner.*, 13:178-180.

BERMAN, R.M. 1957. The role of lead and excess oxygen in uraninite. *Amer. Miner.*, 42:705-731.

BERNER, R.A. 1984. Sedimentary pyrite formation: an update. *Geochim. Cosmochim. Acta*, 48:605-615.

BEST, J.L. & BRAYSHAW, C. 1985. Flow separation - a physical process for the concentration of heavy minerals within alluvial channels. *J. geol. Soc. London*, 142:747-755.

BLATT, H. 1982. Sedimentary Petrology. San Francisco: Freeman. 564 p.

-------, MIDDLETON, G. & MURRAY, R. 1980. Origin of sedimentary rocks, Englewood Cliffs, N.J.: Prentice Hall. 782 p.

BONATTI, S. & GALLITELLI, P. 1951. Sulla torita di nettuno (Roma). *Alli. Soc. toscani Sci. Nal.*, 57:182-183.

BORCHERS, R. 1964. Exploration of the Witwatersrand System and its extensions. (*In* Haughton, S.H., ed. The geology of some ore deposits in southern Africa. Vol. I. Gold deposits of the Witwatersrand Basin. Johannesburg: Geol. Soc. S. Afr. p. 1-23.)

BORCHERT, H. 1934. Uber Entmischungen im System Cu-Fe-S und ihre Bedeutung als geologische Thermometer. *Chemie der Erde*, 9:145-172.

BOSTICK, N.H. 1979. Microscopic measurement of the level of catagenesis of solid organic matter in sedimentary rocks to aid exploration for petroleum and to determine former burial temperatures - A review. (*In* Scholle, P.A. & Schluger, P.R., eds. Aspects of diagenesis. Tulsa, USA: Soc. Econ. Paleont. Mineral. Spec. Publ. 26:17-43.)

BOWIE, S.H.U. & TAYLOR, K. 1958. A system of ore mineral identification. (*In* Proc. 2nd U.N. Intern. Conf. on Peaceful uses of atomic energy. Geneva: United Nations. Vol. 3:527-540.)

BOYLE, R.W., ALEXANDER, W.M. & ASLIN, G.E.M. 1975. Some observations on the solubility of gold. *Geol. Surv. Can.*, Paper 75-24:6 p.

BRANCHE, G., CHERVET, J. & GUILLEMIN, C. 1951. Nouvelles espèces uranifères françaises. *Bull. Soc. Franc., Min. Crist.*, 74:457-488.

BREGER, I.A. 1974. The role of organic matter in the accumulation of uranium. The organic geochemistry of the coal-uranium association. (*In* Formation of uranium ore deposits. Vienna: Intern. Atomic Energy Agency. 748 p.)

BREWER, R. 1960. Cutans: their definition, recognition, and interpretation. *J. Soil Sc.*, 11:280-292.

--------- 1964. Fabric and mineral analysis of soils. New York, Wiley. 470 p.

BROOKINS, D.G. 1975. Coffinite-uraninite stability relations in Grants Mineral Belt, New Mexico. *Amer. Ass. Petrol. Geol.*, 59:905.

BROWN, B.E. & BAILEY, S.W. 1962. Chlorite polytypism: I. Regular and semi-random one-layer structures. *Amer. Miner.*, 47:819-850.

BURGER, A.J., NICOLAYSEN, L.O. & DE VILLIERS, J.W.L. 1962. Lead isotopic compositions of galenas from the Witwatersrand and Orange Free State, and their relation to the Witwatersrand and Dominion Reef uraninites. *Geochim. Cosmochim. Acta*, 26:25-29.

BURNELL, J.R. & RUTHERFORD, M.J. 1984. An experimental investigation of the chlorite terminal equilibrium in pelitic rocks. *Amer. Miner.*, 69:1015-1024.

CAMDEN-SMITH, P.M. 1980. The sedimentology, geochemistry and diagenesis of West Rand Group sediments in the Heidelberg Area, Transvaal. Cape Town. (Dissertation (M.Sc.) - Univ. of Cape Town.)

CAMERON, E.M. 1982. Sulphate and sulphate reduction in early Precambrian oceans. *Nature*, 296:145-148.

CARROLL, D. 1970. Rock weathering. New York: Plenum Press. 203 p.

CARUBA, R., BAUMER, A., GANTEAUME, M. & IACCONI, P. 1985. An experimental study of hydroxyl groups and water in synthetic and natural zircons: a model of the metamict state. *Amer. Miner.*, 70:1224-1231.

CLARINGBULL, G.F. & HEY, M.H. 1953. A re-examination of churchite. *Miner. Mag.*, 30:211-217.

CLEMMEY, H. 1981. Some aspects of the genesis of heavy mineral assemblages in Lower Proterozoic uranium-gold conglomerates. *Miner. Mag.*, 44:399-408.

CLOUD, P. 1976. Major features of crustal evolution. Alex L. du Toit Memorial Lecture, no. 14. Ann. *Trans. Geol. Soc. S. Afr.*, 79:33 p.

-------- 1988. Oasis in space - Earth's history from the beginning. New York: Norton & Coy. 508 p.

COETZEE, F. 1965. Distribution and grain-size of gold, uraninite, pyrite and certain other heavy minerals in gold-bearing reefs of the Witwatersrand Basin. *Trans. geol. Soc. S. Afr.*, 68:61-88.

COIPEL, J. & DIMANCHE, F. 1981. Evolution diagénétique des oxydes de fer, chrome et titane. *Bull. Mineral.*, 104:64-69.

COOPER, R.A. (1923). Mineral constituents of Rand concentrates. *J. Chem. Metall. Min. Soc. S. Afr.*, 24:90-95.

COUSINS, C.A. 1973. Platinoids in the Witwatersrand System. *J. S. Afr. Inst. Min. Metall.*, 73:184-199.

CURTIS, C.D., HUGHES, C.R., WHITEMAN, J.A. & WHITTLE, C.K. 1985. Compositional variation within some sedimentary chlorites and some comments on their origin. *Miner. Mag.*, 49:375-386.

DAVIDSON, C.F. & BOWIE, S.H.U. 1951. On thucholite and related hydrocarbon-uraninite complexes with a note on the origin of the Witwatersrand gold ores. *Bull. Geol. Surv. Gt. Britain*, 3:1-18.

DAVIES, R.V., KENNEY, J., MELLROY, R.W., SPENCE, R.H. & HILL, K.M. 1964. Extraction of uranium from sea water. *Nature*, 203:1110-1115.

DEELMAN, J.C. Von. 1979. Low-temperature synthesis of anatase ($TiO_2$). *N. Jb. Miner. Mh.*, 6:253-261.

DEER, W.A., HOWIE, R.A. & ZUSSMAN, J. 1962. Rock-forming minerals. Vol. 3. Sheet silicates. London: Longmans and Green. 270 p.)

DE KOCK, W.P. 1964. The geology and economic significance of the West Wits Line. (*In* Haughton, S.H., ed. The geology of some ore deposits in southern AFrica. Vol. I. Gold deposits of the Witwatersrand Basin. Johannesburg: Geol. Soc. S. Afr. p. 323-386.)

DEXTER-DYER-GROSOVSKY, B. 1983. Microbial role in Witwatersrand gold deposition. (*In* Westbroek, P. & De Jong, E.W., eds. Biomineralization and biological metal accumulation. Dordrecht: Reidel. p. 495-498.)

DILL, H. 1980. Neue Ergebnisse zur Mineralogie der primären Uranträger auf den Gruben Hohenstein/Poppenreith und Waldel/Mahring in Nordostbayern mit besonderer Berücksichtigung der Uran-Titan- und Phosphor-Kohlenstoff-Verbindungen. *Geol. Jb. D.*, 42:3-39.

DILL, H. 1985. The polymetallic and monotonous uranium parageneses - A contribution to the position of endogenous uranium mineralization at the western edge of the Bohemian Massif. *N. Jb. Miner. Mh*, 4:184-192.

DIMANCHE, F. & BARTHOLOME, P. 1976. The alteration of ilmenite in sediments. *Miner. Sci. Eng.*, 8:187-201.

DIMROTH, E. 1979. Significance of diagenesis for the origin of Witwatersrand-type uraniferous conglomerates. *Phil. Trans. R. Soc. London*, A291:277-287.

DISSANAYAKE, C.B. & KRITSOTAKIS, K. 1984. The geochemistry of Au and Pt in peat and algal mats - A case study from Sri Lanka. *Chem. Geol.*, 42:61-76.

DUNOYER DE SEGONZAC, G.D. 1970. The transformation of clay minerals during diagenesis and low-grade metamorphism: A review. *Sedimentology*, 15:281-346.

DURAND, B. 1985. Diagenetic modification of kerogens. *Phil. Trans. R. Soc. London*, A315:77-90.

EALES, H.V. & REYNOLDS, I.M. 1983. Factors influencing the composition of chromite and magnetite in some southern african rocks. (*In* De Villiers, J.P.R. & Cawsthorn, P.A., eds. ICAM 81. Johannesburg: Geol. Soc. S. Afr. Spec. Publ. 7:5-22.)

EICHMANN, R. & SCHIDLOWSKI, M. 1974. Isotopic composition of carbonaceous matter from the Precambrian uranium deposits of the Blind River District, Canada. *Naturwiss.*, 61:449-451.

ELLSWORTH, H.V. 1928. Thucholite, a remarkable primary carbon mineral from the vicinity of Parry Sound, Ontario. *Amer. Miner.*, 13:419-448.

ERASMUS, C.S., SELLSCHOP, J.P.R & HALLBAUER, D.K. 1982. Major amounts of mercury in native gold from upper Witwatersrand sediments. Johannesburg: Council for Mineral Technology. Rep. M54:16 p.

EVARTS, R.C. & SCHIFFMAN, P. 1983. Submarine hydrothermal metamorphism of the Del Puerto ophiolite, California. *Amer. J. Sc.*, 283:289-340.

FAWCETT, J.J. & YODER, H.S. 1966. Phase relationships of chlorites in the system $MgO-Al_2O_3-SiO_2-H_2O$. *Amer. Miner.*, 51:353-380.

FEATHER, C.E. 1976. Studies on the mineralogy and geochemistry of the Witwatersrand Supergroup. Johannesburg. (Dissertation (Ph.D.) - Univ. Witwatersrand)

-------- & DUGGAN, L.W. 1974. Investigation of arsenosulphides in the Witwatersrand reefs. *Proc. Electron Microscopy Soc. Southern Afr.*, 4:73-74.

FEATHER, C.E. & KOEN, G.M. 1875. The mineralogy of the Witwatersrand reefs. *Miner. Sc. Eng.*, 7:189-224.

FERRIS, C.S. & RUUD, C.O. 1971. Brannerite: Its occurrences and recognition by microprobe. *Quarterly Colorado School of Mines*, 66:1-35.

FILIPENKO, Y.S. 1958. Coffinite. (*In* Int. A.E.A. Proc. 2nd Conf. on Peaceful uses of atomic energy. Vol. 2:302-304.)

FINKELMAN, R.B. & KLEMIC, H. 1976. Brannerite from the Penn Haven Junction uranium occurrence, Carbon County, Pennsylvania. *J. Res. U.S. Geol. Surv.*, 4:715-716.

FINKELSTEIN, N.P. 1972. The chemistry of the extraction of gold from its ores. (*In* Adamson, R.J., ed., Gold metallurgy in South Africa. Cape Town: Cape and Transvaal Printers Ltd. 452 p.)

FITZPATRICK, R.W., LE ROUX, J. & SCHWERTMANN, U. 1978. Amorphous and crystalline titanium and iron-titanium oxides in synthetic preparations, at near ambient conditions, and in soil clays. *Clays and Clay Miner.*, 26:189-201.

FLEISCHER, N. (1983). Glossary of mineral species. Tucson: The Mineralogical Record Inc. 202 p.

FOORD, E.E., COBRAN, R.R. & BROWNFIELD, I.K. 1985. Uranoan thorite in lithophysal rhyolite - Topaz Mountain, Utah, U.S.A. *Miner. Mag.*, 49:729-731.

FOSTER, M.D. 1962. Interpretation of the composition and a classification of the chlorites. *Prof. Paper U.S. Geol. Surv.*, 414A:A1-A33.

FRANKEL, J.J. 1952. Silcrete near Albertina, Cape Province. *S. Afr. J. Sci.*, 48:173-182.

FREY, M. 1972. Geol. Soc. Amer. Ann. Meeting (abs). (*In* Winkler, H.G.F. 1979. Petrogenesis of metamorphic rocks. New York: Springer Verlag. 348 p.)

------ 1987. Very low-grade metamorphism of clastic sedimentary rocks. (*In* Frey, M. Low temperature metamorphism. Glasgow: Blacke & Son. p. 9-58.)

FRONDEL, C. 1953. Hydroxyl substitution in thorite and zircon. *Amer. Miner.*, 38:1007-1018.

------ 1958. Systematic mineralogy of uranium and thorium. Bull. Geol. Surv. 1064, U.S. Washington: Gov. Print. Off. 400 p.

------ & COLETTE, R.L. 1957. Hydrothermal synthesis of zircon, thorite, and huttonite. *Amer. Miner.*, 42:759-765.

FUCHS, L.H. & GEBERT, E. 1958. X-ray studies of synthetic coffinite, thorite and uranothorites. *Amer. Miner.*, 43:243-248.

FUCHS, L.H. & HOEKSTRA, H.R. 1959. The preparation and properties of uranium (IV) silicate. *Amer. Miner.*, 44:1057-1063.

FULLER, A.O. 1958. A contribution to the petrology of the Witwatersrand System. *Trans. geol. Soc. S. Afr.*, 61:19-50.

GARRELS, R.M. & CHRIST, C.L. 1965. Solutions, minerals and equilibria. New York, Harper and Row. 450 p.

GAY, N.C. 1968. The composition of gold from the Barberton Mountain Land. *Trans. geol. Soc. S. Afr.*, 71:274-289.

GEORGE, d'A. 1949. Mineralogy of uranium and thorium bearing minerals. RMO-563, USAEC. 198 p.

GIUSTI, L., HALLBAUER, D.K., ALLSOPP, H.L., EVANS, I.B. & WELKE, J.H. 1986. Dating and isotopic characterization of components of Witwatersrand conglomerates and possible source rocks. (*In* Extended abstracts Geocongress '86. Johannesburg, Geol. Soc. S. Afr. 123-127.)

GLATTHAAR, C.W. & FEATHER, C.E. 1985. Predicting the hydrometallurgical recovery of uranium by mineralogical mass-balance study of the uranium-bearing minerals in Dominion Reef, South Africa. (*In* Park, W.C., Hausen, D.M. & Hagni, R.D., eds. Applied mineralogy. Metal. Soc. AIME. p. 617-628.)

GOLEVA, G.A., KRIVENKOV, V.A. & GUTZ', Z.G. 1970. Geochemical trends in the occurrence and migration forms of gold in natural water. *Geochem. Int.*, 7:518-529.

GOTMAN, Y.D., POLYAKOVA, V.M. & MIGUTA, A.K. 1968. Another variety of brannerite. *Doklady Akad. Nauk, SSSR*, 179:429-430.

GRANDSTAFF, D.E. 1974. Microprobe analyses of uranium and thorium in uraninite from Witwatersrand, South Africa, and Blind River, Ontario, Canada. *Trans. geol. Soc. S. Afr.*, 77:291-294.

---------- 1976. A kinetic study of the dissolution of uraninite. *Econ. Geol.*, 71:1493-1506.

---------- 1980. Origin of uraniferous conglomerates at Elliot Lake, Canada and Witwatersrand, South Africa; Implications for oxygen in the Precambrian atmosphere. *Precambrian Res.*, 18:1-26.

--------, EDELMAN, M.J., FOSTER, R.W., ZBINDEN, E. & KIMBERLEY, M.M. 1986. Chemistry and mineralogy of Precambrian paleosols at the base of the Dominion and Pongola Groups (Transvaal, South Africa). *Precambrian Res.*, 32:97-131.

GRATON, L.C. 1930. Hydrothermal origin of the Rand gold deposits. *Econ. Geol.*, 25:1-185.

GROVES, D.I., BARRETT, F.M., BINNS, R.A. & McQUEEN, K.G. 1977. Spinel phases associated with metamorphosed volcanic-type iron-nickel sulfide ores from Western Australia. *Econ. Geol.*, 72:1224-1244.

GRUNER, J.W. & SMITH, D.K. 1954. The problem of coffinite. *Ann. rep. April 1954 to March 1955*. Oak Ridge, Tennessee: U.S. At. En. Commission, Techn. Inf. Service. p. 16-24.

GYBBON SPILSBURY, E. 1908. Contributed remarks. (*In* The origin of the gold in the Rand Banket. *Trans. Inst. Min. Metall.* 17:66-69.)

HAAS, H. & HOLDAWAY, M.J. 1973. Equilibria in the system $Al_2O_3$-$SiO_2$-$H_2O$ involving the stability limits of pyrophyllite, and thermodynamic data of pyrophyllite. *Amer. J. Sci.*, 273:449-464.

HALFERDAHL, L.B. 1961. Chloritoid; its composition, X-ray and optical properties, stability, and occurrence. *J. Petrol.*, 2:49-135.

HALLBAUER, D.K. 1975. The plant origin of the Witwatersrand 'carbon'. *Miner. Sc. Eng*, 7:111-131.

---------- 1981. Geochemistry and morphology of mineral components from the fossil gold and uranium placers of the Witwatersrand. (*In* Genesis of the uranium- and gold-bearing quartz-pebble conglomerates in the Witwatersrand and the Blind River. Prof. Paper U.S. Geol. Surv. 1161-A-BB: p.M1-M22.)

---------- 1983. Geochemistry and fluid inclusions in detrital minerals as guides to their provenance and distribution. (*In* De Villiers, J.P.R. & Cawthorn, P.A., eds., ICAM 81. Johannesburg: Geol. Soc. S. Afr. Spec. Publ. 7:39-57.)

-------- & JOUGHIN, N.C. 1973. The size distribution and morphology of gold particles in Witwatersrand reefs and their crushed products. *J. S. Afr. Inst. Min. Metall.*, 73: p.395-405.

------- & UTTER, T. 1977. Geochemical and morphological characteristics of gold particles from recent river deposits and the fossil placers of the Witwatersrand. *Mineral. Deposita*, 11:293-306.

------- & VAN WARMELO, K.T. 1974. Fossilized plants in thucholite from Precambrian rocks of the Witwatersrand, South Africa. *Precambrian Res.*, 1:199-212.

------- & VON GEHLEN, K. 1983. The Witwatersrand pyrites and metamorphism. *Miner. Mag.*, 47:473-479.

-------, UTTER, T. & HIRDES, W. 1978. Size and composition of gold, pyrite and other sulphides in some Wits conglomerates. *Coal, gold and base minerals of S. Afr.*, 65-79.

HARRISON, W.E. 1979. Levels of graphitization of kerogen as a potentially useful method of assessing palaeotemperatures. (*In* Scholle, P.A. & Schluger, P.R., eds. Aspects of diagenesis. Tulsa, USA: Soc. Econ. Paleont. Miner. Spec. Publ. 26:45-53.)

HATTORI, K., KROUSE, H.R. & CAMPBELL, F.A. 1983. The start of sulfur oxidation in continental environments about 2,2 x $10^9$ years ago. *Science*, 121:549-551.

HAYES, J.B. 1970. Polytypism of chlorite in sedimentary rocks. *Clays and Clay Miner.*, 18:285-306.

HEGNER, E., KRONER, A. & HOFMANN, A.W. 1984. Age and isotope geochemistry of the Archaean Pongola and Usushwana suites in Swaziland, southern Africa: A case for crustal contamination of mantle-derived magma. *Earth and Planet. Sc. Letters*, 70:267-279.

HEMINGWAY, B.S. 1982. Thermodynamic properties of selected uranium compounds and aqueous species at 298,15 K and 1 bar and at higher temperatures - Preliminary models for the origin of coffinite deposits. U.S. Geol. Surv. Open file Rep. 82-619: 74 p.

HEMLEY, J.J. & JONES, W.R. 1964. Chemical aspects of hydrothermal alteration with emphasis on hydrogen metasomatism. *Econ. Geol.*, 59:538-569.

HEROUX, Y. CHAGNON, A. & BERTRAND, R. 1979. Compilation and correlation of major thermal maturation indicators. *Amer. Ass. Petrol. Geol. Bull.*, 12:2128-2144.

HESS, F.L., WELLS, A.B. & WELLS, R.C. 1920. Brannerite, a new uranium mineral. *J. Franklin Inst.* 189:225-237.

HEWETT, D.F., STONE, J. & LEVINE, H. 1954. Brannerite from San Bernadino County, California. *Amer. Miner.*, 39: 30-38.

HIEMSTRA, S.A. 1968. The mineralogy and petrology of the uraniferous conglomerate of the Dominion Reefs Mine, Klerksdorp Area. *Trans. geol. Soc. S. Afr.*, 71:1-66.

HIRDES, W. 1984. Different populations of gold particles as outlined by their silver content. A regional investigation in the Precambrian Kimberley Reef placer of the East Rand Goldfield/Witwatersrand/South Africa. (*In* Wauschkun, A., Kluth, C. & Zimmermann, R.A., eds. Syngenesis and epigenesis in the formation of mineral deposits. Berlin: Springer Verlag. p.247-259.)

HIRSCHBERG, A. & WINKLER, H.G.F. 1968. Stabilitätsbeziehungen zwischen Chlorit, Cordierit und Almandin bei der Metamorphose. *Contr. Mineral. Petrol.*, 18:17-42.

HOEFS, J., NIELSEN, H. & SCHIDLOWSKI, M. 1968. Sulfur isotope abundances in pyrite from the Witwatersrand conglomerates. *Econ. Geol.*, 63:975-977.

HOEFS, J. & SCHIDLOWSKI, M. 1967. Carbon isotope composition of carbonaceous matter from the Precambrian of the Witwatersrand System. *Science*, 155:1096-1070.

HOEKSTRA,H.R. & FUCHS, L.H. 1956. Synthesis of coffinite - $USiO_4$. *Science*, 123:105.

HOERING, T.C. 1967. The organic geochemistry of Precambrian rocks. (*In* Abelson, P.H. ed. Researches in geochemistry. New York: Wiley. p.87-111.)

HOLDAWAY, M.J. 1971. Stability of andalusite and the aluminium silicate phase diagram. *Amer. J. Sci.*, 271:97-131.

HOLLAND, H.D. 1978. The chemistry of the atmosphere and oceans. New York: Wiley. 351 p.

HOSCHECK, G. 1969. The stability of staurolite and chloritoid and their significance in metamorphism of pelitic rocks. *Contr. Mineral. Petrol.*, 22:208-232. (German version 1967, 14:123-162).

HOSTETLER, P.B. & GARRELS, R.M. 1962. Transportation and precipitation of uranium and vanadium at low temperatures, with special reference to sandstone-type uranium deposits. *Econ. Geol.*, 57:137-166.

HOWER, J., ESLINGER, E.V., HOWER, M.E. & PERRY, E.A. 1976. Mechanism of burial metamorphism of argillaceous sediment: 1. Mineralogical and chemical evidence. *Geol. Soc. Amer. Bull.*, 87:725-737.

HUTCHINSON, R.W. & VILJOEN, R.P. 1988. Reevaluation of gold source in Witwatersrand ores. *S. Afr. J. Geol.*, 91:157-173.

HUTTON, C.O. 1950. Studies of heavy detrital minerals. *Bull. Geol. Soc. Amer.*, 61:635-716.

HUTTON, J.T., TWIDALE, C.R., MILNES, A.R. & ROSSER, H. 1972. Composition and genesis of silcretes and silcrete skins from the Beda Valley, southern Arcoona Plateau, South Australia. *J. geol. Soc. Austr.*, 19:31-39.

IANOVICI, V., NEACSU, G. & NEACSU, V. 1981. Pyrophyllite occurrences and their genetic relations with the kaolin minerals in Romania. *Bull. Mineral.*, 104:768-775.

IRVINE, T.N. 1965. Chromian spinel as a petrogenetic indicator. Part 1. Theory. *Can. J. Earth Sci.*, 2:648-673.

JAMES, H.L. 1978. Subdivision of the Precambrian - A brief review and a report on recent decisions by the subcommission on Precambrian stratigraphy. *Precambrian Res.*, 7:193-204.

JENSEN, M.L. & DECHOW, E. 1964. Bearing of sulfur isotopes on the origin of southern African ore deposits (Abstr.). Program 1964 Ann. meeting Geol. Soc. Amer.

KAIMAN, S. 1959. Synthesis of brannerite. *Can. Miner.*, 6:380-381

KAJITANI, K. 1970. A geochemical study on the genesis of ningyoite the special calcium uranous phosphate mineral. *Econ. Geol.*, 65:470-480.

KARKHANAVALA, M.D. 1959. X-ray and electron diffraction study of brannerite from Rajasthan. *J. Scient. and Ind. Research, Section B, Physical Sc.*, 18B:7-10.

KASTING, J.F., HOLLAND, H.D. & PINTO, J.P. 1985. Oxidant abundances in rainwater and the evolution of the atmospheric oxygen. *J. geophys. Res.*, 90:10497-10510.

KELLER, C. 1963. Untersuchungen uber die Germanate and Silikate des Typs $ABO_4$ der vierwertigen Elemente Thorium bis Americum. *Nukleonik*, 5:41-48.

KERRICK, D.M. 1968. Experiments on the upper stability limit of pyrophyllite at 1,8 kilobars and 3,9 kilobars water pressure. *Amer. J. Sci.*, 266:204-214.

KIM, S.J. 1978. Chemical composition of the coffinite from the Woodrow Mine, New Mexico, U.S.A. *J. Korea Inst. Mining Geol.*, 11:183-186.

KIMBERLEY, M.M., DIMROTH, E. 1976. Basic similarity of Archaean to subsequent atmospheric and hydrospheric compositions as evidenced in the distributions of sedimentary carbon, sulphur, uranium, and iron. (*In* Windley, B.F., ed. The early history of the Earth. London: Wiley. p.579-585.)

KISCH, H.J. 1983. Mineralogy and petrology of burial diagenesis and incipient metamorphism in clastic rocks - Literature published since 1976. (*In* Larsen, G. & Chilingar, G.V., eds. Diagenesis in sediments and sedimentary rocks. Devel. in Sedimentology 25b. p.289-493.)

KLEMM, D.D. 1965. Syntesen and Analysen in den Dreiecksdiagrammen FeAsS-CoAsS-NiAsS und $FeS_2$-$CoS_2$-$NiS_2$. *N. Jb. Miner. Abh.*, 103:205-255.

KOEN, G.M. 1961. The genetic significance of the size distribution of uraninite in Witwatersrand Bankets. *Trans. geol. Soc. S. Afr.*, 64:23-47.

--------- 1964. Rounded platinoid grains in the Witwatersrand Banket. *Trans. geol. Soc. S. Afr.*, 67:139-146.

KOPPEL, V.H. & SAAGER, R. 1974. Lead isotope evidence on the detrital origin of Witwatersrand pyrites and its bearing on the provenance of the Witwatersrand gold. *Econ. Geol.*, 69:318-331.

KOROBUSHKINA, E.D., MINEEV, G.G. & PRADED, G.P. 1976. Mechanism of the microbiological process of dissolution of gold. *Microbiology*, 45:463-465.

KRAPEZ, B. 1979. A sedimentological study of the Ventersdorp Contact Reef at East Driefontein Gold Mine, Carletonville, South Africa. Johannesburg (Dissertation (M.Sc.) - Univ. Witwatersrand.)

KRENDELEV, F.P., ZOZULENKO, L.B. & ORLOVA, L.M. 1973. Properties of solutions that have metamorphosed metalliferous conglomerate as shown by the study of gas-liquid inclusions in quartz pebbles and regenerated minerals. *Doklady Akad. NAUK SSSR*, 212:160-163.

KURAT, G., SIMOVA, F. & KRACHER, A. 1977. Contribution to the uranium mineralogy of some sandstone-type deposits of central Europe. Lusaka, Zambia: Adv. Group meeting on uranium deposits in Africa. 11 p.

LAKIN, H.W., CURTIN, G.C. & HUBERT, A.E. 1974. Geochemistry of gold in the weathering cycle. Washington: U.S. Geol. Surv. Gov. Print. Off. Bull. 1330:80 p.

LANDIS, C.A. 1971. Graphitization of dispersed carbonaceous material in metamorphic rocks. *Contr. Mineral. and Petrol.*, 30:34-45.

LANGMUIR, D. 1978. Uranium solution-mineral equilibria at low temperatures with applications to sedimentary ore deposits. *Geochim. Cosmochim. Acta*, 42:547-569.

LASKORIN, B.N., METALNIKOV, S.S. & TERENTIEV, A.S. 1956. Extraction of uranium from natural water. (*In* Proc. 2nd United National Int. Conf. on the peaceful uses of atomic energy. Geneva: United Nations. 211-215.)

LAXEN, P.A. 1972. A fundamental study of the dissolution in acid solutions of uranium minerals from South Africa ores. Johannesburg. p. 143. (Dissertation (Ph.D.) - Univ. Witwatersrand.)

LIEBENBERG, W.R. 1955. The occurrence and origin of gold and radioactive minerals in the Witwatersrand System, the Dominion Reef, the Ventersdorp Contact Reef and the Black Reef. *Trans. geol. Soc. S. Afr.*, 58:101-228.

---------- 1972. Mineralogical features of gold ores in South Africa. (*In* Adamson, R.J., ed. Gold metallurgy in South Africa, Johannesburg: Cham. of Min. S. Afr. p. 352-446.)

LING ONG, H. & SWANSON, V.E. 1974. Natural organic acids in the transportation, deposition, and concentration of gold. *Quarterly J. Colorado School of Mines*, 64:395-425.

LOUGHNAN, F.C. 1969. Chemical weathering of the silicate minerals. New York: Elsevier. 154 p.

LOUW, J.D. 1954. Geological age determinations on Witwatersrand uraninite using the lead isotope method. *Trans. geol. Soc. S. Afr.*, 57:209-227.

LOWE, D.R. & KNAUTH, L.P. 1978. The oldest marine carbonate ooids reinterpreted as volcanic accretionary lapilli, Onverwacht Group, South Africa. *J. Sed. Petr.*, 48:709-722.

LUDWIG, K.R. & GRAUCH, R.I. 1980. Coexisting coffinite and uraninite in some sandstone-host uraninite ores of Wyoming. *Econ. Geol.*, 75:296-302.

MAIR, J.A., MAYNES, A.D., PATCHETT, J.E. & RUSSELL, R.D. 1960. Isotopic evidence on the origin and age of the Blind River uranium deposits. *J. Geophys. Res.*, 65:341-348.

MANN, A.W. 1984. Mobility of gold and silver in lateritic weathering profiles: some observations from Western Australia. *Econ. Geol.*, 79: 38-49.

MARTINI, J.E.J. 1986. Stratiform gold mineralization in palaeosol and ironstone of Early Proterozoic age, Transvaal Sequence, South AFrica. *Miner. Deposita*, 21:306-312.

McCARTHY, T.S., CADLE, A.B. & HORROCKS, P. 1982. Thrust faulting in Witwatersrand rocks at Langerman's Kop, Johannesburg. *Trans. geol. Soc. S. Afr.*, 85:189-201.

McKINNEY, J.S. *et al*. 1964. Geology of the Anglo American Group Mines in the Welkom Area, Orange Free State Goldfield. (*In* Haughton, S.H., ed. The geology of some ore deposits in southern Africa. Vol. I. Johannesburg: Geol. Soc. S. Afr. p.451-506.)

MEADE, R.H. 1982. Sources, sinks, and storage of river sediment in the Atlantic drainage of the United States. *J. Geol.*, 90:235-252.

MELLOR, E.T. 1916. The conglomerates of the Witwatersrand. *Trans. Inst. Min. Met.*, 23:226-348.

MEYER, M., & TAINTON, S. 1986. Characteristics of small-pebble conglomerates in the Promise Formation of the West Rand Group. (*In* Extended Abstracts Geocongress '86. Johannesburg: Geol. Soc. S. Afr. p.155-160.)

MIHALIK, P. 1968. The geochemistry of some uranium minerals of the Dominion Reef and Witwatersrand System. Johannesburg: Nat. Inst. for Met. Rep. 414:20p.

--------- & SAAGER, R. 1968. Chromite grains showing altered borders from the Basal Reef, Witwatersrand System. *Amer. Miner.*, 53:1543-1550.

MILNES, A.R. & HUTTON, T.J. 1974. The nature of microcrypto-crystalline titania in 'silcrete' skins from the Beda Hill Area of South Asutralia. *Search*, 5:153-154.

MILTON, Ch., MURATA, K.J. & KNECHTEL, M.M. 1944. Weinschenkite, yttrium phosphate dihydrate from Virginia. *Amer. Miner.*, 29:92-107.

MINTER, W.E.L. 1972. Sedimentology of the Vaal Reef in the Klerksdorp Area. Johannesburg. p.170. (Dissertation (Ph.D.) - Univ. Witwatersrand.)

MIYASHIRO, A. 1973. Metamorphism and metamorphic belts. London: Allen and Unwin. 492 p.

MODDLE, D.A. 1957. Brannerite from eastern Ontario. *Can. Miner.*, 6:155-157.

MOENCH, R.H. 1962. Properties and paragenesis of coffinite from Woodrow Mine, New Mexico. *Amer. Miner.*, 47:26-33.

MOSSMAN, D.J. & DEXTER-DYER, B. 1985. The geochemistry of Witwatersrand-type gold deposits and the possible influence of ancient prokaryotic communities on gold dissolution and precipitation. *Precambrian Res.*, 30:303-319.

MOSSMAN, D.J. & HARRON, G.A. 1983. Origin and distribution of gold in the Huronian Supergroup, Canada - The case for Witwatersrand-type paleoplacers. *Precambrian Res.*, 20:543-583.

MUFF, R. & SAAGER, R. 1979. Petrographic and mineragraphic investigation of the Archaean gold placer at Mt. Robert in the Pietersburg Greenstone Belts, N. Transvaal. Geokongress 77. *Geol. Soc. S. Afr.*, Spec. Publ. 6:23-32.

MURCHISON, D.G., COOK, A.C. & RAYMOND, A.C. 1985. Optical properties of organic matter in relation to thermal gradients and structural deformation. Lonfon: Phil. Trans. R. Soc., A315:157-186.

NAMI, M. 1982. Small-scale gold distribution pattern on Carbon Leader Placer at Blyvooruitzicht Gold Mine. Part 1: Sedimentological investigation. Johannesburg: Cham. of Mines. Res. Rep. 39/82:37 p.

NICCOLI, H.B. 1980. Geochemical characteristics and genesis of sandstone type uranium deposits, Sierra Pintada District, San Rafael, Mendoza, Argentina. Paris: 26th Intern. Geol. Congress.

NICKEL, E.H. & MANDARINO, J.A. 1987. Procedures involving the IMA Commission on new minerals and mineral names, and guidelines on mineral nomenclature. *Can. Miner.*, 25:353-377.

NICOLAYSEN, L.O., BURGER, A.J. & LIEBENBERG, W.R. 1962. Evidence for the extreme age of certain minerals from the Dominion Reef conglomerates and the underlying granite in the Western Transvaal. *Geochim. Cosmochim. Acta*, 26:15-23.

NISBET, E.G. 1987. The young earth. An introduction to Archaean geology. London: Allen & Unwin. 402 p.

NORD, G.L. 1977. Characterization of fine-grained black uranium ores by transmission electron microscopy. Short paper U.S. Geol. Surv. Uranium-thorium symposium 1977. Circ. 753:29-31.

OBERTHUR, Th. 1983. Metallogenetische Uberlegungen zur Bildung des Carbon Leader Reef, Carletonville Goldfield, Witwatersrand, Süd Afrika. Köln. 214 p. (Dissertation (Ph.D.) - Univ. Köln.)

-------- & SAAGER, R. 1986. Silver and mercury in gold particles from the Proterozoic Witwatersrand placer deposits of South Africa; metallogenic and geochemical implications. *Econ. Geol.* 81:20-31.

OEHLER, D.Z., SCHOPF, J.W. & KVENVOLDEN, K.A. 1972. Carbon isotopic studies of organic matter in Precambrian rocks. *Sciencce*, 175:1246-1248.

ORTLEPP , R.J. 1962. On the occurrence of uranothorite in the Dominion Reef. *Trans. geol. Soc. S.A.*, 65:197-201.

OZTUNALI, O. 1959. Uber die Struktur von Brannerit. *N. Jb. Miner. Mh.*, 187-188.

PABST, A. 1952. The metamict state. *Amer. Miner.*, 37:137-157.

-------- 1954. Brannerite from California. *Amer. Miner.*, 39:109-117.

PALACHE, Ch., BERMAN, H. & FRONDEL, C. 1944. The system of mineralogy of James Dwight Dana and Edward Salisbury Dana, Yale Univ. Vol. I. Elements, sulphides, sulphosalts, oxides. 7th ed., New York: Wiley. 834 p.

PARES, Y., MARTINET, R., CUPER, J., GIRAUD, J., LOKO, H., GAGNAIRE, L., MAUVIEUX, L. & PREIRA, M. 1965. Utilisation de milieux de culture de faible prix de revient pour la mise en solution de l'or par voie bactérienne. *Ann. Inst. Pasteur, Paris*, 108:674-681.

PARIS, I.A. 1984. The geology of the farms Josefsdal, Dunbar and part of the Diepgezet in the Barberton Greenstone Belt. Johannesburg. p.258. (Dissertation (D.Sc.) - Univ. Witwatersrand.)

PATCHETT, J.E. & NUFFIELD, E.W. 1960. Studies of radioactive compounds. X. - The synthesis and crystallography of brannerite. *Can. Miner.*, 6:483-490.

PEKING INSTITUTE OF URANIUM GEOLOGY, X-ray Laboratory, Wuhan Geological College. 1978. Orthobrannerite, a new mineral of the brannerite group. *Acta. Geol. Sinica*, 52:241-251.

PERRY, E.C., MONSTER, K., & REIMER, Th. 1971. Sulfur isotopes in Swaziland System barites and the evolution of the earth's atmosphere. *Science*, 171:1015-1016.

PETTIJOHN, F.D. 1957. Sedimentary rocks. New York: Harper and Row. 718 p.

PHILLIPS, G.N. 1987. Metamorphism of the Witwatersrand goldfields: conditions during peak metamorphism. *J. metam. Geol.*:307-322.

PIROW, H. 1920. The distribution of the pebbles in the Rand Banket and other features of the rock. *Trans. geol. Soc. S. Afr.*, 23:64-97.

PODPORINA, Y.K., BURKOV, V.V. & DANILOVA, K.N. 1983. Neodymium churchite from weathered mantle of metamorphic rocks in Kazakhstan. *Doklady Akad. NAUK SSSR*, 268:195-198.

POURBAIX, M. 1963. Atlas d'équilibres électrochimiques à 25°C. Parks: Gauthier-Villars. 644 p.

PRETORIUS, D.A. 1976. The nature of the Witwatersrand gold-uranium deposits. (*In* Wolf, K.H., ed. Handbook of strata-bound and stratiform ore deposits. II. Regional studies and specific deposits. Amsterdam: Elsevier. p.29-88.)

---------- 1981. Gold and uranium in quartz-pebble conglomerates. *75th Ann. vol. Econ. Geol.*, 117-138.

---------- 1986. Witwatersrand gold: The men, the money, the mineralization (*In* Extended Abstracts Geocongress '86. Johannesburg: Geol. Soc. S. Afr. p. 1-4.)

RAMDOHR, P. 1955. Neue Beobachtungen an Erzen des Witwatersrandes in Südafrika und ihre genetische Bedeutung. *Abh. Dt. Akad. Wissensch, Berlin, Kl. Chem, Geol., Biol.*, 5:43 p.

---------- 1957. Die "Pronto-Reaktion". *N. Jhb. Miner.*, 217-222.

---------- 1958a. New observations on the ores of the Witwatersrand in South Africa and their genetic significance. *Annexure Trans. geol. Soc. S. Afr.*, 61:55 p.

---------- 1958b. Die Uran- und Goldlagerstätten Witwatersrand - Blind River District - Dominion Reef - Serra de Jacobina: Erzmikroskopische Untersuchungen und ein geologischer Vergleich. *Abh. Dt. Akad. Wissensch., Berlin, Kl. Chem., Geol., Biol.*, 3:1-35.

--------- 1961. Das Vorkommen von Coffinit in hydrothermalen Uranerzgangen, besonders vom Co-Ni-Bi-Typ. *N. Jb. Miner. Abh.*, 95:313-324.

READING, H.G. 1979. Sedimentary environments and facies. London: Blackwell Scientific Publ. 557 p.

REID, I. & FROSTICK, L.E. 1985. Role of settling, entrainment and dispersive equivalence and of interstice trapping in placer formation. *J. geol. Soc. London*, 142:739-746.

REIMER, T.O. 1979. Platinoids in auriferous Proterozoic conglomerates of South Africa. Evaluation of existing data. *N. Jb. Miner. Abh.*, 135:287-314.

REIMER, T.O. 1983. Accretionary lapilli and other spheroidal rocks from the Archaean Swaziland Supergroup, Barberton Mountain Land, South Africa. (*In* Peryt. T., ed. Coated grains. Berlin: Springer-Verlag. 655 p.

---------- 1984. Alternative model for the derivation of gold in the Witwatersrand Supergroup. *J. geol. Soc. London*, 141:263-272.

ROBB, L.J. & MEYER, M. 1985. The nature of the Witwatersrand Hinterland: Conjectures on the source-area problem. Johannesburg: Univ. Witwatersrand. Econ. Geol. Res. Unit. Inf. Circ. 178:25 p.

ROBINSON, A. & SPOONER, T.C. 1982. Source of the detrital components of uraniferous conglomerates, Quirke ore zone, Elliot Lake, Ontario, Canada. *Nature*, 299:622-624.

ROCK-COLOR CHART COMMITTEE. 1963. Rock-color chart. New York: Geol. Soc. Amer.

ROERING, C. 1984. The Witwatersrand Supergroup at Swartkops: A re-examination of the structural geology. *Trans. geol. Soc. S. Afr.*, 87:87-99.

---------- 1986. Aspects of thrust faulting on the northern margin of the Witwatersrand Basin. (*In* Extended Abstracts Geocongress '86, Johannesburg, Geol. Soc. S. Afr. 59-62.)

ROJKOVIC, I. & BORNICHIN, V.A. 1982. U-Ti minerals at the deposit Novoveska Huta (Slovenske Rudohorie Mts). *Geol. Zvornik - Geol. Carpathica*, 33:321-330.

RUHLMANN, F. 1980. Quelques examples de relation uranium-titane. *Bull. Mineral.*, 103:240-244.

RUNDLE, C.G. & SNELLING, N.J. 1977. The geochronology of uraniferous minerals in the Witwatersrand Triad; an interpretation of new and existing U-Pb age data on rocks and minerals from the Dominion Reef, Witwatersrand and Ventersdorp Supergroups. *Phil. Trans. R. Soc. London*, A286:567-583.

SAAGER, R. 1968. Structures in pyrite from the Basal Reef in the Orange Free State Goldfield. Johannesburg: Univ. Witwatersrand. Econ. Geol. Res. Unit. Inf. Circ. 45:25 p.

--------- 1969. The relationship of silver and gold in the Basal Reef of the Witwatersrand System, South Africa. *Miner. Deposita*, 4:93-113.

------- & MIHALIK, P. 1967. Two varieties of pyrite from the Basal Reef of the Witwatersrand System. *Econ. Geol.* 62: 719-731.

SAAGER, R. & OBERTHUR, T. 1984. Nickel-cobalt sulfides in Precambrian gold and uranium-bearing quartz-pebble conglomerates of South Africa. (*In* Waunschkuhn, A., Kluth, C. & Zimmermann, R.A., eds. Syngenesis and epigenesis in the formation of mineral deposits. Berlin: Springer Verlag. p. 237-245.)

-------- & STUPP, H.D. 1983. U-Ti phases from Precambrian quartz-pebble conglomerates of the Elliot Lake Area, Canada, and the Pongola Basin, South Africa. *Tschermak Min. Petr. Mitt.*, 32:83-102.

--------, UTTER, T. & MEYER, M. 1982. Pre-Witwatersrand and Witwatersrand Conglomerates in Southern Africa; A mineralogical comparison and bearings on the genesis of gold-uranium placers. (*In* Amstutz, G.C., El Goresy, A., Frenzel, G., Kluth, C., Moh, G., Wauschkuhn, A., Zimmerman, R.A., eds. Ore genesis. Berlin: Springer Verlag. p. 38-56.)

SCHIDLOWSKI, M. von. 1966a. Beitrage zur Kenntnis der radioaktiven Bestandteile der Witwatersrand-Konglomerate. II. Brannerit und "Uranpecherzgeister". *N. Jb. Miner. Abh.*, 105:310-324.

------------------ 1966b. Beitrage zur Kenntnis der radioaktiven Bestandteile der Witwatersrand-Konglomerate. I. Uranpecherz in den Konglomeraten des Oranje-Frei-Staat-Goldfeldes. *N. Jb. Miner. Abh.*, 105:183-202.

------------------ 1966c. Beitrage zur Kenntnis der radioaktiven Bestandteile der Witwatersrand-Konglomerate. III. Kohlige Substanz ("Thucholith"). *N. Jb. Miner. Abh.*, 106:55-71.

------------------ 1966d. Zellulier strukturierte Elemente aus dem Praekambrium des Witwatersrand-Systems (Südafrika). *Z. Dt. geol. Ges.*, 115:783-786.

------------------ 1966e. Mineralbestand und Gefügebilder in Faseraggregaten von kohliger Substanz ("Thucholith") aus den Witwatersrand-Konglomeraten. *Contr. Miner. and Petrol.*, 12:365-380.

------------------ 1967. Note on graphite in the Witwatersrand conglomerates. *Trans. geol. Soc. S. Afr.*, 70:65-66.

------------------ 1968. The gold fraction of the Witwatersrand conglomerates from the Orange Free State Goldfield (South Africa). *Miner. Deposita*, 3:344-363.

------------------ 1985. Early life and mineral resources. *Nature and Resources, Unesco*, 21:11-17.

------------------ 1988. A 3.800-million-year isotopic record of life from carbon in sedimentary rocks. *Nature*, 333:313-318.

SCHIDLOWSKI, M. von., HAYES, J.M. & KAPLAN, I.R. 1983. Isotopic inferences of ancient biochemistries: carbon, sulfur, hydrogen, and nitrogen. (*In* Schopf, J.W., ed., Earth's earliest Biosphere: Its origin and evolution. Princeton: Princeton Univ. Press. p. 149-186.)

--------- & OTTEMANN, J. 1966. Mackinawite from the Witwatersrand conglomerates. *Amer. Miner.*, 51:1535-1541.

SCHMIDT, V. & McDONALD, D.A. 1979. The role of secondary porosity in the course of sandstone diagenesis. (*In* Scholle, P.A. & Schluger, P.R., eds. Aspects of diagenesis. Tulsa, USA: Soc. Econ. Paleont. Mineral. *Special publ.* 26:175-207.)

SCHMIDT-COLLERUS, J.J. 1969. Research in uranium geochemistry: Investigations of the relationship between organic matter and uranium deposits. Part 2: Experimental investigation. Grand Junction, Colorado: U.S. Atom. En. Comm. 192 p.)

SCHREYER, W. & BISCHOFF, A.A. 1982. Kyanite as a metamorphic mineral in Witwatersrand sediments at Johannesburg and Krugersdorp, South Africa. *Trans. geol. Soc. S. Afr.*, 85:211-214.

SCHROECKE, H. 1958. Zur Synthese von $AB_2O_6$-Verbindungen. *N. Jb. Miner. Mh*, 70-71,

SEELIGER, E. & STRUNTZ, H. 1965. Erzpetrographie der Uran-Mineralien von Wolsendorf. *N. Jb. Miner. Abh.*, 103:163-178.

SEWARD, T.M. 1973. Thiocomplexes of gold and the transport of gold in hydrothermal ore solutions. *Geochim. Cosmochim. Acta*, 37:379-399.

---------- 1984. The transport and deposition of gold in hydrothermal systems. (*In* Foster, R.P., ed. Gold '82: The geology, geochemistry and genesis of gold deposits. Rotterdam: Balkema. Spec. Publ. Geol. Soc. Zimbabwe, 1. p. 165-181.)

SHARPE, J.W.N. 1949. The economic auriferous bankets of the Upper Witwatersrand beds and their relationship to sedimentation features. *Trans. geol. Soc. S. Afr.*, 52: 265-330.

SIEVER, R. & WOODFORD, N. 1979. Dissolution kinetics and the weathering of mafic minerals. *Geochim. Cosmochim. Acta*, 43:717-724.

SIMOVA, F.G. 1981. Uranium silicates from two deposits in Permian sediments, Central Europe. *Comptes rendus de l'Académie Bulgare de Sciences*, 34:1693-1696.

SIMPSON , P.R. & BOWLES, J.F.M. 1977. Uranium mineralization of the Witwatersrand and Dominion Reef Systems. Phil. Trans. R. Soc. London, A286:527-548.

SMITS, G. 1978. Mineralogy and uranium-mineralization of conglomeratic sandstones from northern Natal. Pelindaba: At. Energy Board. Rep. PIN 316 (NIM 7129). 14p.

SMITS, G. 1984a. Some aspects of the uranium minerals in Witwatersrand sediments of the Early Proterozoic. *Precambrian Res.*, 25:37-59.

-------- 1984b. Mineral modifications observed in uranium-bearing reefs of the Witwatersrand, South Africa. *Trans. geol. Soc. S. Afr.*, 87:245-256.

-------- 1985a. Behaviour of mineals in Witwatersrand ores during the leaching stage of the uranium-extraction process. (*In* Park, W.C., Hausen, D.M. & Hagni, R.D., eds. Applied mineralogy. Metall. Soc. AIME. p.599-616.)

-------- 1985b. Uranium-bearing minerals in Witwatersrand rocks and their behaviour during leaching. (*In* Haughton, L.F., ed., Proceedings of MINTEK 50, International Conference on Mineral Science and Technology. Vol. 2. 992 p.)

-------- 1985c. Randburg: Council for Mineral Technology. Conf. Rep.

-------- 1985d. Archives in the reefs. *Nuclear Active*, 32:6-10.

-------- 1986. The mobility of uranium during Witwatersrand times. (*In* Extended Abstracts Geocongress '86. Johannesburg, Geol. Soc. S. Afr. 203-206.)

-------- 1987. Uranium-thorium silicates with specific reference to the species in the Witwatersrand Reefs. Randburg: Council for Mineral Technology. Rep. M278. 33 p.

-------- 1989. (U,Th)-bearing silicates in reefs of the Witwatersrand, South Africa. *Can. Miner.*, 27:643-655.

------- & GRIMBEEK, J.C. 1987. Randburg: Council for Mineral Technology. Conf. Rep.

------- & UITERWIJK, B.H. 1983. The uranium mineralization in the south-western Karoo: its mineralogy and genesis. (*In* De Villiers, J.P.R. & Cawthorn, P.A., eds. ICAM 81. Johannesburg: Geol. Soc. S. Afr., Spec. Publ. 7:39-57.)

SNYMAN, C.P. 1965. Possible biogenetic structures in Witwatersrand thucholite. *Trans. geol. Soc. S. Afr.*, 68:225-235.

SOBOLEVA, M.V. & PUDOVKINA, I.A. 1958. New mineral names - Lodochnikite. *Amer. Miner.*, 43:380.

SOUTH AFRICAN COMMITTEE FOR STRATIGRAPHY (SACS). 1980. Kent, L.E., ed. Stratigraphy of South Africa Part 1. Pretoria: Geol. Surv. S. Afr., Gov. Print. Handbook 8. 960 p.

SPRY, A. 1969. Metamorphic textures. Oxford: Pergamon Press. 350 p.

STACH, E., MACKOWSKY, M.Th., TEICHMULLER, M., TAYLOR, G.H., CHANDRA, D. & TEICHMULLER, R. 1982. Stach's textbook of coal petrology. 3rd ed. Berlin: Brontraeger. 535 p.

STEACY, H.R. 1953. An occurrence of uraninite in black sand. *Amer. Miner.*, 38:549-550.

STEVENS, R.E. 1944. Composition of some chromites of the western hemisphere. *Amer. Miner.*, 29:1-34.

STIEFF, L.R., STERN, T.W. & SHERWOOD, A.M. 1955. Preliminary description of coffinite - a new mineral. *Science*, 121:608-609.

------, -----, & ---------- 1956. Coffinite, a uranous silicate with hydroxyl substitution: a new mineral. *Amer. Miner.*, 41:675-688.

SUMMERFIELD, M.A. 1983. Petrography and diagenesis of silcrete from the Kalahari Basin and Cape Coastal Zone, Southern Africa. *J. Sedim. Petr.*, 53:895-909.

SUTHERLAND, D.G. 1985. Geomorphological controls on the distribution of placer deposits. *J. geol. Soc. London*, 142:727-737.

SWEENEY, R.E. & KAPLAN, I.R. 1973. Pyrite framboid formation: Laboratory syunthesis and marine sediments. *Econ. Geol.*, 68: 618-634.

SWIEGERS, J.U. 1939. Gold, carbon, pyrite and other sulphides in the Black Reef. *Trans. geol. Soc. S. Afr.*, 42:35-45.

SZYMANSKI, T.J. & SCOTT, J.D. 1982. A crystal-structure refinement of synthetic brannerite, $UTi_2O_6$, and its bearing on rate of alkaline-carbonate leaching of brannerite in ore. *Can. Miner.*, 20:271-279.

TANKARD, A.J., ERIKSSON, K.A., HUNTER, D.R., JACKSON, M.P.A., HOBDAY, D.K. & MINTER, W.E.L. 1982. Crustal evolution of Southern Africa. 3.8 billion years of Earth History. Berlin: Springer Verlag. 523 p.

TEMPLE, A.K. 1966. Alteration of ilmenite. *Econ. Geol.* 61:695-714.

THEIS, N.J. 1976. Uranium-bearing and associated minerals in their geochemical and sedimentological context, Elliot Lake, Ontario. Kingston, Ontario. p. 158. (Dissertation (Ph.D.) - Queen's Univ.)

---------- 1979. Uranium-bearing and associated minerals in their geochemical and sedimentological context, Elliot Lake, Ontario. *Bull. Geol. Surv. Can.*, 304:50 p.

THIEL, K., SAAGER, R. & MUFF, R. 1979. Distribution of uranium in early precambrian gold-bearing conglomerates of the Kaapvaal Craton, South Africa: A review of a case study for the application of fission track micromapping of uranium. *Miner. Sci. Eng.*, 11:225-245.

THOMPSON, A.B. 1970. A note on the kaolinite-pyrophyllite equilibrium. *Amer. J. Sci.* 268:454-458.

THOMPSON, J.B. & NORTON, S.A. 1968. Palaeozoic regional metamorphism in New England and adjacent areas. (*In* E-an Zen *et al.*, eds. Studies of Appalachian Geology. New York: Interscience Publisher Wiley.)

TROEGER, W.E. 1967. Optische Bestimmung der gesteinsbildende Minerale. Teil. 2. Stuttgart: Republ. by Braitsch, O., Schweizerbart'sche Verlagsbuchhandlung. 822 p.

TUCKER, R.F. 1980. The sedimentology and mineralogy of the Composite Reef on Cooke Section, Randfontein Estates G.M. Johannesburg. p. 348. (Dissertation (M.Sc.) - Univ. Witwatersrand.)

UTTER, Th. 1978. Raster-elektronmikroskopische und geochemische Untersuchungen an Erzmineralien aus dem Oberen Witwatersrand- und Ventersdorp-System des Klerksdorp-Goldfeldes, Südafrika. Frankfurt. p. 159. (Dissertation (Ph.D.) - Goethe Univ.)

--------- 1980. Rounding of ore particles from the Witwatersrand gold and uranium deposit (South Africa) as an indicator of their detrital origin. *J. Sedim. Petr.*, 50:0071-0076.

UYTENBOGAARDT, W., and BURKE, E.A.J. 1971. Tables for microscopic identification of ore minerals. Amsterdam: Elsevier. 430 p.

VAN DER WESTHUYZEN, C. & SMITS, G. 1985. Randburg: Council for Mineral Technology. Conf. Rep.

VAN NIEKERK, C.B. & BURGER, A.J. 1964. The age of the Ventersdorp System. *Ann. Geol. Surv. S. Afr.*, 3:75-86.

---------- & ---------- 1969a. A note on the minimum age of the acid lava of the Onverwacht Series of the Swaziland System. *Trans. geol. Soc. S. Afr.*, 72:9-21.

---------- & ---------- 1969b. Lead isotopic data relating to the age of the Dominion Reef Lava. *Trans. geol. Soc. S. Afr.*, 72:37-45.

---------- & ---------- 1978. A new age for the Ventersdorp acidic lavas. *Trans. geol. Soc. S. Afr.*, 81:155-163.

VASSILOU, A. 1980. The form of occurrence of uranium in deposits associated with organic matter. *Econ. Geol.* 75:609-617.

VASSILOU, A. & KERR, P.F. 1972. Uranium-organic matter association at La Bajada, New Mexico. *Econ. Geol.* 67:41-54.

VELDE, B. 1983. Diagenetic reactions in clays. (*In* Parker, A. & Sellwood, B.W., eds. Sediment diagenesis. Series C: Math. Phys. Sci. Vol. 115. Dordrecht: Reidel. 427 p.)

VILJOEN, E.A. 1971. An electron-microprobe analysis of gold in the Witwatersrand banket and in ores from the Barberton Mountain Land. Johannesburg, Nat. Inst. for Metall. Rep. 1361. 7 p.

---------- 1977. The composition of chromite grains from various Witwatersrand reefs. Johannesburg, Nat. Inst. for Metall., Rep. 1924. 3 p.

VILJOEN, R.P. 1963. Petrographic and mineragraphic aspects of the Main Reef and Main Reef Leader of the Main-Bird Series, Witwatersrand System. Johannesburg. 193 p. (Dissertation (M.Sc.) - Univ. Witwatersrand.)

----------, SAAGER, R., & VILJOEN, M.J. 1970. Some thoughts on the origin and processes responsible for the concentration of gold in the early Precambrian of Southern Africa. *Miner. Deposita*, 5:164-180.

VON GEHLEN, K. 1983. Silver and mercury in single gold grains from the Witwatersrand and Barberton, South Africa. *Miner. Deposita*, 18:529-534.

VOS, R.G. 1975. An alluvial plain and lacustrine model for the Precambrian Witwatersrand deposits of South Africa. *J. Sedim. Petr.*, 45:480-493.

WALKER, J.L., SHERMAN, G.D. & KATSURA, T. 1969. The iron and titanium minerals in the titaniferous ferruginous latosols of Hawaii. *Pacific Sci.* 23:291-304.

WALTER, M.R. 1983. Archaean stromatolites: Evidence of the earth's earliest benthos. (*In* SCHOPF, J.W., ed. Earth's earliest biosphere: Its origin and evolution. Princeton: Princeton Univ. Press. 187-213.)

WATCHORN, M.B. 1980. The stratigraphic and sedimentological development of the Witwatersrand West Rand Basin in the Klerksdorp Area. Johannesburg, Univ. Witwatersrand, Econ. Geol. Res. Unit. Inf. Circ. 148: 9 p.

WEIS, P. 1980. Graphite skeleton crystals - A newly recognized morphology of crystalline carbon in metasedimentary rocks. *Geology*, 8:296-297.

WETHERILL, G.W. 1956. An interpretation of the Rhodesia and Witwatersrand age patterns. *Geochim. Cosmochim. Acta*, 9:290-292.

WHITE, A.F. & YEE, A. 1985. Aqueous oxidation-reduction kinetics associated with coupled electron-cation transfer from iron-containing silicates at 25°C. *Geochim. Cosmochim. Acta.* 49:1263-1275.

WHITE, S.H., HUGGETT, J.M. & SHAW, H.F. 1985. Electron-optical studies of phyllosilicate intergrowths in sedimentary and metamorphic rocks *Miner. Mag.*, 4:413-423.

WHITESIDE, H.C.M. 1970. Uraniferous Precambrian conglomerates of South Africa. (*In* Uranium exploration geology. Vienna: Intern. At. En. Ag. p.49-75.)

WIEBOLS, J.H. 1961. Note on chloritoid in the Witwatersrand System. *Trans. geol. Soc. S. Afr.*, 64:85-98.

WILLEMSE, J. 1948. Die chromiet-voorkoms op Lemoenfontein 893, Pietersburg Distrik. *Trans. geol. Soc. S. Afr.*, 1:195-212.

WILSON, M.J. 1970. A study of weathering in a soil derived from a biotite-hornblende rock. I. Weathering of biotite. *Clay Minerals*, 8:291-303.

WILSON, N.L., OOSTHUIZEN, D.H., BRINK, W.C.M. & TOENS, P.D. 1964. The geology of the Vaal Reef Basin in the Klerksdorp area . (*In* Haughton, S.H., ed. The geology of some ore deposits in southern Africa. Vol. I. Johannesburg: Geol. Soc. S. Afr. p. 399-416.)

WINKLER , H.G.F. 1979. Petrogenesis of metamorphic rocks. New York: Springer Verlag. 348 p.

WYBRECHT, E., DUPLAY, J., PIQUE, A. & WEBER, F. 1985. Mineralogical and chemical evolution of white micas and chlorites from diagenesis to low-grade metamorphism data from various size fracxtions of greywackes (Middle Cambrian, Morocco). *Mineral. Magazine*, 49:401-411.

YOUNG, R.B. 1917. The banket of the South African Goldfields. London: Gurnsey and Jackson.

ZEN, E.An. 1960. Metamorphism of Lower Palaeozoic rocks in the vicinity of the Taconic Range in west-central Vermont. *Amer. Miner.*, 45:129-175.

ZESCHKE, G. 1960. Transportation of uraninite in the Indus River, Pakistan. *Trans. geol. Soc. S. Afr.*, 68:87-97.

ZUMBERGE, J.E., SIGLEO, A.C. & NAGY, B. 1978. Molecular and elemental analyses of the carbonaceous matter in the gold and uranium bearing Vaal Reef carbon seams, Witwatersrand Sequence. *Miner. Sci. Eng*, 10:223-246.

# APPENDIX A

Figure A.1 Photomicrographs of phyllosilicates
Transmitted light

a. Ghost texture of a flexed, silicified flake of a pseudomorph after biotite, in which rutile (black) precipitated along the cleavage. The quartz crystallized in optical continuity with the grains bordering the flake. Vaal Reef, Western Reefs G.M.

b. Chloritoid porphyroblast (SE direction), which precipitated across a pseudomorph after biotite, as is suggested by the wavy texture of the network of minute rutile prisms (SW direction). Carbon Leader, West Driefontein G.M.

c. Ghost texture of silicified phyllosilicate, from which chlorite (dark grey stripes) was preserved. Vaal Reef, Vaal Reefs South G.M.

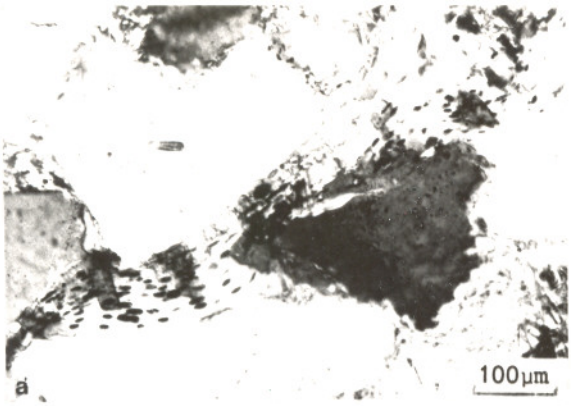
d. Vertical section across thin layer of pyrite (white), chloritoid (grey, cd), and fine-grained rutile (pale grey) overlying fine-grained quartzite (dark grey at bottom), and overlain by coarser quartzite (dark grey at top). Incident light in air. Carbon Leader, Western Deep Levels G.M.

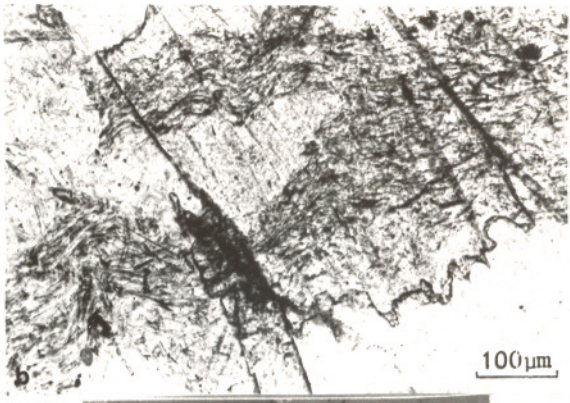
e. Interstitial sericite (grey) displaying straight contacts with quartz (pale grey). Vaal Reef, Harte-beestfontein G.M.

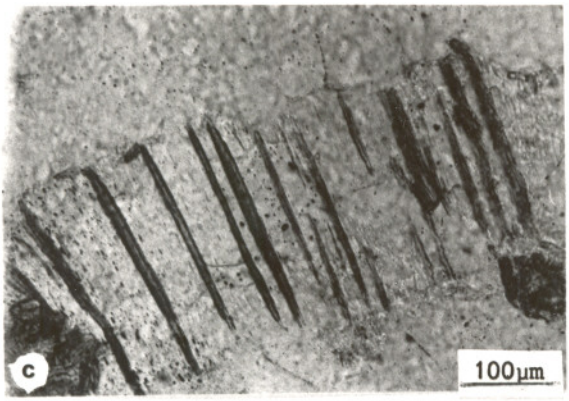
f. Argillaceous footwall quartzite in which flakes of chlorite (dark grey) intergrown with little sericite (pale grey) lie parallel to the plane of deposition. The quartz and chlorite grains are cemented by a fine-grained mixture of sericite and pyrophyllite. Leader Reef, Virginia G.M.

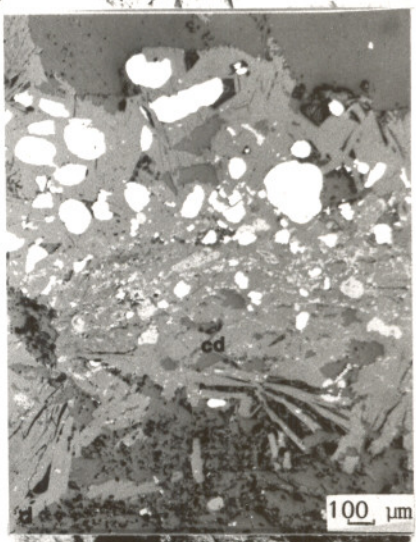
g. Chloritoid porphyroblast (grey) with quartz inclusions (dark grey). The microstylolite running SW-NE consists mainly of minute rutile prisms (white spots). Incident light in oil. Carbon leader, West Driefontein G.M.

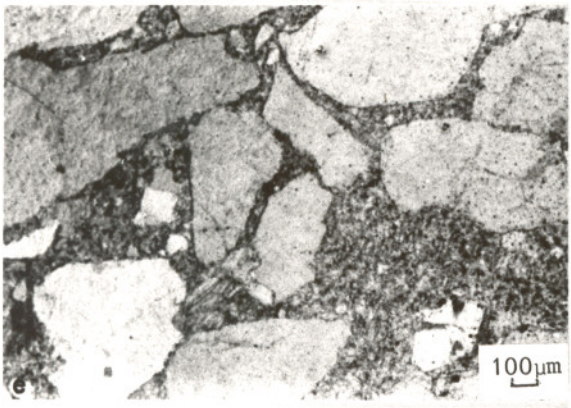
h. Groups of chloritoid porphyroblasts in quartz. Some of the blades formed at the expense of pyrite (black). Monarch Reef, West Rand Consolidated G.M.


a
100μm

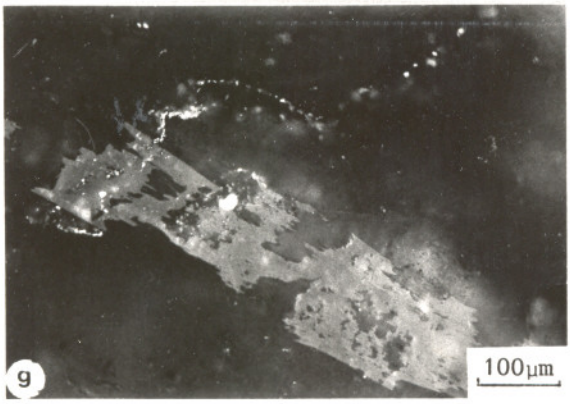

b
100μm


c
100μm


cd
100 μm


e
100μm


100μm


g
100μm

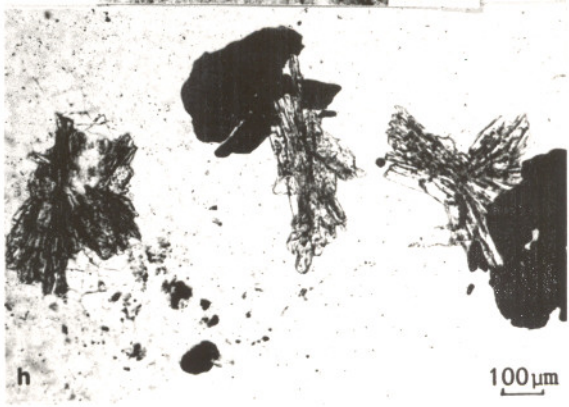

h
100μm

Figure A.2 Photomicrographs of chlorite
Transmitted light

a. Boudinaged flake of chlorite (black) bordered by pyrophyllite (pale grey). Basal Reef, Harmony G.M.

b. Kinked muscovite (pale grey) in which iron sulphide (black spots and kinked stripe) precipitated along the cleavage. Black detrital grains are pyrite and rutile-leucoxene pseudomorphs. Monarch Reef, West Rand Consolidated G.M.

c. Kinked flake of pseudomorph after biotite. Vaal Reef, Vaal Reefs East G.M.

d. Whorls of chlorite (grey) along a microstylolite at the contact of two quartz particles (pale grey). Kalkoenkrans Reef, Oryx G.M.

e. Stacked basal sections of authigenic chlorite (grey) forming curved trails in quartz (white) referred to as vermicular chlorite or 'helminth' (Troger, 1967). Carbon Leader, West Driefontein G.M.

f. Partly chloritized (shades of grey, fibrous) detrital pyrite (black). Vaal Reef, Vaal Reefs East G.M.

g. Partly chloritized (dark grey) arsenopyrite (white), enveloped by film of minute brannerite crystals (pale grey). Incident light in oil. Carbon Leader, West Driefontein G.M.

h. Detrital chromite (grey) partly replaced by chlorite (black). Incident light in oil. Basal Reef, President Brand G.M.

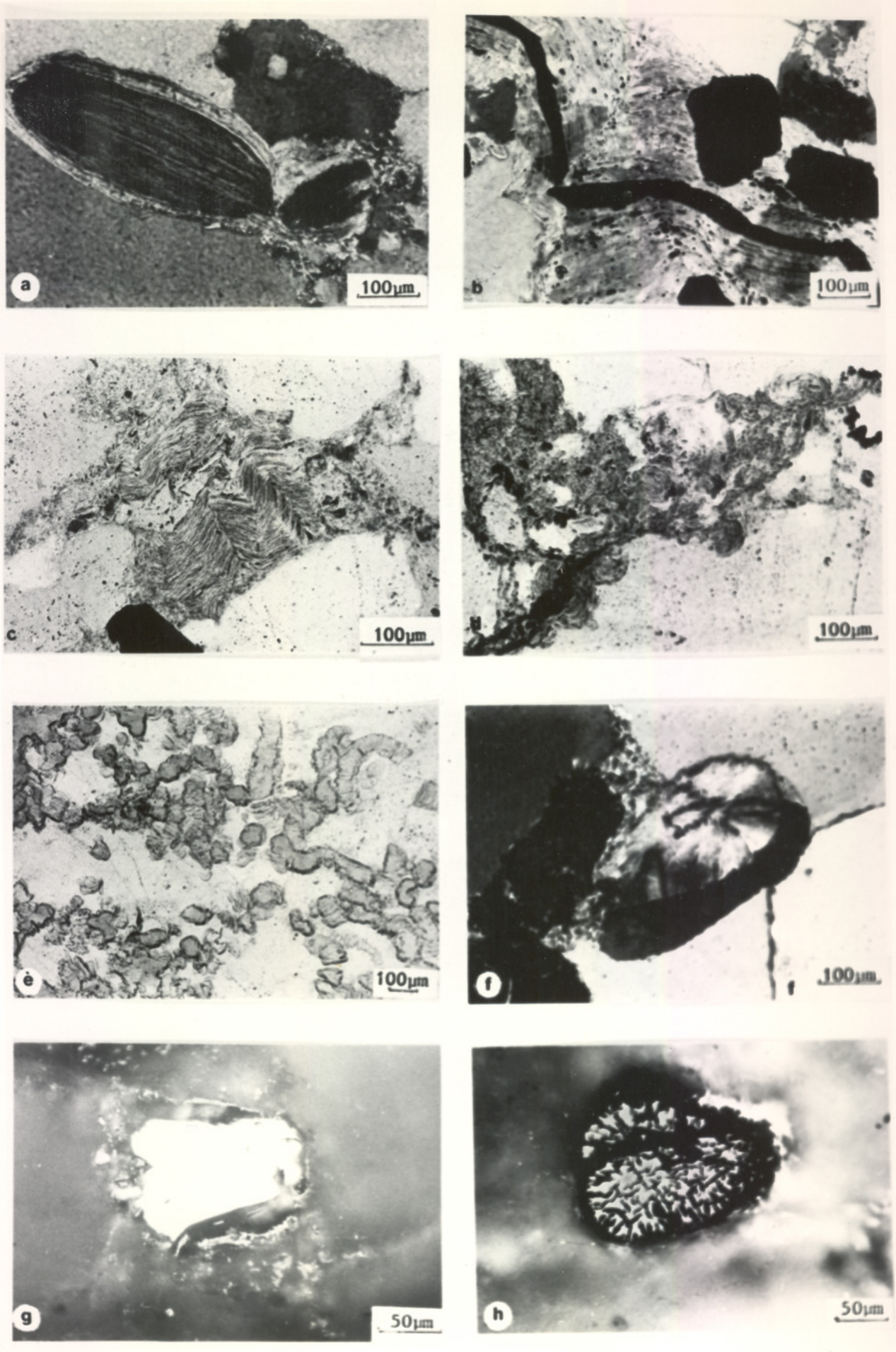

a
100µm
b
100µm
c
100µm
d
100µm
e
100µm
f
100µm
g
50µm
h
50µm

Figure A.3 Photomicrographs of phyllosilicates

**a.** Interstitial chlorite (black) in which minute haloes (white) round uraniferous leucoxene (black) are dispersed. Incident light in oil. Carbon Leader, West Driefontein G.M.

**b.** Pseudomorph after biotite composed of chlorite (dark grey) and muscovite (black), the latter enclosing pyrite (white) along its cleavage. Incident light in oil. Kimberley Reef, Grootvlei G.M.

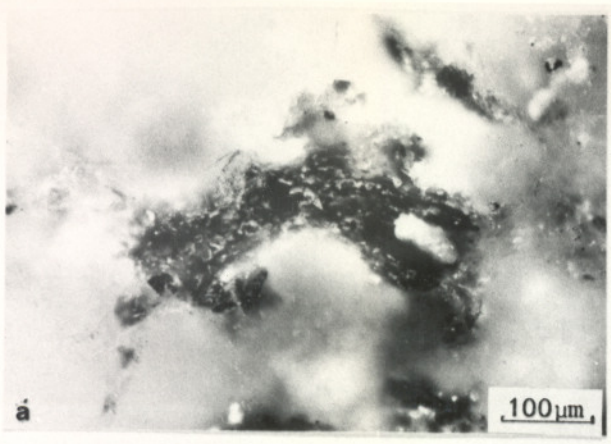
**c.** Interstitial fine-grained chlorite mixed with quartz (both grey) enclosing skeletal gold (white in centre, Au). Incident light in air. Kalkoenkrans Reef, Oryx G.M.

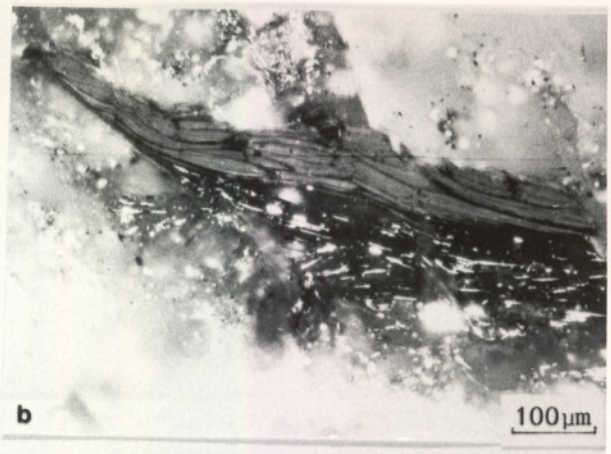
**d.** Chlorite aggregate (dark grey) enclosing galena (black). Transmitted light. Vaal Reef, Hartebeestfontein G.M.

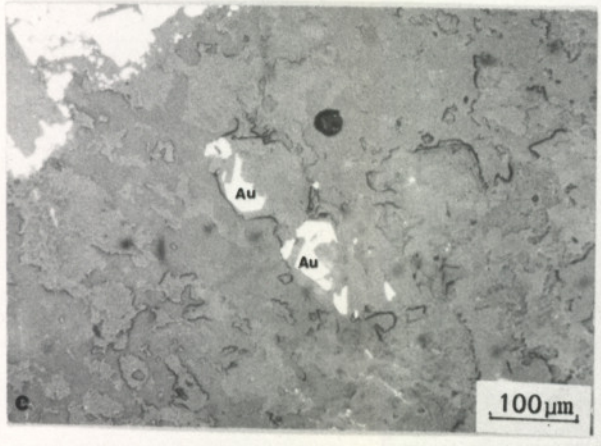
**e.** Coarse chlorite aggregate (white) enclosing sphalerite (black). Transmitted light. Vaal Reef, Buffelsfontein G.M.

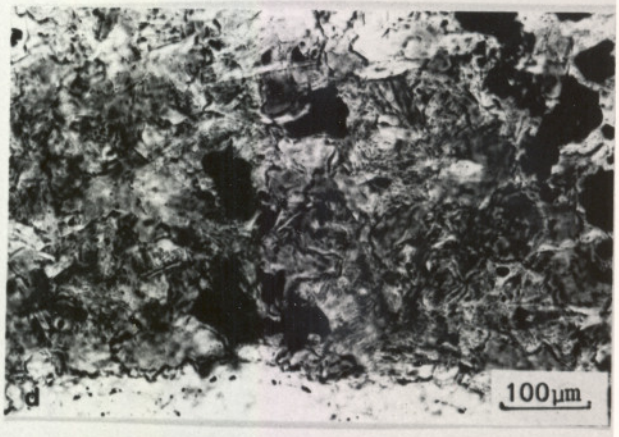
**f.** Chlorite (black) with brannerite inclusions (pale grey). Incident light in oil. Carbon Leader, Western Deep Levels G.M.

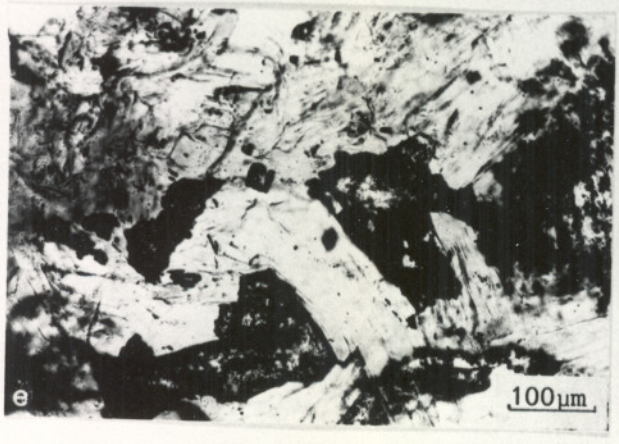
**g and h.** Haloes of iron-rich chlorite (pale grey) round uraniferous leucoxene (black), outlined by film of black spots which probably consist of iron dust. The haloes occur within a mixture of sericite and pyrophyllite (pale grey). Transmitted light. Carbon Leader, West Driefontein G.M.

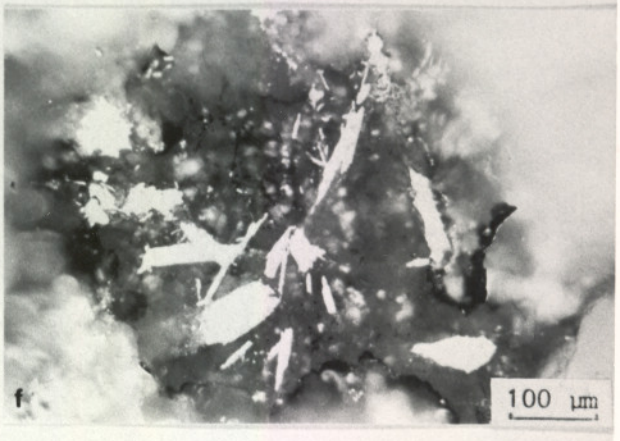

á
100µm

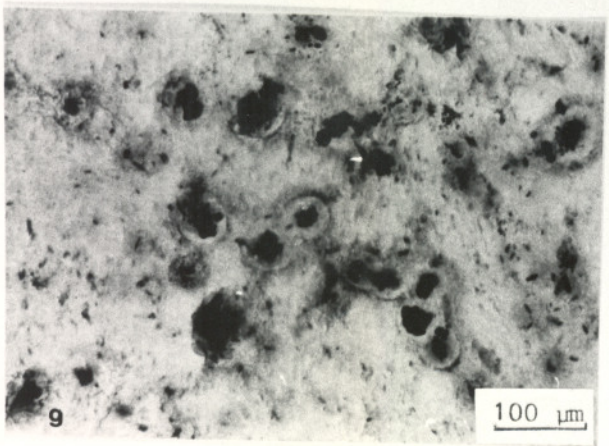

b
100µm


Au
Au
c
100µm


d
100µm


e
100µm


f
100 µm


g
100 µm

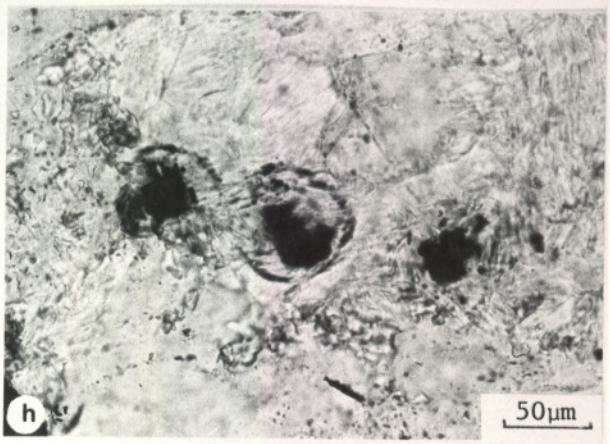

h
50µm

Figure A.4 Photomicrographs of phyllosilicates
Transmitted light

**a.** Sericite and/or pyrophyllite aggregate (pale grey), in which abundant rutile prisms (black) are dispersed. Leader Reef, Virginia G.M.

**b.** Film of parallel sericite (white) shreds at the contact of two quartz grains (pale grey and black). Leader Reef, Virginia G.M.

**c.** Whorly muscovite (white) which formed at the expense of quartz grains (pale grey). Carbon Leader, Blyvooruitzicht G.M.

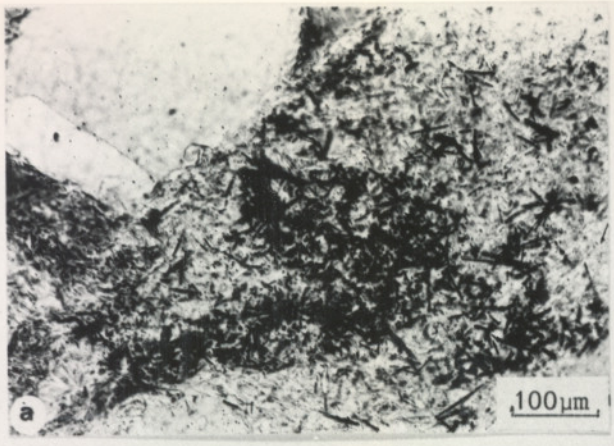
**d.** Whorls of pyrophyllite (grey) in quartz (white and black). Carbon Leader, West Driefontein G.M.

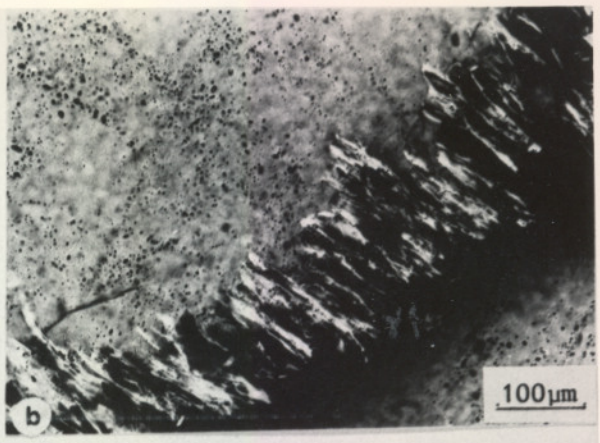
**e.** Whorls of pyrophyllite (grey), in which minute specks of iron sulphide (black) are dispersed in recrystallized quartz (shades of grey) displaying triple point contacts. Monarch Reef, West Rand Consolidated G.M.

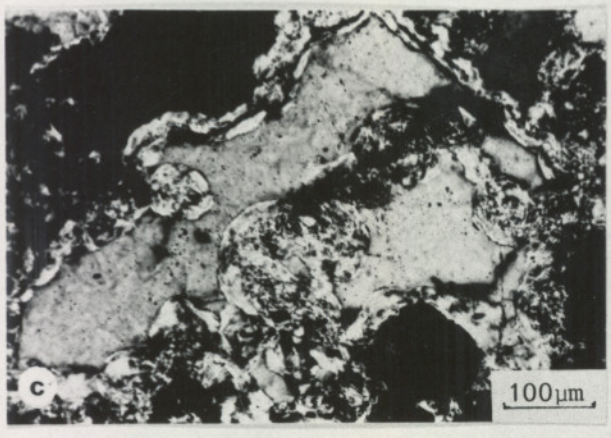
**f.** Spheres of undeformed muscovite enveloped by concentric phyllosilicate are enclosed by a mudclast silicified to microquartz. Kalkoenkrans Reef, Oryx G.M.

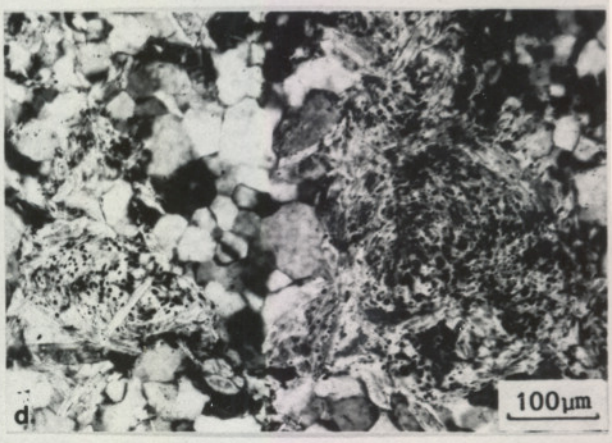
**g.** Remnants of sericite or pyrophyllite, or a mixture of the two (white spots in centre) which was silicified; the quartz crystallized in optical continuity with the adjacent quartz grains. Microquartz formed to the right. Vaal Reef, Vaal Reefs South G.M.

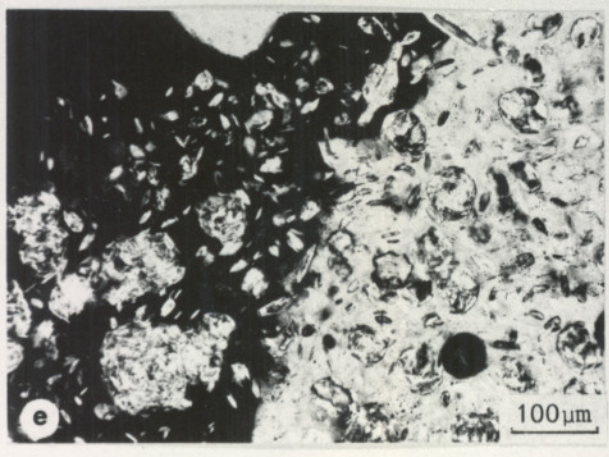
**h.** Rare occurrence of overgrowth of secondary quartz (white) on detrital quartz grains (white, grey, and black, q). Carbon Leader, Blyvooruitzicht G.M.

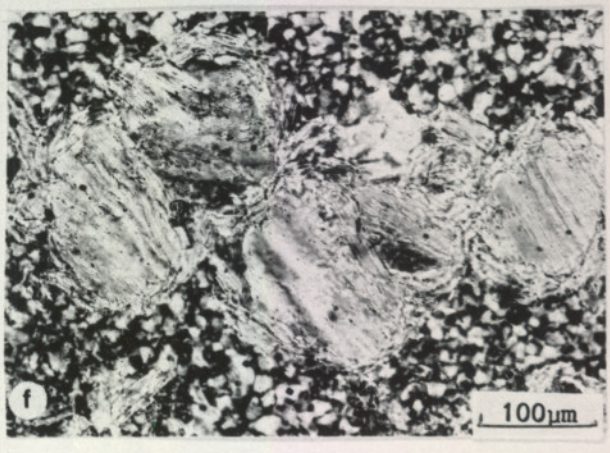

a
100μm

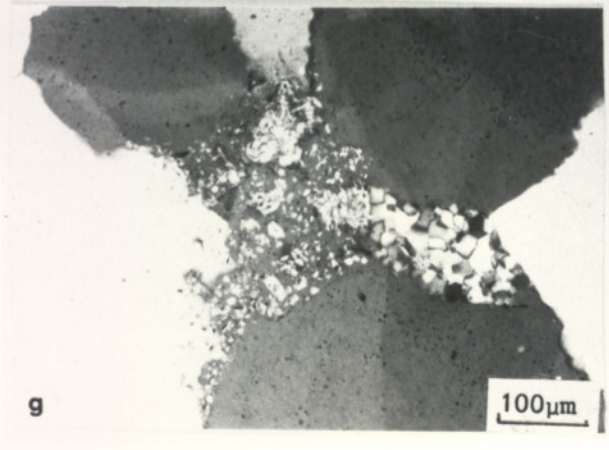

b
100μm


c
100μm


d
100μm


e
100μm


f
100μm


g
100μm

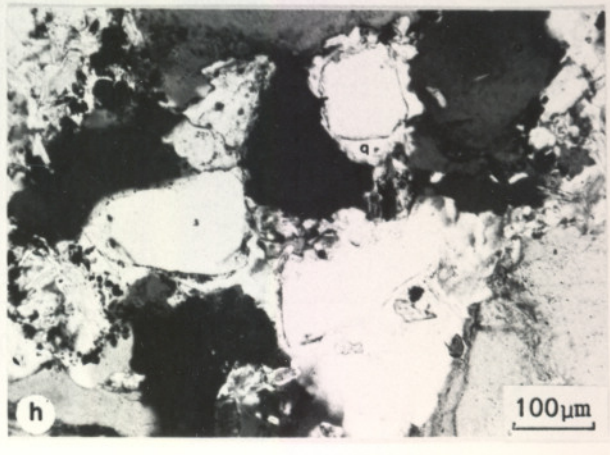

h
100μm

Figure A.5 Photomicrographs of chloritoid and pyrite

**a.** Hour-glass texture in chloritoid blades produced by the presence of impurities. Transmitted light. Basal Reef, Harmony G.M.

**b and c.** Chloritoid (grey) blades which precipitated at the expense of detrital pyrite (white). Incident light in oil. Kalkoenkrans Reef, Oryx G.M.

**d and e.** Haloes of chlorite around uraniferous leucoxene in chloritoid. (b) taken in transmitted light, (c) in incident light in oil. Carbon Leader, Western Deep Levels G.M.

**f.** Partly chloritized (black) pyrite (mottled) grain. Transmitted light. Vaal Reef, Buffelsfontein G.M.

**g.** Two chlorite (black) particles of detrital origin and some of the pyrite (white) grains are coated by a film of brannerite crystals (grey). At left centre is a uraninite (pale grey, u) grain enclosed by kerogen (k). Incident light in oil. Carbon Leader, Blyvooruitzicht G.M.

**h.** Brannerite and uraniferous leucoxene (both dark grey) which corroded the surfaces of two pyrite grains (white). Minute pyrrhotite laths (white) and galena specks are dispersed in the uranous titanates. Incident light in oil. Vaal Reef, Vaal Reefs East G.M.

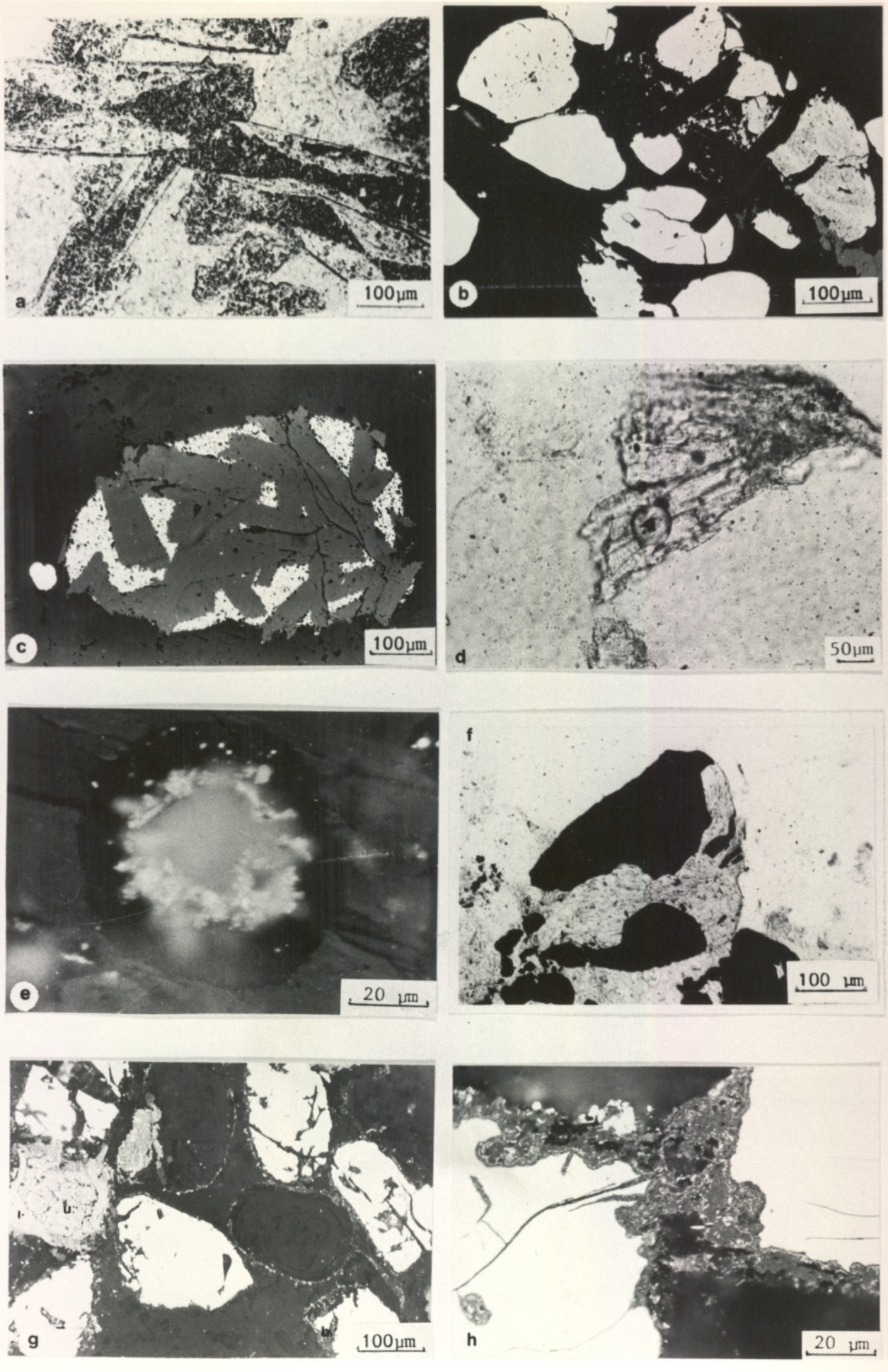

a
100µm
b
100µm
c
100µm
d
50µm
e
20 µm
f
100 µm
g
100µm
h
20 µm

Figure A.6 Photomicrographs of pyrite
Incident light in oil

**a to e.** Detrital concretionary pyrite grains of different textures. The oolitic texture in (d) has only been noticed once in the Kalkoenkrans Reef, Oryx G.M. The individual oolites (30 μm) are made up of layers of pyrite, galena, chalcopyrite, pyrrhotite (all pale grey), and gangue (black). The texture of the grain in (e) was enhanced because the polished section was subjected to leaching with dilute sulphuric acid. The darker etched patches (shades of grey) contain trace amounts of Co, Ni, and As. The youngest pyrite (white) is pure. Basal Reef, Harmony G.M.

**f.** Consolidated mudball composed of fine-grained pyrite (white, p), chalcopyrite (pale grey, c), and gangue (black). E9Ec, Western Areas G.M.

**g.** Consolidated 'mudball' composed of minute gersdorffite crystals (white, <40 μm) with cores of galena and pyrite, which are cemented by a mixture of phyllosilicate and quartz (black). E9Gd Reef, Cooke Section.

**h.** Detrital pyrite (white) intergrown with gangue (black) encrusted by authigenic, euhedral pyrite (white). Carbon Leader, Blyvooruitzicht G.M.

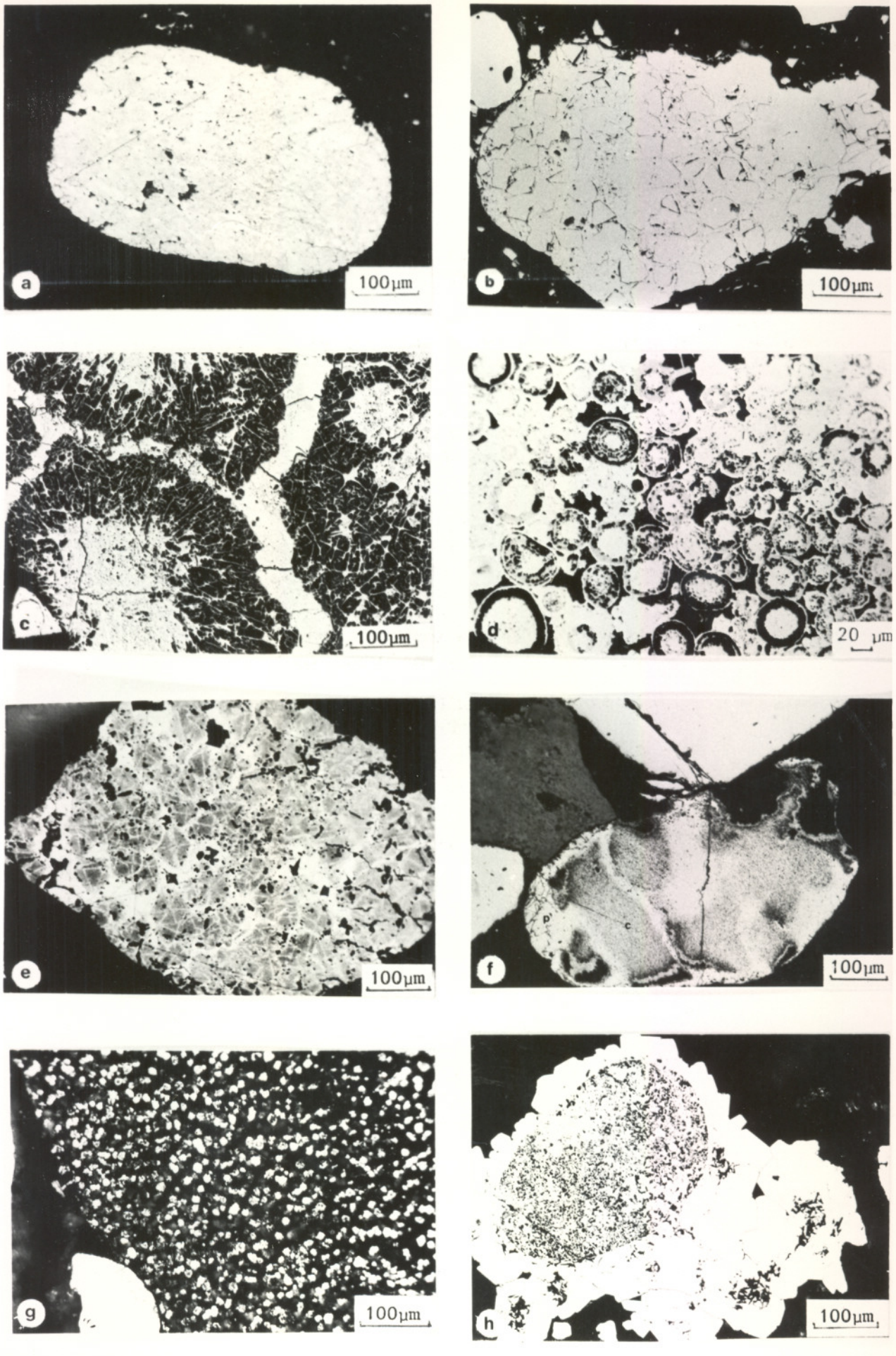

a
100μm
b
100μm
c
100μm
d
20 μm
e
100μm
f
100μm
g
100μm
h
100μm

Figure A.7 Photomicrographs of pyrite
Incident light in oil

**a.** Inclusion of gold (white), pyrrhotite (grey), and chalcopyrite (pale grey), measuring 60 μm, in detrital pyrite (white). Vaal Reef, Western Reefs G.M.

**b.** Pyrite grain (pale grey) intersected by veinlets of pyrrhotite (medium grey). Inherited texture. Kalkoenkrans Reef, Oryx G.M.

**c.** Detrital laminated pyrite (white)-rutile (grey) grain, most likely pseudomorph after ilmeno-hematite. Kalkoenkrans Reef, Oryx G.M.

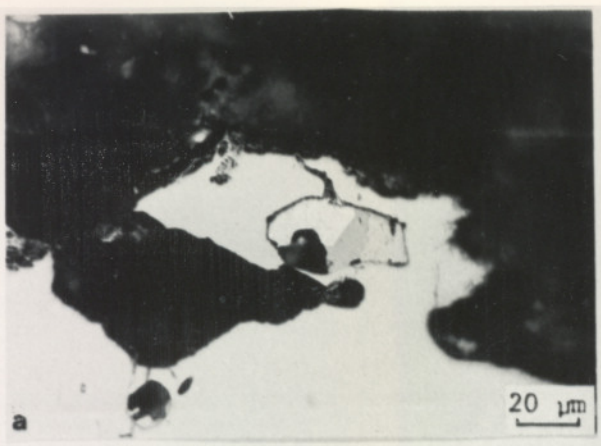
**d.** Concretionary pyrite (white) composed of skeletal, octahedral pyrite crystals, which represent terrace-faced crystal growth, also referred to as hopper crystals. The voids were filled by galena (grey) and some sphalerite (dark grey, on the right). Composite Reef, Cooke Section.

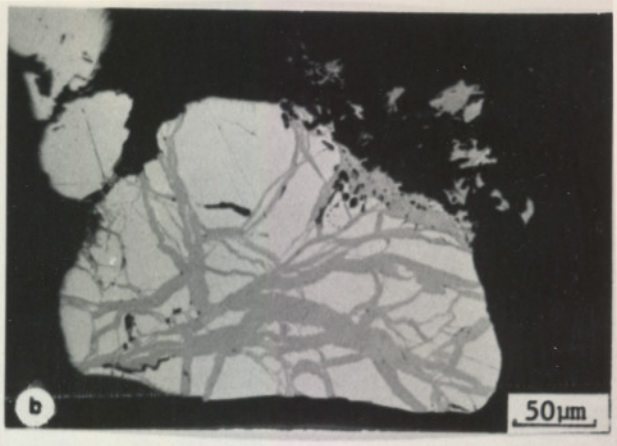
**e.** Concretionary pyrite with colloform texture of alternating pyrite (pale grey), chalcopyrite (dark grey), and quartz (black) lamellae. Composite Reef, Cooke Section.

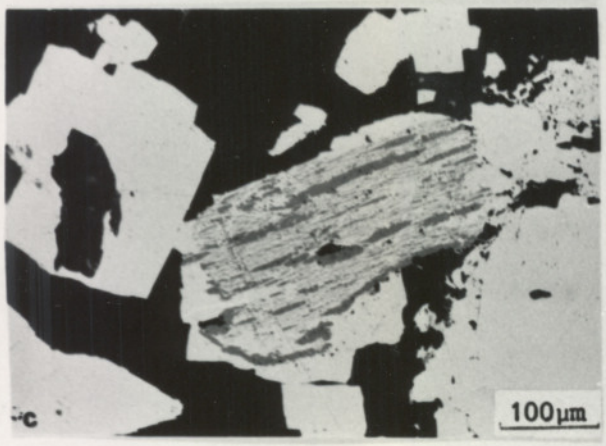
**f.** Gold (white) and chalcopyrite (grey, c) inclusions of irregular, angular outline in concretionary pyrite (pale grey). Gangue is black. UE1a Reef, Cooke Section.

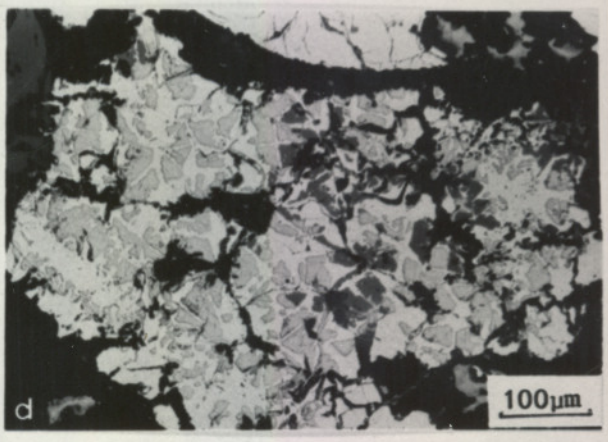
**g.** Detrital chloritized (black) chromite (grey) and pyrite (white) corroded by uranous titanate (black) and cemented by pyrite. Vaal Reef, Western Reefs G.M.

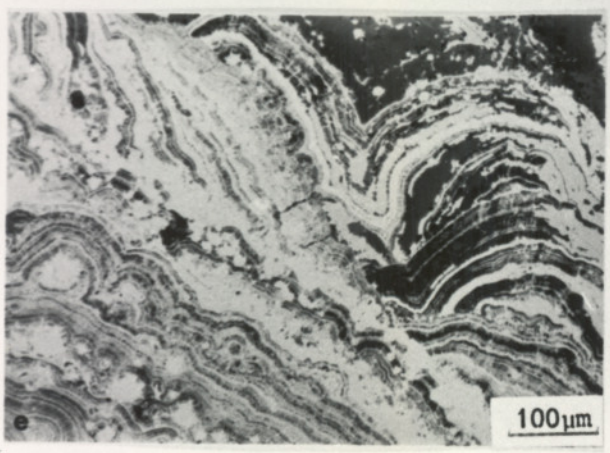
**h.** Uraniferous leucoxene (dark grey) particles cemented by pyrite in pyrite-rich horizon at the area where the UE1a Reef is transgressively overlain by the E9 Reef. Composite Reef, Cooke Section.

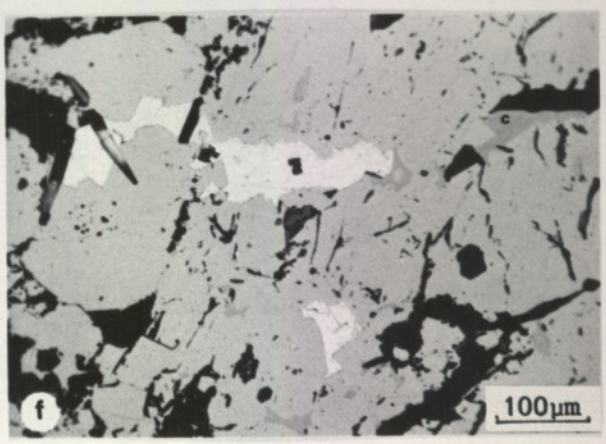

a
20 µm

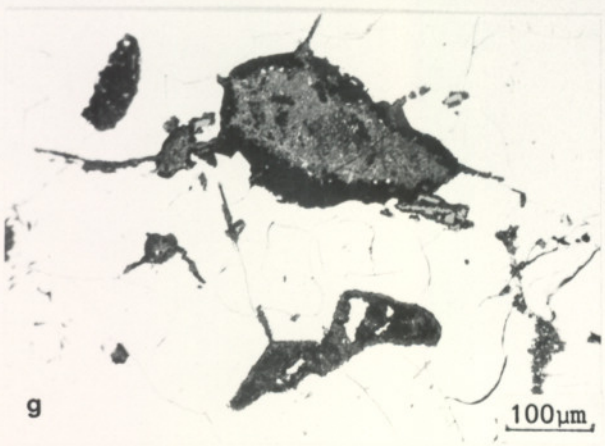

b
50µm


c
100µm


d
100µm


e
100µm


f
100µm


g
100µm

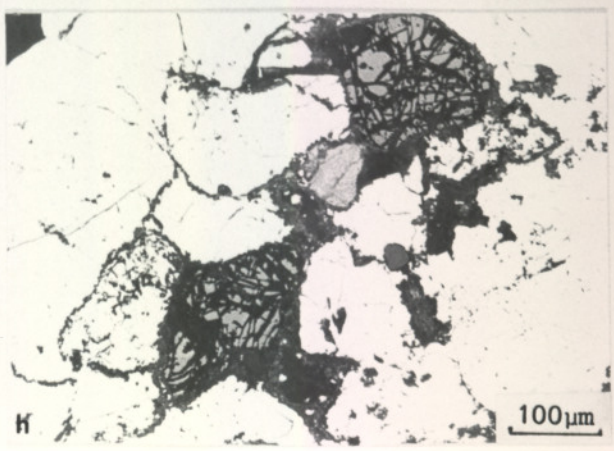

h
100µm

Figure A.8 Photomicrographs of sulphides, chromite, tantalaeschynite, and garnet
Incident light in oil

**a.** Boudinage texture of detrital sphalerite (pale grey, sl) enclosed by kerogen (grey). The voids between the sphalerite and neighbouring quartz (dark grey, q) fragments were filled by chlorite (black). Vertical direction from left to right. The polished section was subjected to leaching tests, so that the very small uraninite inclusions (5 μm) were replaced by anglesite (black). Basal Reef, President Brand G.M.

**b.** 1 to 2 mm-wide compact layer of a mixture of pyrite, marcasite, and pyrrhotite (white to pale grey, pmp) underlain by a quartzite (dark grey), and overlain by a horizon of heavy minerals (small white grains) and quartz, about 5 mm thick, which was deposited before the small-pebble conglomerate with larger pyrite grains (white) above it. Leader Reef, Harmony G.M.

**c.** Close up of the pyrite-marcasite-pyrrhotite layer (pmp) in (b). At the base, pyrrhotite blades were replaced pseudomorphously by a mixture of pyrite (white) and marcasite (pale-grey, irregular shaped). In upward direction this mixture is followed by massive pyrrhotite (grey) which locally encloses galena (grey). Leader Reef, Harmony G.M.

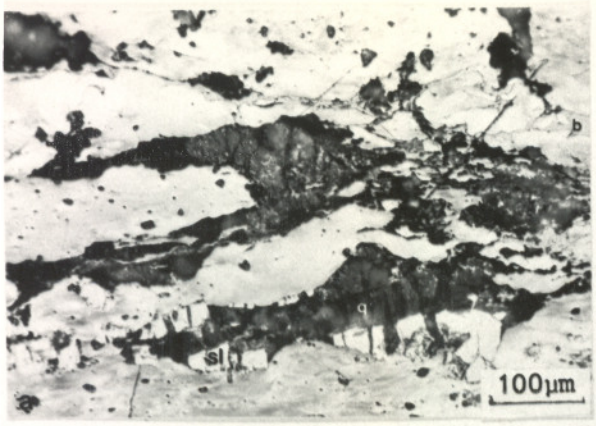
**d.** Molybdenite flake (pale grey). Kalkoenkrans Reef, Oryx G.M.

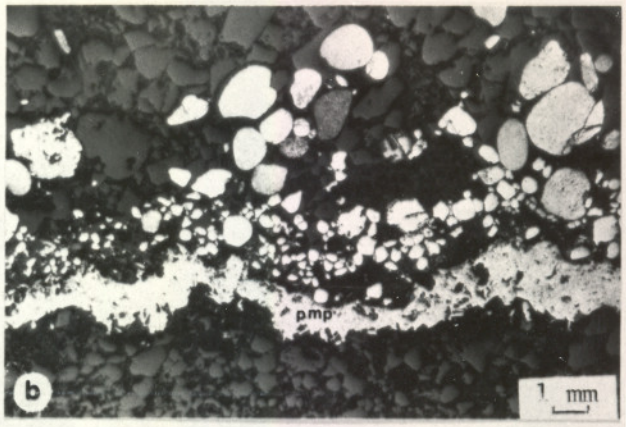
**e.** Fractured, detrital arsenopyrite (white) partly replaced by chlorite (black) and rutile (grey in the left portion), covered by a film of minute brannerite crystals (pale grey). The arsenopyrite encloses galena (g). Leader Reef, Virginia G.M.

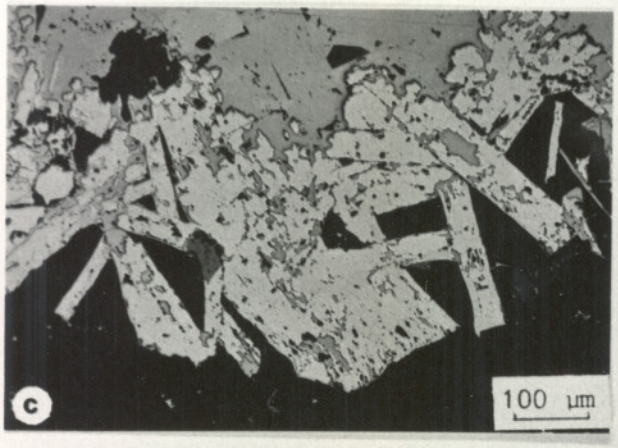
**f.** Chromite grain partly replaced by oriented rutile prisms. Kalkoenkrans Reef, Oryx G.M.

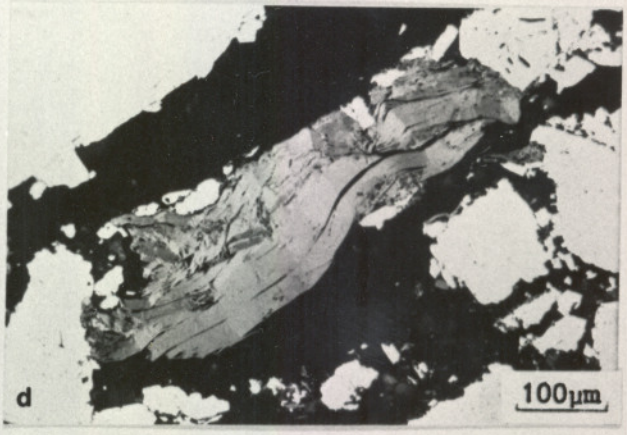
**g.** Detrital grain of fractured tantalaeschynite (grey), a (Ta,Ti,Nb)-oxide, intergrown with a component of slightly different composition (darker grey). Rutile (darkest grey) healed some of the fractures, and enveloped a hackly gold particle (white). Kalkoenkrans Reef, Oryx G.M.

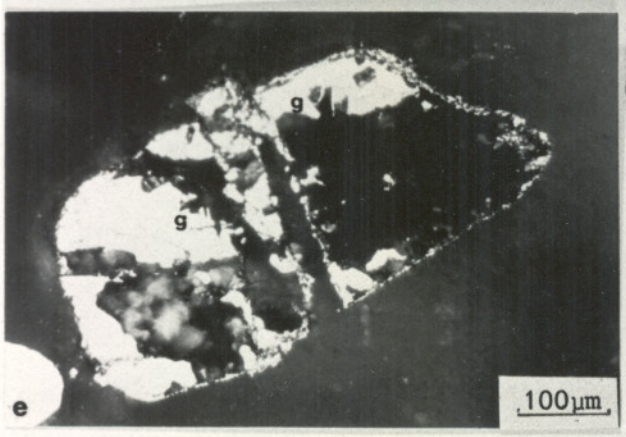
**h.** Garnet (grey) partly replaced by quartz (white and pale grey), and little chlorite (dark grey, feathery). To the right of the garnet are numerous uraninite grains (black). Transmitted light. Uraninite-rich layer overlying the Upper Reef of the Dominion Reef, Bramley G.M.

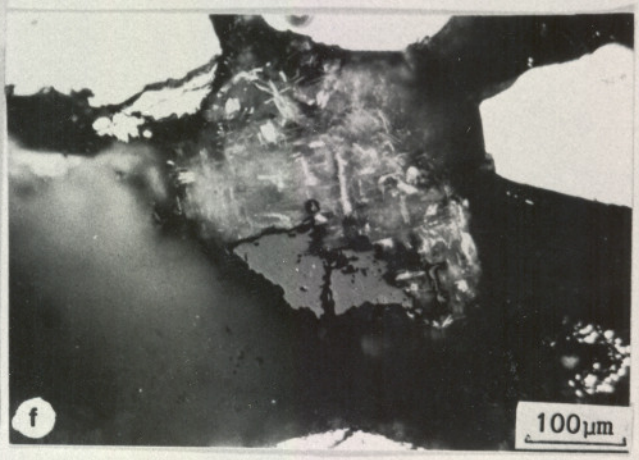

b
q
sl
100µm

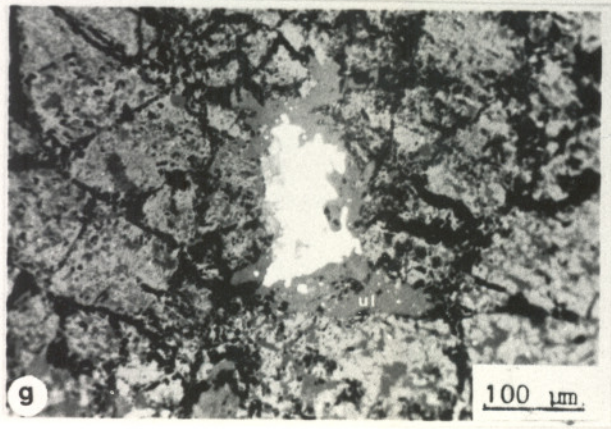

pmp
b
1 mm


c
100 µm


d
100µm


g
g
e
100µm


f
100µm


ul
g
100 µm

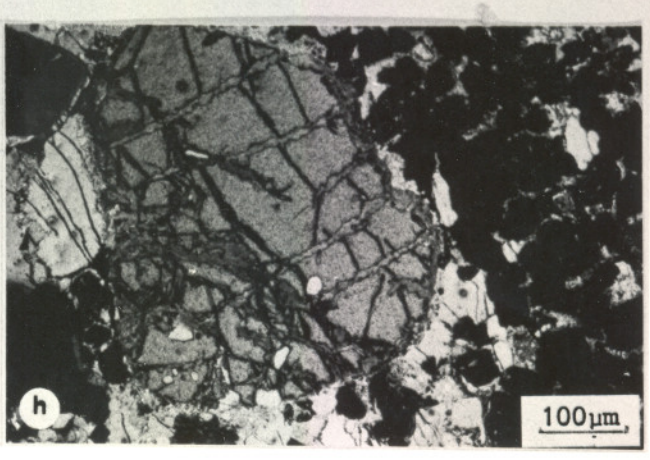

h
100µm

Figure A.9 Photomicrographs of gersdorffite
Incident light in oil

**a.** Partly chloritized (black) pyrite (white) enveloped by a film of minute gersdorffite (white) particles. Pale grey particles are kerogen nodules. Gangue is quartz (dark grey). Beisa Reef, Beisa G.M.

**b.** Reconstituted gold (white) surrounded by authigenic gersdorffite (pale grey). Vaal Reef, Western Reefs G.M.

**c.** Cutan of minute gersdorffite crystals enveloping a uraninite grain (grey) which is incipiently altered to coffinite along crystal planes (black). Basal Reef B3, Harmony G.M.

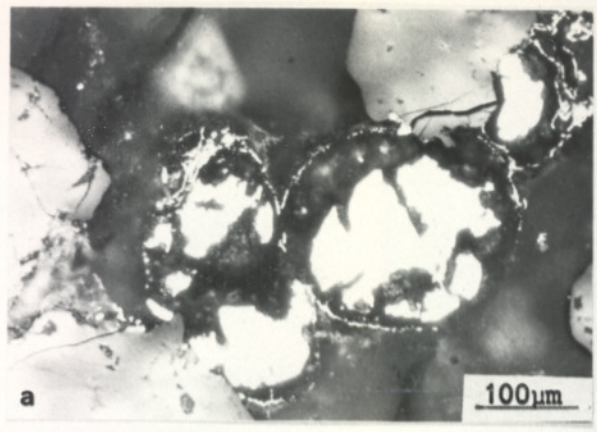
**d.** Group of relict uraninite grains, the shape of which has been preserved by gersdorffite cutans (white). The leached space was filled by quartz (q). Two anatase (a) grains in left top corner. Leader Reef, Harmony G.M.

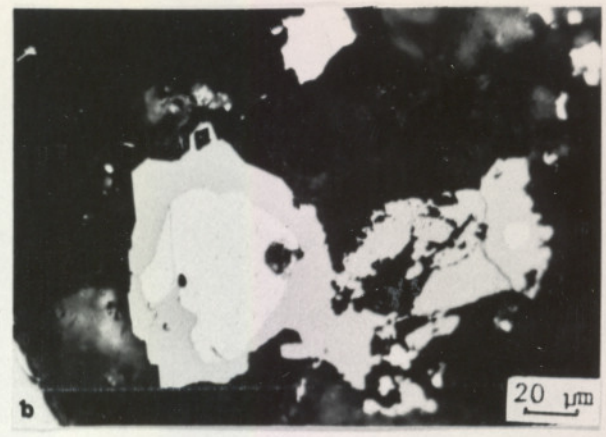
**e.** Two kerogen (k) nodules enclosing uraninite (grey, u) are covered by gersdorffite (white) crystals. Vaal Reef, Buffelsfontein G.M.

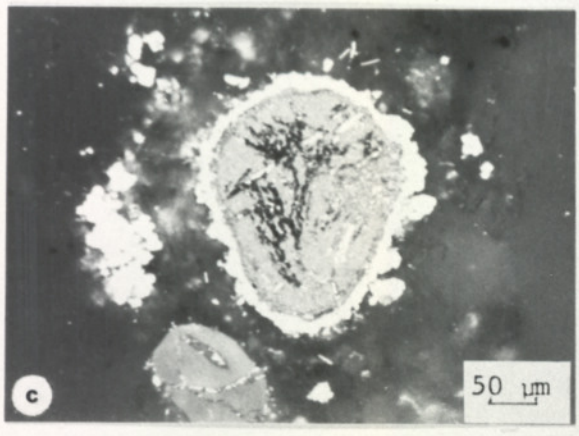
**f.** Kerogen nodule (grey) enclosing uraniferous leucoxene (pale grey) was first covered by a gersdorffite cutan (white), and then overgrown by a younger generation of kerogen (dark grey) devoid of uraninite. Basal Reef, Harmony G.M.

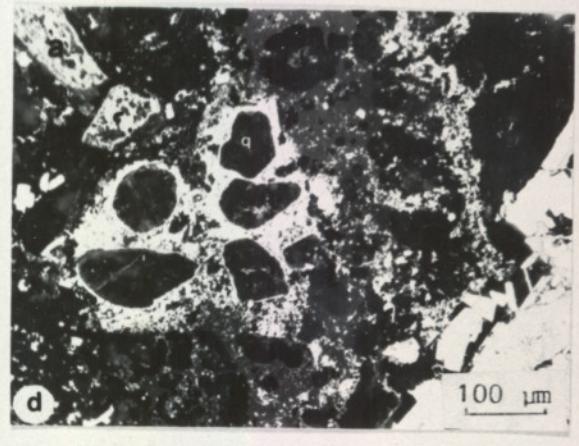
**g.** Crystal, 40 μm in diameter, composed of a core of pyrite (white) overgrown by a zone of galena (grey), and then by gersdorffite (g). Basal Reef B3, Harmony G.M.

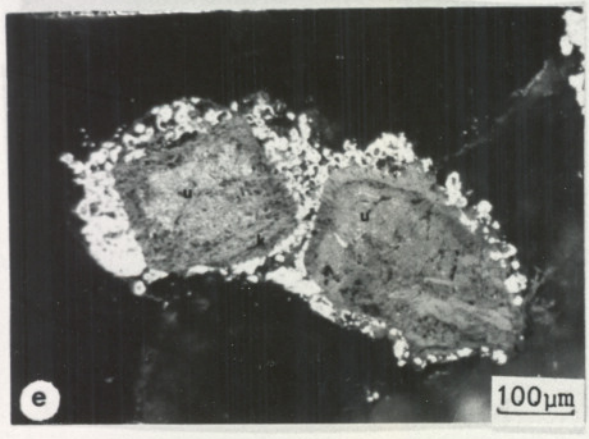
**h.** Two generations of kerogen; the oldest (pale grey), which encloses uraninite, displays pregraphitic optical properties. The younger generation (darker grey) is devoid of uraninite and encloses gersdorffite crystals. Vaal Reef, Buffelsfontein G.M.

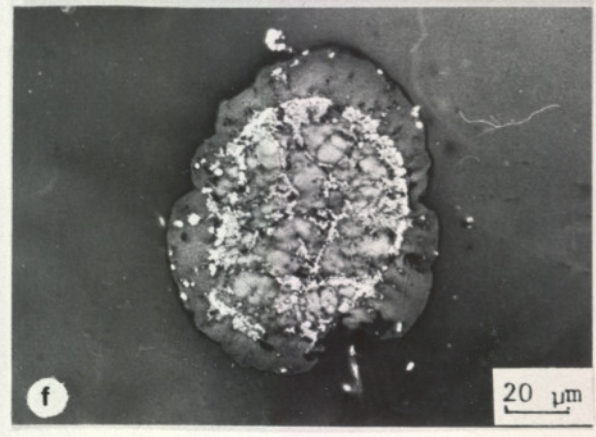

a
100µm

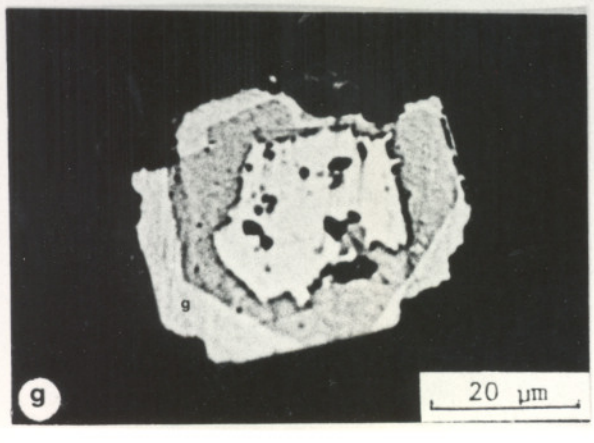

b
20 µm


c
50 µm


d
100 µm


e
100µm


f
20 µm


g
20 µm

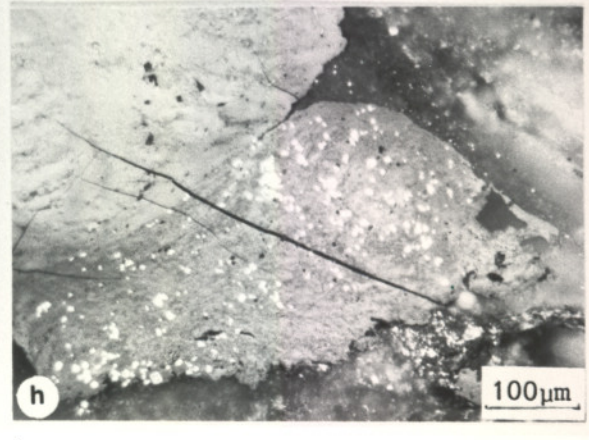

h
100µm

Figure A.10 Photomicrographs of cheralite, titania, and chromite
Incident light in oil

**a.** A grain of the thorium phosphate cheralite (very pale grey) with a core of thorite (black) surrounded by a sericite-quartz (white) matrix and quartz grains (black). Dominion Reef, Bramley G.M.

**b.** Detrital grain of intergrown rutile and pyrite. Kalkoenkrans Reef, Oryx G.M.

**c.** Geode-like fillings represent pseudomorphs after ilmenite. In the large pseudomorph after ilmenite, stubby rutile crystals (white), which possibly formed from anatase, lined the cavity, whereas chlorite (black) filled the open space in the centre. Dominion Reef, Bramley G.M.

**d.** Submicroscopic Ti-bearing spherules (white spots), measuring <2 μm, at the surface of quartz (dark grey) grains. The bigger white spots (<10 μm) are gold grains. Carbon Leader, Blyvooruitzicht G.M.

**e.** Cluster of chromite (grey) and pyrite (white) grains. E9Ec Reef, Western Areas G.M.

**f.** Chromite grain (grey) with thin iron-enriched margin of brighter reflectance. Vaal Reef, Hartebeestfontein G.M.

**g.** Chromite (grey) pervaded by zinc (dark grey) and rutile (pale grey), which precipitated along crystal planes and cracks. Basal Reef, Harmony G.M.

**h.** Chromite grain marginally altered to brannerite in which radiogenic galena occurs. Carbon Leader, Blyvooruitzicht G.M.

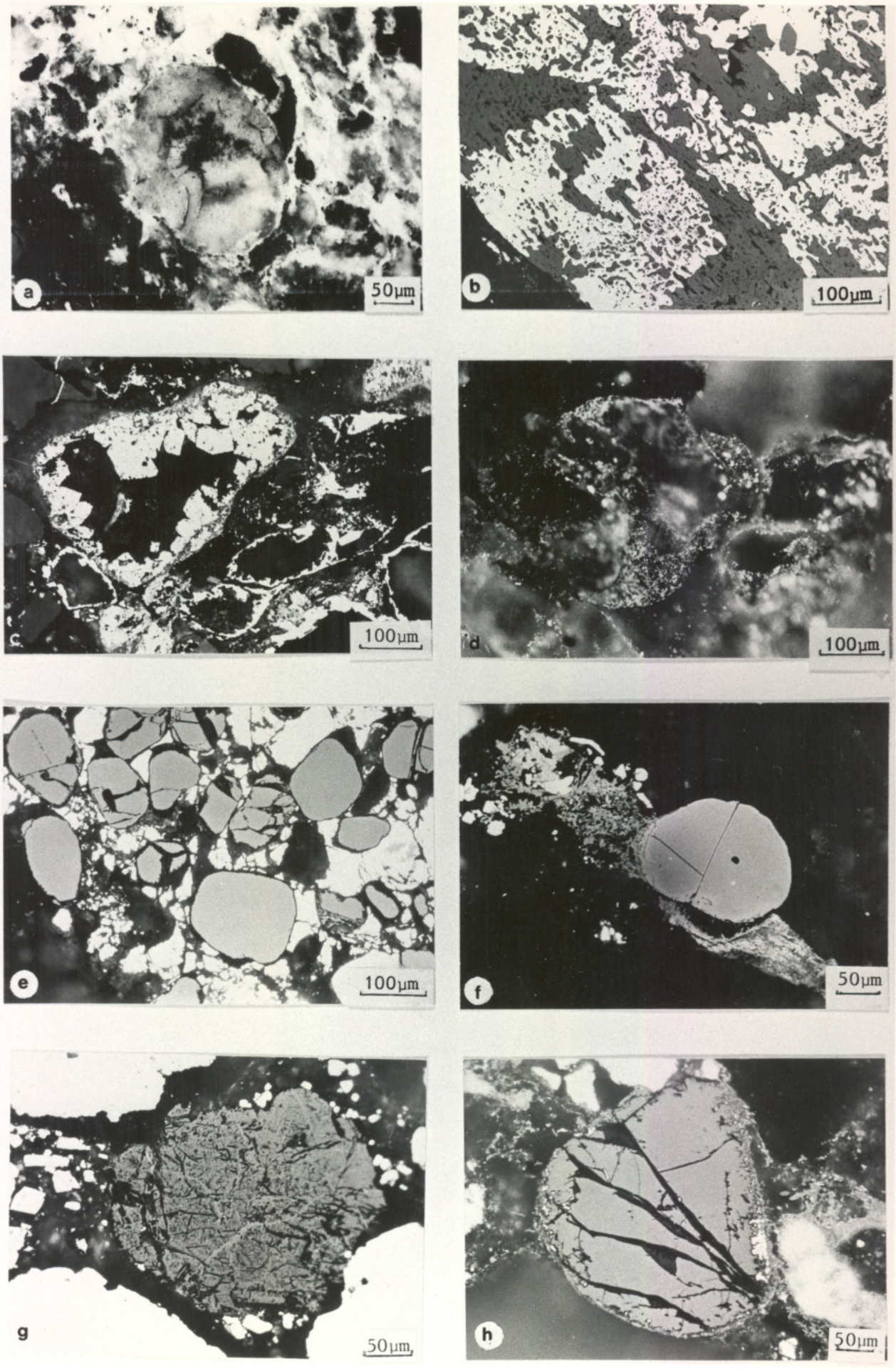

a
50µm
b
100µm
c
100µm
d
100µm
e
100µm
f
50µm
g
50µm
h
50µm

Figure A.11 Photomicrographs of titania
Incident light in oil

**a.** Polished section of footwall quartzite (grey and pale grey mixture) overlain by a thin pyrite-rich heavy-mineral concentration (white speckled) which was deposited before the overlying gritty quartzite, again followed by fine-grained quartzite devoid of heavy minerals. The footwall quartzite is in the upper part over 1 cm strongly enriched in rutile (pale grey, laminated). Macrophotograph. Incident light in air. Carbon Leader, Western Deep Levels G.M.

**b.** Rounded rutile-leucoxene pseudomorph moulded onto pyrite (white). The compact rutile core (pale grey, r) is separated from the leucoxene margin (paler grey, lc) by an interrupted film of pyrite (white). Basal Reef, Harmony G.M.

**c.** Rutile-leucoxene (resp. pale grey and white) pseudomorph moulded by pyrite (black) and quartz (dark grey). Basal Reef, Harmony G.M.

**d.** Rutile-leucoxene pseudomorph (white) in which compact rutile (pale grey) occurs in the margin. The grain is moulded by surrounding quartz grains (black) and overgrown by minute prisms of authigenic rutile. Carbon Leader, Western Deep Levels G.M.

**e.** Rutile-leucoxene pseudomorph (white) enclosing uranous titanate (grey) which precipitated in available open space and at the surface of the grain. Vaal Reef, Buffelsfontein G.M.

**f.** Leucoxene pseudomorph (white) onto which brannerite (dark grey at right bottom) precipitated in which minute specks of radiogenic galena (white) are dispersed. Basal Reef, Harmony G.M.

**g.** Brannerite crystals (dark grey) and quartz (black) precipitated in the central void of the rutile (grey)-leucoxene (speckled pale grey) pseudomorph. Monarch Reef, West Rand Consolidated G.M.

**h.** Rutile-leucoxene (white) pseudomorph exhibiting relict cleavage. Brannerite (grey, b) filled voids in the lower half and upper part, and also precipitated at the surface of the grain (at the top and at right bottom). Leader Reef, Virginia G.M.

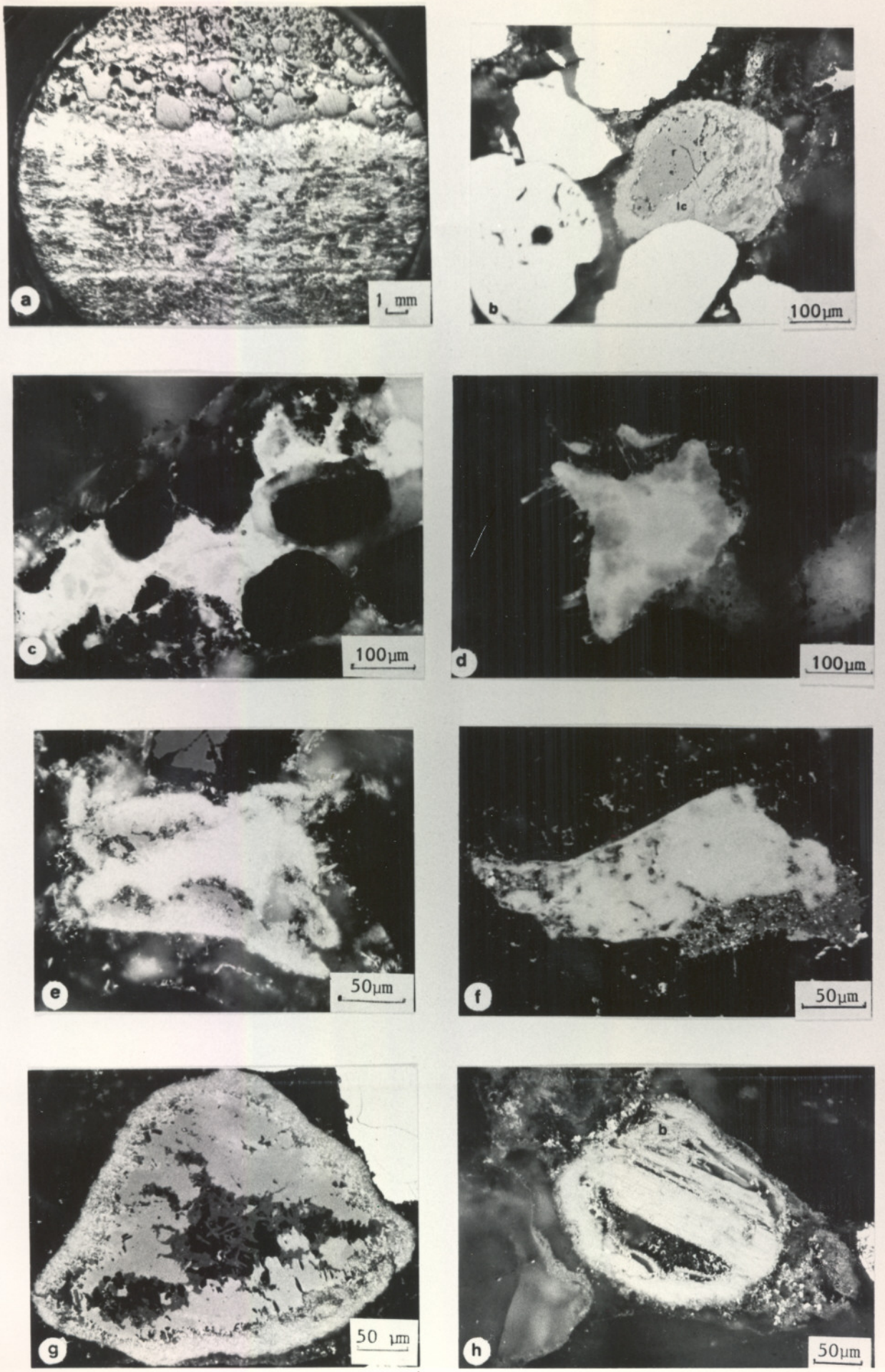

a
1 mm
b
lc
100µm
c
100µm
d
100µm
e
50µm
f
50µm
g
50 µm
h
b
50µm

Figure A.12 Photomicrographs of chromite
ıncident light in oil

**a to e.** Chromite grains (dark grey in (a), (b), and (d), pale grey in (c)) in different stages of replacement by rutile (white) intergrown with phyllosilicate. In (e) the shape of the grain (compare with grain in Figure A.9a) suggests that it is a chromite which has been completely replaced by chlorite and rutile; the grain is outlined by small pyrite particles. In (a) and (b), rutile prisms occur at random, in (c) the rutile is leucoxenic, and in (d) and (e) the prisms are oriented. Figs. a, d and e: Kalkoenkrans Reef, Oryx G.M.; Fig. b: Vaal Reef, Western Reefs G.M.; Fig. c: Carbon Leader, West Driefontein G.M.

**f.** Chromite (dark grey) enveloped by uraniferous leucoxene. Galena (white) precipitated in the margin of the grain. Vaal reef, Vaal Reefs South G.M.

**g.** Euhedral chromite (pale grey) with rounded corners marginally corroded by brannerite; radiogenic galena (white) precipitated in the margin. Zircon to the right, and a leucoxene grain replaced by brannerite to the left. Vaal Reef, Vaal Reefs East G.M.

**h.** Chromite (grey) pervaded by zinc (dark grey dendrites). Basal Reef, Harmony G.M.

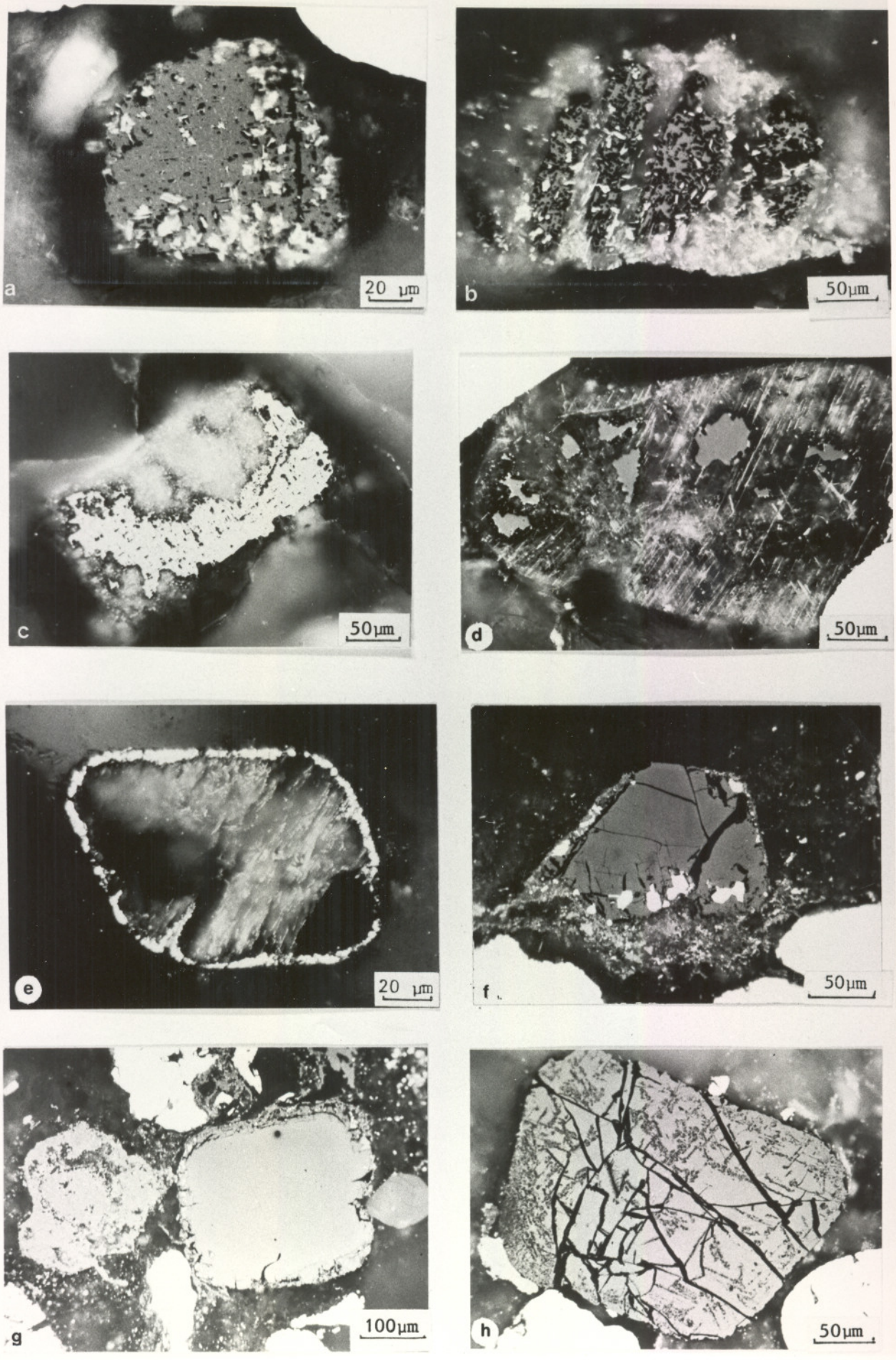

a
20 µm
b
50µm
c
50µm
d
50µm
e
20 µm
f
50µm
g
100µm
h
50µm

Figure A.13 Photomicrographs of chromite, zircon, and gold
Incident light in oil

**a and b.** Chromite (spotted grey) in which zinc is homogeneously distributed, imparting a micro-dot texture to the grain. (a) UE1a Reef, Cooke Section; (b) White Reef, West Rand Consolidated G.M.

**c.** Zoned zircon in which radioactive zones predominate. The metamict zones (slightly darker than the pure zircon) reacted when the polished section was subjected to leaching in dilute sulphuric acid. Leader Reef, Virginia G.M.

**d.** Euhedral zircon (grey) with a metamict core of crumbled texture, in which white spots of radiogenic galena are dispersed. Cracks in the unaltered, marginal zircon result from expansion of the core. Basal Reef, President Brand G.M.

**e.** Gold particles (white, scratched surface) between detrital pyrite (white) and in quartz (black). Carbon Leader, Western Deep Levels G.M.

**f.** Gold (white) inclusions in pyrite (pale grey) and 'free' gold particles at quartz (black) boundaries. A concretionary pyrite grain is present in the bottom part of the micrograph. Kalkoenkrans Reef, Oryx G.M.

**g.** Several 'free' gold particles (white) between compact and concretionary pyrite (pale grey), associated and intergrown with small chlorite flakes (black). Kalkoenkrans Reef, Oryx G.M.

**h.** Gold (white, scratched surface) of irregular outline, displaying crystal faces, is surrounded by quartz (black) grains. Vaal Reef, Vaal Reefs East G.M.

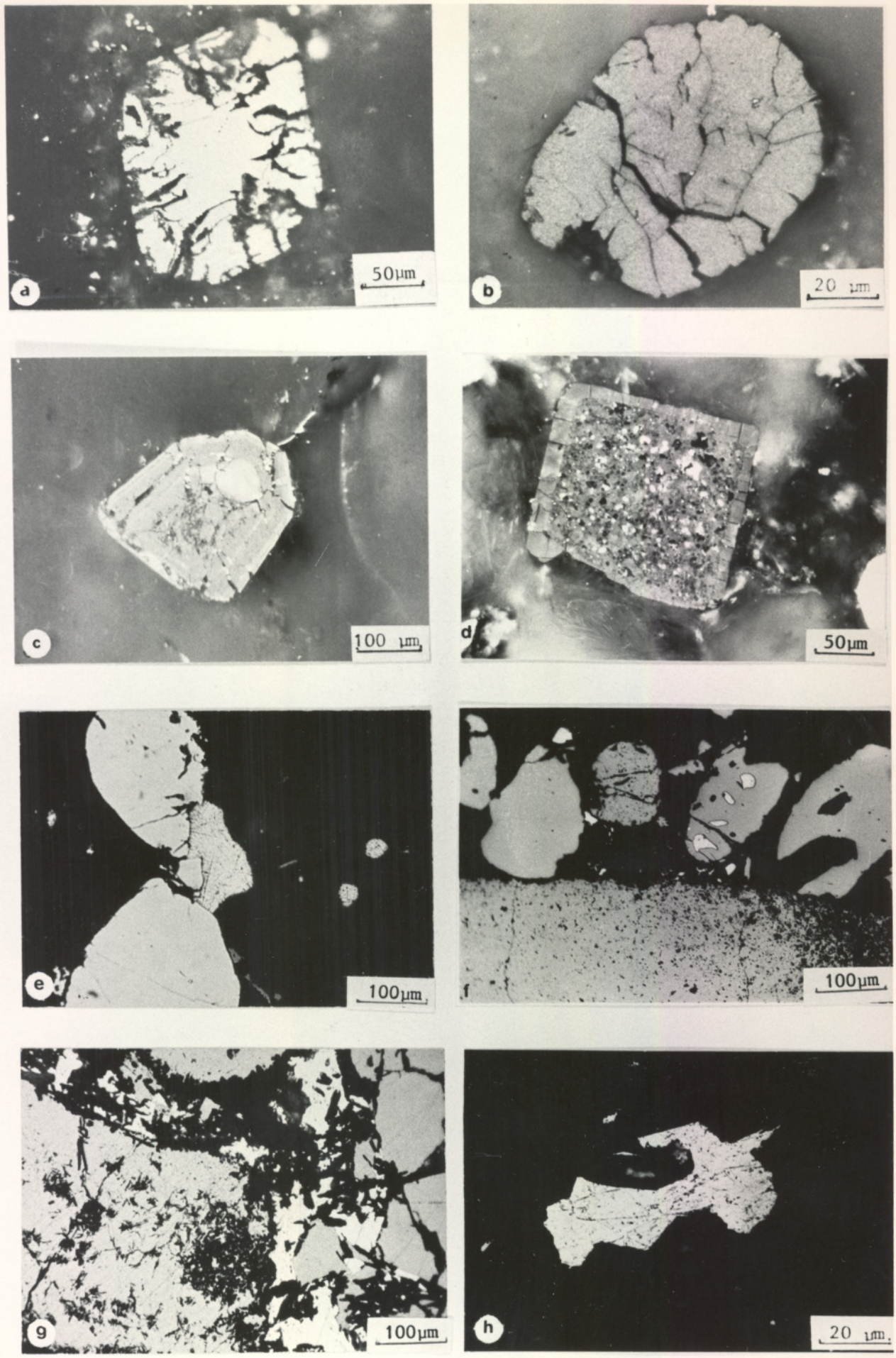
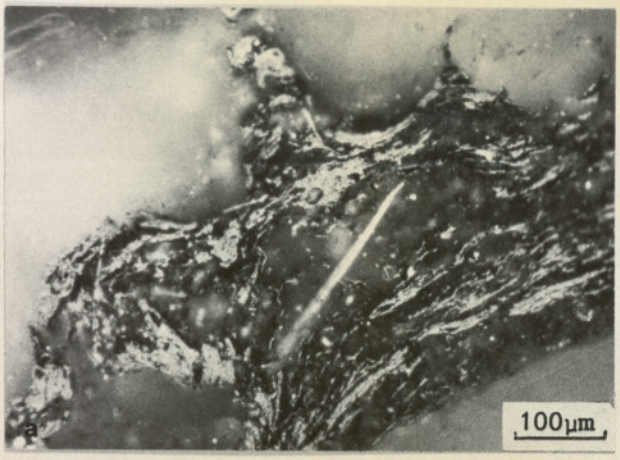

a
50µm
b
20 µm
c
100 µm
d
50µm
e
100µm
f
100µm
g
100µm
h
20 µm

Figure A.14 Photomicrographs of graphite intergrown with chlorite, Kalkoenkrans Reef, Oryx G.M.

**a and b.** Intimate intergrowth of graphite (pale grey in (a) and white in (b)) and chlorite (black) in microstylolites along quartz grains (white and pale grey). Incident light in oil.

**c and d.** SEM photomicrographs of the same feature at large magnification. Graphite is black, chlorite of different compositions in shades of grey. Small elliptic grains are monazite (grey, m) and the minute euhedral crystals are galena (white, g).


a
100µm


b


c

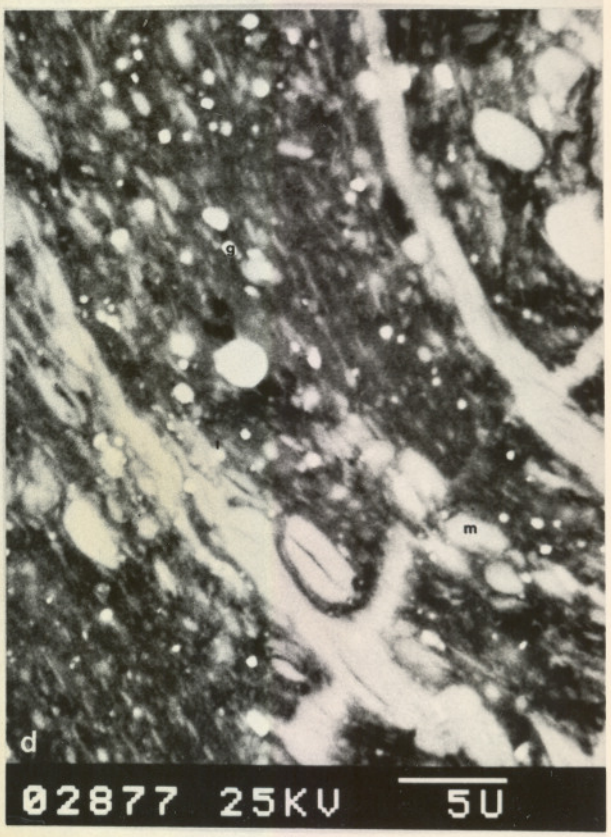

g
m
d
02877 25KV
5U

Figure A.15 Photomicrographs of graphite inclusions in quartz in the Kalkoenkrans Reef, Oryx G.M. (a to f), and Sheba G.M., Barberton (g and h).

**a.** Round, porous particle of very fine-grained flaky graphite.

**b.** Half sphere of flaky graphite aggregate, the texture of which becomes coarser towards the straight boundary on the right.

**c.** Graphite grain of smooth outline composed of spherules of radiating platelets (10 μm in diameter) embedded in finer spherulitic graphite, surrounded by a 15 μm-wide film of columnar graphite.

**d.** Very fine, spherulitic graphite enclosing porous flaky graphite possibly intergrown with phyllosilicate.

**e.** Half sphere of graphite composed mainly of randomly oriented flakes, bordered on flat side by very fine, spherulitic graphite.

**f.** Irregular-shaped particle with coarse, porous texture on the left, grading into very fine spherules (<1 μm) towards the right.

**g.** Boudinaged graphite (pale grey) with geode-like texture in quartz veinlet (dark grey) intersecting metagreywackes.

**h.** Close up of a fragment of graphite from a quartz veinlet, disclosing the coarser flaky texture in the centre, enclosed by very fine spherulitic graphite.

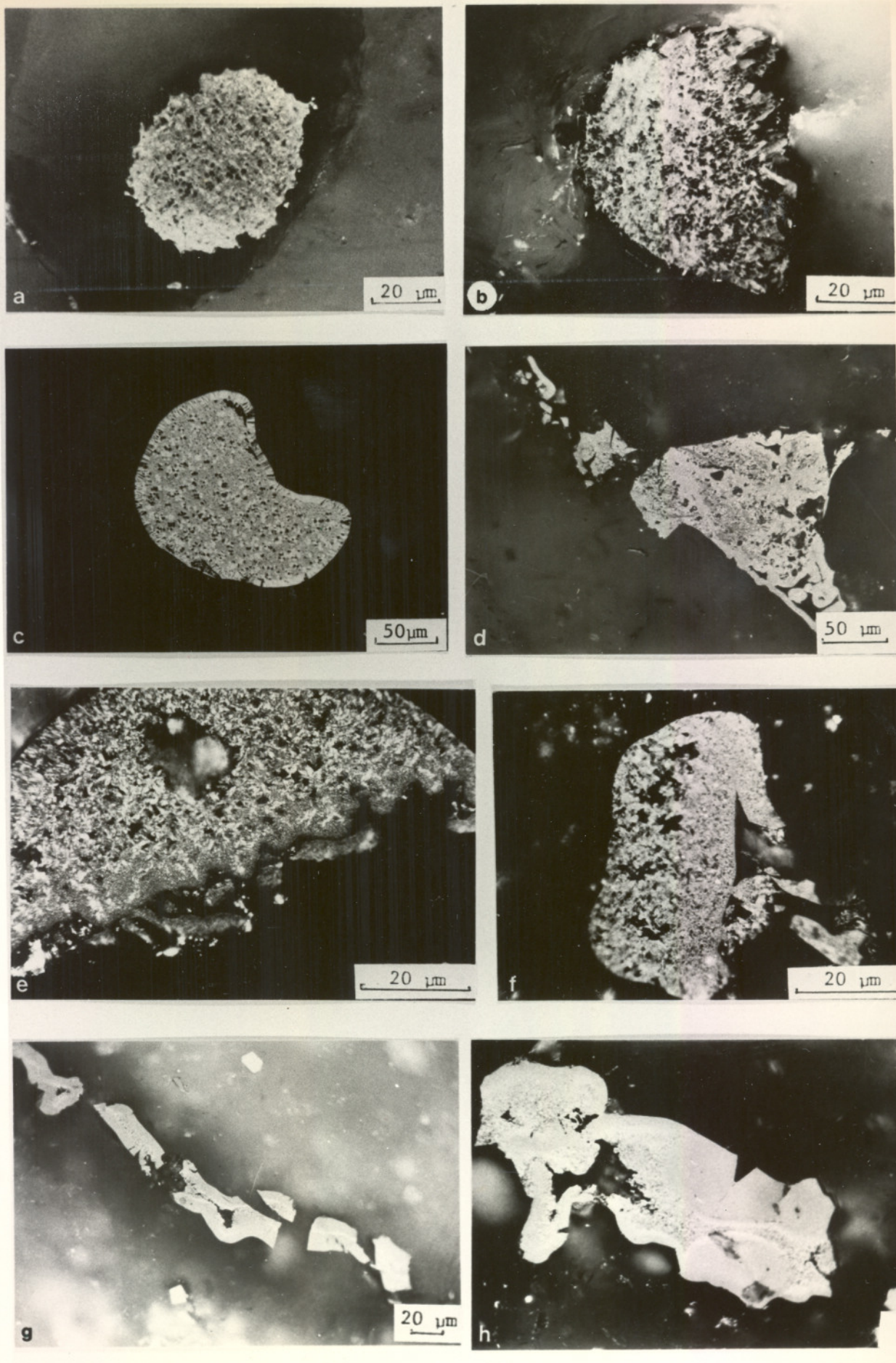

a
20 µm
b
20 µm
c
50µm
d
50 µm
e
20 µm
f
20 µm
g
20 µm
h

Figure A.16 Photomicrographs of polymineralic spheroids
Transmitted light

**a.** Spheroid in which concentric muscovite or pyrophyllite (pale grey, m) surrounds a core of quartz (q). Kalkoenkrans Reef, Oryx G.M.

**b.** Two spheroids composed of a chlorite core (grey), surrounded by concentric muscovite or pyrophyllite (pale grey). A few quartz inclusions (almost white) are present. The cross-section of the particle on the right is six-sided. Kalkoenkrans Reef, Oryx G.M.

**c.** Chloritized (dark grey) spheroid of isometric shape, with few, small remnants of garnet (pale grey), and sericite filling cracks (pale grey). Kalkoenkrans Reef, Oryx G.M.

**d.** Six-sided cross-section of spheroid composed of zoned muscovite or pyrophyllite and chlorite, surrounding a core of quartz. Kimberley Reef, Grootvlei G.M.

**e.** Chlorite (grey) and quartz (white) fill cracks in garnet (pale grey). Small black particles around altered garnet are mostly uraninite grains. Dominion Reef, Bramley G.M.

**f.** Spheroid composed of a mixture of chlorite (grey), quartz (white and pale grey), and apatite (white, a). The speroid is outlined by a film of minute pyrite particles (black). Kimberley Reef, Grootvlei G.M.

**g and h.** Spheroids in which chlorite (black) enclosing some dispersed rutile (white) envelopes a core of titania (white) mixed with quartz and/or sericite or pyrophyllite. Incident light in oil. Kalkoenkrans Reef, Oryx G.M.

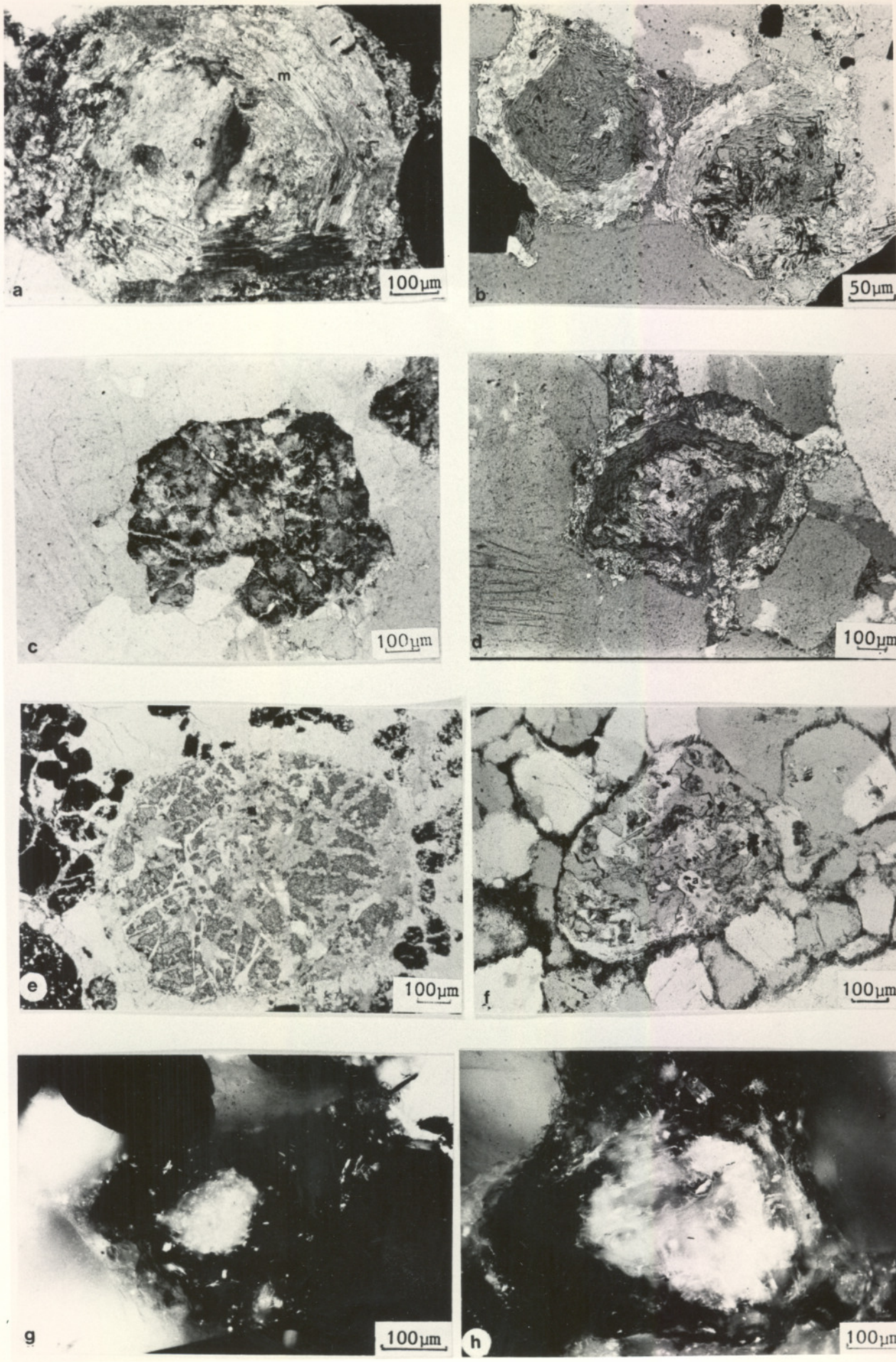

m
α
a
100μm
b
50μm
c
100μm
d
100μm
e
100μm
f
100μm
g
100μm
h
100μm

Figure A.17 Photomicrographs of gold
Incident light in oil

**a.** Detrital cobaltite (pale grey) encloses irregular-shaped gold (white), chalcopyrite (grey), and sphalerite (dark grey). Kalkoenkrans Reef, Oryx G.M.

**b.** Detrital pentlandite (pale grey) intergrown with phyllosilicate (black), which contains about 70 particles of gold (white), most of which measure less than 10 μm. Kalkoenkrans Reef, Oryx G.M.

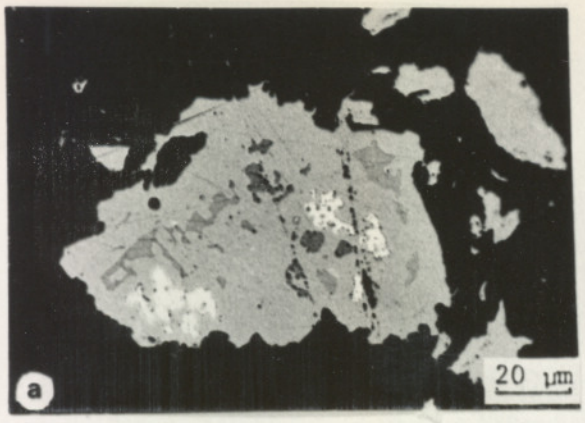
**c.** Recrystallized gold (white, scratched surface) between compact pyrite (grey) grains and concretionary pyrite (grey, porous), and quartz (black). Basal Reef, President Brand G.M.

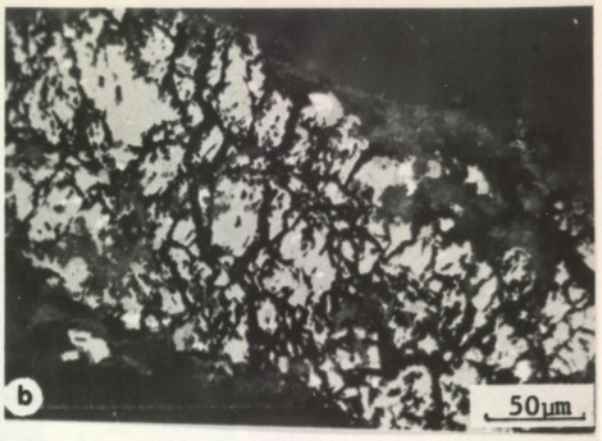
**d.** Gold (white) and pyrrhotite (dark grey) filling a crack in pyrite (pale grey). Vaal Reef, Buffelsfontein G.M.

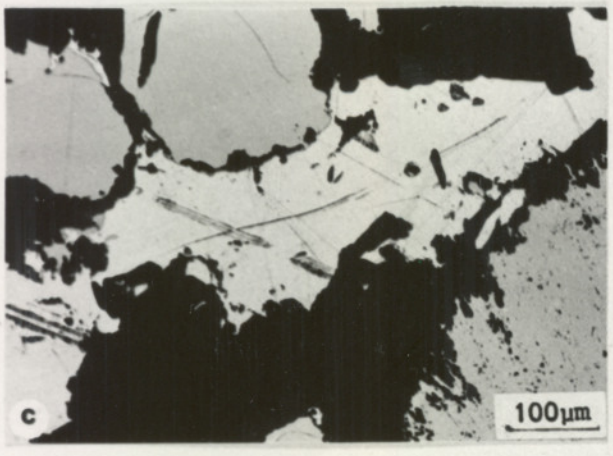
**e.** Shattered zircon (grey) in which gold (white) precipitated in a crack. A large part of the grain is metamict (dark grey, left side, m). White patches are leucoxene; quartz is black. Vaal Reef, Western Reefs G.M.

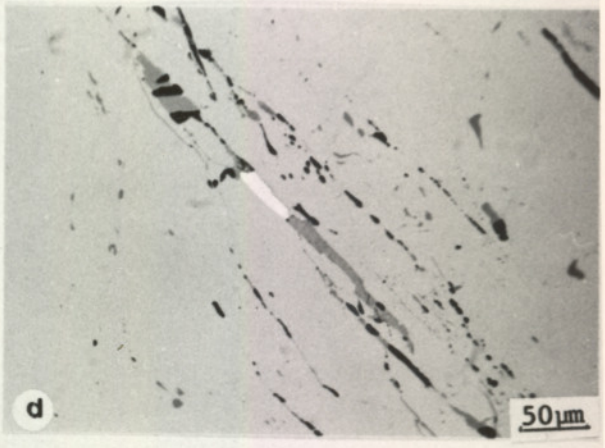
**f.** Group of detrital uraninite (dark grey) pigmented by minute galena specks (white), partly altered to coffinite (black), and coated by a film of uraniferous leucoxene (pale grey). In the muffin-shaped grain on the left, gold (white) is present. Basal Reef, President Brand G.M.

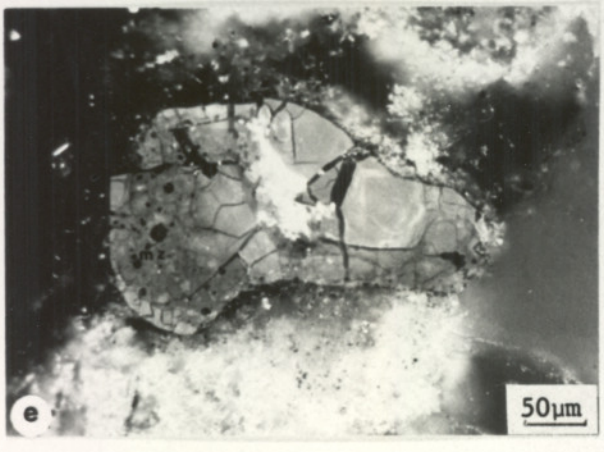
**g and h.** Gold (white) filling interfilamental space and other voids in uraninite-bearing kerogen (shades of grey). Basal Reef, President Brand G.M.

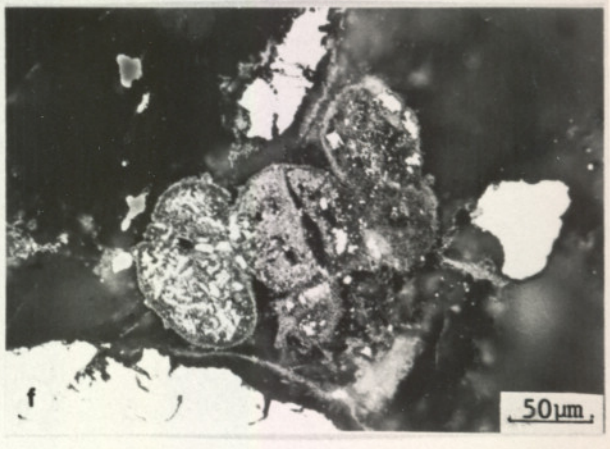

a
20 µm

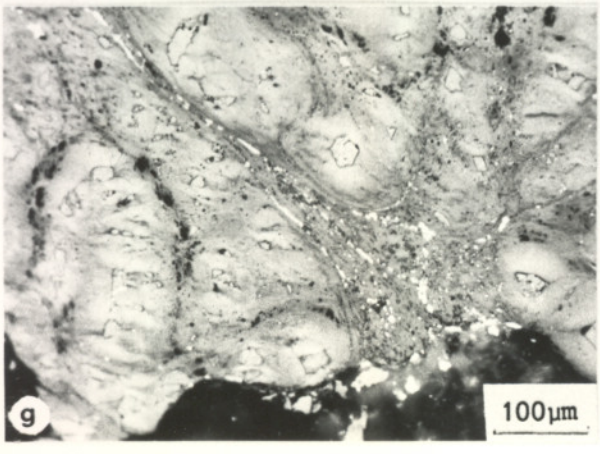

b
50µm


c
100µm


d
50µm


e
50µm


f
50µm


g
100µm

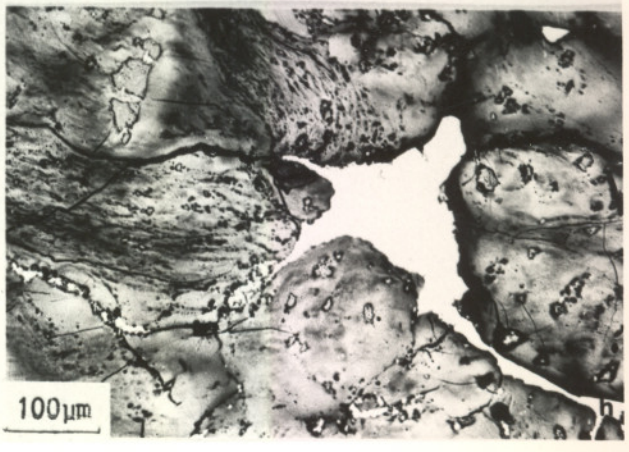

100µm

Figure A.18 Photomicrographs of gold
Incident light in oil

**a.** Gold (white) which precipitated with authigenic pentlandite (pale grey, p) at the base of a pyrite layer. Compact pyrite (pale grey) at top, and concretionary pyrite (pale grey, porous) at bottom right. Elsburg Reef, Western Reefs G.M.

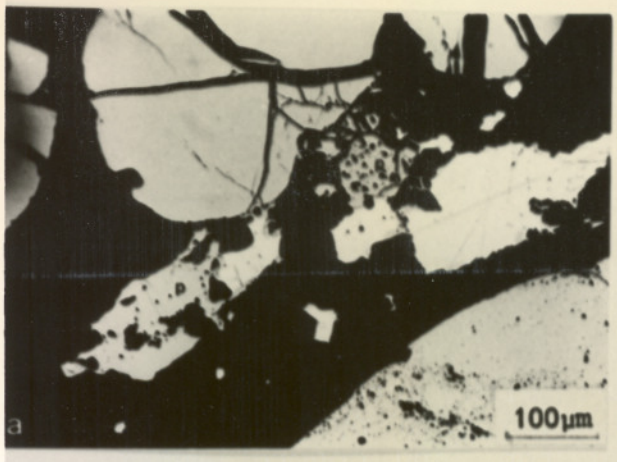
**b.** Gold, (white, Au) which recrystallized together with pyrrhotite (po) at the surface of a kerogen seam (shades of grey). The pyrrhotite is boudinaged (minute parallel cracks) but not the enclosed gold. Cleats (black) formed in the kerogen parallel to the plane of deposition. Carbon Leader, Blyvooruitzicht G.M.

**c.** Horizontal cross-section at base of kerogen seam ashed at $300^0$C. Several gold platelets (white) are present. The porous residue consists of a phyllosilicate (pale grey) and uraninite fragments (black spots). The larger black areas are cracks. Basal Reef, President Brand G.M.

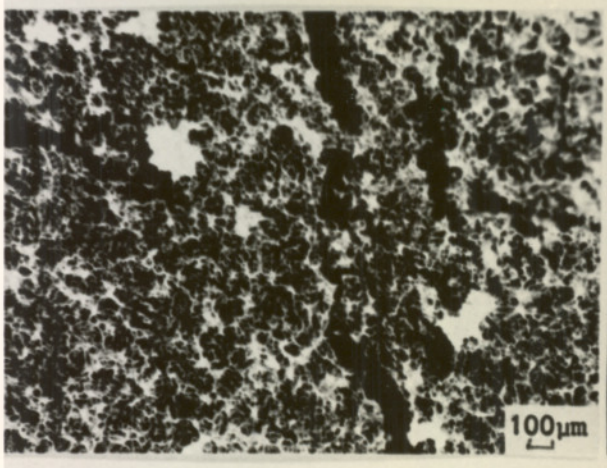
**d.** Detrital cobaltite (grey) overgrown by authigenic gersdorffite (grey, g) which encloses gold particles (white). Vaal Reef, Vaal Reefs East G.M.

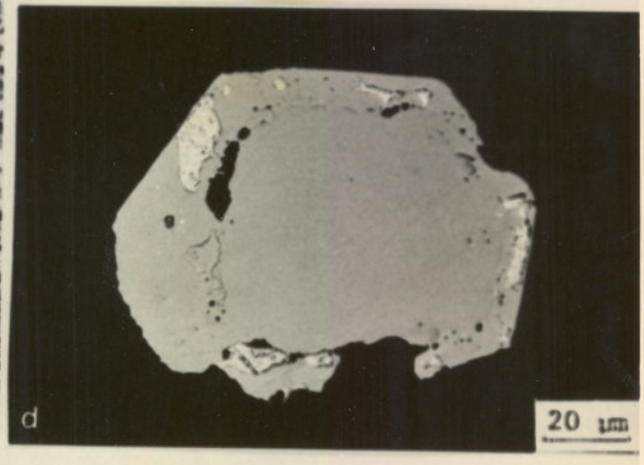
**e.** Angular inclusions of gold (white, Au) and of silver-bearing tetrahedrite (grey) in pyrite (white) occurring at the contact (indistinguishable in the micrograph) of two generations of pyrite. The younger, outer portion is idiomorphic. Consort Gold Mine, Barberton.

**f.** Gangue minerals (black) cemented by reconstituted gold (white), with a round inclusion of tetrahedrite (pale grey, top centre). Monarch Reef, Randfontein Estates G.M.


a
100μm


Au
b
50μm


100μm


d
20 μm


Au
e
50μm

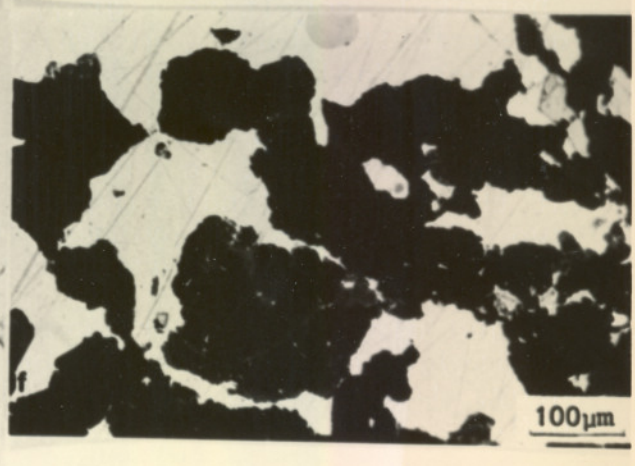

f
100μm

Figure A.19 Photomicrographs of uraninite
Incident light in oil

**a.** Spherical uraninite grain, flattened on right-hand side. Radiogenic galena (white) migrated to cracks or coalesced to larger grains. Basal Reef, President Brand G.M.

**b.** Cluster of uraninite grains (grey) spotted by radiogenic galena (white). Monarch Reef, West Rand Consolidated G.M.

**c.** Well-packed cluster of uraninite grains, which are incipiently altered to coffinite (black rims). Radiogenic galena (white) migrated to grain boundaries and to fracture in centre. Compare with Figure A.22a. Monarch Reef, East Champ d'Or G.M.

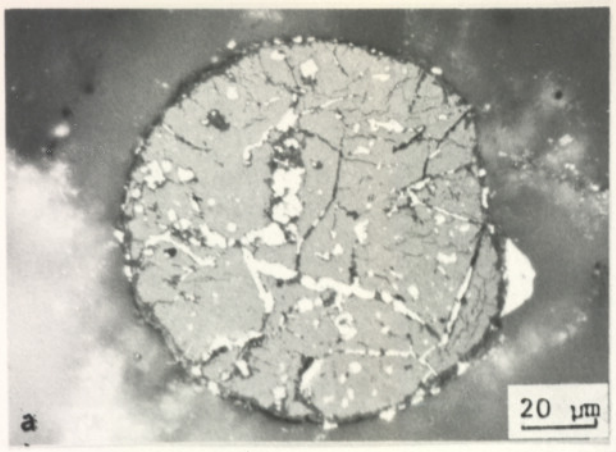
**d.** Kerogen (shades of grey) enclosing well-outlined uraninite fragments (grey, u) spotted by radiogenic galena (white). Basal Reef, President Brand G.M.

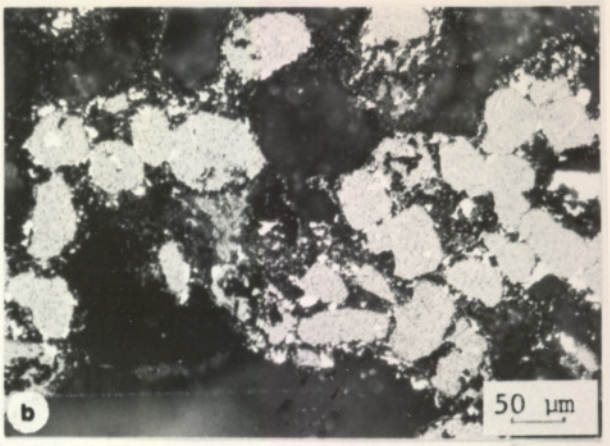
**e.** Euhedral uraninite grain (grey, u) covered by a gersdorffite (white) cutan. Leader Reef, Virginia G.M.

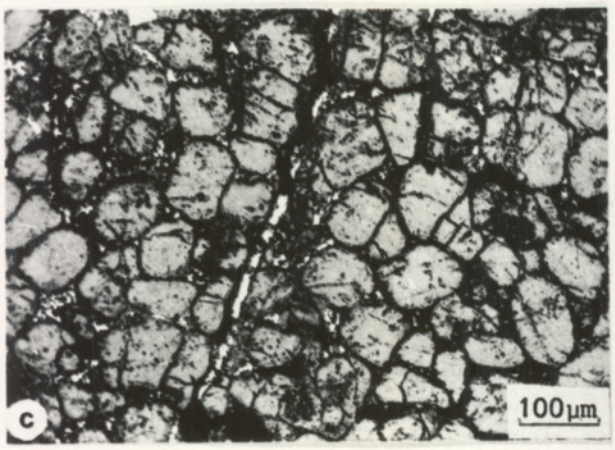
**f.** Large cataclastic uraninite particle (grey) about 8 times the average size of uraninite grains (75 μm), enveloped and cemented by coffinite (black). Both are pigmented by galena (white). Vaal Reef, Vaal Reefs East G.M.

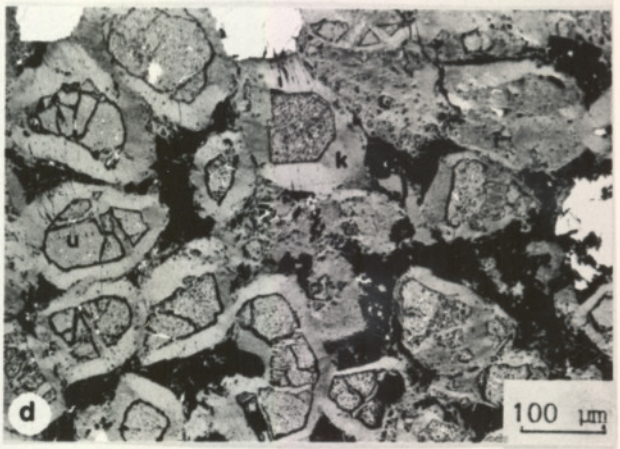
**g.** Fractured uraninite grain (grey) held together by quartz (black), illustrating how euhedral grains of uraninite could have formed. Basal Reef, President Brand G.M.

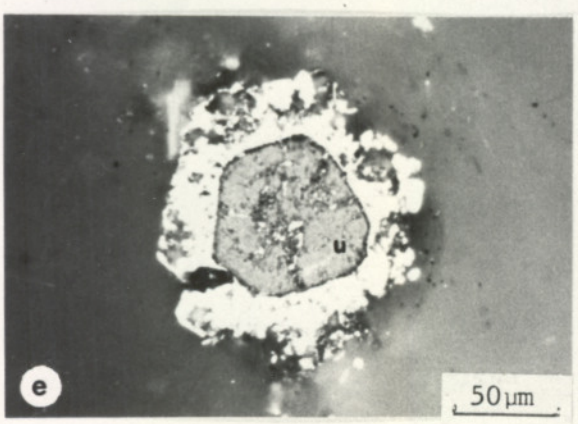
**h.** Three discrete uraninite grains (grey) which can be fitted together to form one grain. Dominion Reef, Bramley G.M.

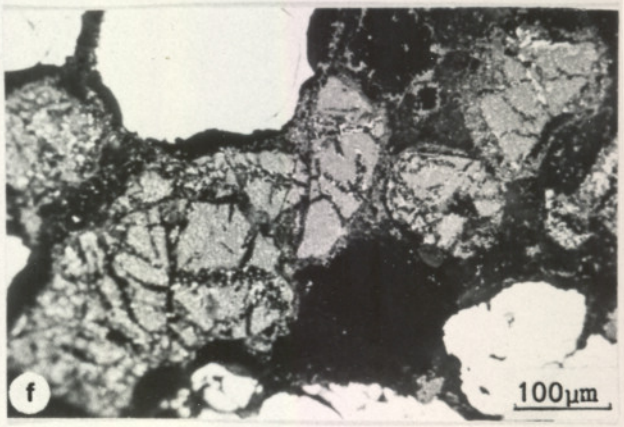

a
20 µm

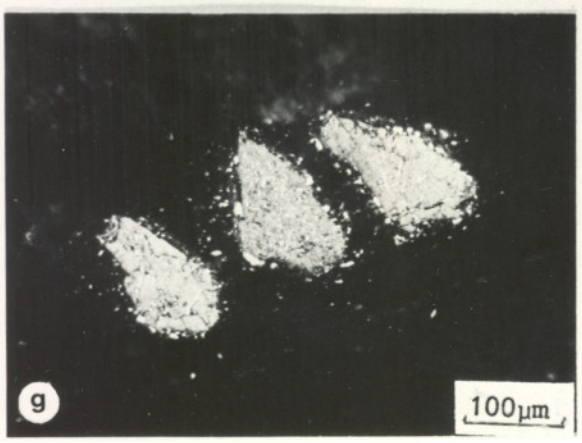

b
50 µm


c
100µm


d
k
u
100 µm


e
u
50µm


f
100µm


g
100µm

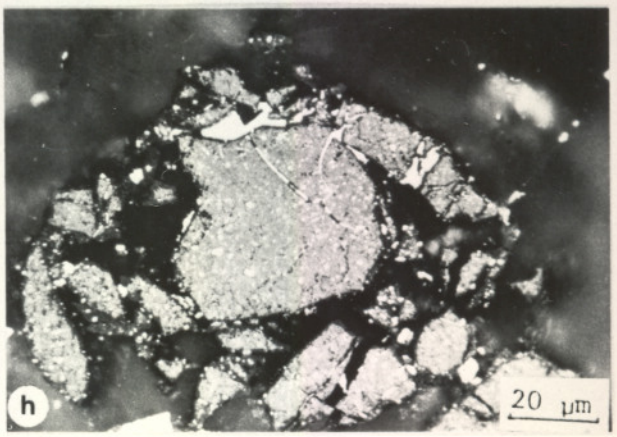

h
20 µm

Figure A.20 Photomicrographs of altered uraninite and seam of kerogen
Incident light in oil

**a.** Uraninite grain (grey) in the matrix in which the dissolution of uranium started along the crystal planes. The voids were filled by quartz (dark grey). Radiogenic galena (minute white specks) migrated to the surfaces of the remaining uraninite fragments. Vaal Reef, Vaal Reefs East G.M.

**b.** Uraninite (black) grain broken up and cemented by uraniferous leucoxene (pale grey). Basal Reef, Harmony G.M.

**c.** Uraninite (grey, u) in which coffinite (black) precipitated along crystal planes in the core. Basal Reef, President Brand G.M.

**d and e.** Rectangular and oval cross-sections of relict uraninite grains defined by a gersdorffite (white) cutan. The grains were replaced by quartz (smooth, black or grey core), while uraniferous leucoxene (grey, ul) precipitated just in- and outside the cutan. Monarch Reef, West Rand Consolidated G.M. and Basal Reef, Harmony G.M. respectively.

**f.** Relict uraninite replaced by pyrrhotite (po) crystals surrounding core of pyrite (p). Uraniferous leucoxene (grey) occurs to the left of the iron sulphides. Basal Reef, Harmony G.M.

**g.** Macrophotograph of a 12 mm-wide kerogen seam (black), in the centre interrupted by horizontally boudinaged quartz which is overlain by a quartz pebble (dark grey, q). The quartz below the pebble is infiltrated by barite (black, filling oblique fissures). The kerogen seam developed on a footwall quartzite (speckled grey) in which two heavy-mineral foresets (f), enriched in pyrite, occur. Basal Reef, President Brand G.M.

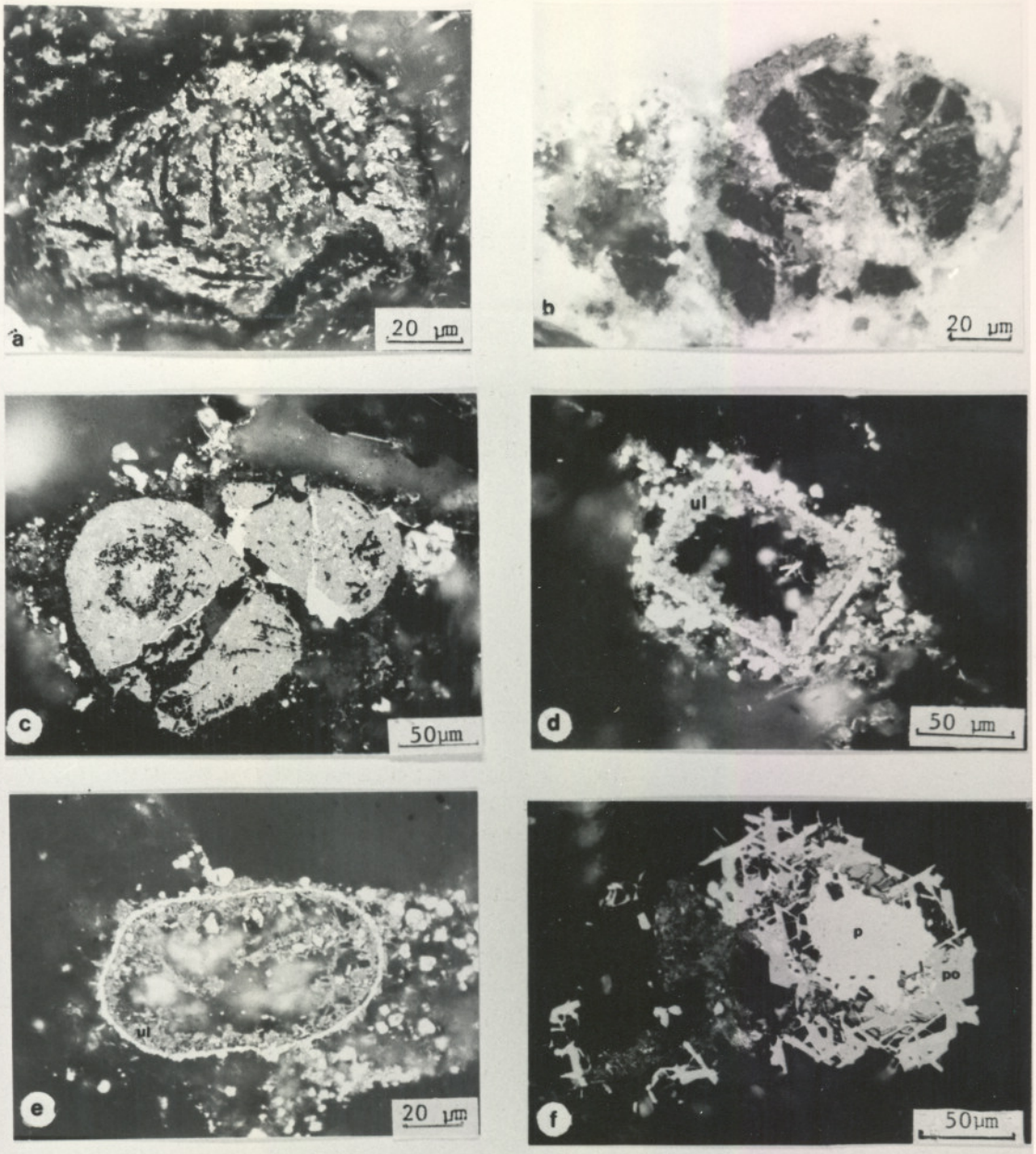

a
20 µm
b
20 µm
c
50µm
ul
d
50 µm
ul
e
20 µm
p
po
f
50µm
q
g

Figure A.21 Photomicrographs of uraninite-bearing kerogen
Incident light in oil

**a.** Kerogen nodule (grey) enclosing one uraninite (darker grey) grain. Organisms grew onto, and penetrated the grain along cracks pushing the fragments apart. Basal Reef, President Brand G.M.

**b.** Clast of a kerogen seam (shades of grey) broken up during reworking of sediment, enclosing uraninite (slightly paler grey) fragments. The surface of the kerogen grain runs across the uraninite inclusions. Radiogenic galena (white) migrated to open space in kerogen, and gersdorffite crystals precipitated at the surface of the fragment after burial on the fan. At top centre is a small zoned zircon (pale grey). Basal Reef, Harmony G.M.

**c.** Columnar habit of kerogen (grey) which encloses minute uraninite fragments. Vertical direction from the base at the right to the left. Vaal Reef, Buffelsfontein G.M.

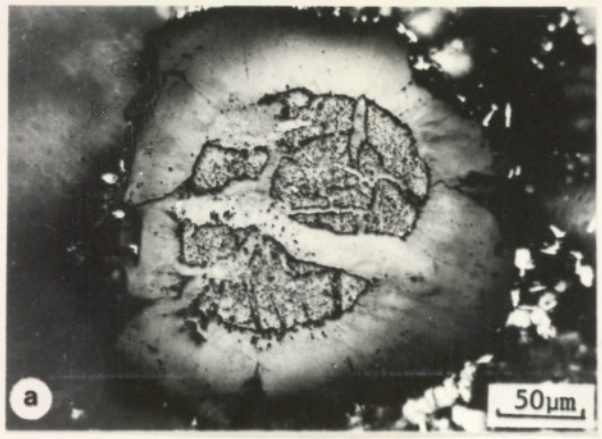
**d.** Finger-shaped kerogen columns. Picture taken on SEM by Hallbauer (1975).

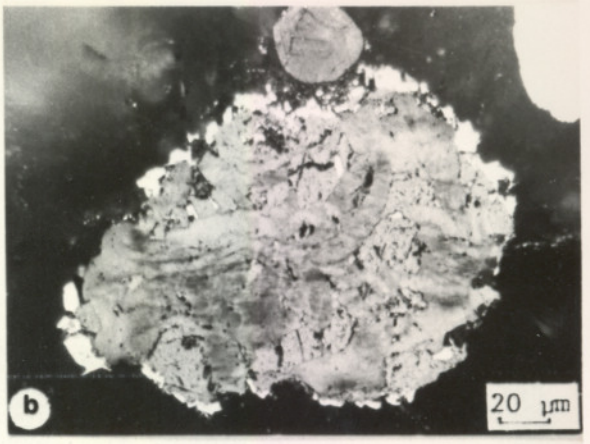
**e.** Segmented texture of kerogen seam produced by individual fragmented uraninite (grey) grains, which are each surrounded by uranium-free kerogen (pale grey aureole). N-S running cleats (black) are parallel to the base of the kerogen seam. Beisa Reef, Beisa G.M.

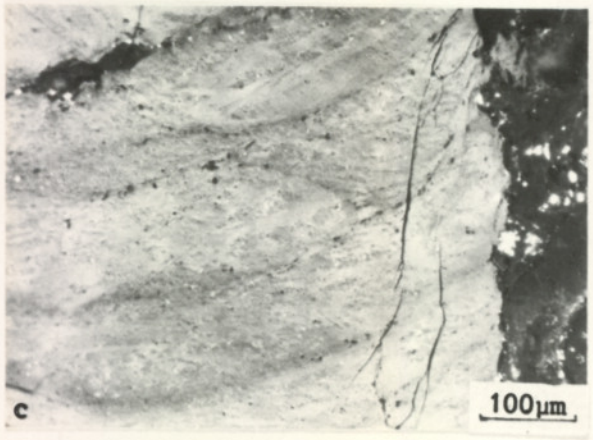
**f.** Similar to (e) but uraninite fragments are smaller so that it is less easy to reconstruct the grains. Carbon Leader, West Driefontein G.M.

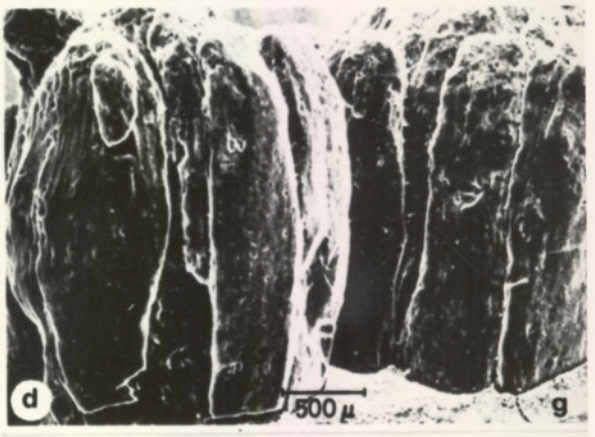
**g.** Fragmented uraninite grains (grey) oriented in vertical direction (NE in micrograph) in kerogen (pale grey). The fragments which were pushed apart during the growth of the microorganisms can be fitted together like pieces of a puzzle. Basal Reef, President Brand G.M.

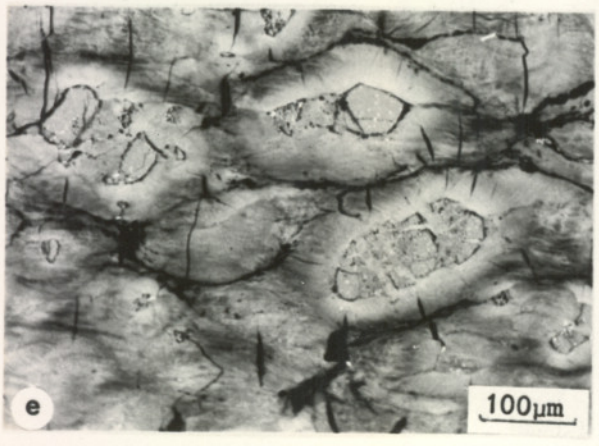
**h.** Kerogen with minute uraninite inclusions. The segmented texture of the kerogen is accentuated by interfilamental quartz (black). White mineral is gold. Vaal Reef, Western Reefs G.M.

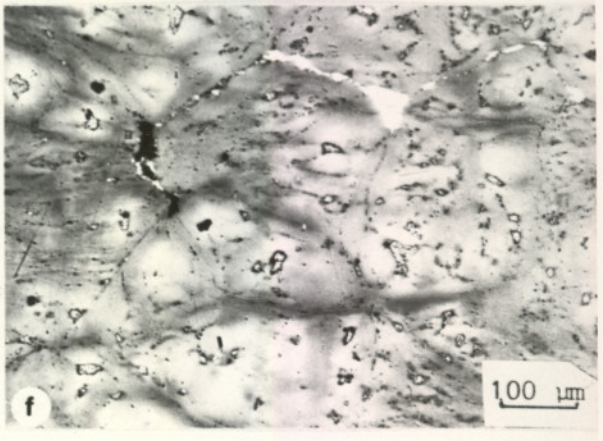

a
50µm

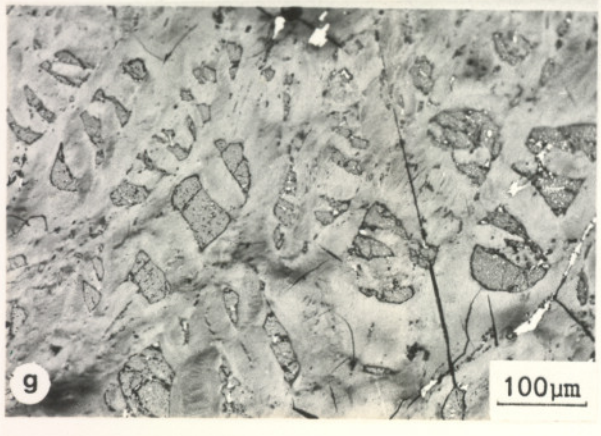

b
20 µm


c
100µm


d
500 µ
g


e
100µm


f
100 µm


g
100µm

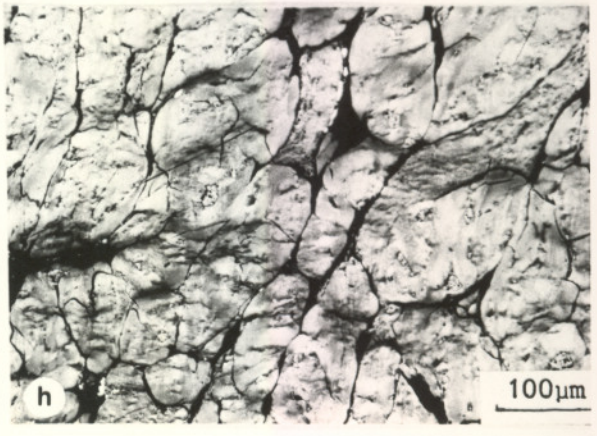

h
100µm

Figure A.22 Photomicrographs of kerogen
Incident light in oil

**a.** The residue which remains after ashing kerogen at 300$^0$C is a phyllosilicate which displays filamental texture elongated in the vertical direction (in micrograph from left to right). Basal Reef, President Brand G.M.

**b.** Cross-section of ashed kerogen seam of previous photograph. The segments are outlined by phyllosilicate (pale grey, p) which encloses uraninite particles (black spots). Pores are grey and black. Basal Reef, President Brand G.M.

**c.** Kerogen speckled by minute uraninite (dark grey) inclusions. Radiogenic galena (white) migrated to interfilamental voids. Basal Reef, Harmony G.M.

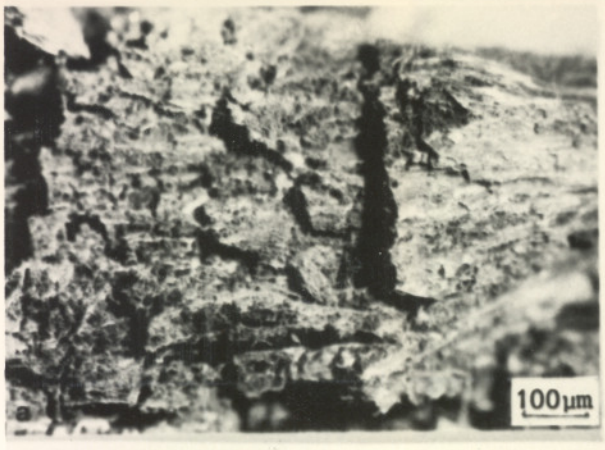
**d.** Continuous vertical (right to left) kerogen column (dark grey; bottom section), speckled by very fine-grained uraninite (black) inclusions. In centre, brannerite (dark grey, b) penetrated the kerogen from the top of the seam at the left. The polished section was subjected to leaching in a dilute sulphuric acid, so that all uraninite inclusions were dissolved and replaced by anglesite (black). Brannerite remained unaffected. Basal Reef, President Brand G.M.

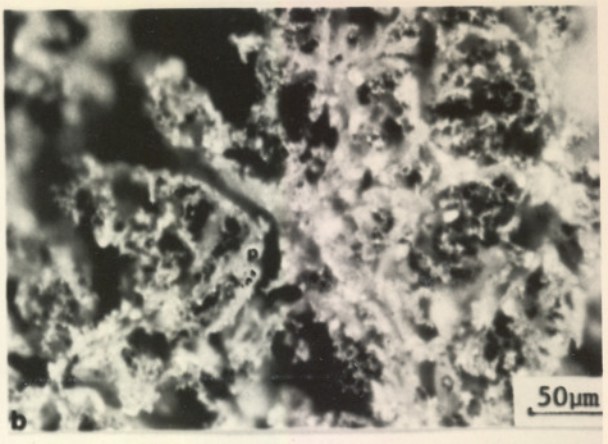
**e.** Kerogen (shades of grey) nodule surrounded by uranous titanate (spotted pale grey), which formed at the expense of the kerogen. The reflectance of the kerogen suggests that it was thermally cracked, possibly as a result of the nearby introduction of magmatic matter. Kalkoenkrans Reef, Oryx G.M.

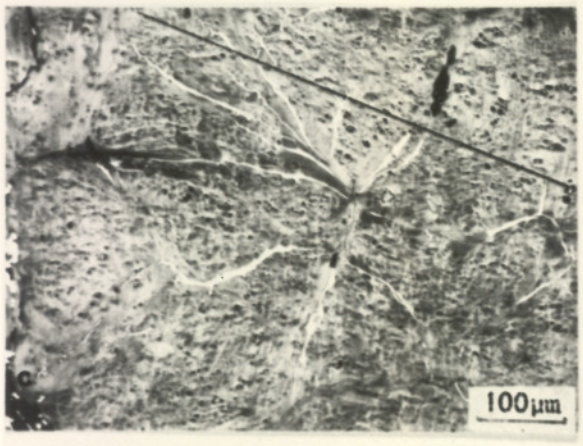
**f.** Brannerite penetrated kerogen breaking it up in roundish fragments. The uranous titanate corroded the pyrite (white). Leader Reef, Virginia G.M.

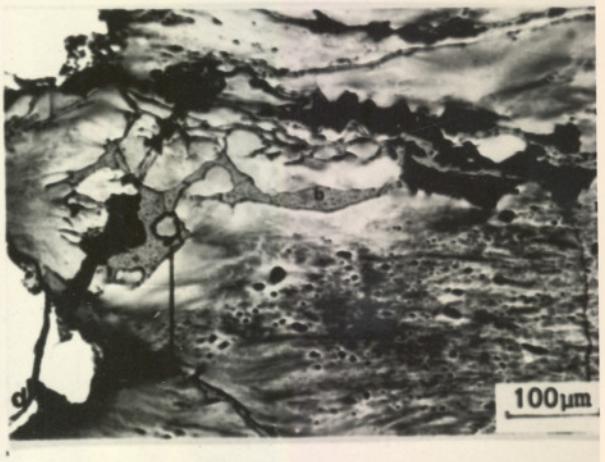
**g.** Coffinite (black) which formed from uraninite inclusions, penetrated the kerogen (grey) in a dendritic manner to accommodate for the added silica. UE1a Reef, Cooke Section.

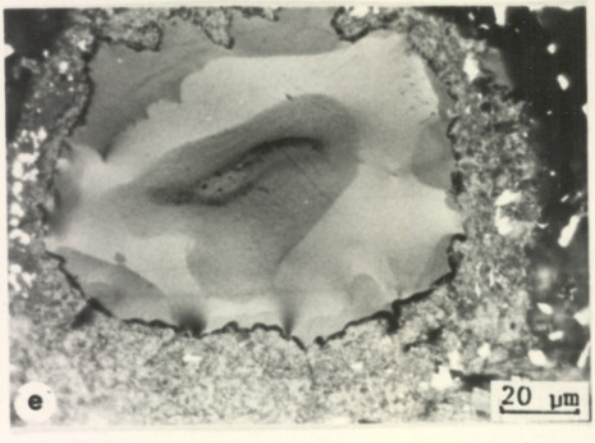
**h.** Uraninite inclusions in kerogen (grey) were replaced by dendritic coffinite (black spots). Beisa Reef, Beisa G.M.

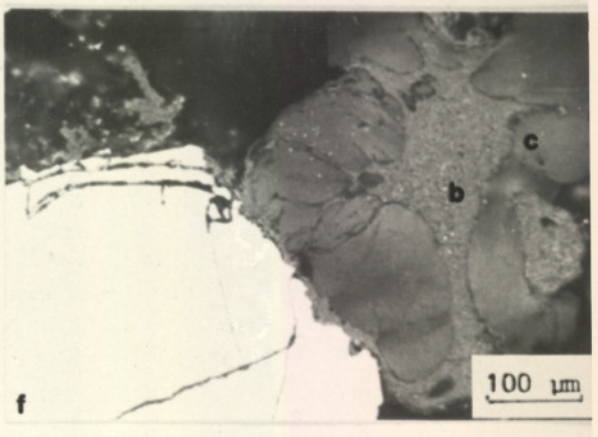

100µm

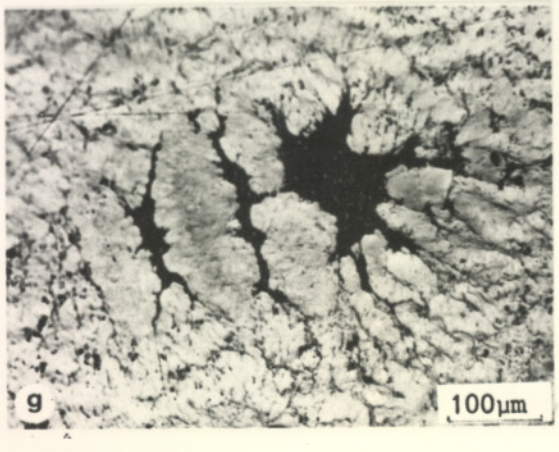

50µm


100µm


100µm


20 µm


c
b
100 µm


100µm

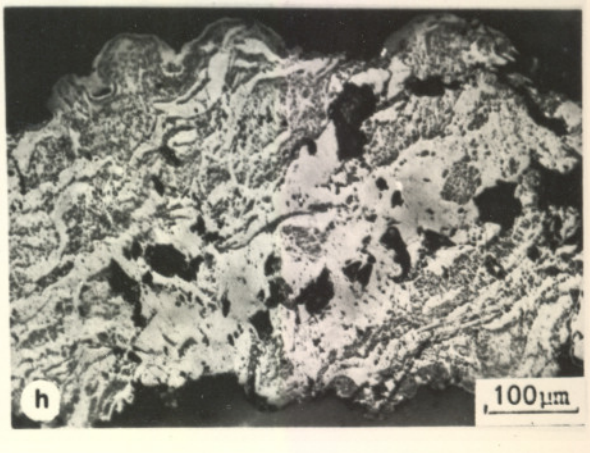

100µm

Figure A.23 Photomicrographs of uranous titanates and kerogen
Incident light in oil

**a.** Two relict uraninite grains. The top grain has been entirely replaced by uranous titanate (pale grey, ul), whereas the bottom grain was covered by a gersdorffite cutan (g), and the grain itself completely leached and replaced by a quartz core (q) and marginal brannerite (b). Basal Reef, Harmony G.M.

**b.** Relict uraninite grain in thin section, which was replaced by a chlorite core (mixed grey colours) and brannerite (black) in the margin. Transmitted light, crossed nicols. UE1a Reef, Cooke Section.

**c.** Two structureless kerogen nodules, devoid of uraninite. Leader Reef, Virginia G.M.

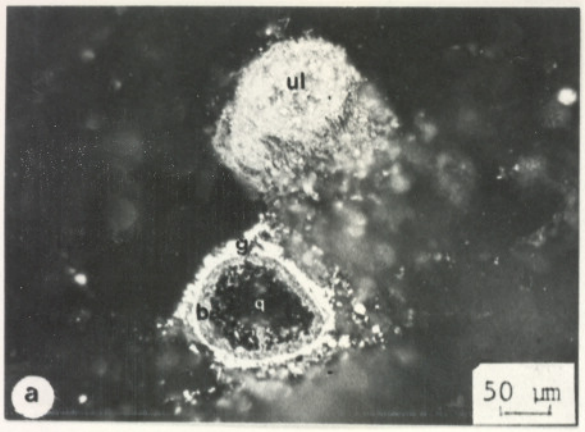
**d.** Kerogen (grey) of spongy texture at the base of a seam, which is younger than the kerogen with uraninite inclusions (pale grey) at left. White particles at top are gersdorffite. Vaal Reef, Buffelsfontein G.M.

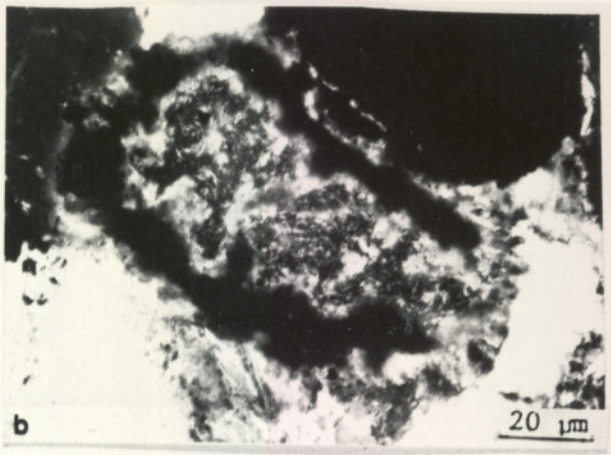
**e.** Kerogen (dark grey) devoid of uraninite, which is spotted and surrounded by gersdorffite (white) shows an embayed outline produced by authigenic quartz (q) which suggests that the organic matter was not solid at the time of the precipitation of quartz. Leader Reef, Virginia G.M.

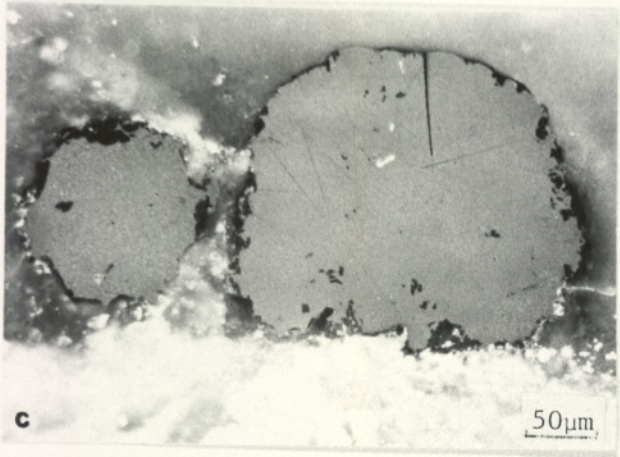
**f.** Kerogen (pale grey), which encloses very fine-grained uraninite. At the base of the seam, a younger generation of kerogen (dark grey) is present which encloses quartz (black) some uraniferous leucoxene (grey, 1c), and crystals of gersdorffite (white). Vaal Reef, Buffelsfontein G.M.

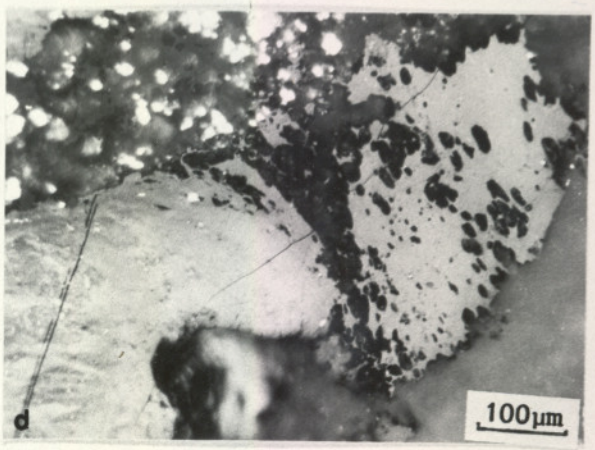
**g.** Kerogen (shades of grey) enclosing very fine-grained uraninite fragments displays a higher reflectance than normal and pronounced cleats (black). Both features are probably caused by the nearby introduction of magmatic matter. Vaal Reef, Vaal Reef South G.M.

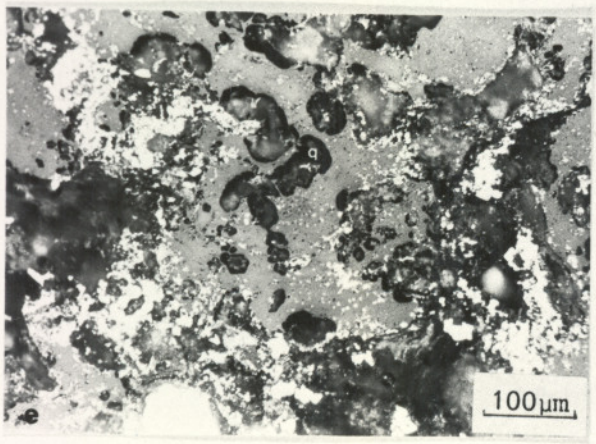
**h.** Chloritic leucoxene (grey and medium grey core) enveloped by a film of brannerite (pale grey, b) and then overgrown by the younger generation of non-uraniferous kerogen (black). Vaal Reef, Buffelsfontein G.M.

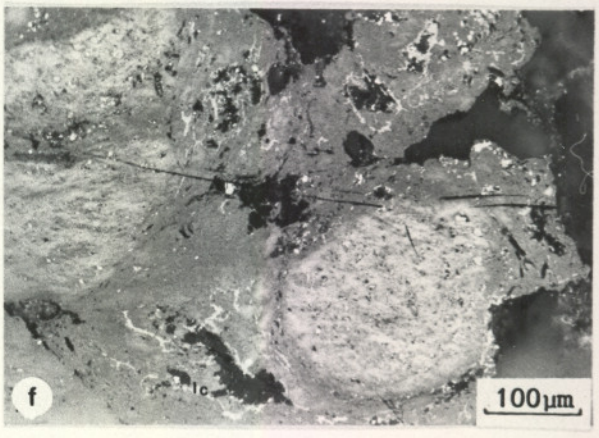

ul
g
b
q
a
50 µm


b
20 µm


c
50µm


d
100µm


q
e
100µm


f
100µm


g
100µm

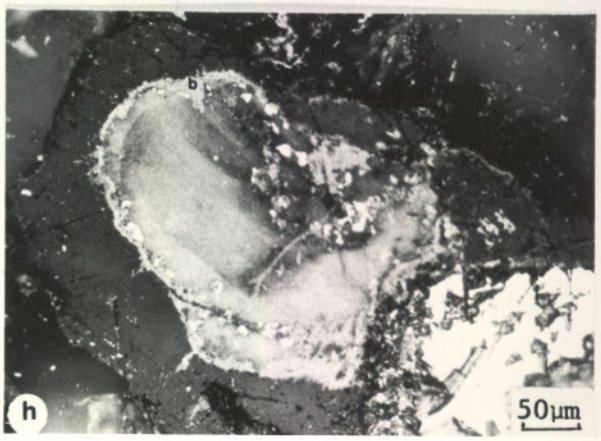

b
h
50µm

Figure A.24 Photomicrographs of kerogen
Incident light in oil

**a.** Black, structureless kerogen which encloses unaltered uraninite (pale grey). White Reef, West Rand Consolidated G.M.

**b.** Kerogen (shades of grey) which grew onto pyrite at the expense of the sulphide. Kerogen encloses coffinite (black) of a dendritic texture. UE1a Reef, Western Areas G.M.

**c, d, and e.** Kerogen nodules in which the kerogen (grey, k) has been partly or entirely destroyed and replaced by quartz and phyllosilicate (both black), coffinite (very dark grey, spongy) and uraniferous leucoxene (pale grey, ul), which also enveloped the nodules. (e) is a close up at greater magnification. E9Gc Reef, Cooke Section.

**f.** Kerogen (grey) enclosing very fine-grained coffinite (black) imparting a dendritic texture to the kerogen. UE1a Reef, Cooke Section.

**g.** Authigenic quartz (white) which filled interfilamental space in the kerogen seam displayed in Fig. A.15g. The quartz was boudinaged in a vertical direction (from left centre to right bottom) and the open space then filled by columnar chlorite (dark grey, striped). The organic matter (black bulge at centre right) protruded into the open space before it was filled with chlorite. Transmitted light. Basal Reef, President Brand G.M.

**h.** Parallel fissures (from left to right) intersect pyrite (white) and quartz (black) which, in pyrite, were filled by quartz (black) and in the quartz pebble by pyrrhotite (white, po). The boudinage texture runs parallel to the bedding plane and is invariably associated with uraninite-bearing kerogen (grey), which itself is not fractured. Vaal Reef, Vaal Reefs East G.M.

Figure A.25 Photomicrographs of boudinage by kerogen and of uranous titanates
Incident light in oil

**a.** Subhedral zircon (high relief, z) has been pulled apart in vertical direction (from left to right). Kerogen is present just outside the micrograph. The open space was filled by pyrite (spotted dark grey, p). Transmitted light. Basal Reef, President Steyn G.M.

**b.** Fractures in quartz parallel to the bedding plane were filled by organic matter (shades of grey). Kerogen encloses fine-grained coffinite (black). White patches are radiogenic galena. Beisa Reef, Beisa G.M.

**c.** Uraninite replaced by brannerite crystals (grey, b) and quartz (black). Pyrite (white) in contact with brannerite, or uraniferous leucoxene (inclusion in pyrite, ulc) is corroded. Basal Reef, Harmony G.M.

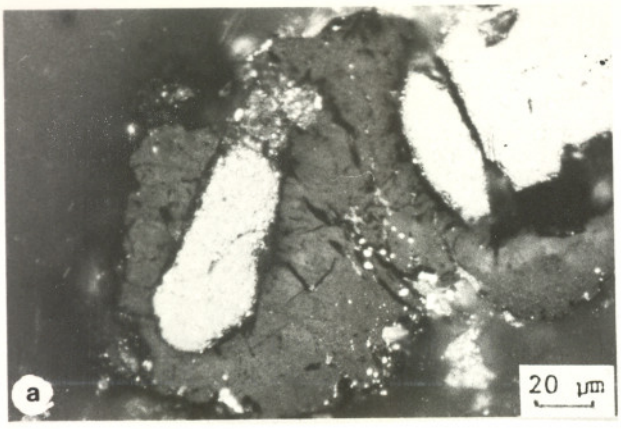
**d.** Uraninite grains replaced by quartz (black) and brannerite crystals (grey) spotted by radiogenic galena (white) and coated by gersdorffite (white). Leader Reef, Virginia G.M.

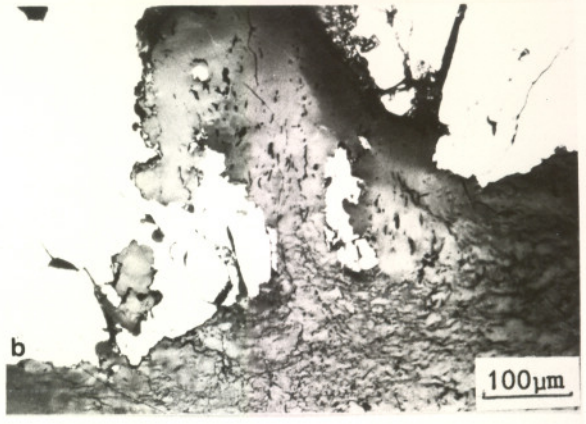
**e.** Leucoxene pseudomorph replaced by brannerite crystals (grey) and quartz (black). Pyrite (white) in contact with the brannerite is corroded. Vaal Reef, Vaal Reefs South G.M.

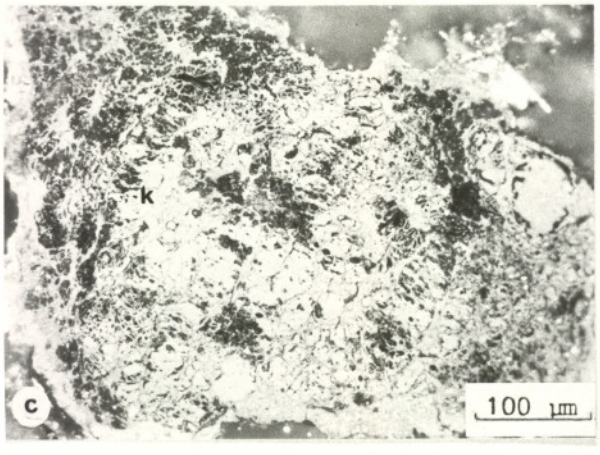
**f.** Group of detrital grains which were first covered by a film of titania (black), then by a film of gersdorffite crystals (white, g). Chloritized (black) chromite (grey) at bottom left covered by a film of minute brannerite crystals (grey). Above the chromite is a detrital chlorite grain (dark grey); the other grains are pyrite (white), two of which are partly chloritized (dark grey). Same photo with nicols crossed in A.20h. Vaal Reef, Western Reefs G.M.

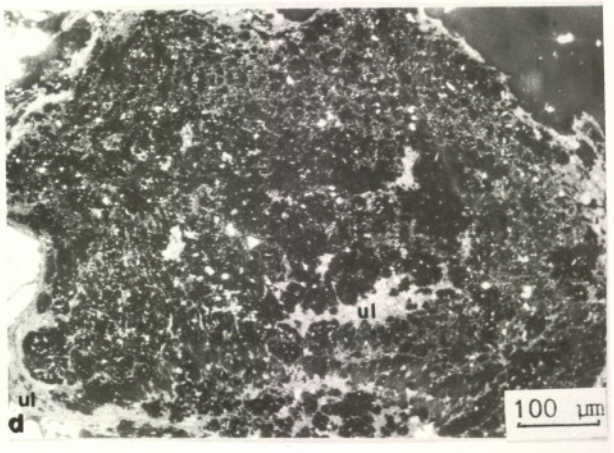
**g.** Leucoxene pseudomorph replaced by cryptocrystalline brannerite (grey). Cubes and round grains of galena (white), and pyrrhotite laths (white) are dispersed in the brannerite. Carbon Leader, Western Deep Levels G.M.

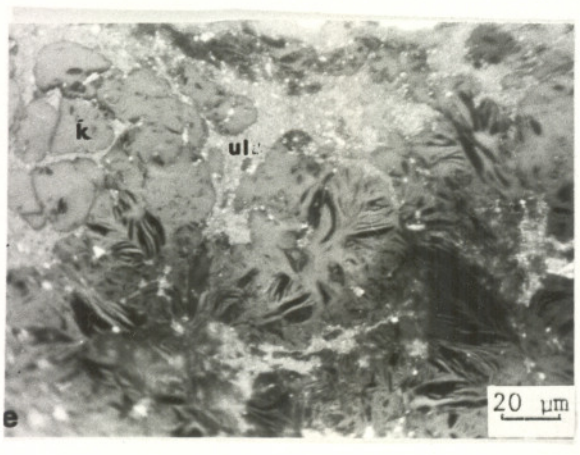
**h.** Two detrital leucoxene pseudomorphs (pale grey) in which brannerite (grey, b) and uraniferous leucoxene crystals (grey, ulc) precipitated. Leader Reef, Virginia G.M.

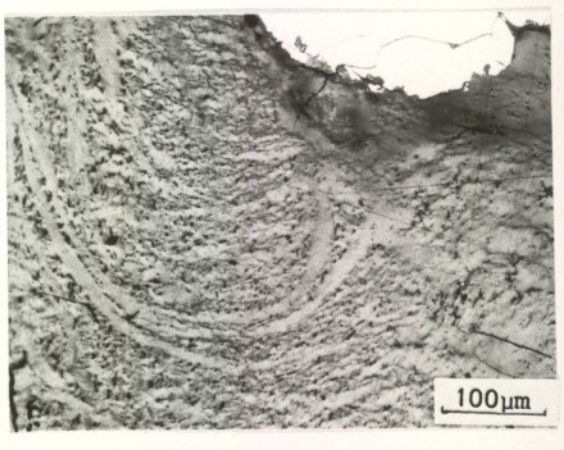

a
20 µm

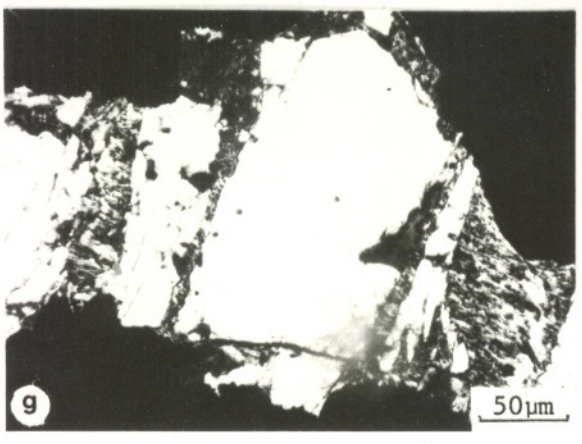

b
100µm

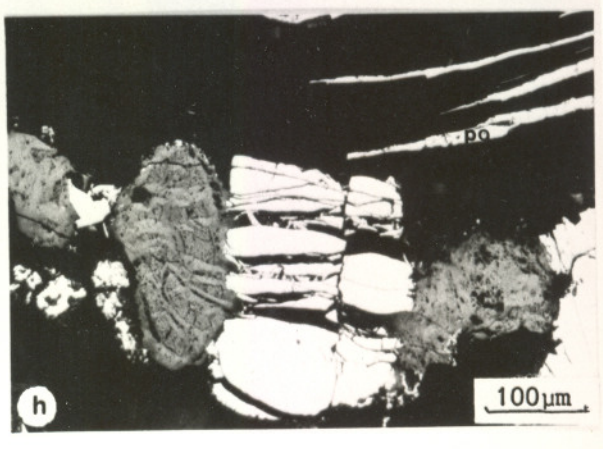

k
c
100 µm

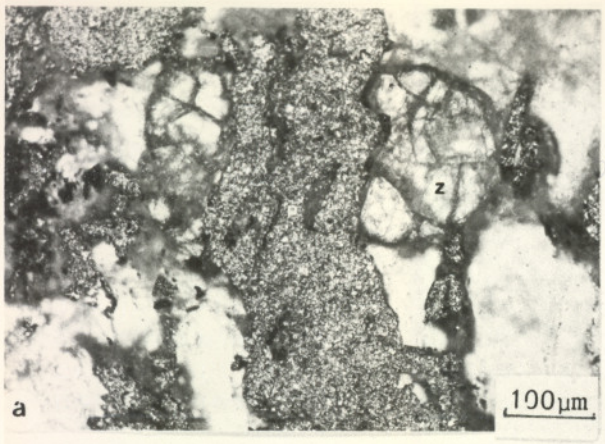

ul
ul
d
100 µm

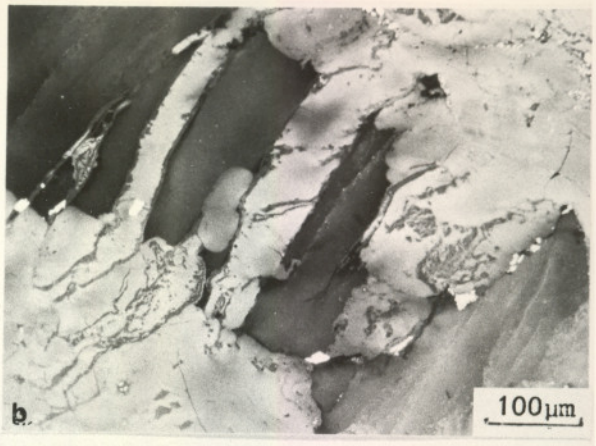

k
e
20 µm

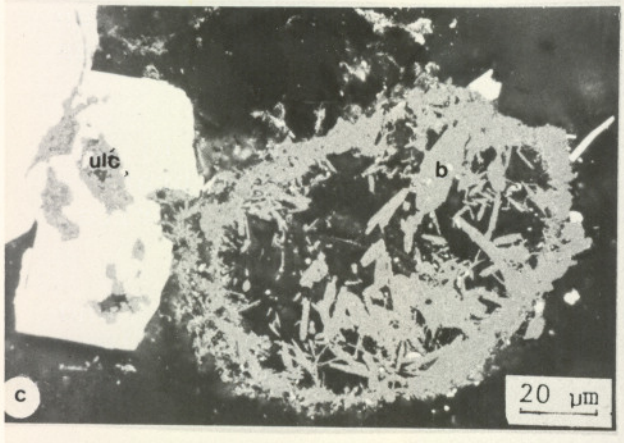

f
100µm

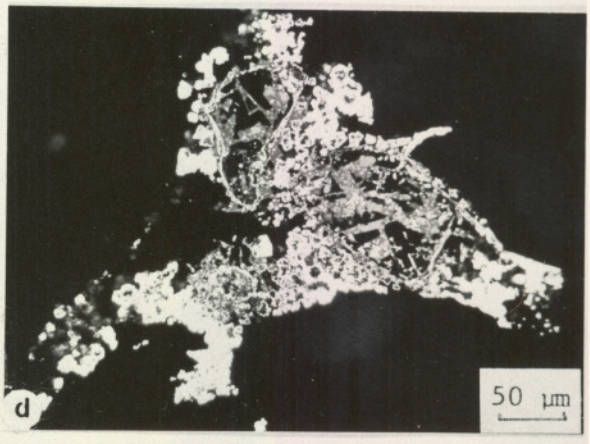

g
50µm


h
100µm


z
100µm
a

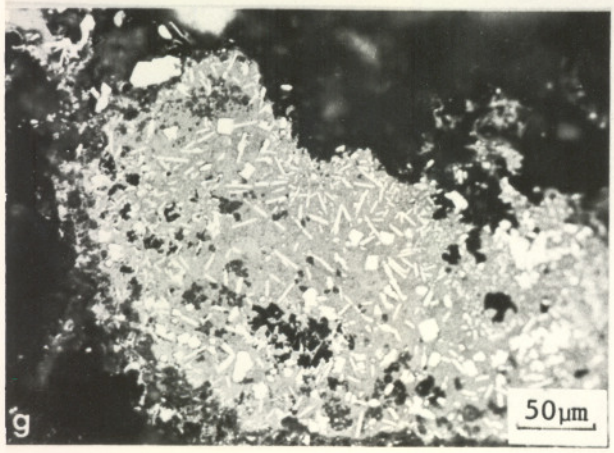

100µm
b


ulc
b
20 µm
c


50 µm
d


50 µm
e


100 µm
f


50µm
g

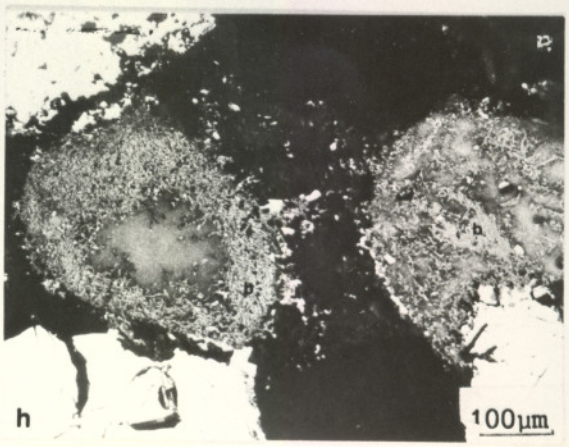

100µm
h

Figure A.26 Photomicrographs of uranous titanates
Incident light in oil

**a.** Stubby pyrrhotite crystals (white) precipitated onto uraninite altered to brannerite (grey), and filled cracks in the grain. This type of pseudomorph occurs in pyrite-rich horizons in a quartzite. Basal Reef, Harmony G.M.

**b.** 'Uraninite ghost' composed of a shell of brannerite (grey) onto which pyrrhotite crystals (white) precipitated. The initial uraninite, the core of the ghost, was replaced by quartz (core, q). Basal Reef, Harmony G.M.

**c.** Leucoxene grain (pale grey, 1c) in which brannerite (dark grey, b) spotted by galena (white) precipitated in cracks and in the core which was further filled by quartz (black). Basal Reef, Harmony G.M.

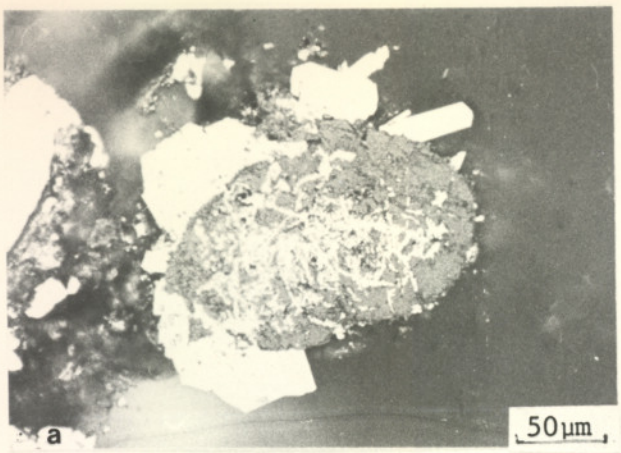
**d.** Streaky uranous titanate (grey) along boundaries of quartz (q) and chlorite (chl), which encloses gersdorffite (g) and chalcopyrite (c). Vaal Reef, Hartebeestfontein G.M.

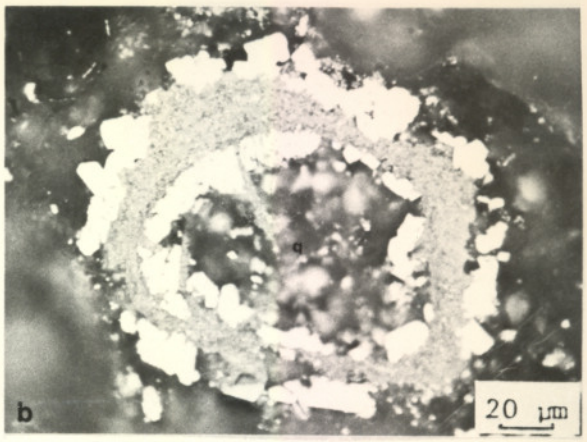
**e.** Cluster of uraninite grains which have been replaced by uranous titanates (speckled pale grey, u) enclosing galena (white). Smooth, white particles on the left are pyrite. Vaal Reef, Western Reefs. G.M.

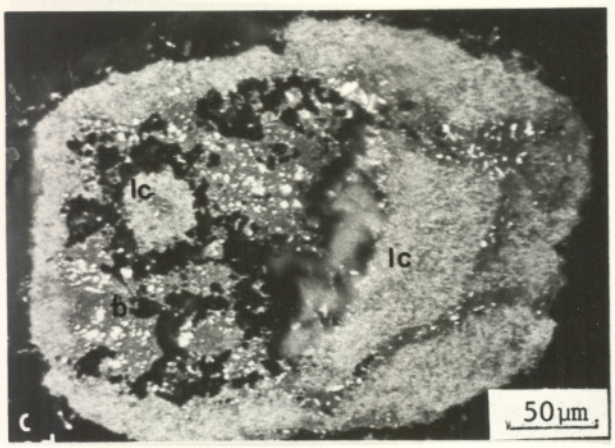
**f.** Leucoxene grain replaced by uranous titanate. Vaal Reef, Western Reefs G.M.

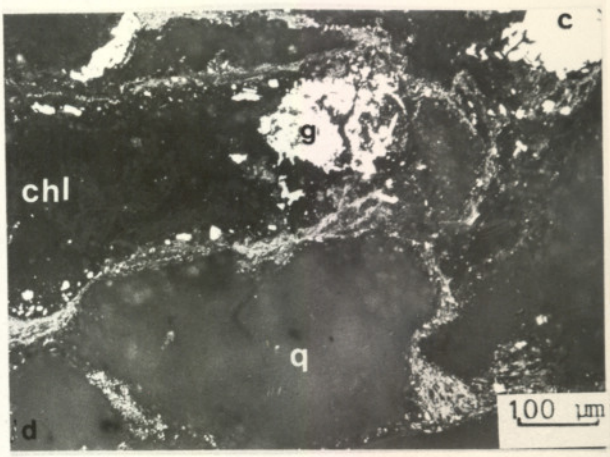
**g.** Cluster of uraninite grains (black) altered to uranous titanate (dark grey) and coffinite (black), spotted by pyrrhotite laths and galena specks (both white). The grains are cemented by mushy anatase (speckled, pale grey). A considerable portion of the uranium was leached and replaced by quartz (dark grey, q) and phyllosilicate (dark grey). Monarch Reef, Randfontein Estates G.M.

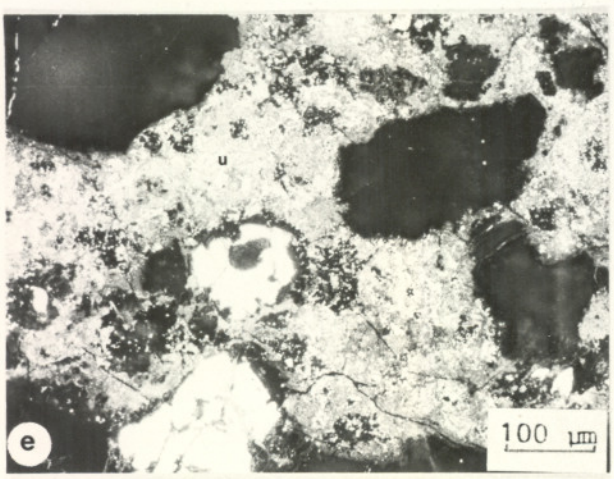
**h.** Same group of minerals as in A.19f, but taken with the nicols crossed. Vaal Reefs, Western Reefs G.M.

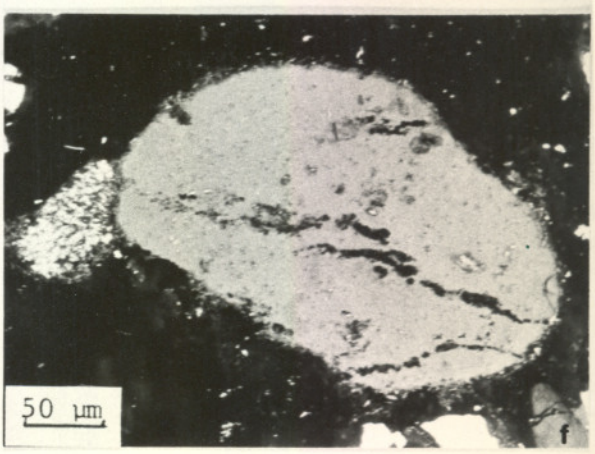

a
50µm

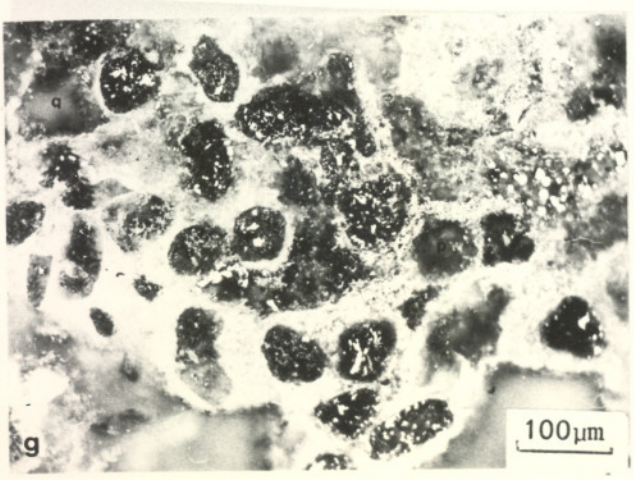

q
b
20 µm


lc
lc
b
c
50µm


c
g
chl
q
d
100 µm


u
e
100 µm


50 µm
f


q
g
100µm

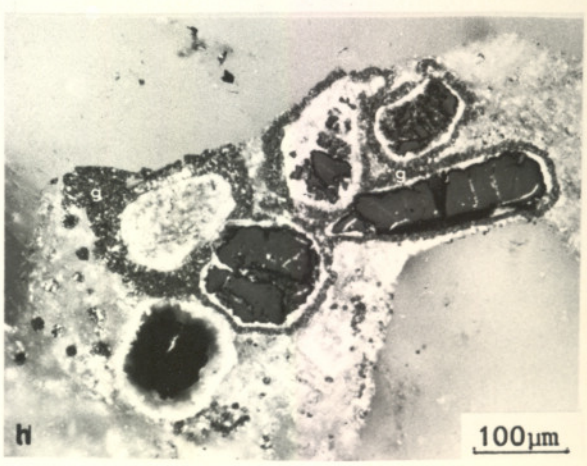

h
100µm

Figure A.27 Photomicrographs of uraniferous leucoxene and coffinite
Incident light in oil

**a.** Kerogen nodule (grey) with minute uraninite inclusions (pale grey) covered by a film of leucoxene (white), possibly uraniferous. Basal Reef, Harmony G.M.

**b.** Streaky uraniferous leucoxene (pale grey) intergrown with phyllosilicate in quartz matrix (dark grey to black). Vaal Reef, Western Reefs G.M.

**c.** Rutile-leucoxene pseudomorph replaced by brannerite (dark grey). Streaky uraniferous leucoxene (pale grey at right bottom corner) intergrown with phyllosilicate. Vaal Reef, Western Reefs G.M.

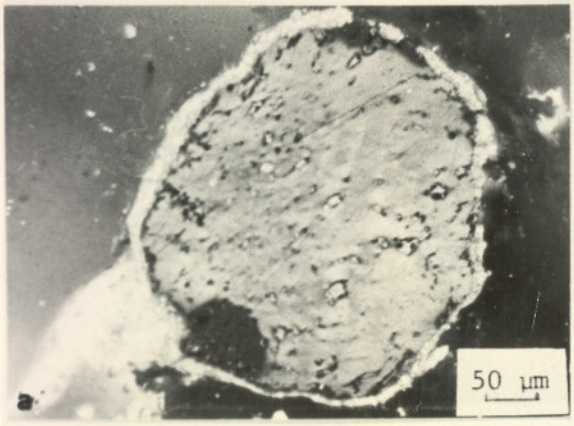
**d.** Rounded anhydrous thorian coffinite (black) enclosing galena (white) and minute laths of pyrrhotite (white) which also occur at the contacts with the surrounding quartz grains (dark grey). E9Gc Reef, Western Areas G.M.

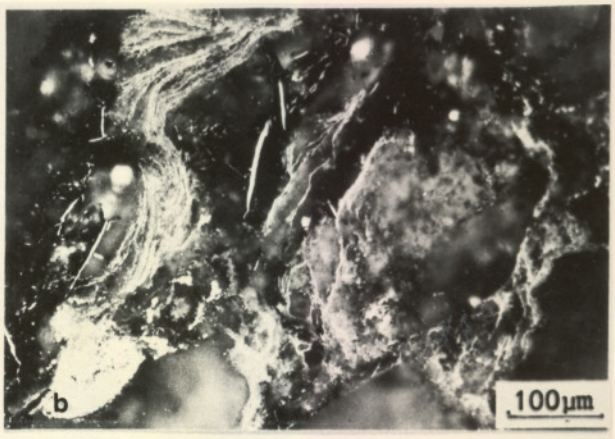
**e.** Group of uraninite (dark grey) grains spotted by galena (pale grey) and almost entirely transformed to coffinite (dark grey) are enveloped by a mixture of uraniferous leucoxene, quartz and phyllosilicate (pale grey). The original shape of the uraninite grains is faintly visible. Where in contact with pyrite (white), the uraniferous leucoxene corroded the iron sulphide. Quartz and pores are black. Composite Reef, Cooke Section.

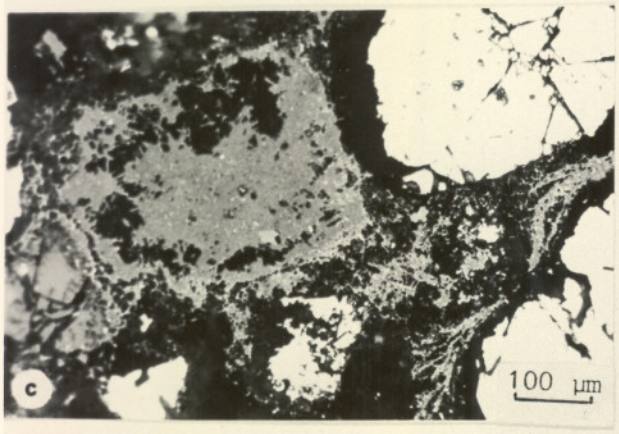
**f.** Amoeboid-shaped coffinite grain (black) at the surface of a concretionary pyrite (white). The admixture is composed of coffinite (black), gold (white patches), galena (white spots), quartz (black), phyllosilicate (black), and minute pyrrhotite laths (white); it is enveloped by a film (pale grey) of uraniferous leucoxene mixed with quartz and phyllosilicate. Composite Reef, Cooke Section.

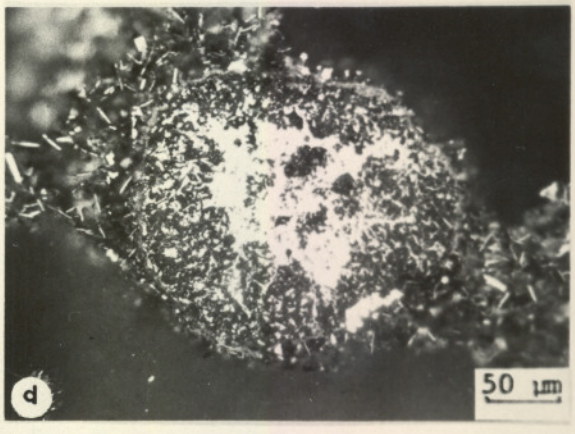
**g.** Detrital uraninite (grey) marginally transformed *in situ* into anhydrous thorian coffinite (black). In the uraninite, radiogenic galena (white) migrated into cracks and in the coffinite it occurs as irregular-shaped specks. E9Gc Reef, Western Areas G.M.

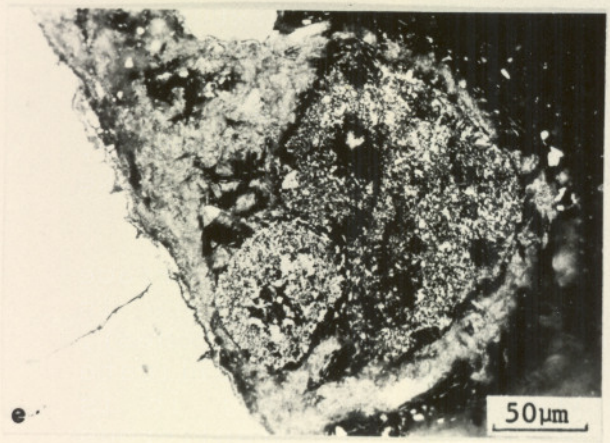
**h.** Kerogen (grey) enveloped by galena-pigmented coffinite (black). Larger white grains are pyrrhotite. Elsburg no. 5 Reef, Western Reefs G.M.

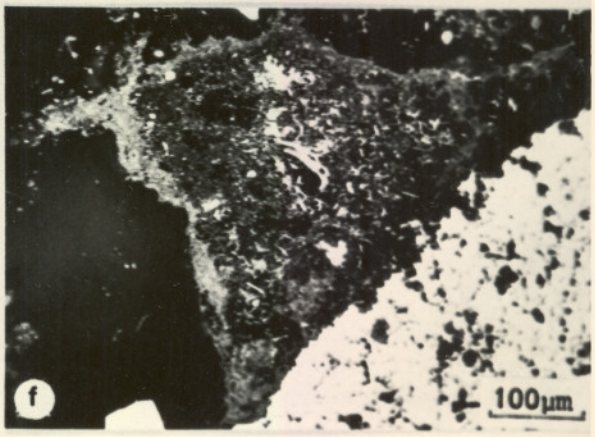

50 µm

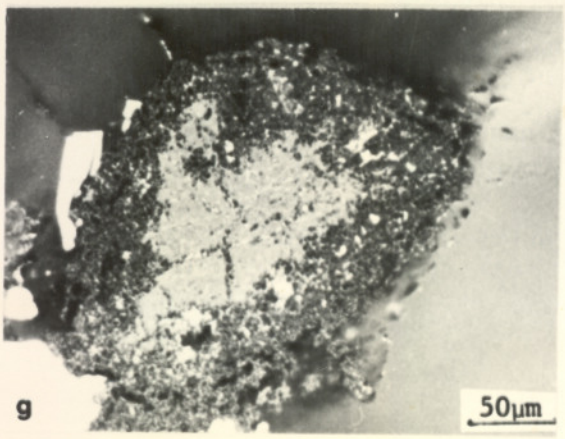

100µm


100 µm


50 µm


50µm


100µm


50µm

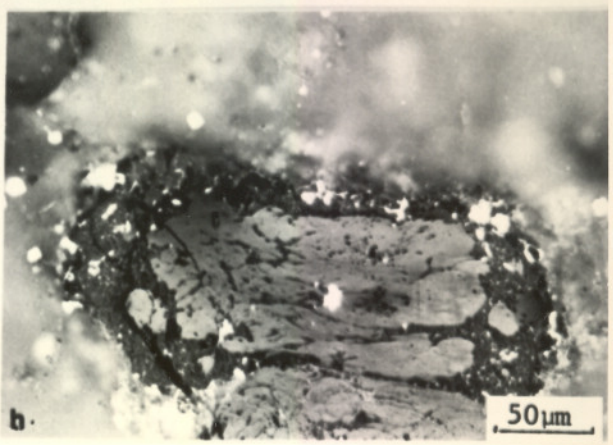

50µm

Figure A.28 Photomicrographs of coffinite, pitchblende and secondary coffinite
Incident light in oil

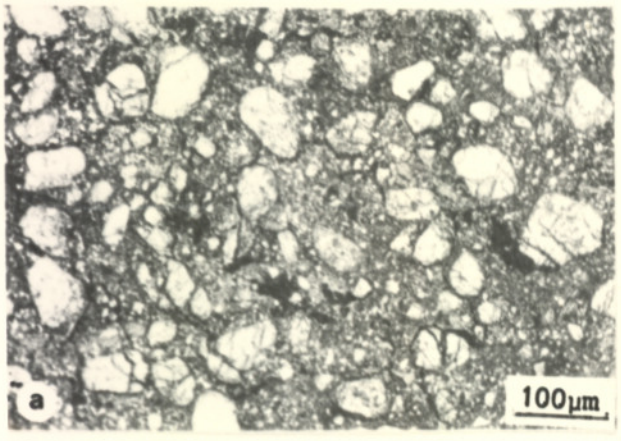
**a.** Dense cluster of uraninite grains (grey) partly altered to coffinite (dark grey). Compare with Figure A.14c. Monarch Reef, East Champ d'Or G.M.

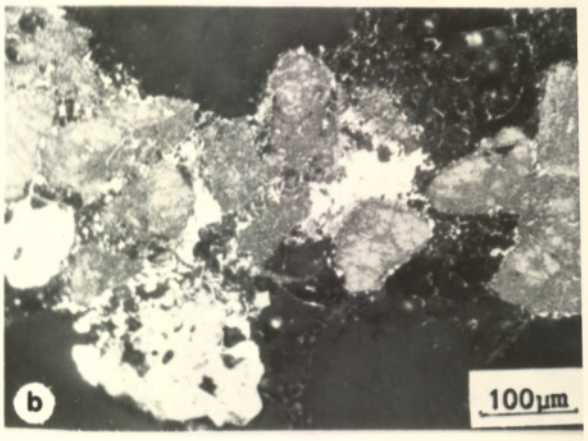
**b.** Group of uraninite (grey) grains, which are partly or entirely replaced by hydrated thorian coffinite (dark grey). Radiogenic galena migrated to the grain surfaces (white spots). Small patches of pyrite (white) and secondary ilmenite (pale grey at left bottom) are also present. Dominion Reef, Bramley G.M.

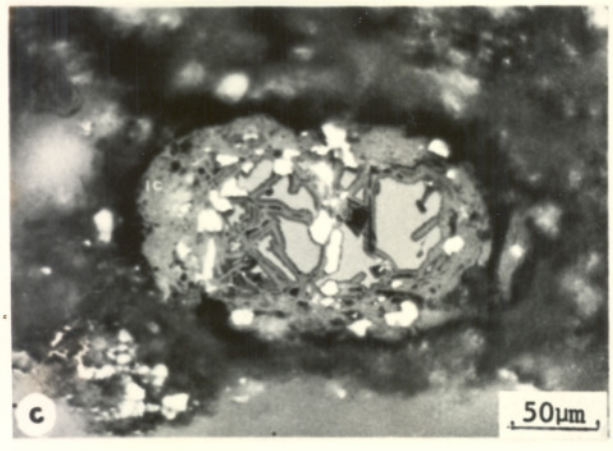
**c.** Grain of uraninite (grey) and coffinite (dark grey) bordering cracks, pseudomorphous after detrital uraninite, which formed relatively recently in a supergene environment. The grain is enveloped by uraniferous leucoxene (pale grey, 1c). Galena (white) coalesced to larger grains, but is absent in the secondary uraninite and coffinite. Monarch Reef, Randfontein Estates G.M.

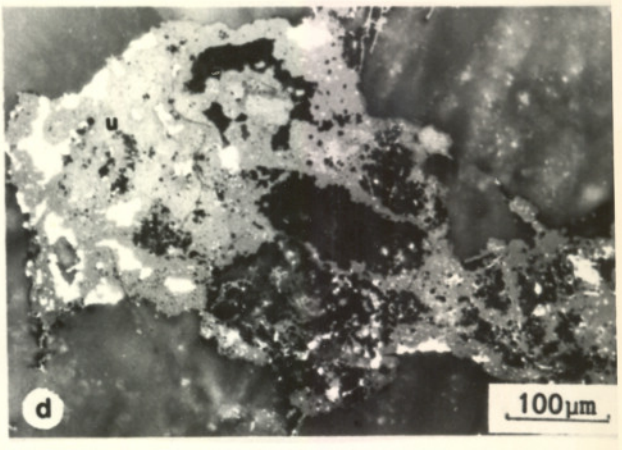
**d.** Colloform uraninite (grey) and coffinite (dark grey) of supergene origin, which formed from allogenic uraninite (pale grey, u) present in the left portion. Galena (white) coalesced to larger patches. Monarch Reef, Randfontein Estates G.M.

**e.** Colloform coffinite (black) enveloped by a film of secondary pyrite (white); both formed relatively recently in a supergene environment. Monarch Reef, Randfontein Estates G.M.


a
100µm


b
100µm


c
50µm


d
100µm

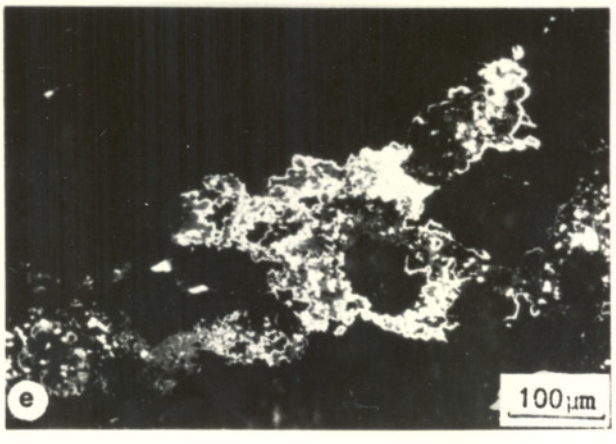

e
100µm

Figure A.29 Photomicrographs of brannerite
Incident light in oil

**a.** Detrital uraninite (grey) altered to coffinite (black) along crystal planes. Qualitative analysis on the EMP suggests that the grain is overgrown by a brannerite-type mineral (dark grey). Authigenic ilmenite (pale grey) occurs at top left. Dominion Reef, Dominion Reefs G.M.

**b.** Detrital anhydrous brannerite (grey) grain. Leader Reef, Virginia G.M.

**c.** Detrital brannerite (grey, b) grain enclosing quartz (dark grey) and galena (white, g) surrounded by rutile (white, r). Leader Reef, Virginia G.M.

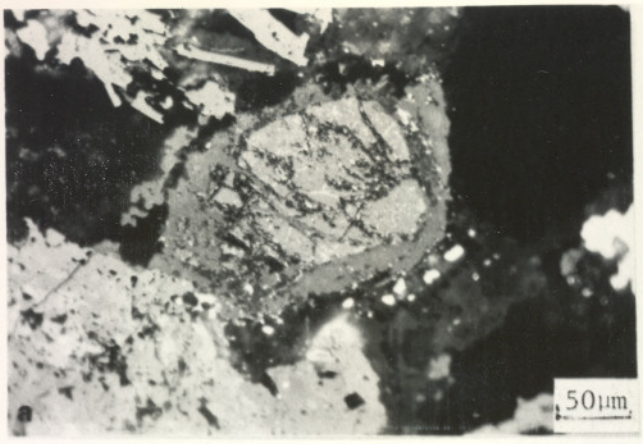
**d.** Uranous titanate of lacy texture in contact with pyrite which is corroded. Leader Reef, Virginia G.M.

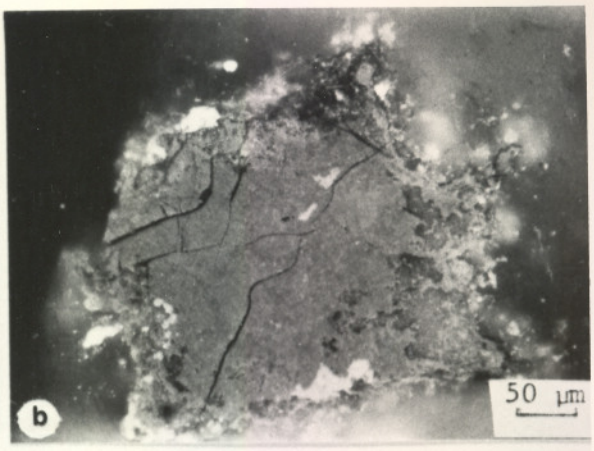
**e.** Leucoxene pseudomorph replaced by brannerite. Carbon Leader, Blyvooruitzicht G.M.

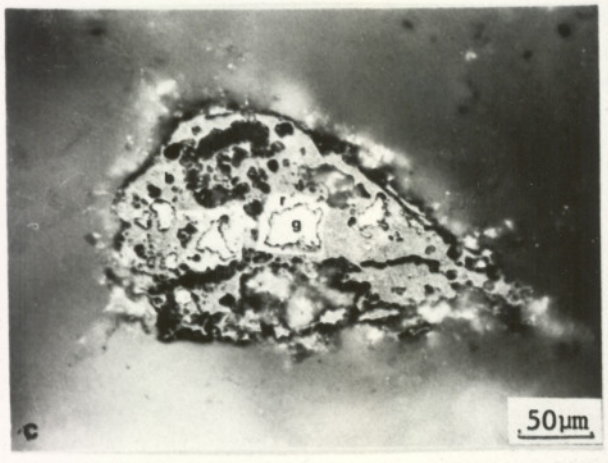
**f.** Massive brannerite (grey) grain enclosing round kerogen particles (dark grey). Incident light in oil. Leader Reef, Virginia G.M.

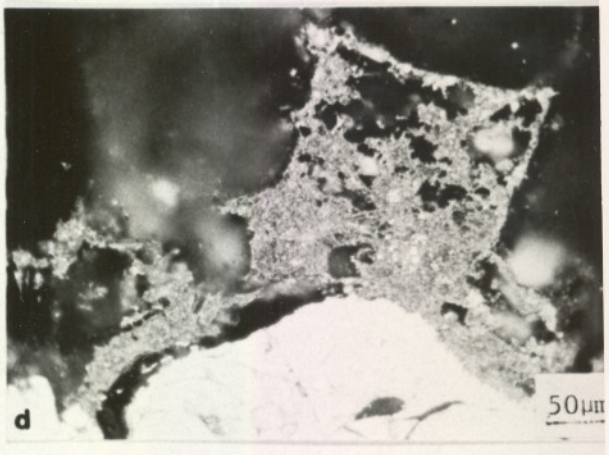
**g.** Two chloritized leucoxene (medium grey) enveloped by a film of brannerite crystals (pale grey), which also filled cracks, and then overgrown by non-uraniferous kerogen (dark grey). The pyrite (white) at top left were corroded by uranous titanate and then covered by uraninite-free kerogen. The two partly chloritized pyrite grains (white and black margin) left on centre wer coated by a thin film of brannerite crystals (pale grey). Vaal Reef, Buffelsfontein G.M.

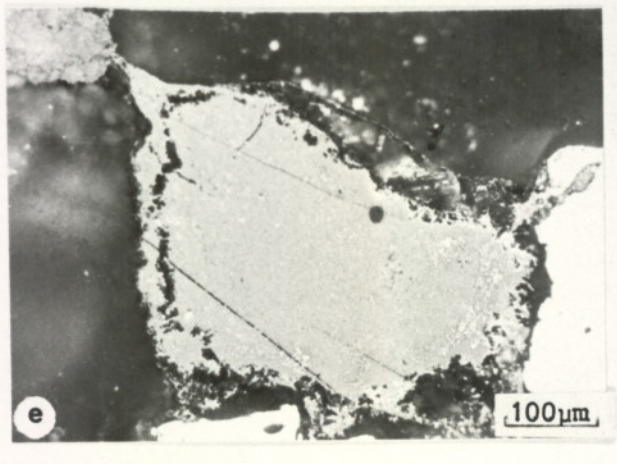
**h.** Microstylolite at quartz boundary (medium grey, q) which contains brannerite (grey, b) and pyrite (white). Carbon Leader, Western Deep Levels G.M.

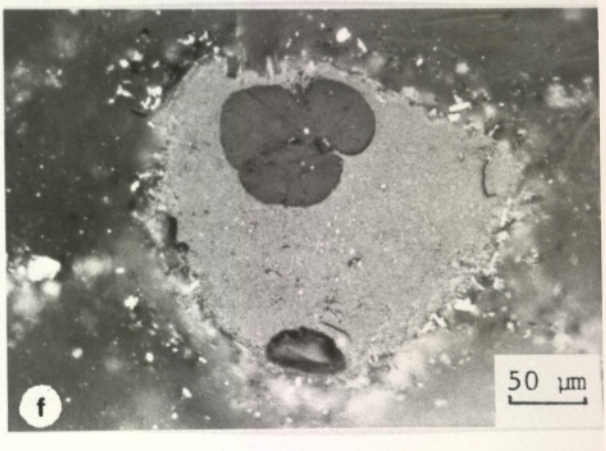

a
50µm

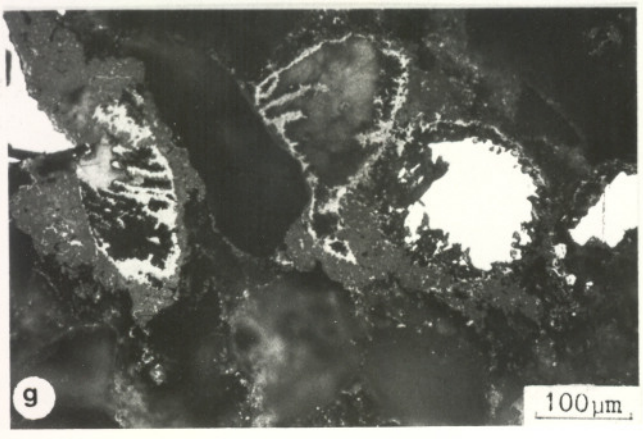

b
50 µm


c
50µm


d
50µm


e
100µm


f
50 µm


g
100µm

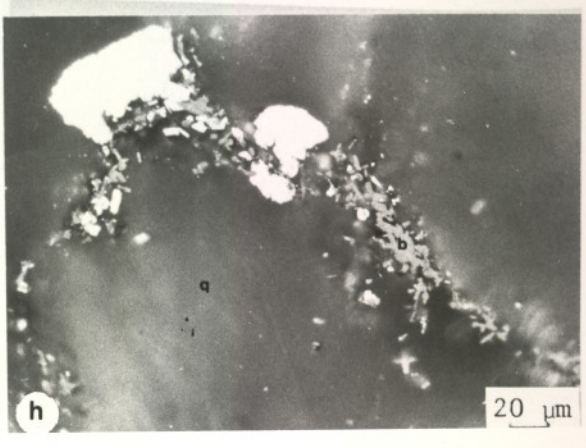

h
20 µm

Figure A.30 Photomicrographs of thorite and mushy anatase
Incident light in oil

**a.** Euhedral, detrital thorite (dark grey, spongy) spotted by galena specks (white) and quartz (black) filling pores. Authigenic ilmenite (grey) at right bottom. Dominion Reef, Bramley G.M.

**b.** Detrital chlorite grain in which spindle-shaped thorite crystals (dark grey, spotted white by galena) are dispersed together with chalcopyrite and pyrrhotite crystals (larger white grains). Kalkoenkrans Reef, Oryx G.M.

**c.** Mushy anatase (speckled pale grey) cementing chloritized pyrite (white cores with dark grey rim of chlorite). Vaal Reef, Western Reefs G.M.

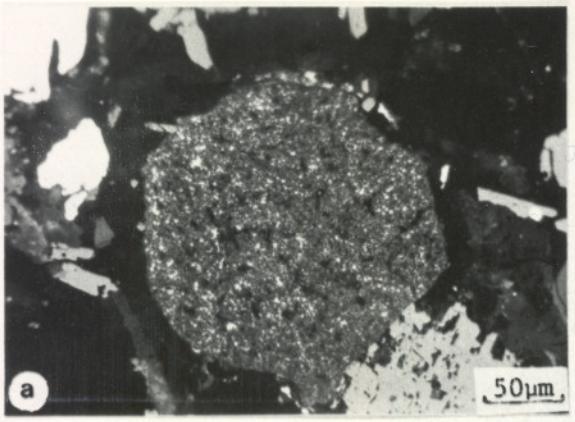
**d.** BSE image of mushy anatase (pale grey) mixed with coffinite, uraniferous leucoxene, quartz (black), and phyllosilicate (black). Galena stands out as white spots (g, 0,5 μm), while uraniferous leucoxene and coffinite (both very pale grey) can barely be distinguished, because of the similar grey tones. Carbon Leader, West Driefontein G.M.

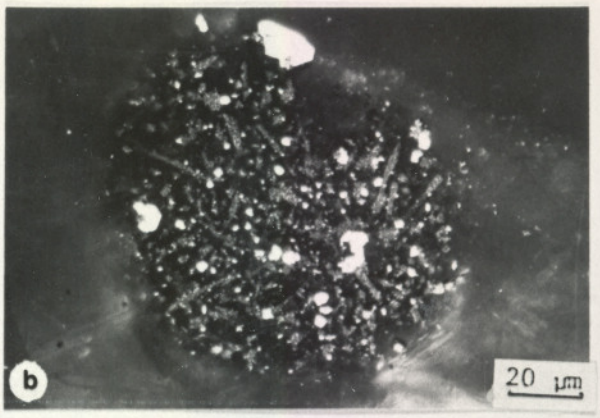
**e.** Uraninite grain (centre) replaced by brannerite crystals (grey) and quartz (black) is coated by a thick layer of crystalline gersdorffite (white) which also precipitated beyond the cutan around chromite (pale grey) and pyrite (white, top centre). Basal Reef, Harmony Complex.

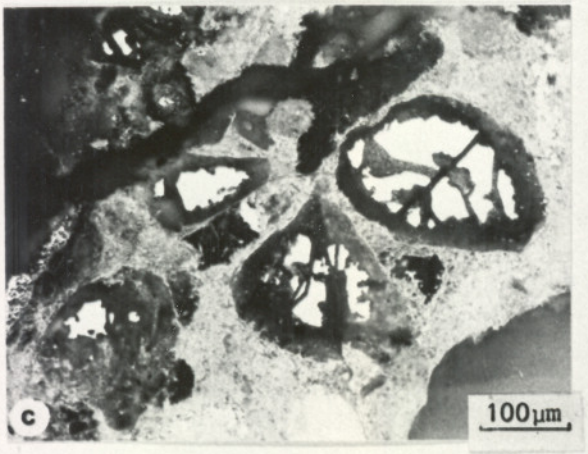
**f.** Kerogen (shades of grey) enclosing fragmented uraninite (grey, dark grey). Quartz (black) with minute gersdorffite crystals (white) filled open space in the organic matter. Vaal Reef, Vaal Reefs South G.M.

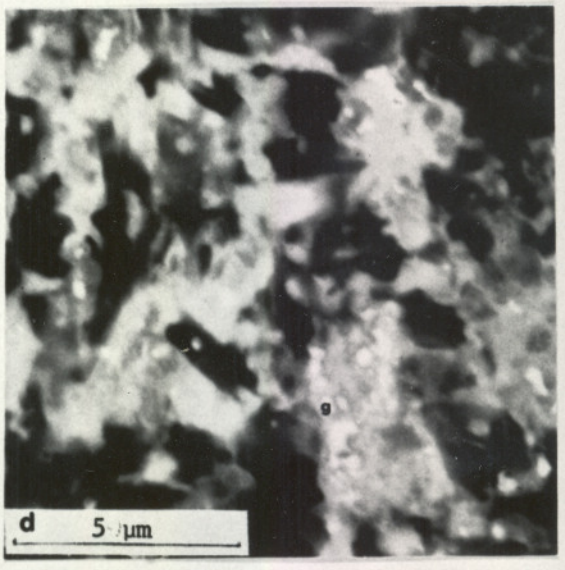
**g.** Detrital chlorite (black) which was first coated by a film of brannerite (grey) and then by non-uraniferous kerogen (dark grey). A film of brannerite crystals (pale grey) coats the pyrite (white) at top left. Vaal Reef, Buffelsfontein G.M.

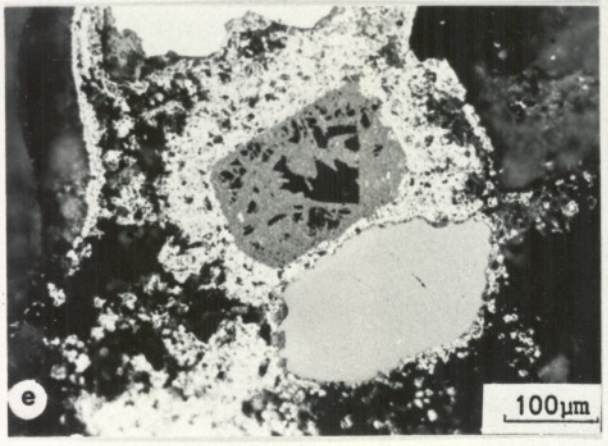
**h.** Microstylolite at contact between two quartz grains (black and white) filled with chlorite (white to grey). Transmitted light, crossed nicols. Carbon Leader, Blyvooruitzicht.

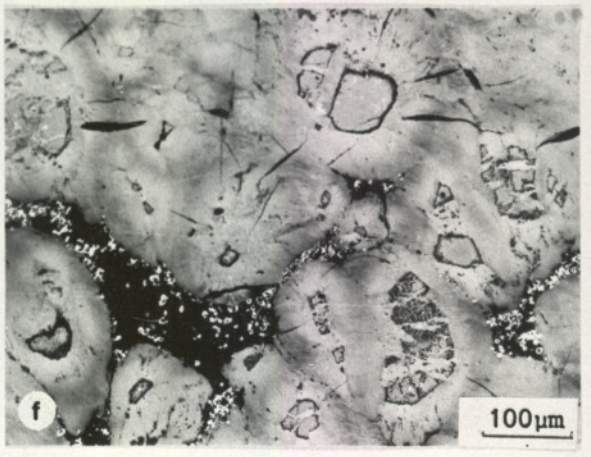

a
50µm

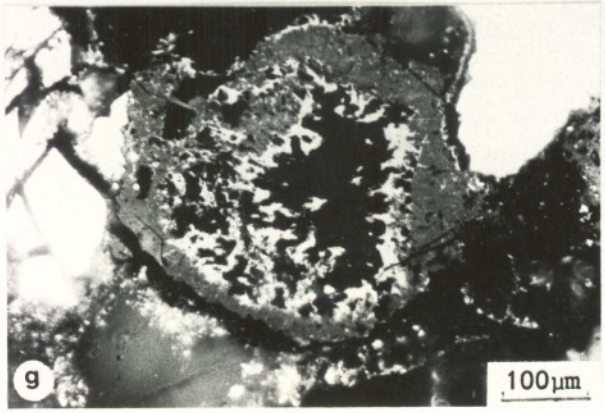

b
20 µm

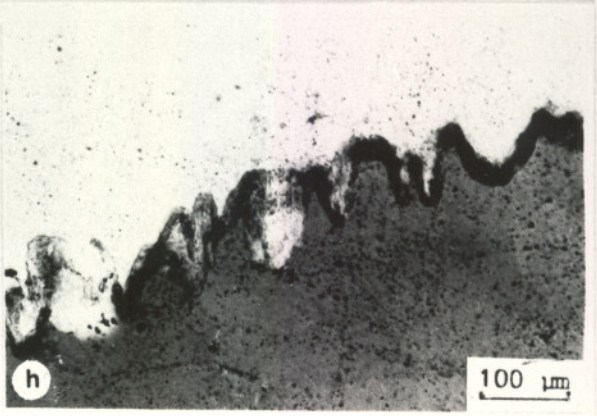

c
100µm


d
5 µm


e
100µm


f
100µm


g
100µm


h
100 µm

APPENDIX B

# LIST OF ABBREVIATIONS

## MINERALS

| | | | |
|---|---|---|---|
| ab | albite | lc | leucoxene |
| an | anatase | magn | magnetite |
| alm | almandite | montm | montmorillonite |
| and | andalusite | mus | muscovite |
| asp | arsenopyrite | ort | orthoclase |
| bio | biotite | PGE | platinum group elements |
| br | brannerite | PGM | platinum group minerals |
| cf | coffinite | ph | pyrophyllite |
| chl | chlorite | ph.sil. | phyllosilicate |
| chlort | chloritoid | pn | pentlandite |
| chr | chromite | po | pyrrhotite |
| chur | churchite | py | pyrite |
| cob | cobaltite | q | quartz |
| cor | cordierite | rut | rutile |
| cp | chalcopyrite | ser | sericite |
| fsp | feldspar | sil | silimanite |
| gar | garnet | sl | sphalerite |
| gd | gersdorffite | smec | smectite |
| gn | galena | staur | staurolite |
| hem | hematite | ulc | uraniferous leucoxene |
| ill | illite | ur | uraninite |
| ilm | ilmenite | ur. tit. | uranous titanate |
| kaol | kaolinite | usp | ulvospinel |
| ker | kerogen | verm | vermiculite |
| ky | kyanite | zr | zircon |

## GENERAL

| | |
|---|---|
| BIF | banded iron formation |
| BSE | back scattered electron |
| CRG | Central Rand Group |
| DTA | differential temperature analysis |
| EMP | electron microprobe |
| G.F. | goldfield |
| G.M. | gold mine |
| HREE | heavy rare earths |
| LREE | light rare earths |
| ML | mixed-layered |
| OFS | Orange Free State |
| PAL | present atmospheric level |
| SEM | scanning electron microscope |
| TEM | transmission electron microscope |
| UDC | uranyl dicarbonate |
| UTC | uranyl tricarbonate |
| VCR | Ventersdorp Contact Reef |
| VHN | Vickers hardness numbers |
| WRG | West Rand Group |
| XRD | X-ray diffraction |

59 327/41